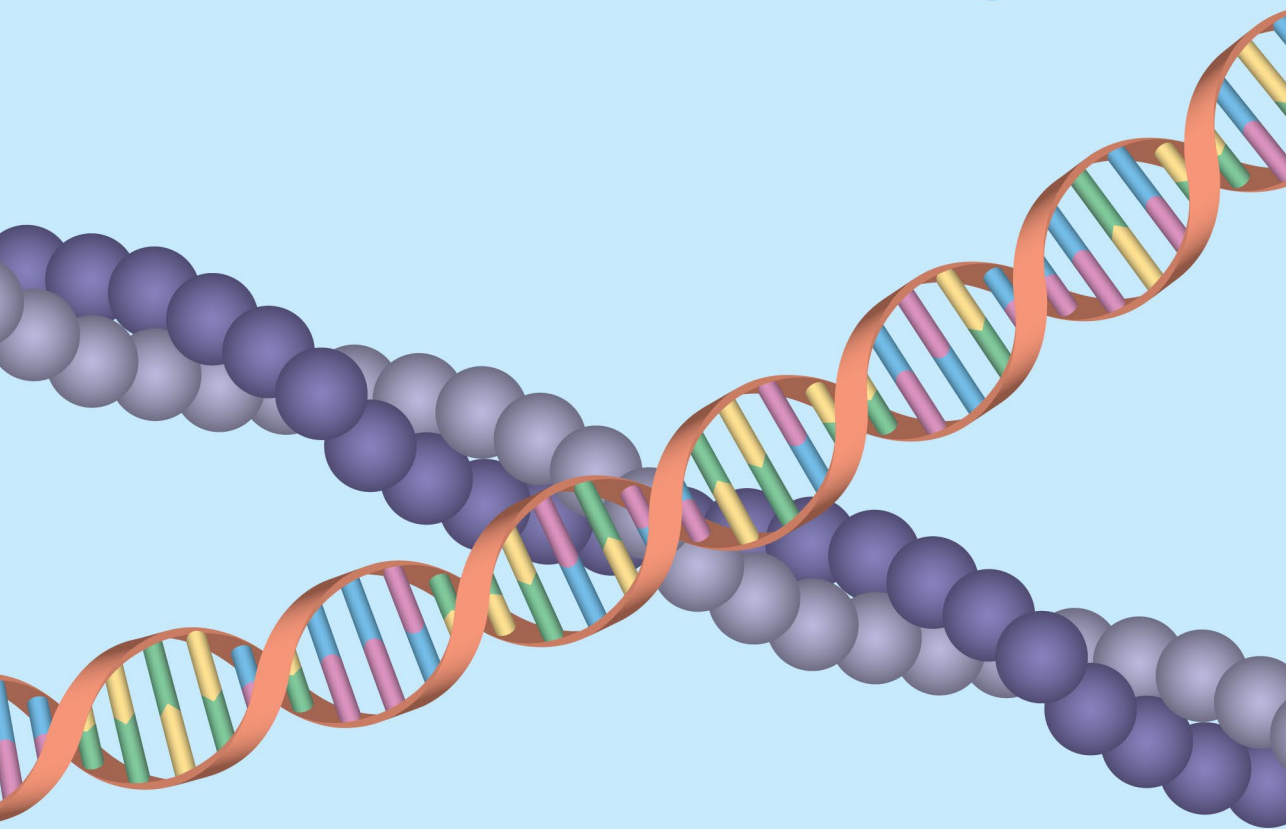


Unraveling intestinal lumen formation in *Caenorhabditis elegans*



Jorian J. Sepers

Unraveling intestinal lumen formation in *Caenorhabditis elegans*

Jorian J. Sepers

DOI: <https://doi.org/10.33540/2167>

ISBN: 978-94-6483-853-4

Printed by Ridderprint

Cover, design & layout by Jorian J. Sepers

Copyright © 2024 by Jorian J. Sepers. All rights reserved.

Unraveling intestinal lumen formation in *Caenorhabditis elegans*

Het ontrafelen van de formatie van het darm-lumen
in *Caenorhabditis elegans*
(met een samenvatting in het Nederlands)

Proefschrift

ter verkrijging van de graad van doctor aan de Universiteit Utrecht op gezag
van de rector magnificus, prof. dr. H.R.B.M. Kummeling, ingevolge het besluit
van het college voor promoties in het openbaar te verdedigen op maandag 25
maart 2024 des middags te 2.15 uur

door

Johannes Jan Sepers
geboren op 22 juni 1994 te Gorinchem

Promotoren:

Prof. dr. M. Boxem

Prof. dr. S.J.L. van den Heuvel

Beoordelingscommissie:

Dr. M. Galli

Prof. dr. S.C.D. van IJzendoorn

Prof. dr. L.C. Kapitein

Prof. dr. J. Klumperman

Prof. dr. H.C. Korswagen

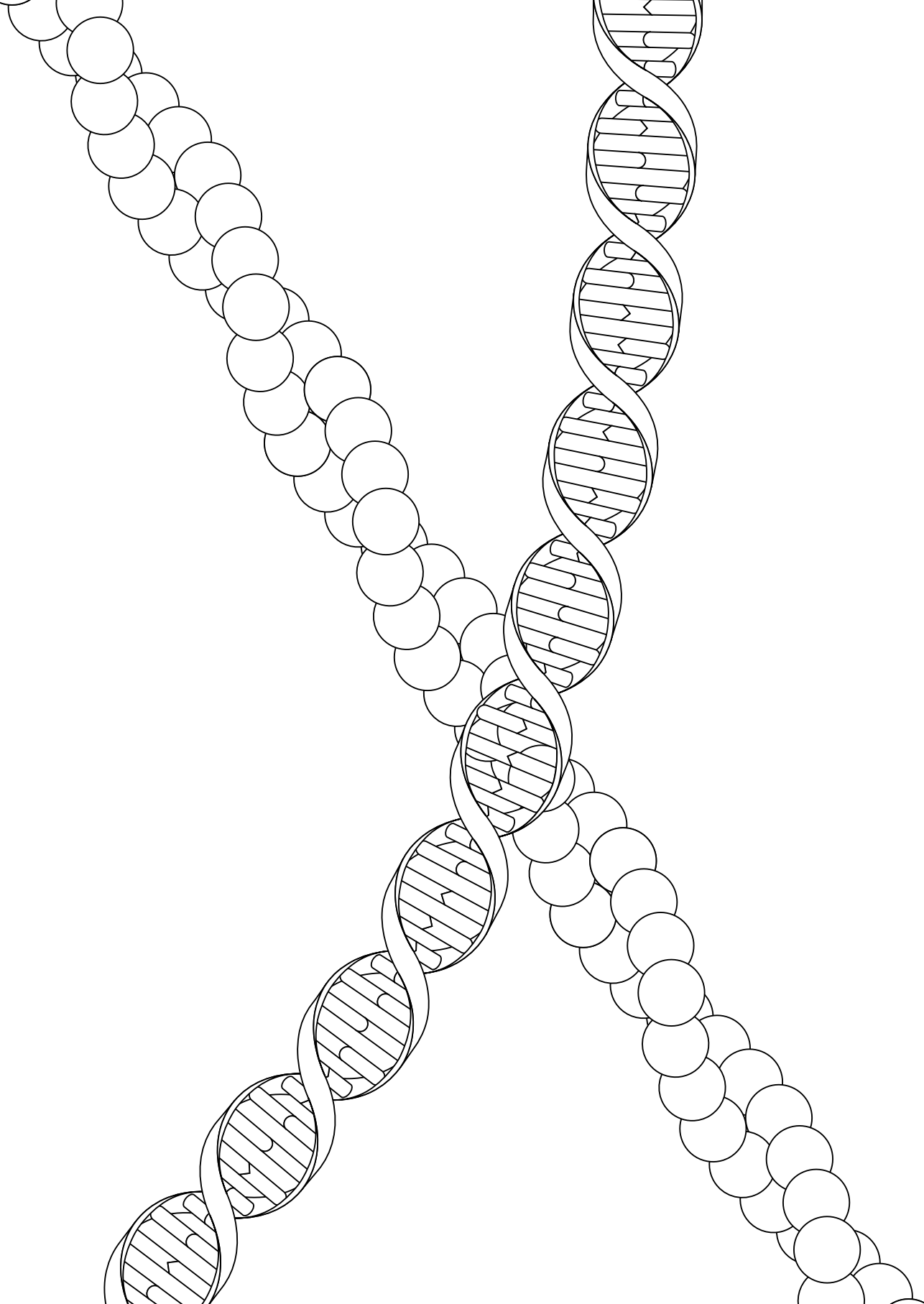
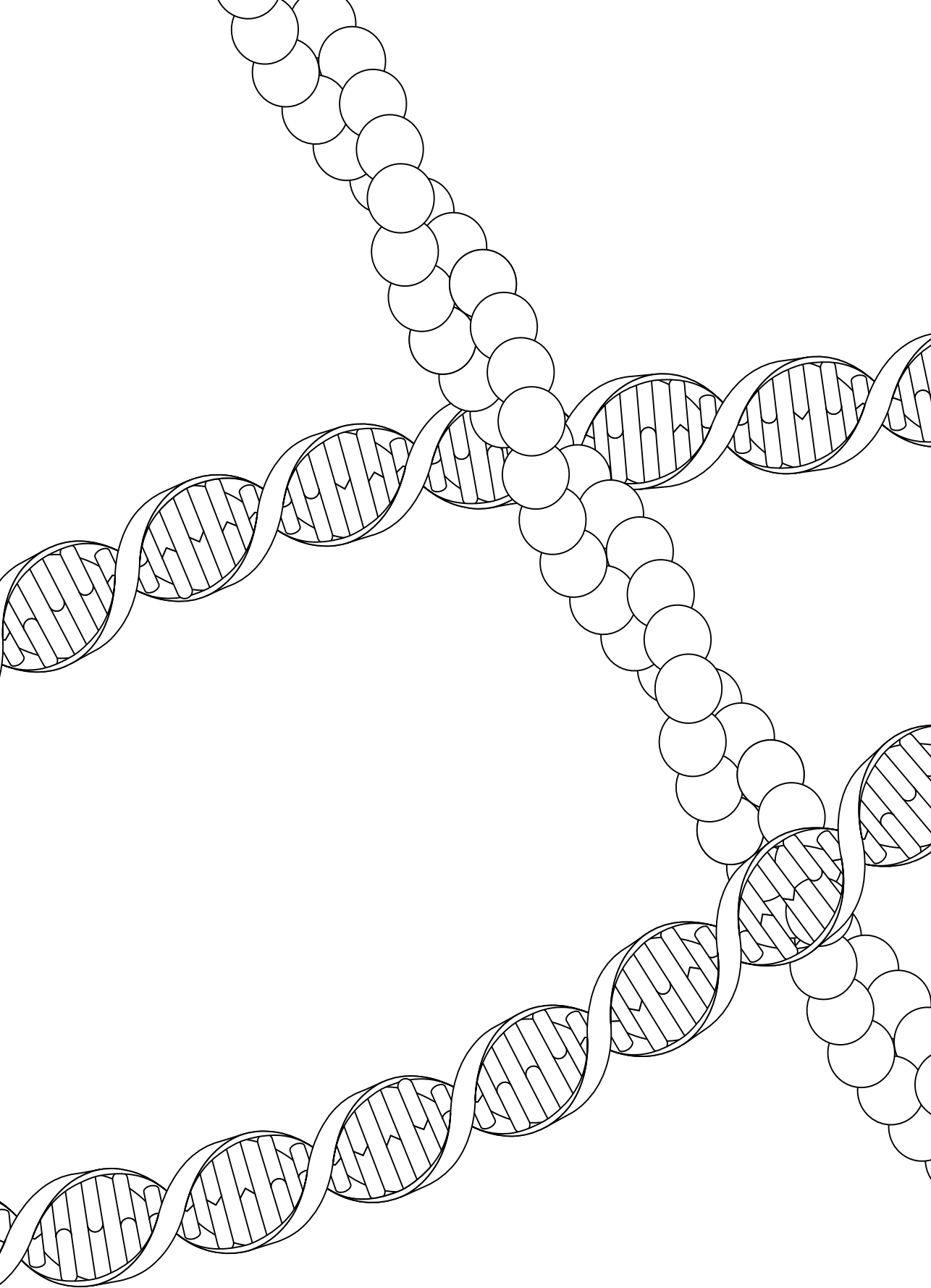


Table of contents

Chapter 1	Introduction	10
	Scope of the thesis	32
Chapter 2	C-terminal phosphorylation modulates ERM-1 localization and dynamics to control cortical actin organization and support lumen formation during <i>Caenorhabditis elegans</i> development	35
Chapter 3	ERM-1 phosphorylation and NRFL-1 redundantly control lumen formation in the <i>C. elegans</i> intestine	77
Chapter 4	Regulation of <i>Caenorhabditis elegans</i> intestinal lumen formation by the Ste20-family kinase GCK-4 ^{Lok/Sik}	107
Chapter 5	The mIAA7 degron improves auxin-mediated degradation in <i>Caenorhabditis elegans</i>	143
Chapter 6	General discussion	177
Appendix	References	192
	English summary	224
	Dutch summary (Nederlandse samenvatting)	228
	Curriculum vitae	234
	List of publications	235
	Acknowledgments (Dankwoord)	236



Chapter 1

General introduction

Jorian J. Sepers

Division of Developmental Biology, Institute of Biodynamics and Biocomplexity, Department of Biology, Faculty of Science, Utrecht University, Utrecht, The Netherlands

Introduction

Caenorhabditis elegans is an important model organism, driving numerous foundational biological breakthroughs. For example, the identification of programmed cell death regulation, later revealed to be conserved in numerous species including humans (ELLIS & HORVITZ, 1986). Additionally, the identification of RNA interference (RNAi) in *C. elegans* opened up new avenues for gene regulation studies (FIRE *et al.*, 1998). These and many other discoveries were possible due to a number of key features of the *C. elegans* model system. For instance, the nematode allows for efficient genetics as they have a short life cycle and have hermaphroditic lifestyle. The animal also has a completely defined developmental cell lineage and a transparent body allowing for investigating detailed developmental events and biological processes.

C. elegans, as a differentiated multi-cellular organism, mirrors various aspects of mammalian physiology. A prime example is the intestine, the focal point of this thesis. The worm's intestine exhibits similar properties to humans, such as the ability to digest and absorb food. Additionally, it exerts influence over other organs systems, including the nervous and immune systems, and it can host a microbiome. Due to these diverse functions while having a simplistic morphology, the *C. elegans* intestine serves as an outstanding model system for investigating a wide array of biological processes. This chapter aims to provide an overview of the research conducted using the *C. elegans* intestine. By the end, readers should be well-equipped to delve into the intestinal research presented in the subsequent chapters of this thesis.

C. elegans development and intestine formation

The *C. elegans* development is initiated in the spermatheca, where the oocyte undergoes fertilization. The zygote, or one-cell stage embryo, then progresses towards the uterus where it undergoes several rounds of asymmetrical divisions. Somewhere between the 16-cell and 32-cell stages, the egg is laid, and the embryo continues its development outside the parent. Around this time, gastrulation takes place, during which the germ layers form. In *C. elegans*, gastrulation is not as dramatic as in many other animal embryos, with cells moving only short distances and the blastocoel space being relatively small. Following gastrulation, morphogenesis ensues, a critical phase where cells and tissues intricately shape and position themselves, establishing the fundamental body plan along different body axes. From this point onward, the embryonic stages are identified by the shape of the embryo (Figure 1A). The first of these stages is known as the (lima) bean stage, characterized by an oval shape with a small ventral dent around 2/3 from the anterior side of the embryo. In the subsequent stage, the dent deepens, and the embryo is referred to as the comma stage embryo. As the embryo elongates, the posterior side folds over at the location of the dent. From this juncture, embryos are denoted by the

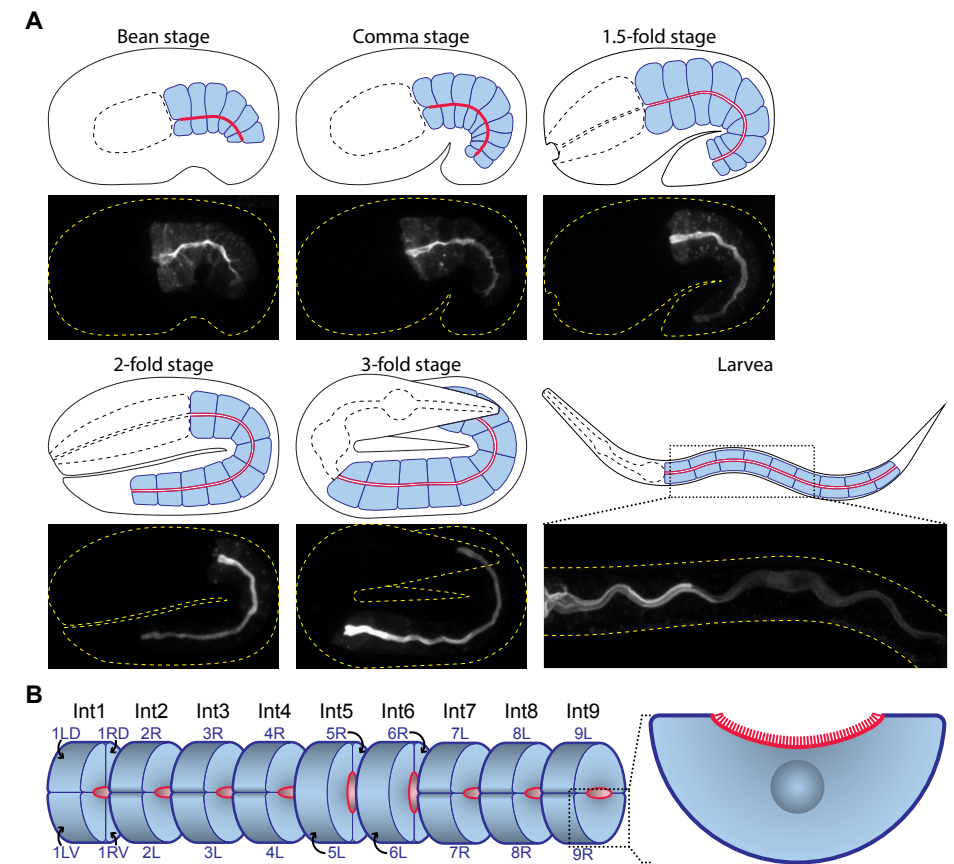
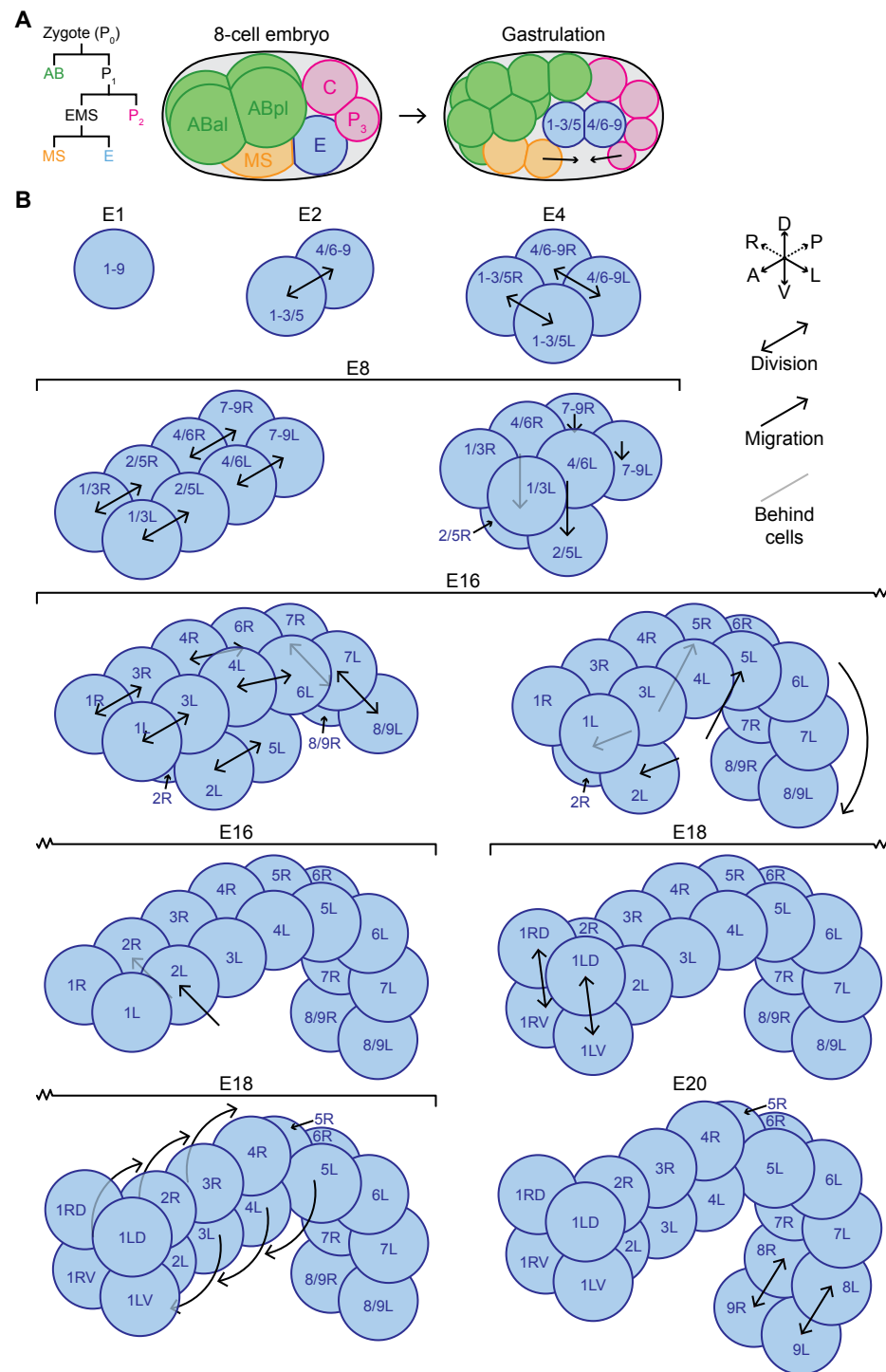


Figure 1: Overview of the *C. elegans* intestine throughout development. (A) Spinning disk microscopy images with complementary schematic illustrations of the intestine during various developmental stages. **(B)** A schematic illustration of a mature intestine with the names for the intestinal rings and cells indicated.

number of times they fold over within the egg. For instance, an embryo that folds over one and a half times the length of the egg is termed a 1.5-fold embryo. This nomenclature is used until the animal hatches, although around the 2-fold stage, the embryo starts to move, and exact stages become more challenging to discern. After hatching, *C. elegans* goes through four larval stages, designated as L1, L2, L3, and L4. During these stages, the worm undergoes growth spurts and molts, shedding its old cuticle and replacing it with a new one. Following the fourth and final molt, the animal attains adulthood and gains the ability to reproduce through either self-fertilization or mating with others.

Intestinal development initiates at the 8-cell stage, when the embryo gives rise to a single intestinal precursor cell known as the E cell. Through a series of cell divisions and morphological events, discussed in the “Embryonic morphogenesis” section, the E cell forms a tube composed of nine rings, collectively referred to as the intestine. Each ring consists of two half-moon



~ Figure description on the next page ~

Figure 2: Schematic overview of the E cell lineage and morphogenesis of the intestinal primordium. (A) The cell lineage from a one-cell embryo up to an 8-cell embryo. In addition, an illustration of an 8-cell embryo and an embryo during gastrulation. **(B)** A series of illustrations of the different cell divisions and morphological changes through the early development of the intestine. The six-sided compass in de legenda indicate the different body axes, A-P, D-V and L-R are anterior-posterior, dorsal-ventral and left-right, respectively.

shaped cells, except for the most anterior ring that comprises four cells, totaling 20 cells (Figure 1B). In a mature intestine, the rings are denoted as Int followed by a number, ranging from 1 to 9, with Int1 representing the most anterior ring. During intestinal development, the various stages are characterized by the number of E cell descendants. Thus, after the initial division, the primordium is referred to as E2, and after the final cell division, as E20.

There is no standardized nomenclature for individual cells within the E lineage. However, these cells do undergo consistent and organized changes in their order and position throughout development. In this chapter, each cell will be assigned a number corresponding to the Int-ring it will become a part of in the mature intestine (Figure 1B). Prior to reaching E20, cells may be identified with multiple numbers, as they continue to divide, and their descendants contribute to multiple rings. For example, after the first E cell division, the ancestral cell of Int1, Int2, Int3, and Int5 arises and is termed 1-3/5. The two cells within each Int-ring will be referred to as L or R for left and right, respectively, as they initially align along the left-right axis during development. Finally, in Int1, which contains four cells, the two ventral and two dorsal cells will be marked as V and D, respectively.

Embryonic morphogenesis

After fertilization, the one-cell embryo, with the initial cell referred to as P_0 , and its daughter cells go through three cycles of asymmetric divisions. Among the resulting eight cells, the E cell emerges at the ventral-posterior side (Figure 2A – “8-cell stage embryo”; Figure 2B – “E1”) (DEPPE *et al.*, 1978; SULSTON *et al.*, 1983). Initially, the E cell divides along the anterior-posterior axis, giving rise to the 1-3/5 and 4/6-9 cells, commonly referred to as Ea and Ep, respectively (Figure 2B – “E2”) (ASAN *et al.*, 2016; DEPPE *et al.*, 1978; LEUNG *et al.*, 1999; SULSTON *et al.*, 1983). After this division, the embryo undergoes gastrulation during which the two E cell daughters located on the surface migrate inwards and become surrounded by neighboring cells (Figure 2A – “Gastrulation”) (NANCE, 2005; SULSTON *et al.*, 1983).

Following gastrulation, the two intestinal cells undergo two rounds of division, resulting in eight daughter cells (SULSTON *et al.*, 1983). The initial division occurs along the left-right axis, resulting in the formation of left and right pairs that ultimately constitute the final intestinal rings (Figure 2B – “E4”). Subsequently, the second set of divisions takes place along the anterior-posterior axis, resulting in four pairs (Figure 2B – “E8”). At the E8 stage, the 2/5 cell pair

migrates ventrally beneath the other E cells while maintaining contact with the 1/3 and 4/6 pairs (MADURO, 2017). While the exact reason for this migration remains elusive, it has been postulated that it could play a crucial role in the development of the pharyngeal-intestinal valve. This valve connects the intestine to the pharynx, the organ responsible for food intake. The valve cells require an interaction with the adjacent four Int1 cells to establish polarity and a seamless lumen connection with the intestine. As the Int1 pair only divides later during development, the Int2 pair may temporarily establish contact with the valve cells to facilitate pharyngeal-intestinal valve development (RASMUSSEN *et al.*, 2013).

In the subsequent round of E cell divisions, most cells divide along the anterior-posterior axis, including the ventral positioned 2/5 cells giving rise to the Int2 and Int5 cells. During the E16 stage, these ventral cells undergo dorsal migration to form a monolayered sheath (Figure 2B – “E16”). As the non-chronological numbering of the cells indicates, these cell pairs do not intercalate in the same position within the sheath (LEUNG *et al.*, 1999). Initially, the Int5 cells migrate between the Int4 and Int6 cell pairs, in a coordinated manner as the neighboring cells reshape to accommodate the intruding Int5 cells (ASAN *et al.*, 2016). Next, the Int2 pair migrate between the Int1 and Int3 cell pairs, however this migration is more variable and chaotic as the duration can vary dramatically and the neighboring cells do not seem to accommodate the Int2 cells. Moreover, the manner in which this migration occurs can differ depending on the division of the Int1 cells and the rotations of various cell pairs that take place shortly after or sometimes even during the Int2 intercalation (ASAN *et al.*, 2016). These Int1 cell divisions and rotations will be discussed below. During the E8 to E16 transition, the posterior 7-9 cells divide diagonal between the anterior-posterior and dorsal-ventral axes (Figure 2B – “E16”). Additionally, these cells begin to curve downward, as the animal starts to fold over itself within the egg (Figure 1A; Figure 2B – “E16”).

In addition to intercalation, the intestinal lumen is formed through means of cord hollowing during the E16 stage. Cord hollowing is a type of *de novo* lumen formation in which a space is formed between cells that were previously tightly connected together (LEUNG *et al.*, 1999; MADURO, 2017; SIGURBJÖRNSDÓTTIR *et al.*, 2014). The initial step in this lumen formation process is to establish the side of the cells where the future lumen will be formed (SIGURBJÖRNSDÓTTIR *et al.*, 2014). This is accomplished by establishing epithelial cell polarity, wherein the apical membrane is designated as the site of the future lumen. Polarization occurs approximately 30 minutes into the E16 stage, when organelles are polarizing along the apical-basolateral axis. One prominent example is the nucleus, which migrates toward the prospective apical membrane. At this point the intestine has radial symmetry with respect to the midline, an imaginary line running anterior-posterior through the center of the primordium (LEUNG *et al.*, 1999).

During the next step, the apical membrane is enlarged to expand the lumen (SIGURBJÖRNSDÓTTIR *et al.*, 2014). This becomes apparent shortly after polarization, as separations between the cell pairs become discernible and apical vesicles begin to form. These separations are initially unstable and collapse frequently, but after a while more stable separations emerge, ultimately coalescing into a continuous lumen (LEUNG *et al.*, 1999).

Following the E16 stage, the 1L and 1R cells undergo division along the dorsal-ventral axis, resulting in the four cells that compose the Int1 ring (Figure 1A; Figure 2B – “E18”) (ASAN *et al.*, 2016; LEUNG *et al.*, 1999). Concurrently, the Int2–Int4 rings execute a clockwise rotation of 90 degrees, resulting in the right cells assuming a dorsal position and the left cell aligning ventrally, stacked atop one another (LEUNG *et al.*, 1999). Notably, these individual rings appear to undergo these movements autonomously as the timing of each rotation varies. For example, there are instances where Int3 initiates rotation prior to full intercalation of Int2, while in other cases, Int2 might commence rotation during interactions before the rotation of Int3 has even begun (ASAN *et al.*, 2016). These rotations hinge on interactions between the Int rings with the ventral neurons and dorsal hypodermis, possibly providing cues for orientation guidance or timing (ASAN *et al.*, 2016). The reason for these rotations is probably not for intestinal function, but to facilitate pharyngeal-intestinal valve development and body movement. After the rotations, the oval lumen’s longest diameter aligns along the horizontal axis rather than the ventral axis (LEUNG *et al.*, 1999). This orientation is believed to better align with the valve cell lumen and aids in the dorsal-ventral bending of the body necessary for the animal’s movement (ASAN *et al.*, 2016).

The last cells to divide are the 8/9 cells, giving rise to the Int8 and Int9 cell pairs (Figure 2B – “E20”) (ASAN *et al.*, 2016; LEUNG *et al.*, 1999). Following this, the intestine undergoes further development and growth, ultimately forming a functional intestine by the time the animal hatches. For example, the lumen will now fully mature, gaining an oval shape and forming a brush border (BIDAUD-MEYNARD *et al.*, 2021; MADURO, 2017; SIGURBJÖRNSDÓTTIR *et al.*, 2014). Microvilli can be observed as early as the 1.5-fold stage, and by the 3-fold stage the lumen has a regular brush border that will become thicker and taller throughout development (BIDAUD-MEYNARD *et al.*, 2021). In the later stages of embryonic development, the Int7 to Int9 rings execute a 90-degree counter-clockwise rotation, causing the cell pairs to align directly above one another (LEUNG *et al.*, 1999). These rotations are poorly understood as they transpire while the animal is moving in the egg, rendering live imaging complicated (ASAN *et al.*, 2016). The rationale for the Int5 and Int6 rings abstaining from rotation likely stems from the necessity for them to partially surround the primordial germ cells (ASAN *et al.*, 2016; CHIHARA & NANCE, 2012).

Postembryonic polyploidy

During embryonic stages, intestinal development yields a functional intestine consisting of 20 cells, each possessing a single $2n$ nucleus. However, by the end of larval development, the intestine still comprises 20 cells, but now harbors 30 to 34 $32n$ nuclei, leading to a 24- to 27.2-fold increase in genomic copies compared to pre-larval development (SULSTON *et al.*, 1983). This is achieved through two distinct types of non-canonical cell cycles: endoreplication and endomitosis (Figure 3A) (EDGAR *et al.*, 2014). In endomitosis, the mitosis step (M phase) is partially skipped, resulting in the duplication of only the nucleus without a complete cell duplication. Conversely, endoreplication entails the complete omission of mitosis, leading to DNA duplication without cell or nucleus duplication. Most intestinal cells undergo a round of endomitosis during the L1 larval stage, with the exception of the six cells composing the Int1 and Int2 rings (Figure 3B). Additionally, the four cells of Int8 and Int9 may or may not undergo endomitosis in L1 (SULSTON *et al.*, 1983). Following the L1 endomitosis, all cells undergo endoreplication and will do so in all the subsequent larval stages resulting in total of four endoreplication cycles (SULSTON *et al.*, 1983).

Polyploidy is a natural occurrence observed across the plant and animal kingdoms, often associated with terminally differentiated tissues. It serves a crucial purpose in enhancing cellular capacity, enabling cells to grow larger and produce more materials (EDGAR *et al.*, 2014). As *C. elegans* larvae grow, the intestine grows with it, which is achieved by growth of the individual cells and not cell division. This indicates that to accommodate this growth, there needs to be an increase in the production of proteins, achieved by amplifying the number of genomic copies within the cells (SULSTON *et al.*, 1983). This phenomenon aligns with the polyploidy observed in the hypodermis, where there exists a dose-dependent correlation between polyploidy and body size (LOZANO *et al.*, 2006; MORITA *et al.*, 2002). Polyploidy can also allow for increased production of secreted proteins, which might be true for the *C. elegans* intestine as they nurture germ cells by producing yolk proteins. In support of this, recent research has demonstrated that inhibiting nuclear division in the intestine disrupts the rapid upregulation of certain genes specific to intestinal development, ultimately leading to reduced fitness in the progeny (RIJNBEEK *et al.*, 2022).

Transcriptional regulation of endoderm fate

The transcriptional regulation of the *C. elegans* intestine starts with the activation of the EMS cell, under the control of the SKN-1 transcription factor (Figure 4) (MCGHEE, 2013). Depletion of SKN-1 leads to a disruption in the MS and E lineages, causing them to adopt the C lineage (BOWERMAN *et al.*, 1992; BOWERMAN *et al.*, 1993). SKN-1 is maternally provided in the oocyte and eventually localizes within the P1 cell due to its asymmetric distribution towards the posterior side

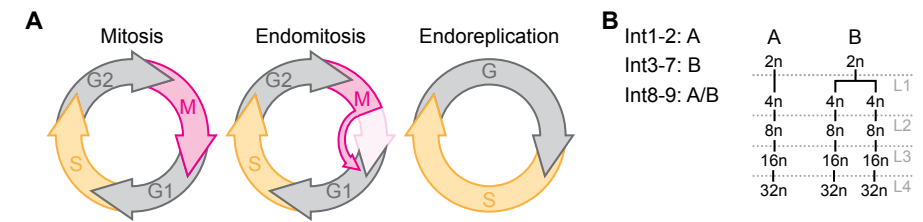


Figure 3: Schematic illustration of polyploidy in the intestine. (A) An illustration of the mitotic, endomitotic and endoreplication cell cycles. **(B)** The endomitosis and endoreplication events for the different intestinal rings during larval development.

of the one-cell embryo (FARLEY *et al.*, 2008; PAGE *et al.*, 2007). Following the division of the P1 cell, SKN-1 triggers the EMS program in the posterior daughter cell (BOWERMAN *et al.*, 1992; BOWERMAN *et al.*, 1993). Concurrently, SKN-1 undergoes transcriptional inactivation in the anterior P2 cell, mediated by the RNA binding protein PIE-1. Loss of PIE-1 leads to the emergence of two EMS lineages, as the P2 cell adopts the EMS program (BOWERMAN *et al.*, 1993; MELLO *et al.*, 1992; TENENHAUS *et al.*, 2001). SKN-1 is crucial for both the MS and E lineages, as SKN-1 transcriptionally activates *tbx-35*, vital for the MS program, and regulators of the E cell program that will be described in detail in the following paragraphs (BROITMAN-MADURO *et al.*, 2006; MCGHEE, 2013).

The endoderm lineage is initiated by SKN-1, which triggers a cascade of GATA-like transcription factors (Figure 4) (MCGHEE, 2013). The first in this sequence are MED-1 and MED-2, direct targets of SKN-1 (MADURO *et al.*, 2001). MED-1 and MED-2 are 98 % identical, and are unsurprisingly largely functionally redundant (CAPTAN *et al.*, 2007; MADURO *et al.*, 2007). Following MED-1 and MED-2, the subsequent GATA-like transcription factors are END-1 and END-3, which exhibit a 51 % similarity in their binding targets and display considerable phenotypic redundancy (MADURO *et al.*, 2005a; MCGHEE, 2013). These factors become active in the early E lineage and are recognized as the primary inducers of endoderm, as ectopic expression can induce at least partial endoderm programming in nearly every other cell type (MADURO *et al.*, 2005a; ZHU *et al.*, 1997; ZHU *et al.*, 1998). The final GATA-like transcription factors in this cascade are ELT-2 and ELT-7, which serve as the main activators of genes associated with endoderm differentiation (FUKUSHIGE *et al.*, 2003; SOMMERMANN *et al.*, 2010). They become expressed as early as the E2 stage and are the only two GATA-like transcription factors that remain active in the intestine throughout the entirety of the animal's life (FUKUSHIGE *et al.*, 1998; FUKUSHIGE *et al.*, 2003; RAJ *et al.*, 2010). ELT-2 and ELT-7 exhibit a synergistic and redundant relationship, with ELT-2 considered to play a more critical role in endoderm induction (FUKUSHIGE *et al.*, 2003). Ectopic expression of either ELT-2 or ELT-7 can reprogram certain non-endodermal differentiated cells towards an endoderm program (RIDDLE *et al.*, 2013; RIDDLE *et al.*, 2016).

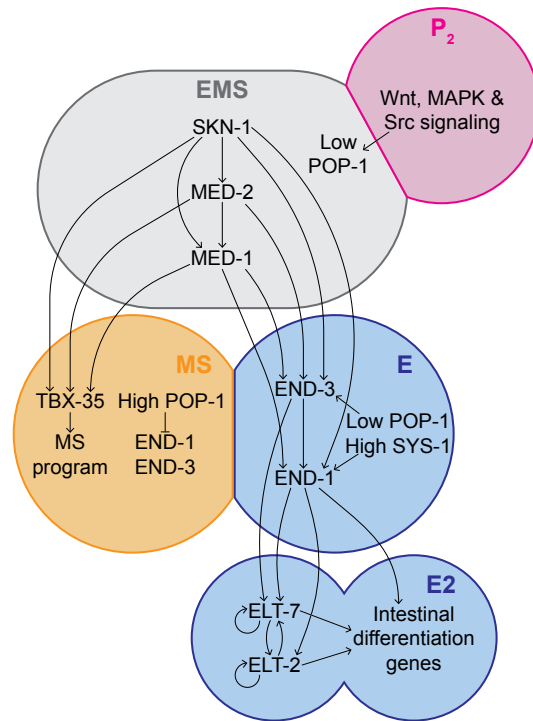


Figure 4: Schematic overview of the signaling pathways responsible for endoderm induction.

SKN-1, MED-2, and END-3 collaboratively activate *end-1* (BROITMAN-MADURO *et al.*, 2005; MADURO *et al.*, 2005a; MADURO *et al.*, 2015; OWRAGHI *et al.*, 2010; ZHU *et al.*, 1997). Subsequently, END-1 and END-3 work together to activate *elt-7*, and END-1, along with ELT-7, activate *elt-2* (FUKUSHIGE *et al.*, 1999; FUKUSHIGE *et al.*, 2003; SOMMERMANN *et al.*, 2010). Finally, ELT-2 and ELT-7 have the capacity to stimulate their own transcription and that of each other, maintaining continuous expression throughout the worm's lifespan. END-1, ELT-2, and ELT-7 collectively drive the activation of genes essential for intestinal differentiation, although END-1 expression is lost around the E8 stage (EWE *et al.*, 2022; RAJ *et al.*, 2010).

SKN-1 plays a crucial role in inducing both the E and MS cells, and it is present in similar levels within these cells (BOWERMAN *et al.*, 1992; BOWERMAN *et al.*, 1993; PAGE *et al.*, 2007). Additionally, MED-1 and MED-3 also have the capacity to transcriptionally activate *tbx-35*, thereby initiating the MS lineage (BROITMAN-MADURO *et al.*, 2006; BROITMAN-MADURO *et al.*, 2009). If SKN-1, MED-1 and MED-3 can initiate both the E and MS programs, what determines which EMS daughter cell becomes the E, and which the MS cell? It has long been known that the P2 cell, located posterior to the EMS cell, is essential for inducing the endoderm fate, and that repositioning the P2 cell can reverse the E and MS lineages (GOLDSTEIN, 1993; SCHIERENBERG, 1987). Through various genetic screens, it

Initially, it was believed that SKN-1 and the downstream GATA-like transcription factors operated in a linear pathway, but more recent data has revealed a more intricate network (Figure 4) (EWE *et al.*, 2022; MCGHEE, 2013). All these components function in a feed-forward-loop, meaning they not only activate the next component but also one or more components further down the pathway, introducing significant redundancy into the system (EWE *et al.*, 2022). SKN-1 activates *med-2* transcriptionally, and both SKN-1 and MED-2, in turn, activate *med-1* (EWE *et al.*, 2022; MADURO *et al.*, 2001). SKN-1, MED-1, and MED-2 jointly induce *end-3* expression, and

was discovered that Wnt, Src, and MAPK signaling from the P2 cell redundantly trigger the E lineage in the posterior EMS daughter cell. This occurs through the phosphorylation and subsequent nuclear export of the TCF/LEF ortholog POP-1 in the future E cell nucleus (Figure 4) (BEI *et al.*, 2002; MADURO *et al.*, 2002; MENEGHINI *et al.*, 1999; SHIN *et al.*, 1999; THORPE *et al.*, 1997). TCF are DNA binding proteins and downstream effectors of the Wnt pathway, but POP-1 in the E cell seems to act in an inverted way to canonical Wnt signaling (CADIGAN & WATERMAN, 2012; LIN *et al.*, 1995). Loss of Wnt signaling between the P2 and EMS cell leads to the formation of two MS daughter cells, while loss of POP-1 results in two E daughter cells (BEI *et al.*, 2002; LIN *et al.*, 1995; THORPE *et al.*, 1997).

In canonical Wnt signaling activation, TCF interacts with β -catenin to promote the transcription of target genes (CADIGAN & WATERMAN, 2012). In the E cell, POP-1 interacts with at least two orthologs of β -catenin, WRM-1 and SYS-1, upon induction of the P2 cell. These β -catenins, however, serve distinct functions (Figure 4) (MCGHEE, 2013). Upon P2 signaling, WRM-1 prompts the MAPK-like kinase LIT-1 to undergo autophosphorylation, after which they form a complex together (ROCHELEAU *et al.*, 1999). Subsequently, LIT-1 phosphorylates POP-1, causing POP-1 to exit the nucleus (LO *et al.*, 2004; YANG *et al.*, 2011). SYS-1 is counter-polarized relative to POP-1, orienting towards the posterior side, and it stimulates the endodermal program (HUANG *et al.*, 2007; PHILLIPS *et al.*, 2007). It has been proposed that the nuclear levels of POP-1 are regulated through a mutually exclusive binding of the two β -catenins (YANG *et al.*, 2011). The nuclear levels of POP-1 are lower, although not entirely absent, in the future E nucleus, with approximately a two-fold difference between the E and MS nuclei (LIN *et al.*, 1998). This is by design, as POP-1 inhibits the expression of the *end-1* and *end-3* genes at high nuclear levels but stimulates their expression at lower levels (CALVO *et al.*, 2001; MADURO *et al.*, 2005b; SHETTY *et al.*, 2005). Hence, it has been suggested that it is not the absolute levels of POP-1, but rather the ratio between SYS-1 and POP-1, that is crucial for inducing the E and MS lineages (HUANG *et al.*, 2007; ZACHARIAS *et al.*, 2015). To summarize, POP-1 governs the E and MS lineages in a concentration-dependent manner based on signaling input from the P2 cells.

Cytoskeletal organization

The cytoskeleton serves as an internal network of polymeric bundles that provide essential structural support and organization for both the cell and its organelles. It governs the cell's overall shape, as well as smaller membrane features like microvilli. Moreover, the cytoskeleton plays a pivotal role in orchestrating the distribution of molecules and organelles within the cell, acting as pathways along which cargo can travel. Comprising microtubules (MTs), actin, and intermediate filaments (IFs), the cytoskeleton encompasses three major structural components, each of which will be explored in greater detail below (GOODSON & JONASSON, 2018; HERRMANN & AEBI, 2016; POLLARD, 2016).

Microtubules

MTs are approximately 25 nanometer wide hollow polymers composed of tubulin and can typically be found throughout the cytoplasm of cells (GOODSON & JONASSON, 2018). These structures are formed by α - and β -tubulin that combine to create tubulin dimers, known as protofilaments, which are connected side-by-side in a spiral arrangement, ultimately forming the tubular structure (Figure 5 – “Microtubules”) (AKHMANOVA & STEINMETZ, 2015; GOODSON & JONASSON, 2018). Polarized in nature, MTs possess a fast-growing plus end, characterized by exposed β -tubulin, and a slow-growing minus end, featuring exposed α -tubulin (Figure 5 – “Microtubules”) (AHER & AKHMANOVA, 2018). The minus ends typically attach to a MT organizing center (MTOC), providing stability, while the unbound plus ends extend outward. While centrosomes are the most extensively studied MTOCs, visibly active during mitosis as they generate MTs to construct the mitotic spindle, other organelles or intracellular structures can also function as MTOCs, particularly in post-mitotic differentiated cells. For example, in many neurons, the Golgi apparatus serves as the MTOC (SANCHEZ & FELDMAN, 2017). The MT network acts as a cellular highway for the transportation of cargo and organelles. MTs can be decorated with MT binding proteins and undergo post-translational modifications, governing MT stability, enabling other proteins and structures to attach, and facilitating coordinated transport (GOODSON & JONASSON, 2018). Additionally, the growth rate and stability of MTs are influenced by the binding of β -tubulin to either GDP or GTP, corresponding to unstable and stable polymers, respectively. Generally, the majority of MTs are GDP-bound, with their ends featuring a significant presence of GTP-bound protofilaments, commonly referred to as the GTP cap (AHER & AKHMANOVA, 2018).

In the early stages of intestinal development, the centrosomes serve as the MTOCs. This is evident from the radial arrangement of MTs around the centrosome, along with the presence of most components associated with a mature MTOC situated at this central point (FELDMAN & PRIESS, 2012; LEUNG *et al.*, 1999). Shortly after the E8 to E16 divisions, these centrosomal components undergo a relocation towards the future apical membrane, resulting in a noticeable enrichment of MTs at this specific site (FELDMAN & PRIESS, 2012; LEUNG *et al.*, 1999). Subsequently, the MTOC becomes positioned at the apical membrane, with MTs aligning along the apical-basal axis, where the plus ends extend towards the basal side, mirroring the MT organization of most mature epithelia (Figure 5) (QUINTIN *et al.*, 2016; SANCHEZ & FELDMAN, 2017). Depletion of these centrosomal components and minus end binding proteins leads to a disruption of the MT network within the intestine (SALLEE *et al.*, 2018). During the divisions that occur as the endoderm progresses from E16 to E20, the apical MTOC undergoes temporary inactivation in the dividing cells, probably to facilitate the formation of the mitotic spindle (SALLEE *et al.*, 2021).

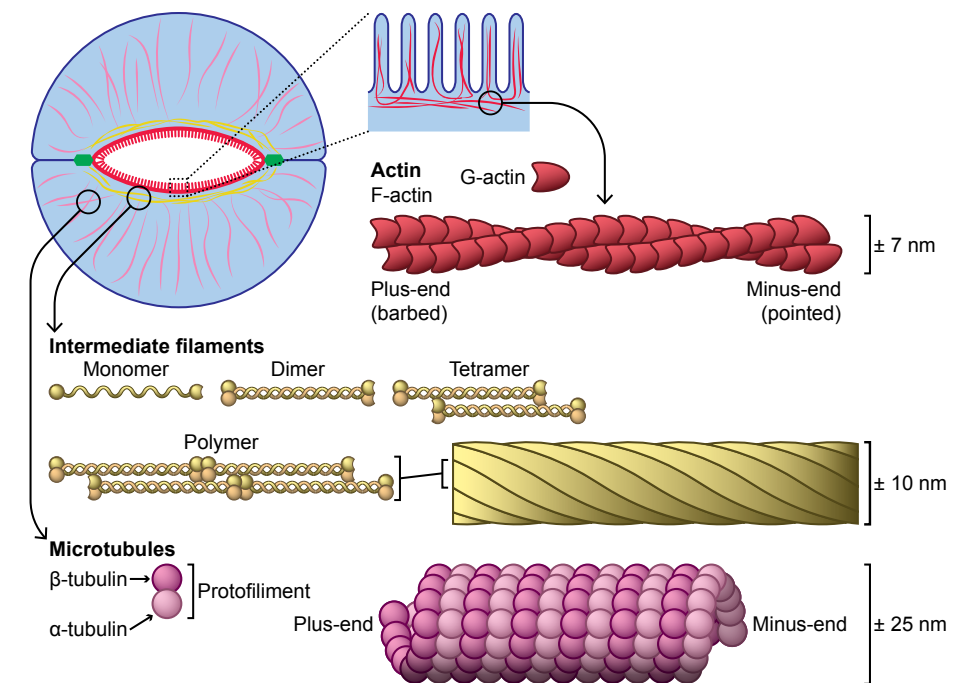


Figure 5: Schematic overview of the different cytoskeletal components and their location in the intestinal cells.

Actin

Actin is widely recognized for its pivotal role in muscle cells where it together with the motor protein myosin forms sarcomeres essential for generating contractile forces. However, actin is essential in other cell types as well, generally influencing cell morphology, contributing membrane features such as microvilli, and contributes to contractile forces essential for cell migration. Typically, actin is concentrated at the cell cortex, providing structural support (DOMINGUEZ & HOLMES, 2011; POLLARD, 2016). Actin exists in two forms: the monomeric G-actin (globular) and the polymeric F-actin (filamentous) (Figure 5 – “Actin”). G-actin is a single protein comprised of four subdomains, featuring an opening on one side where either ADP or ATP can bind, influencing actin polymerization dynamics. The side with the opening is referred to as the barbed side, while the opposite side is the pointed side. F-actin is the result of polymerized G-actin, which has a minus end with pointed side exposed and a plus end with barbed side exposed. The way the G-actin interacts with one another, makes it so that the monomers form a roughly 7 nanometer wide double spiral of interlaced actin monomers (POLLARD, 2016). The assembly of the F-actin network is a tightly regulated process involving various proteins that govern filament nucleation, stabilization, and disassembly (POLLARD, 2016). One mechanism for controlling F-actin formation involves regulating the presence of ATP-bound G-actin, where ATP-bound G-actin is primarily utilized for polymerization,

and subsequently, F-actin gradually converts ATP to ADP. ADP-bound F-actin is less stable, allowing for rapid disassembly and recycling of actin filaments (DOMINGUEZ & HOLMES, 2011). Actin is typically found in mesh networks, bundles, or together with myosin to form contractile bundles (DOMINGUEZ & HOLMES, 2011).

Before the polarization of E cells, actin is predominantly distributed evenly along the cortex. However, there are indications that during cellular rearrangements and intercalations, actin might exhibit some degree of enrichment in specific areas of the cortex (ASAN *et al.*, 2016; LEUNG *et al.*, 1999). Following polarization, actin regulators become concentrated at the midline, with the predominant intestinal actin isoform, ACT-5, following shortly after (Figure 5) (BIDAUD-MEYNARD *et al.*, 2021; LEUNG *et al.*, 1999; MACQUEEN *et al.*, 2005). The apical actin network forms a structure, in conjunction with the IF network, located between the cell-cell junctions just beneath the apical membrane, known as the terminal web or endotube. Disruption of apical actin or its regulators leads to a widening of the lumen and a loss of its oval shape, indicating the crucial role of actin in controlling luminal morphology. Additionally, actin is an integral component of microvilli, and disruptions in the apical actin network can adversely affect or even lead to the absence of the brush border (BERNADSKAYA *et al.*, 2011; CROCE *et al.*, 2004; GÖBEL *et al.*, 2004; MACQUEEN *et al.*, 2005; VAN FÜRDEN *et al.*, 2004). The absence of ERM-1, the sole Ezrin, Radaxin, and Moesin ortholog, which acts as an actin- and membrane-crosslinker and scaffold for other actin regulators, further underscores the importance of actin in lumen formation, as its loss results in a discontinuous intestinal lumen (GÖBEL *et al.*, 2004; VAN FÜRDEN *et al.*, 2004).

Intermediate filaments

IFs encompass a diverse group of stable polymers that function to withstand mechanical stresses exerted on the cell and its organelles. Examples of IFs include keratins that strengthen and protect epithelia, laminins that provide stability to the nucleus, and neurofilaments that regulate the axon diameter (HERRMANN & AEBI, 2016). Despite their diversity, these polymers share a common assembly pattern, resulting in filaments approximately 10 nanometers in width (HERRMANN & AEBI, 2016). IF monomers consist of an elongated structure with three domains: a helical rod domain, and globular head and tail domains. (Figure 5 – “Intermediate filaments”) (ELDIRANY *et al.*, 2021). These monomers have the capacity to form hetero- and homodimers by forming coiled-coils with their rod domains, aligning their head and tail domains in the same direction. These dimers then combine to create tetramers, arranging themselves side by side in an anti-parallel manner. Subsequently, tetramers link together from head to tail, forming strands. Finally, eight of these strands coil together to constitute the complete IF structure (ELDIRANY *et al.*, 2021). Unlike MTs and actin, IFs lack polarity due to the antiparallel orientation of dimers in the tetramers.

As with MTs and actin, the stability and polymerization of IFs are typically tightly regulated processes, involving various IF binding proteins (HERRMANN & AEBI, 2016).

During the division of the E cells, IF components are primarily localized at the centrosomes (LEUNG *et al.*, 1999). However, around the 1.5-fold stage, these components migrate to the apical membrane (BIDAUD-MEYNARD *et al.*, 2021; BOSSINGER *et al.*, 2004). As mentioned earlier, here they collaborate with the actin cytoskeleton to form the endotube structure (Figure 5) (BOSSINGER *et al.*, 2004; CARBERRY *et al.*, 2009; GEISLER *et al.*, 2020). Small disruptions in the apical IF network can lead to local cytoplasmic invaginations, while complete disruption results in the widening of the intestinal lumen (GEISLER *et al.*, 2016; GEISLER *et al.*, 2020; HÜSKEN *et al.*, 2008; REMMELZWAAL *et al.*, 2021). This suggests that the primary function of the IF cytoskeleton is to regulate the size of the intestinal lumen. IFs and actin appear to work synergistically in controlling luminal width, as the loss of the endotube leads to the mislocalization of the apical actin bundler PLST-1 (HÜSKEN *et al.*, 2008). However, it is worth noting that microvilli formation does not appear to be dependent on the IF network, as intestines with a disrupted apical IF network do not exhibit overt brush border defects (GEISLER *et al.*, 2020; REMMELZWAAL *et al.*, 2021).

Cell-cell junction

Cell-cell junctions are protein structures that play a vital role in connecting neighboring cells, enabling intercellular communication, establishing a protective barrier, and fortifying the integrity of the tissue. In *C. elegans* epithelia, these junctions manifest as a distinctive electron-dense structure located just below to the apical membrane, recognized as the *C. elegans* apical junction (CeAJ) (LYNCH & HARDIN, 2009; PÁSTI & LABOUESSE, 2018).

The CeAJ is composed of at least two protein complexes: the Cadherin/Catenin complex (CCC) and DLG-1/AJM-1 complex (DAC) (LYNCH & HARDIN, 2009; PÁSTI & LABOUESSE, 2018). The CCC comprises HMR-1, HMP-1, HMP-2, and JAC-1, which are orthologs of E-cadherin, α -catenin, β -catenin, and p120-catenin, respectively (Figure 6A – “Cadherin/Catenin complex (CCC)”) (COSTA *et al.*, 1998; PETTITT *et al.*, 2003). HMR-1, a transmembrane protein, engages in homophilic interactions with neighboring cell HMR-1 proteins via its extracellular domain, while its intracellular domain binds HMP-2 and JAC-1. HMP-2 links with F-actin through HMP-1, establishing a connection between the CCC and the cytoskeleton (COSTA *et al.*, 1998). JAC-1 plays a regulatory role, modulating the local actin network and aiding in anchoring F-actin to the CCC (KLOMPSTRA *et al.*, 2015; PETTITT *et al.*, 2003). Basal of the CCC, the DAC encompasses the mostly nematode-specific protein AJM-1 and the evolutionarily conserved polarity protein DLG-1 (Figure 6A – “DLG-1/AJM-1 complex (DAC)"). DLG-1 is crucial for the proper localization of

AJM-1, while the loss of AJM-1 has a mild impact on DLG-1 localization (KÖPPEN *et al.*, 2001; McMAHON *et al.*, 2001). The exact mechanism by which AJM-1 and DLG-1 connect to the membrane at the CeAJ remains unknown.

In addition to the CCC and DAC, a potential third complex has been identified: the SAX-7/MAGI-1/AFD-1 complex (SMAC) (Figure 6A – “SAX-7/MAGI-1/AFD-1 complex (SMAC)”) (LYNCH *et al.*, 2012; STETAK & HAJNAL, 2011). SAX-7, an ortholog of L1CAM, is a transmembrane protein capable of homophilic interactions with SAX-7 proteins on adjacent cells, akin to HMR-1. The intracellular portion of SAX-7 binds MAGI-1, which in turn binds AFD-1 (GRANA *et al.*, 2010; LYNCH *et al.*, 2012). It has been postulated that AFD-1 interacts with F-actin (LYNCH *et al.*, 2012). In the epidermis, SAX-7 and MAGI-1 exhibit partial interdependence for their localization, while AFD-1 relies entirely on the other two for CeAJ localization (LYNCH *et al.*, 2012; STETAK & HAJNAL, 2011). The precise positioning of the SMAC relative to the CCC and DAC remains uncertain, as earlier observations suggest that the SMAC may be situated either between or apical to the other complexes in the epidermis (LYNCH *et al.*, 2012; STETAK & HAJNAL, 2011). However, these conclusions were drawn from conventional fluorescent microscopy, and given that the CeAJ measures approximately 200 nm in length, future studies employing super-resolution microscopy techniques may provide clarity on this matter. While research on the SMAC has predominantly centered on the worm’s epidermis, it’s noteworthy that the components of this complex have also been detected in the intestine (CHEN *et al.*, 2001; PICKETT *et al.*, 2022).

The three CeAJ complexes generally operate independently in terms of their localization and assembly, and they do not appear to have direct physical interactions with one another, hence they are considered separate complexes (BERNADSKAYA *et al.*, 2011; BOSSINGER *et al.*, 2001; COSTA *et al.*, 1998; GRANA *et al.*, 2010; KÖPPEN *et al.*, 2001; LYNCH *et al.*, 2012; NATURALE *et al.*, 2022; STETAK & HAJNAL, 2011). However, they do function in a redundant and synergistic manner, enhancing each other’s phenotypes upon depletion (LYNCH & HARDIN, 2009; PÁSTI & LABOUESSE, 2018). For instance, when one complex is disrupted, it leads to early embryonic defects due to a failure in cell adhesion or actin disruption. This phenotype is significantly exacerbated when a second complex is also depleted (KÖPPEN *et al.*, 2001; McMAHON *et al.*, 2001; STETAK & HAJNAL, 2011). Additionally, both the CCC and SMAC redundantly play a crucial role in the ingression of the E cells during gastrulation (GRANA *et al.*, 2010; MINNA ROH-JOHNSON *et al.*, 2012; SAWYER *et al.*, 2010).

During intestine polarization, the components of CCC and SMAC, followed by DAC with a slight delay, initially concentrate at the apical membrane in foci, and later enrich at the midline. Around the time that the Int2 cells undergo intercalation, these junctional components transition from the apical to the subapical domain, where they form the mature CeAJ (ACHILLEOS *et al.*, 2010; LEUNG *et al.*, 1999; NATURALE *et al.*, 2022; TOTONG *et al.*, 2007). In a mature intestine, the junctions display a distinctive ladder-like pattern, characterized by junctions between

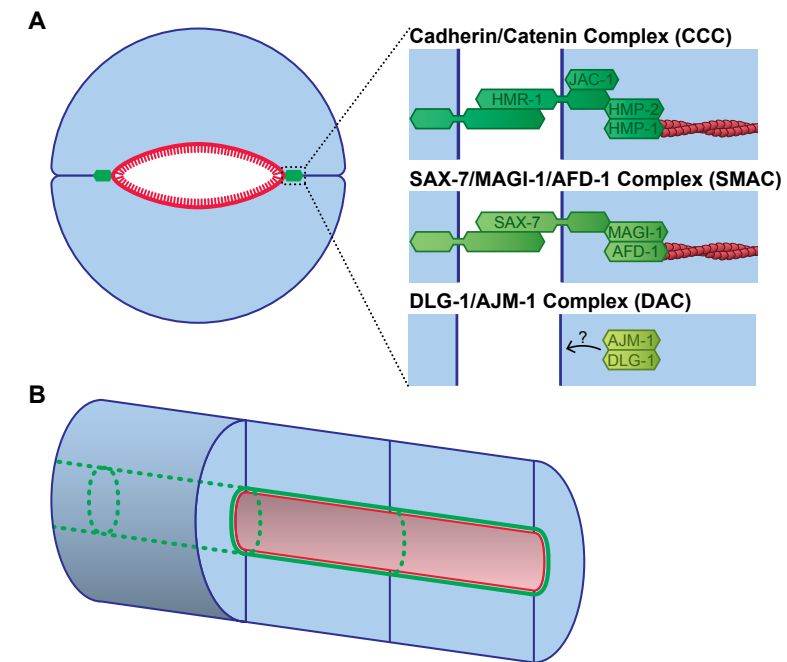


Figure 6: Schematic overview of the CeAJ in the intestine. (A) The different CeAJ components and their location. **(B)** The ladder-like pattern of the CeAJ.

cell pairs in each ring forming two parallel lines from anterior to posterior, with perpendicular junctions connecting the intestinal rings (Figure 6B) (LEUNG *et al.*, 1999). Surprisingly, the depletion of CeAJ components does not seem to lead to significant leakages in the intestine, as there have been no observable instances of obvious ruptures or spillages of intestinal content. Instead, complete disruptions of the CeAJ in the intestine result in tubulogenesis defects, leading to a discontinuous lumen (NATURALE *et al.*, 2022; SEGBERT *et al.*, 2004). The CeAJ are intertwined with the cytoskeletal and epithelial cell polarity networks, as disruptions in these networks lead to CeAJ defects, and *vice versa* (ACHILLEOS *et al.*, 2010; BERNADSKAYA *et al.*, 2011; CARBERRY *et al.*, 2012; NATURALE *et al.*, 2022; SEGBERT *et al.*, 2004; TOTONG *et al.*, 2007). The precise relationship between the CeAJ and the polarity network will be explored in greater detail in the “Epithelial cell polarity establishment” section.

Epithelial cell polarity establishment

In most cells, an inherent asymmetry known as cell polarity is pivotal for the formation of distinct molecularly and functionally specialized intercellular domains. In epithelial cells, two domains emerge: the apical domain, projecting outward from the body or toward the lumen of a tube, and the basolateral domain, which face the neighboring epithelial cells and towards the body. These domains are demarcated by cell-cell junction complexes. The establishment and maintenance of epithelial cell polarity exhibit remarkable diversity, varying

not only between species but also within tissues of the same species (RIGA *et al.*, 2020; RODRIGUEZ-BOULAN & MACARA, 2014). However, it generally relies on the Crumbs complex, PAR complex, the Scribble group and the Par1/MARK protein.

The Crumbs complex encompasses the transmembrane protein Crumbs, which intracellularly binds with PALS/Stardust. PALS, in turn, recruits PATJ and LIN-7 (BULGAKOVA & KNUST, 2009). The PAR complex comprises Par3/Baz, Par6, aPKC, and Cdc42 and resides together with the Crumbs complex apically (GOLDSTEIN & MACARA, 2007). aPKC directly interacts with Par6 and is a central factor in determining the apical domain through protein phosphorylation. Par6 exerts regulatory control over aPKC, both directly by modulating kinase activity and indirectly by interacting with other polarity determinants. Par3, Cdc42, and the Crumbs complex are required for aPKC localization by binding to Par6 (RIGA *et al.*, 2020; RODRIGUEZ-BOULAN & MACARA, 2014). The Scribble group, consisting of Scribble, Lgl, and Dlg, along with Par1 are located in the basolateral domain (STEPHENS *et al.*, 2018; WU & GRIFFIN, 2017). The apical and basolateral components orchestrate polarity through mutual exclusion from their respective domains. For example, Lgl binds to and Par1 phosphorylates Par3, preventing its basolateral recruitment of Par6 and aPKC. Conversely, aPKC phosphorylates Lgl and Par1, impeding their apical localization (RIGA *et al.*, 2020; RODRIGUEZ-BOULAN & MACARA, 2014). As part of the polarity establishment process, certain polarity regulators, such as Scribble and Par3, play a pivotal role in laying the foundation for cell-cell junctions (RODRIGUEZ-BOULAN & MACARA, 2014).

In the E cell lineage, the initial signs of polarization emerge during the E4 stage. Here, the Par3 ortholog, PAR-3, alongside CCC and SMAC components gather in foci distributed randomly across the cortex (Figure 7). Over time, some of these foci vanish while others coalesce and grow larger. By the onset of the E16 stage, only a single bright foci remains at the center of each membrane shared with a neighboring E cell. At this juncture, PAR-6 and PKC-3, corresponding to Par6 and aPKC orthologs, and, with a slight delay, the DAC components, integrate into these foci as well (ACHILLEOS *et al.*, 2010; NATURALE *et al.*, 2022; TOTONG *et al.*, 2007). It has been postulated that these foci exclusively occur between the E cells, as these foci require time to mature. Given that the surrounding cells divide in different orientations and timings, these foci do not have sufficient time to mature between the E cells and their non-E cell neighbors (NATURALE *et al.*, 2022). At the beginning of the E16 stage, all foci migrate toward the midline, and merge to form a common apical domain (LEUNG *et al.*, 1999). Simultaneously, the nucleus and centrosome are drawn towards the apical domain. Subsequently, the centrosome and the associated MTs play a pivotal role in establishing the apical domain as the MTOC (FELDMAN & PRIESS, 2012). Up to now, the junctional components remain apical. However, at the initiation of the bean stage, they shift subapically, culminating in the distinctive ladder-like pattern (PICKETT *et al.*, 2022).

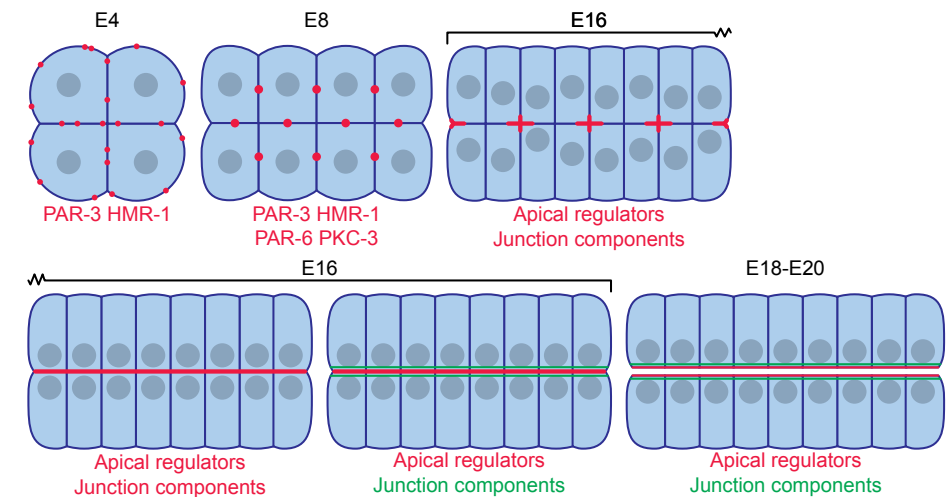


Figure 7: Schematic overview of epithelial cell polarity establishment in the intestinal primordium.

PAR-3 and HMR-1 are considered the initiators of polarity, demonstrating mutual interdependence for sufficient recruitment to the initial foci. While both are instrumental in recruiting PKC-3, they have been postulated to assume slightly distinct roles in polarization. Depletion of PAR-3 leads to the loss of intercellular polarization, impeding the apical migration of the nucleus. Conversely, HMR-1 loss triggers tissue polarization complications, resulting in improper migration and fusion of the foci at the midline (NATURALE *et al.*, 2022). Collectively, the apical PAR proteins and HMR-1 emerge as primary determinants in establishing apical polarity within the intestine. Depletion of any of these proteins culminates deficiencies in recruiting apical components, impairs CeAJ establishment, and disrupts the exclusion of basolateral proteins from the apical membrane. Additionally, the absence of these proteins results in a discontinuous apical surface, giving rise to a disrupted lumen and other tubulogenesis anomalies (ACHILLEOS *et al.*, 2010; FELDMAN & PRIESS, 2012; NATURALE *et al.*, 2022; PICKETT *et al.*, 2022; SALLEE *et al.*, 2018; SALLEE *et al.*, 2021; TOTONG *et al.*, 2007). The depletion of other CeAJ components also sporadically induces defects in lumen formation, and this phenotype can be enhanced by concurrent depletion of multiple components. Therefore, the remaining CeAJ components also contribute to the polarization process (NATURALE *et al.*, 2022; PICKETT *et al.*, 2022; SEGBERT *et al.*, 2004).

Prior to the establishment of apical polarity regulators at the midline, basolateral regulators are uniformly distributed across the cortex of the intestinal cells. However, as junctional components transition subapically in the early bean stage, the Lgl, Scribble, and Par1 orthologs, respectively LGL-1, LET-413 and PAR-1, begin to undergo exclusion from the apical domain. Subsequently, LGL-1 and LET-413 find their residence in the basolateral region,

while PAR-1 becomes enriched near the junctions, adopting a ladder-like pattern (PICKETT *et al.*, 2022). In contrast to the apical regulators, the loss of basolateral regulators yields more nuanced polarity disruptions, as they do not affect the overall morphology of the intestine or physiology of the worm. Depletion of PAR-1 prompts the emergence of ectopic patches featuring apical cytoskeletal regulators in the basolateral domain (WINTER *et al.*, 2012). The absence of LET-413 leads to the disruption of CeAJ, resulting in a reduction of DLG-1, which manifests as a dotted appearance (SEGBERT *et al.*, 2004). Moreover, LET-413 assumes a critical role in the exclusion of apical components, as its depletion triggers the expansion of microvillar and endotube proteins into the basolateral domain (BOSSINGER *et al.*, 2004). Finally, LET-413 is involved in polarized trafficking as a RAB-5 effector, facilitating the activation of RAB-10 (LIU *et al.*, 2018).

In most epithelia, the Crumbs complex assumes a pivotal role in orchestrating epithelial cell polarity (RIGA *et al.*, 2020; RODRIGUEZ-BOULAN & MACARA, 2014). Interestingly, none of Crumbs complex components are essential for intestinal polarization or the overall viability of the worm (CASTIGLIONI *et al.*, 2022; FENG *et al.*, 2005; WAAIJERS *et al.*, 2015). They probably do play a minor role during polarization as the components do enrich at the apical membrane (BOSSINGER *et al.*, 2001; CASTIGLIONI *et al.*, 2022; WAAIJERS *et al.*, 2015). In addition, one of the three Crumbs orthologs, CRB-1, has a subtle role in junction formation. As previously mentioned, proper localization of DLG-1 is depended on LET-413. Interestingly, DLG-1 localization remains unaffected upon combined knockdown of *let-143* and *hmp-1*. However, a triple knockdown involving *let-143*, *hmp-1*, and *crb-1* induces a phenotype akin to that observed with *let-143* knockdown alone (SEGBERT *et al.*, 2004).

Besides the typical polarity proteins, intercellular trafficking and specialized lipids are also imported for polarization of the intestinal cells. Although this is not unique to the *C. elegans* intestine, it is striking that knocking down genes involved in these processes can revert polarity in a mature intestine (ZHANG *et al.*, 2011; ZHANG *et al.*, 2012). The mature intestine is considered to be a robust tissue, as depletion of canonical polarity regulators does not appear to disrupt polarity. For instance, while PAR-3, PAR-6, and PKC-3 are pivotal for establishing polarity, their depletion during larval development does not seem to perturb the intestine (CASTIGLIONI *et al.*, 2020). Disruption of the clathrin complex, responsible for intracellular trafficking, or glycosphingolipid biosynthesis leads to the formation of ectopic lumens at the lateral sides in both embryonic and larval intestines. These ectopic lumens exhibit apical markers and luminal membrane features, including endotube proteins and microvilli, while excluding basolateral components. Moreover, components of the clathrin complex or glycosphingolipid biosynthesis pathway display a genetic interaction, exacerbating intestinal polarity defects in a synergistic

manner (ZHANG *et al.*, 2011; ZHANG *et al.*, 2012). Based on this data, it is proposed that the polarized trafficking of specific membrane components constitutes a pivotal step in polarity establishment and maintenance, operating upstream of the canonical polarity proteins like the PAR complex (ZHANG *et al.*, 2013).

Host-microbe interactions

In the laboratory setting, we grow *C. elegans* on a single mutant *Escherichia coli* strain called OP50, which serve as food for the animals. However, in their natural habitat, *C. elegans* encounters a wide array of microorganisms. These microbes enter the worm's digestive tract, influencing its physiology in both positive and negative manners (JIANG & WANG, 2018; KUMAR *et al.*, 2020).

Just like humans, *C. elegans* suffer from pathogenic microbes that can induce illness or even mortality (JIANG & WANG, 2018; KUMAR *et al.*, 2020). So far, we know that bacteria, fungi, and viruses can infect the worms, although most identified pathogenic fungi primarily exert their effects through the epidermis. In the case of the intestine, the majority of bacteria and fungi tend to impact *C. elegans* by either colonizing the intestinal tract, secreting toxins, or employing a combination of both strategies (JIANG & WANG, 2018; KUMAR *et al.*, 2020). For instance, *Serratia marcescens*, an opportunistic human pathogen, colonizes the intestine of *C. elegans*, leading to distension of the intestinal lumen through the production of lipopolysaccharides and hemolysin toxins (KURZ *et al.*, 2003; PRADEL *et al.*, 2007). In some instances, these bacteria or fungi may even infiltrate the intestinal cells. The fungus *Nematocida parisii*, for example, invades and takes up residence within intestinal cells, where it undergoes proliferation before eventually escaping, resulting in the formation of holes in the endotube (TROEMEL *et al.*, 2008). The response to these infections operates through various pathways, many of which appear to be conserved in humans. The immune response is triggered via signaling pathways, with the MAPK pathway being of particular significance. Downstream, intestinal cells react by among other generating antimicrobial peptides, producing reactive oxygen species, and initiating autophagy (JIANG & WANG, 2018; KUMAR *et al.*, 2020).

Viral research in *C. elegans* initially relied on artificial setups, utilizing techniques such as *C. elegans* cell culture, synthetic viruses, and replicons, since no natural *C. elegans* viruses were known at that time. In these systems, the predominant immune response observed was the anti-viral RNAi response (JIANG & WANG, 2018). This provided a means to explore the initiation and workings of the RNAi system in a more natural context, rather than solely for the purpose of mRNA knockdown. Subsequent advancements in sequencing technologies led to the identification of actual viruses that infect *C. elegans*, with the Orsay virus emerging as the most extensively studied among them. The Orsay virus primarily impacts the intestine, leading to notable alterations in intestinal morphology, including the loss of gut granules and fusion of

intestinal cells (FÉLIX *et al.*, 2011). In addition to the anti-viral RNAi response, *C. elegans* respond to these viral infections through mechanisms involving cell death and ubiquitin-proteasome systems (CHEN *et al.*, 2017; JIANG *et al.*, 2017; TANGUY *et al.*, 2017).

C. elegans not only consume bacteria as a food source but also harbor them within their intestine, forming a microbiome. The composition of these intestinal microbes varies considerably based on the source and geographical origin of the worm. Nonetheless, studies suggest that the *Enterobacteriaceae*, *Pseudomonadaceae*, and *Xanthomonadaceae* families constitute the core microbiota (BERG *et al.*, 2016a; BERG *et al.*, 2016b; DIRKSEN *et al.*, 2016; MONTALVO-KATZ *et al.*, 2013; SAMUEL *et al.*, 2016). In humans, the microbiome exerts a profound influence on physiology, aiding in digestion, stimulating the immune system, and even modulating brain activity. It acts as a barrier against pathogenic bacteria, preventing their colonization. Additionally, it plays a role in safeguarding against neurodegenerative conditions like Alzheimer's and Parkinson's disease (CANI, 2018; SHREINER *et al.*, 2015). Similarly, a diverse microbiome confers benefits to *C. elegans*, rendering them less susceptible to infections, prolonging their lifespan, and inducing neuronal changes based on the encountered bacteria (KUMAR *et al.*, 2020). For instance, a genetic screen involving mutagenized *E. coli* provided to *C. elegans* revealed that bacteria producing an excess of colanic acid polysaccharide extended the worm's lifespan. This extension was attributed to improved mitochondrial function and activation of unfolded protein responses (HAN *et al.*, 2017). Furthermore, exposure to bacteria producing a specific type of amyloid protein in both *C. elegans* and rats led to enhanced amyloid protein aggregation, a phenomenon associated with numerous neuronal degenerative diseases in humans (CHEN *et al.*, 2016). The microbiome is not indispensable for *C. elegans*, as evidenced by the absence of defects in bleach-sterilized animals apart from starvation. Nevertheless, the data described above underscores the significance of the *C. elegans* microbiome in worm physiology, which mirrors its relevance in humans.

Future directions

In this chapter, I have delved into the intricacies of *C. elegans* intestine development, revealing its surprising complexity despite being considered a relatively simple organ. The developmental process entails the collaborative efforts of various intercellular networks and external cues, demonstrating the interdependence of these elements. The insights gained from this research hold relevance beyond this model organism, shedding light on fundamental aspects of organogenesis across the animal kingdom. Nevertheless, how the different intracellular networks act together towards a mature and functional intestine continues to be a subject of ongoing investigation. For instance, we understand the significance of transcription regulators like END-1, ELT-2, and ELT-7 in

determining endodermal fate. However, the precise transcriptional changes they induce to guide the cell towards becoming a functional intestine remain an area of active inquiry. Another example is cell polarization, as we understand the importance of classical polarity proteins and CeA components during polarization. In addition, we observe various defects upon their depletion, such as lumen defects and alterations in intracellular trafficking. However, the precise mechanisms linking cell polarization and to the observed defects remain elusive. Unraveling these intricacies holds the promise of unveiling deeper layers of understanding of organogenesis.

Beyond its significance as a model for organogenesis, the *C. elegans* intestine provides a relevant framework for understanding the physiology of the human intestines. For instance, the *C. elegans* intestine is important for the immune response in the nematode and serves as a first line of defense against infectious diseases, mirroring the role of the human digestive system. *C. elegans* could serve as a simple and efficient model to study viral infections, especially given the recent discovery of innate *C. elegans* viruses and the escalating awareness of viral threats in our society. Additionally, akin to the human intestine, *C. elegans* hosts a microbiome that exerts positive effects on its physiology, sharing substantial parallels with the human microbiome.

Lastly, while not extensively covered in this chapter, the intricate interplay between the intestine and the germline presents a compelling avenue for exploration. The sustained close contact between the endoderm and germline precursor cells throughout development, coupled with the production of yolk proteins by the intestine for oocytes in adult animals, underscores a distinct connection between the two. Various studies have highlighted how dietary and environmental conditions can induce epigenetic changes in offspring through the intestine (NONO *et al.*, 2020; REHAVI & LEV, 2017; REHAVI *et al.*, 2014; TAUFFENBERGER & PARKER, 2014; YU *et al.*, 2021). This process necessitates the transmission of crucial information from the intestine to the germline, offering potential insights into mechanisms that mediate human epigenetic inheritance influenced by diet. Understanding this intricate communication may shed light on broader implications for human biology and health.

Scope of the thesis

This thesis is focused on the molecular mechanisms that underlie lumen formation in the *C. elegans* intestine. Disruption of the endotube, apical polarity network and CeAJ all result in defects in lumen maturation. These defects encompass alterations in the formation of the brush border, changes in the size and shape of the intestinal lumen, and luminal constrictions that impede the passage of food. In the ensuing chapters, I will delve into my research on how these diverse components collectively contribute to the process of lumen formation. A major focus of this investigation revolves around the role of the actin cytoskeleton and some of its associated regulators in orchestrating this intricate process.

In **chapters 2 and 3**, we delved into the roles of the ERM-1 and NRFL-1 proteins, which are the sole orthologs of the Ezrin/Radixin/Moesin (ERM) and Na⁺/H⁺ exchanger regulatory factor (NHERF) protein families, respectively. These proteins are conserved regulators of cortical specialization, functioning as membrane-actin linkers and organizers of molecular hubs. ERM proteins undergo a conformational switch from an inactive cytoplasmic form to an active membrane- and actin-bound form, believed to be mediated by the phosphorylation of a conserved C-terminal threonine residue. In the active conformation, ERM proteins can bind NHERF proteins, which act as scaffolding proteins by exposing multiple PDZ domains. However, *in vivo* data supporting this model is limited, and results regarding the necessity of ERM phosphorylation and NHERF binding are conflicting. Previous studies demonstrated the essential role of ERM-1 in lumen formation in *C. elegans*, as its depletion resulted in a widened lumen and intestinal constrictions (GÖBEL *et al.*, 2004; VAN FÜRDEN *et al.*, 2004). In chapter 2, we show that membrane binding through a conserved PIP₂ binding domain is crucial for ERM-1 function. Additionally, while the conserved C-terminal T544 phosphosite is not essential, it does modulate the stability and apical recruitment of ERM-1. In chapter 3, we reveal that NRFL-1 is dependent on ERM-1 for its microvillar localization in the intestine through its conserved ERM binding domain. Previous studies showed that NRFL-1 is not essential for the worm, as its depletion did not yield any discernible phenotypes (HAGIWARA *et al.*, 2012). However, combined *erm-1* phospho- and *nrfl-1* mutants replicate the *erm-1* null phenotype, underscoring that ERM-1 activity operates through the phosphorylation of its C-terminal T544 residue and the recruitment of NRFL-1.

In a small genetic screen conducted in **Chapter 4**, we identified a kinase named GCK-4, ortholog of the mammalian SLK and LOK, as a lumen formation regulator. Depletion of GCK-4 leads to a widened lumen accompanied by multiple constrictions in the intestine, coupled with alterations in the actin network and adherens junctions. Moreover, our investigation reveals that GCK-4 is localized at the tips of the microvilli in the intestinal brush border. While the orthologs of

GCK-4 participate in a wide array of signaling pathways and cellular processes, they are predominantly recognized for their role as kinases targeting the ERM C-terminal threonine residues (BELKINA *et al.*, 2009; HIPFNER *et al.*, 2004; VISWANATHA *et al.*, 2012). This suggests that GCK-4 may function as the kinase for ERM-1 T544. However, we were unable to detect a change in T544 phosphorylation upon GCK-4 depletion, nor did we detect an interaction between the two proteins. Therefore, ERM-1 and GCK-4 seem to contribute independent of one another to intestinal lumen formation. Finally, we employed two distinct proteomic approaches to identify interactors and kinase substrates of GCK-4.

In **Chapter 5**, we improved the auxin-inducible degradation (AID) system, a commonly used protein degradation system within and beyond the *C. elegans* field. The AID system typically enables efficient degradation of most proteins, rendering it a valuable tool for precisely depleting a target protein with both spatial and temporal control. However, in the case of highly expressed and stable proteins, degradation proves to be inefficient, leading to incomplete degradation or slow degradation dynamics. One such example is ERM-1, which demonstrates minimal degradation over the course of several days upon auxin-mediated degradation. To improve the AID system, we opted to replace the original degron, fused to the target protein, with the mIAA7 degron. This modification resulted in faster degradation for various proteins across different tissues and yielded stronger knockdown phenotypes. Given that the degradation of ERM-1 with a single mIAA7 degron remained insufficient, we also explored and validated that the incorporation of multiple degrons enhances the degradation of ERM-1 even further. In summary, we provided an improvement to the AID system as well as molecular tools for genomic integration of the mIAA7 degron, offering a valuable resource for the *C. elegans* community.



Chapter 2

C-terminal phosphorylation modulates
ERM-1 localization and dynamics to
control cortical actin organization
and support lumen formation during
Caenorhabditis elegans development

João J. Ramalho¹, Jorian J. Sepers¹, Ophélie Nicolle²,
Ruben Schmidt¹, Janine Cravo¹, Grégoire Michaux² &
Mike Boxem¹

1. Division of Developmental Biology, Institute of Biodynamics and Biocomplexity, Department of Biology, Faculty of Science, Utrecht University, Utrecht, The Netherlands
2. Univ Rennes, CNRS, IGDR-UMR 6290, Rennes, France

This chapter is an adapted version of the following publication:

Ramalho, J.J., Sepers, J.J., Nicolle, O., Schmidt, R., Cravo, J., Michaux, G. and Boxem, M., 2020. C-terminal phosphorylation modulates ERM-1 localization and dynamics to control cortical actin organization and support lumen formation during *Caenorhabditis elegans* development. *Development*, 147(14), dev188011.

ERM proteins are conserved regulators of cortical membrane specialization that function as membrane-actin linkers and molecular hubs. The activity of ERM proteins requires a conformational switch from an inactive cytoplasmic form into an active membrane- and actin-bound form, which is thought to be mediated by sequential PIP₂ binding and phosphorylation of a conserved C-terminal threonine residue. Here, we use the single *Caenorhabditis elegans* ERM ortholog, ERM-1, to study the contribution of these regulatory events to ERM activity and tissue formation *in vivo*. Using CRISPR/Cas9-generated *erm-1* mutant alleles, we demonstrate that a PIP₂-binding site is crucially required for ERM-1 function. By contrast, dynamic regulation of C-terminal T544 phosphorylation is not essential but modulates ERM-1 apical localization and dynamics in a tissue-specific manner, to control cortical actin organization and support lumen formation in epithelial tubes. Our work highlights the dynamic nature of ERM protein regulation during tissue morphogenesis and the importance of C-terminal phosphorylation in fine-tuning ERM activity in a tissue-specific context.

Introduction

Morphological and molecular specialization of defined regions at the cell cortex is crucial for the development and function of most animal cell types. The formation of specialized cortical domains relies on local reorganization of membrane composition and the cortical cytoskeleton. Ezrin/Radixin/Moesin (ERM) proteins form an evolutionarily conserved family that plays a major role in organizing the cell cortex and signaling (FEHON *et al.*, 2010; McCLATCHEY, 2014; NEISCH & FEHON, 2011). For example, ERM family members promote the formation of microvilli at the apical surface of epithelial tissues, are required for lumen formation in tubular epithelia, and control the mechanical properties of the cell cortex in processes such as mitosis, cell migration, and immunological synapse formation in B and T cells (KUNDA *et al.*, 2008; McCLATCHEY, 2014; PARAMESWARAN & GUPTA, 2013; PELASEYED & BRETSCHER, 2018). To perform this wide range of functions, ERM proteins can link the plasma membrane physically with the actin cytoskeleton and orchestrate the assembly of a broad array of multiprotein complexes at the cell surface.

ERM proteins consist of an N-terminal band Four-point-one/Ezrin/Radixin/Moesin (FERM) domain that mediates binding to transmembrane and membrane-associated proteins, a C-terminal tail that mediates actin binding, and a central α -helical linker region (FEHON *et al.*, 2010; McCLATCHEY, 2014). The activity of ERM proteins is regulated by a reversible intramolecular interaction. In the inactive closed conformation, extensive interactions between the FERM domain and the C-terminal tail mask the actin-binding site, membrane-binding sites and protein interaction sites (GARY & BRETSCHER, 1995; LI *et al.*, 2007; MAGENDANTZ

et al., 1995; PEARSON *et al.*, 2000). The transition to an open and active conformation involves binding to the plasma membrane lipid phosphatidylinositol 4,5-bisphosphate (PIP₂) and phosphorylation of a specific C-terminal threonine residue (T567 in ezrin, T564 in radixin and T558 in moesin) (BARRET *et al.*, 2000; COSCOY *et al.*, 2002; FIEVET *et al.*, 2004; HAO *et al.*, 2009; NAKAMURA *et al.*, 1999; ROCH *et al.*, 2010; SIMONS *et al.*, 1998; YONEMURA *et al.*, 1998). This transition is thought to occur in a multistep process, in which binding to PIP₂ induces a partial conformational change that enables binding of a kinase and phosphorylation of the C-terminal threonine (BOSK *et al.*, 2011; FIEVET *et al.*, 2004; HAO *et al.*, 2009; PELASEYED *et al.*, 2017).

C-terminal phosphorylation is often considered to be essential for the activity of ERM proteins (GAUTREAU *et al.*, 2000; KUNDA *et al.*, 2008; MATSUI *et al.*, 1998; NAKAMURA *et al.*, 1995; OSHIRO *et al.*, 1998; PARAMESWARAN & GUPTA, 2013; SIMONS *et al.*, 1998; VISWANATHA *et al.*, 2012). However, several studies indicate that phosphorylation might not be a universal requirement. For example, the phosphorylation of ERM proteins appears dispensable for the formation of microvilli-like structures in A431 and MDCK II cells (YONEMURA *et al.*, 2002). Likewise, although some studies have reported that phosphorylation is essential for the activity of *Drosophila* Moesin (KARAGIOSIS & READY, 2004; POLESSELLO *et al.*, 2002), significant rescuing capacity for a non-phosphorylatable variant has been reported (ROCH *et al.*, 2010). Thus, ERM proteins might be activated without phosphorylation, at least in some cell types or biological conditions.

Here, we make use of the nematode *Caenorhabditis elegans* to gain a better understanding of the contributions of PIP₂-binding and C-terminal threonine phosphorylation to the functioning of ERM proteins *in vivo*. *Caenorhabditis elegans* expresses a single ERM protein, termed ERM-1, and the corresponding gene can be engineered endogenously to express mutant variants. Thus, the role of ERM-1 can be studied without the confounding presence of additional family members or non-mutated protein. ERM-1 is highly similar in sequence and domain composition to other ERM proteins, and the residues crucial for PIP₂ binding and the C-terminal threonine residue are fully conserved (Figure 1A). ERM-1 localizes to the apical surface of most polarized tissue types and is essential for apical membrane morphogenesis (GÖBEL *et al.*, 2004; VAN FÜRDEN *et al.*, 2004). Loss of *erm-1* causes early larval lethality, with severe cystic defects in the intestine and excretory canals (GÖBEL *et al.*, 2004). In the intestine, loss of *erm-1* causes constrictions, loss of microvilli, severe reduction in the levels of apical actin, and defects in the accumulation of junctional proteins (BERNADSKAYA *et al.*, 2011; GÖBEL *et al.*, 2004; VAN FÜRDEN *et al.*, 2004). In the excretory canals, ERM-1 controls the extension of the canal lumen in a dose-dependent manner (GÖBEL *et al.*, 2004; KHAN *et al.*, 2013).

We used CRISPR/Cas9 to engineer the *erm-1* locus endogenously to express ERM-1 variants with a mutated PIP₂-binding site, or with a mutated threonine residue that cannot be phosphorylated or that mimics phosphorylation. As in

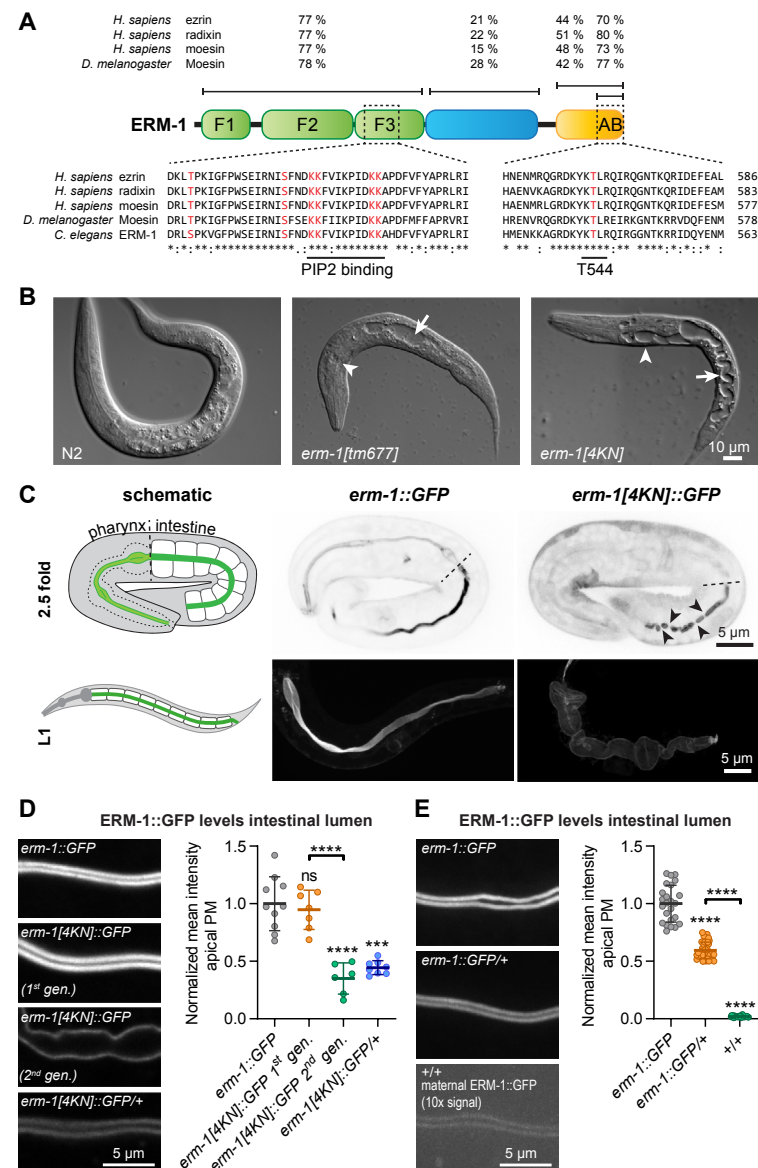


Figure 1. ERM-1 activity and efficient membrane targeting require the PIP₂ binding domain. (A) Conservation and domain organization of ERM-1. AB is the actin-binding domain. (B) Differential interference contrast microscopy images of an N2 animal and *erm-1* mutants. Arrowheads point to the excretory canal and arrows to the intestinal lumen. (C) Intestinal lumen discontinuities (arrowheads) and widened intestinal lumen in *erm-1[4KN]::GFP* second generation homozygous 2.5-fold embryos and L1 larvae. ERM-1 localization in the schematic diagram is in green. Dashed line indicates the boundary between the pharynx and intestine. (D, E) Apical levels of GFP-tagged ERM-1 variants in the intestine of L1 larvae with indicated genotypes. Images were acquired and displayed with the same settings, except *+/+* in E. In this and all other figures, imaging was done with

~ Figure description continues on the next page ~

spinning disk confocal microscopy unless otherwise indicated. PM, plasma membrane. Data shown are means \pm s.d. of six measurements per animal for the apical membrane, normalized to the mean intensity of GFP in *erm-1::GFP* controls ($n = 10, 7, 6$ and 8 in D; and $n = 24, 40$ and 28 in E). Error bars are mean \pm s.d. Tests of significance: Dunnett's T3 multiple comparisons test. ns, not significant. *** $P \leq 0.001$, **** $P \leq 0.0001$. Unless indicated otherwise, statistical comparisons are with *erm-1::GFP*.

other systems, the PIP₂-binding site was essential for the functioning of ERM-1. By contrast, animals expressing only non-phosphorylatable or phosphomimetic ERM-1 protein were viable, demonstrating that C-terminal threonine phosphorylation is not a strict requirement for ERM-1 activity in *C. elegans*. Nevertheless, phosphorylation contributed to multiple aspects of ERM-1 function, including localization, mobility, and the ability to organize an apical actin network. Effects caused by the phosphorylation mutants were often tissue specific, highlighting versatility for C-terminal phosphorylation in controlling ERM-1. Finally, in support of an essential role for phosphorylation cycling, most of the defects we observed were highly similar between non-phosphorylatable and phosphomimetic variants.

Results

A lipid binding site is essential for the activity of ERM-1

Binding to PIP₂ has been shown to be essential for the membrane localization and activity of ERM proteins, but has not been investigated in *C. elegans* (BARRET *et al.*, 2000; COSCOY *et al.*, 2002; FIEVET *et al.*, 2004; HAO *et al.*, 2009; NAKAMURA *et al.*, 1999; ROCH *et al.*, 2010; YONEMURA *et al.*, 2002). We used CRISPR/Cas9 to mutate two pairs of lysine residues within a plasma-binding region to asparagines (K254/255N and K263/264N, hereafter referred to as 4KN) (Figure 1A). This change has been shown virtually to abolish membrane localization of mammalian ezrin and fly Moesin (BARRET *et al.*, 2000; BEN-AISSA *et al.*, 2012; FIEVET *et al.*, 2004; ROCH *et al.*, 2010). The first homozygous generation of *erm-1(mib11[4KN])* is viable, whereas > 95 % of their offspring arrest during larval development, mostly as L1, with cysts in the lumens of the intestine and excretory canals (Figure 1B, C). Both the maternal effect lethality and the cystic luminal phenotypes have been described for the putative *erm-1(tm667)* null allele (GÖBEL *et al.*, 2004). In addition, first generation homozygous *erm-1(mib11[4KN])* animals die prematurely in adulthood and have a greatly reduced brood size, as has been observed for *erm-1(tm667)*. Thus, *erm-1(mib11[4KN])* behaves in a similar manner to a putative null allele.

To examine whether the ERM-1[4KN] mutation prevents membrane association, we generated endogenous COOH-terminal fusions of eGFP (referred to as GFP) with wild-type ERM-1 and ERM-1[4KN]. In early embryogenesis, ERM-1::GFP localized to the entire plasma membrane in addition to the cytoplasm (Supplementary figure 1A). As morphogenesis initiated, ERM-1::GFP was primarily detected at the apical surface of epithelial tissues and in primordial

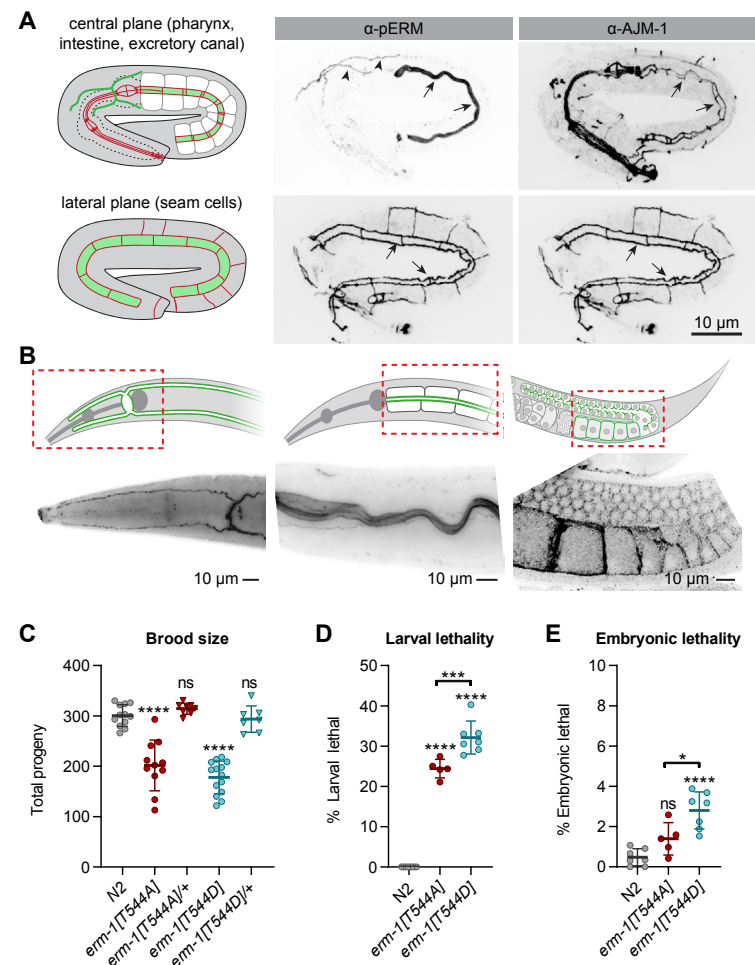


Figure 2: T544 phosphorylation is not essential for ERM-1 activity. (A) Immunostaining of phosphorylated ERM-1 (pERM) and the junctional marker AJM-1 in N2 embryos. Arrows point to the intestinal lumen or seam cells and arrowheads to excretory canals. Images are maximum intensity projections. (B) Immunostaining of pERM in adults. In the graphical representations in A and B, red indicates junctional structures and green areas of ERM-1 localization. Dashed rectangles indicate areas imaged in B. The first two panels in B were imaged on an epifluorescence microscope. (C-E) Quantifications of brood size, larval lethality and embryonic lethality. Each symbol represents the progeny of an individual animal (n = 12, 11, 8, 14 and 7 in C; n = 8, 5 and 7 in D; and n = 7, 5 and 7 in E). Error bars are the mean \pm s.d. Tests of significance: Dunnet's multiple comparisons test for C; Tukey's multiple comparisons test for D and E. ns, not significant. * $P \leq 0.05$, *** $P \leq 0.001$, **** $P \leq 0.0001$. Unless indicated otherwise, comparisons are with N2.

germ cells (PGCs) (Supplementary figure 1A). In larval stages, we observed apical localization of ERM-1::GFP in epithelial tissues including the intestine, seam cells and excretory canals (Figure 1D; Supplementary figure 1B). In the syncytial germline, ERM-1 was associated with the entire plasma membrane but enriched at the apical domain (Supplementary figure 1B).

Addition of N- or C-terminal tags to ERM proteins has been suggested to interfere with the intramolecular interaction between the FERM domain and C-terminus (CHAMBERS & BRETSCHER, 2005; VISWANATHA *et al.*, 2012). Consistent with this, *erm-1::GFP* animals had a reduced brood size and incomplete outgrowth of the excretory canals, but showed no other developmental or morphological abnormalities (Supplementary figure 1C-E). These defects are not likely to be attributable to constitutive ERM-1 activity, because excretory canal defects were absent in *erm-1::GFP/+* heterozygotes (Supplementary figure 1D, E). C-terminal GFP fusions have been used extensively to characterize the distribution of ERM proteins (BABICH & SOLE, 2015; COSCOY *et al.*, 2002; GARBETT & BRETSCHER, 2012; GÖBEL *et al.*, 2004; KHAN *et al.*, 2013; ROCH *et al.*, 2010; VISWANATHA *et al.*, 2012), and the localization of our endogenous ERM-1::GFP fusion mimicked previous reports of ERM-1 localization in *C. elegans* (BERNADSKAYA *et al.*, 2011; GÖBEL *et al.*, 2004; KHAN *et al.*, 2013; VAN FÜRDEN *et al.*, 2004). ERM-1::GFP therefore appears to reflect the localization of the endogenous protein accurately.

ERM-1[4KN]::GFP failed to localize to the plasma membrane in PGCs and seam cells of second generation homozygous *erm-1[4KN]::GFP* L1 larvae (Supplementary figure 1B), and levels in the intestine were severely reduced (Figure 1D, E). Surprisingly, ERM-1[4KN]::GFP appeared still to be restricted to the apical domain of the excretory canal (Supplementary figure 1B).

We also analyzed the distribution of ERM-1[4KN]::GFP in heterozygous *erm-1[4KN]::GFP/+* animals. Although ERM-1[4KN]::GFP still failed to localize to the membrane in PGCs and seam cells, in the intestine, excretory canal and larval germline we observed clear apical localization of ERM-1[4KN]::GFP at the apical membrane domain (Figure 1D; Supplementary figure 1B). Interestingly, in first generation homozygous animals, apical levels of ERM-1[4KN]::GFP were comparable to wild-type ERM-1::GFP (Figure 1D, E). First generation homozygous animals had low levels of maternally contributed wild-type ERM-1 (Figure 1E). Thus, it appears that wild-type ERM-1 can support apical recruitment of ERM-1[4KN], albeit not in all tissues. These results contrast with observations in *Drosophila* and mammalian tissue culture cells, where C-terminally tagged ERM 4KN mutants do not localize to the plasma membrane, even in the presence of wild-type ezrin (BABICH & SOLE, 2015; BARRET *et al.*, 2000; FIEVET *et al.*, 2004; HAO *et al.*, 2009; ROCH *et al.*, 2010).

Based on these observations, we conclude that the N-terminal PIP₂-binding domain is crucial for activity of *C. elegans* ERM-1, as it is for ERM proteins in other organisms. However, the presence of wild-type ERM-1 protein can compensate for the loss of membrane-binding activity of the ERM-1[4KN] mutant in at least some tissues.

Phosphorylation of T544 is not essential for ERM-1 functioning

We next investigated the contribution of phosphorylation of the conserved C-terminal threonine residue to ERM-1 functioning. We used CRISPR/Cas9 to generate *erm-1* mutants in which T544 was replaced with an alanine (T544A) or aspartic acid (T544D), to mimic the non-phosphorylated and phosphorylated states, respectively (Figure 1A). Using an antibody that specifically recognizes C-terminally phosphorylated ERM proteins (pERM), we observed extensive pERM staining at apical membranes of the intestine, seam cells and excretory canals of N2 embryos and larvae, in addition to the larval germline (Figure 2A, B). No staining was observed in *erm-1[T544A]* mutants, indicating that the pERM antibody was specific for the phosphorylated form of ERM-1 (Supplementary figure 2). Thus, ERM-1 is broadly phosphorylated on the conserved C-terminal threonine residue.

Surprisingly, both homozygous *erm-1[T544A]* and *erm-1[T544D]* mutants were viable, demonstrating that T544 phosphorylation is not essential for ERM-1 activity in *C. elegans*. Nevertheless, both mutants had a reduced brood size and increased embryonic and larval lethality compared with wild-type animals (Figure 2C-E). These defects were not observed in heterozygous *erm-1[T544A]/+* and *erm-1[T544D]/+* animals, indicating that neither mutation exerts a dominant effect. Finally, consistent with the broad expression pattern of ERM-1, we observed a variety of partially penetrant phenotypes, including small, dumpy, tail defects, protruding vulva, exploded through vulva, uncoordinated and clear. Together, these results demonstrate that the C-terminal phosphorylation site is important, but not essential, for ERM-1 function in *C. elegans*.

T544 phosphorylation contributes to lumen formation in tubular epithelia

To gain a better understanding of the defects caused by mutation of T544, we investigated the effects on the intestine and excretory canal. We examined the appearance and extension of the canal tubes using a COOH-terminal VHA-5::GFP fusion protein, which localizes to the apical membrane and canaliculi (LIÉGEOIS *et al.*, 2006; LIÉGEOIS *et al.*, 2007). In both *erm-1[T544A]* and *erm-1[T544D]* animals, we observed severe canal extension defects, in addition to cystic canals and widened canal lumens (Figure 3). In accordance with a non-dominant effect of both mutations, canal defects were absent from heterozygous *erm-1[T544A]/+* and *erm-1[T544D]/+* animals (Figure 3B, E). We also examined canal morphology by transmission electron microscopy (TEM) and observed widened lumens and canals in *erm-1[T544A]* and *erm-1[T544D]* animals (Figure 3D). Overexpression of ERM-1 leads to lumen formation defects in the excretory canal, which can be rescued by depletion of the ERM-1 binding partner aquaporin/AQP-8 (KHAN *et al.*, 2013). Given that phosphorylation-mimicking ERM variants are widely assumed to have constitutive activity, we assessed

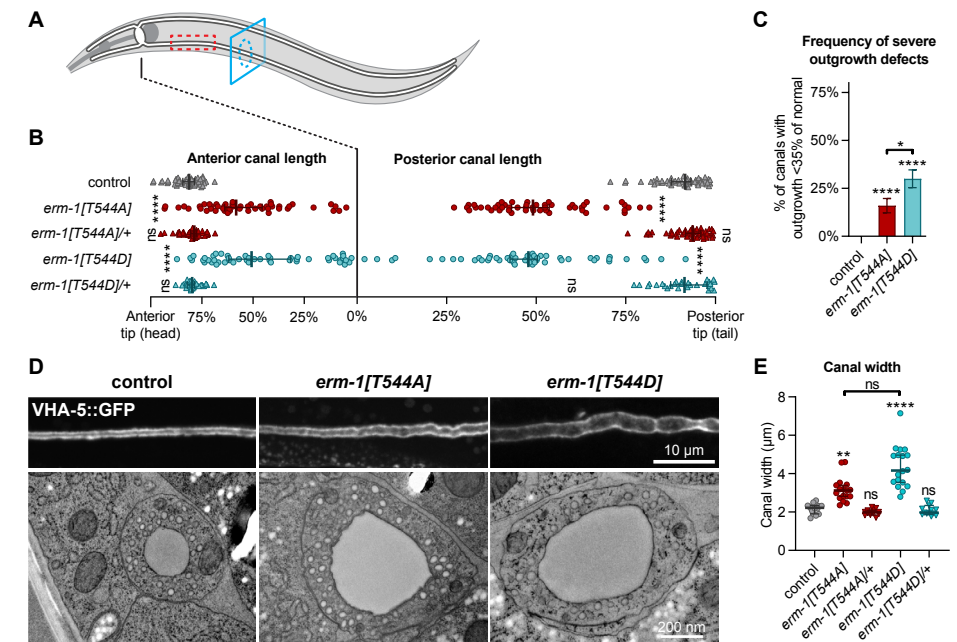


Figure 3: ERM-1 T544 phosphorylation is required for excretory canal lumenogenesis. (A) Schematic drawing of the excretory canal system in an L4 animal. Red dashed rectangle and blue dashed circle indicate areas shown in D by fluorescence and electron microscopy, respectively. (B) Quantification of excretory canal outgrowth in L4 animals. All four canal branches were measured per animal, and each data point represents one branch ($n = 25, 25, 22, 25$ and 14 animals from top to bottom). Error bars are the median \pm 95 % CI. (C) Frequency of anterior and posterior canals from B extending $< 35\%$ of the distance between cell body and tips. (D) Lumen morphology in L4 animals visualized by using a VHA-5::GFP transgene (top panels) or in cross-section by transmission electron microscopy (bottom panels). (E) Quantification of canal width in L4 animals. Each data point represents the average of three measurements at the three widest points in a single posterior canal ($n = 15, 17, 13, 18$ and 13). Error bars are the median \pm 95 % CI. Tests of significance: Dunn's multiple comparisons test for B and E; Fisher's exact test for C. ns, not significant. * $P \leq 0.05$, ** $P \leq 0.01$, **** $P \leq 0.0001$. Outgrowth and width were measured by fluorescence microscopy using VHA-5::GFP as a marker. Unless indicated otherwise, statistical comparisons are with the VHA-5::GFP control line.

whether cyst formation in T544 mutants also required AQP-8 activity. However, depletion of *aqp-8* by RNA interference (RNAi) enhanced the severity of canal defects (Supplementary figure 3), further demonstrating that defects in *erm-1[T544D]* are not attributable to increased ERM-1 activity.

We next investigated intestinal lumen formation by staining T544 mutant embryos with an antibody directed against the junctional protein AJM-1 (Figure 4A). In wild-type embryos, separation of junctions on opposing sides of the lumen was visible from the bean stage. By contrast, in both *erm-1[T544A]* and *erm-1[T544D]* mutants we did not detect clear separation of opposing junctions until the comma stage (Figure 4A). Between comma and 2-fold stages, junction

separation distance was reduced, and constrictions were visible along the length of the intestinal epithelium. At the 2-fold stage, *erm-1[T544D]* animals showed an almost complete separation of junctions throughout the epithelium. In addition, we observed an apparent expansion or ectopic accumulation of junctional material. By contrast, in *erm-1[T544A]* embryos, junction constrictions were still often detected at the 2-fold stage.

We characterized the junction defects of T544 ERM-1 mutants further in living animals during larval stages, using a strain that expresses endogenously tagged DLG-1::mCherry/Discs large and HMR-1::GFP/E-cadherin to mark the *C. elegans* apical junctions (CeAJ). We rarely observed full constrictions in *erm-1[T544D]* at the first larval stage (L1), although junctions had a wavy appearance and formed occasional aggregates and ectopic ring-like structures (Figure 4B). Junctions in *erm-1[T544A]* animals had a higher frequency of partial or full constrictions (Figure 4B). However, we did not detect obvious junction defects in either mutant at subsequent larval stages (data not shown).

The lumen formation defects we observed in early intestinal development are similar to those reported for knockdown of *erm-1* by RNAi (VAN FÜRDEN *et al.*, 2004). The mild defects in intestines of L1 larvae and the observed recovery at later stages are, however, in stark contrast to previous descriptions of *erm-1* mutants or RNAi (GÖBEL *et al.*, 2004; VAN FÜRDEN *et al.*, 2004), suggesting that T544 phosphorylation is important for ERM-1 activity during intestinal lumen formation, but is not strictly required.

ERM proteins in mammals, *Drosophila* and *C. elegans* are all crucial for the formation of microvilli (BONILHA *et al.*, 1999; BONILHA *et al.*, 2006; CASALETTO *et al.*, 2011; GÖBEL *et al.*, 2004; KARAGIOSIS & READY, 2004; SAOTOME *et al.*, 2004; SPECK *et al.*, 2003), and C-terminal phosphorylation is thought to be essential for ERM proteins to support the formation of microvilli (CHEN *et al.*, 1995; GAUTREAU *et al.*, 2000; KONDO *et al.*, 1997; PELASEYED *et al.*, 2017; VISWANATHA *et al.*, 2012). We therefore examined the formation of intestinal microvilli by electron microscopy. Surprisingly, microvilli still formed in *erm-1[T544A]* and *erm-1[T544D]* mutants (Figure 4C), although their length was reduced (Figure 4D). Collectively, our results show that ERM-1 phosphorylation plays a major role in lumen formation during early embryogenesis but is not essential for formation of a functional intestine or formation of microvilli.

Dynamic ERM-1 T544 phosphorylation contributes to molecular specialization of the apical domain

We next addressed whether ERM-1 T544 mutations perturb the functional specialization of the intestinal apical membrane. We introduced the *erm-1* T544 alleles in a strain overexpressing reporters for the peptide transporter PEPT-1::DsRed, which marks the apical membrane, and the small GTPase GFP::RAB-11, which marks apically enriched recycling endosomes (WINTER

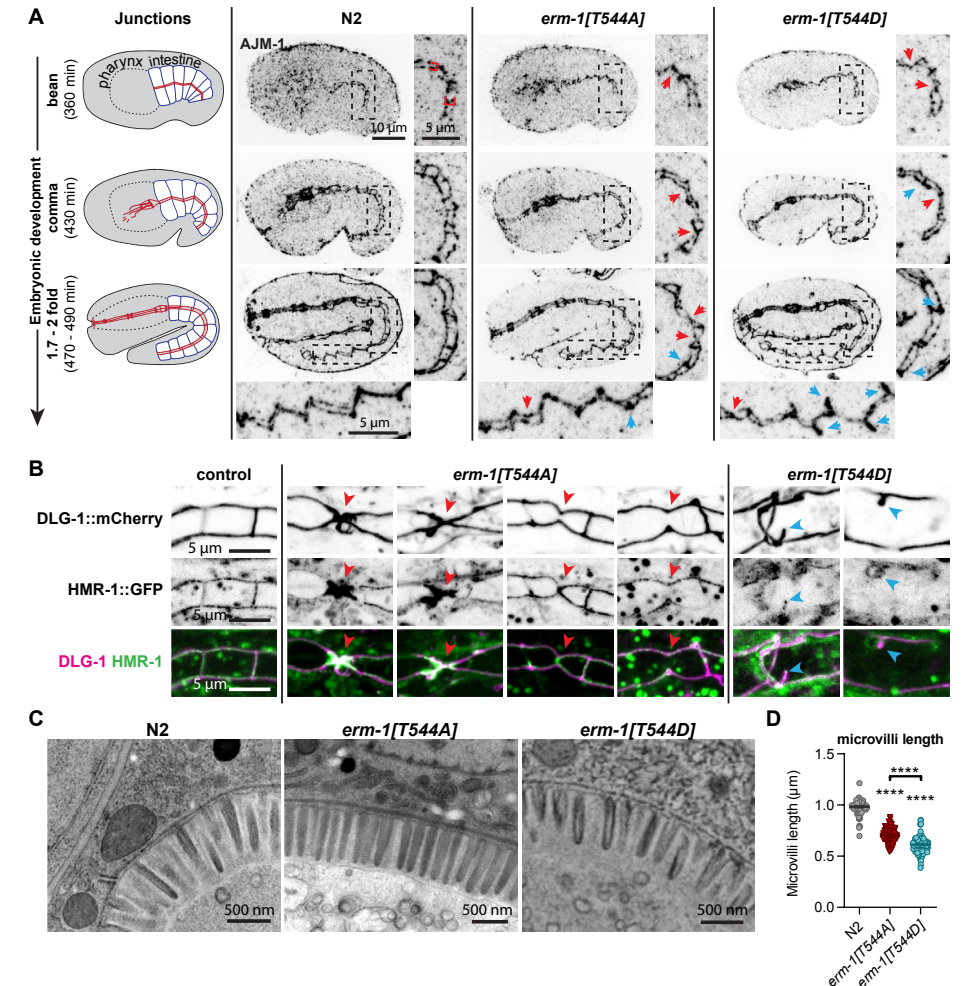


Figure 4: Positioning of cell junctions in intestinal cells requires dynamic regulation of ERM-1 T544 phosphorylation. (A) Junction organization visualized by AJM-1 staining of fixed embryos at different stages. Insets to the right and bottom are enlarged views of the regions indicated by dashed rectangles. Red brackets indicate junction separation in bean stage. Blue arrows point to expansion or ectopic accumulation of junction material, and red arrows point to partial and full constrictions. Images are maximum intensity projections. In all panels, developmental times are the approximate time after fertilization at 20°C. (B) Junction organization in live L1 larvae expressing DLG-1::mCherry and HMR-1::GFP. Blue and red arrows are as in A. (C) Transmission electron microscopy images of intestinal microvilli in L4 animals. (D) Quantification of the length of microvilli (total microvilli quantified: wild type, 88 from five animals; *erm-1[T544A]*, 168 from four animals; *erm-1[T544D]*, 135 from five animals). Error bars are the median ± 95% CI. Dunn's multiple comparisons test of significance, ****P ≤ 0.0001. Unless indicated otherwise, statistical comparisons are with N2.

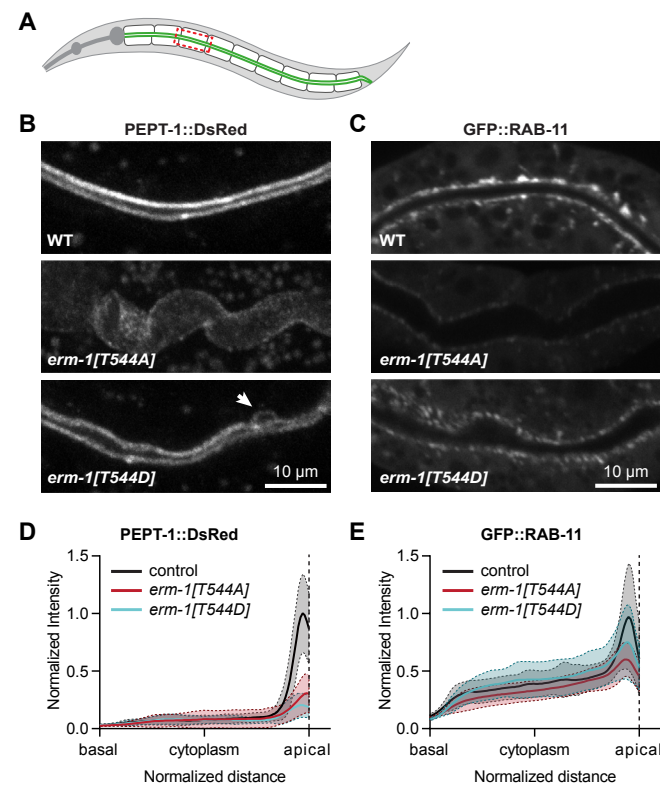


Figure 5: Dynamic T544 phosphorylation is important for molecular specialization of the apical domain. (A) Graphical representation of the area imaged in B and C (dashed red rectangle). (B, C) Intestinal distribution of PEPT-1::DsRed and GFP::RAB-11 transgenes in L1 larvae. Images were acquired and displayed with the same settings for comparison. Images are maximum intensity projections. Arrow in B indicates a small patch of apical membrane observed at the lateral domain, which occurs with low frequency in ERM-1 T544D mutant animals. (D, E) Distribution plots of the mean \pm s.d. fluorescence intensity of PEPT-1::DsRed and GFP::RAB-11 along the apical-basolateral axis in intestinal cells of L1 larvae. Two measurements per animal were plotted separately ($n = 27$ animals for control, $n = 22$ for *erm-1*[T544A] and $n = 19$ for *erm-1*[T544D]).

et al., 2012). Both proteins have important functions in intestinal development and homeostasis across species (SPANIER, 2014; WELZ *et al.*, 2014). In L1 larvae, we observed a dramatic reduction in the levels of PEPT-1::DsRed at the apical membrane in both *erm-1*[T544A] and *erm-1*[T544D] mutants (Figure 5A, B, D). Both mutants also showed a reduction in GFP::RAB-11 enrichment near the apical plasma, although the effect was more pronounced in *erm-1*[T544A] (Figure 5C, E). Thus, the balance between phosphorylated and non-phosphorylated ERM-1 forms contributes to the molecular specialization of the apical domain.

Phosphorylation of T544 controls subcellular localization of ERM-1

Replacing the C-terminal threonine of mammalian ezrin or fly Moesin with a phosphomimetic aspartic acid or glutamic acid causes relocalization to the entire plasma membrane, whereas reported effects of alanine substitutions vary from reduced apical enrichment to loss of membrane localization (BABICH & SOLE, 2015; COSCOY *et al.*, 2002; KARAGIOSIS & READY, 2004; ROCH *et al.*, 2010; VISWANATHA *et al.*, 2012). We therefore investigated the localization of the phosphorylation mutants using an antibody directed against *C. elegans* ERM-1. In the embryonic intestine, ERM-1[T544A] failed to accumulate at the apical membrane (Supplementary figure 4A). ERM-1[T544D] also failed to accumulate during early stages of intestinal development, but apical enrichment was evident by the 2-fold stage (Supplementary figure 4A). Nevertheless, we observed persistent basolateral localization of both ERM-1[T544A] and ERM-1[T544D] throughout embryogenesis, which was not observed for wild-type ERM-1 (Supplementary figure 4A). We were not able to assess ERM-1 distribution accurately in larval stages by antibody staining, owing to limitations in the quality of antibody staining.

To analyze the distribution of ERM-1 T544 mutants in live animals, we engineered *erm-1*[T544A] and *erm-1*[T544D] alleles carrying a COOH-terminal GFP fusion. In the developing embryonic intestine, the GFP-tagged T544 mutants also showed a delay in apical enrichment (Figure 6A). However, we did observe apical enrichment of ERM-1[T544A]:GFP starting from the 2-fold stage (Figure 6A). Strikingly, basolateral localization of ERM-1 persisted throughout development in both mutant variants, albeit more readily visible in *erm-1*[T544A] (Figure 6A-C). In the larval intestine, apical ERM-1[T544A] levels were sharply reduced at the L1 stage, but largely recovered by the L4 stage (Figure 6E; Supplementary figure 7A). In the excretory canal, ERM-1[T544A]:GFP and ERM-1[T544D]:GFP were detected exclusively at the apical plasma membrane (Figure 6D). In the germline, ERM-1[T544A]:GFP levels were lower than those of non-phosphomutant ERM-1::GFP, but still showed apical enrichment (Supplementary figure 5). By contrast, ERM-1[T544D]:GFP showed increased accumulation at the apical domain (Supplementary figure 5). Thus, C-terminal phosphorylation dynamics modulate ERM-1 distribution in a tissue-specific manner.

We also used the *erm-1*[T544A]:GFP and *erm-1*[T544D]:GFP alleles to examine intestinal lumen morphology. We observed discontinuities in the GFP signal along the lumen of *erm-1*[T544A]:GFP and *erm-1*[T544D]:GFP embryos, which largely resolved by the L1 stage (Figure 6F). These presumably correspond to the junction constrictions shown in Figure 4. The penetrance of intestinal phenotypes was slightly higher than in untagged T544 mutants

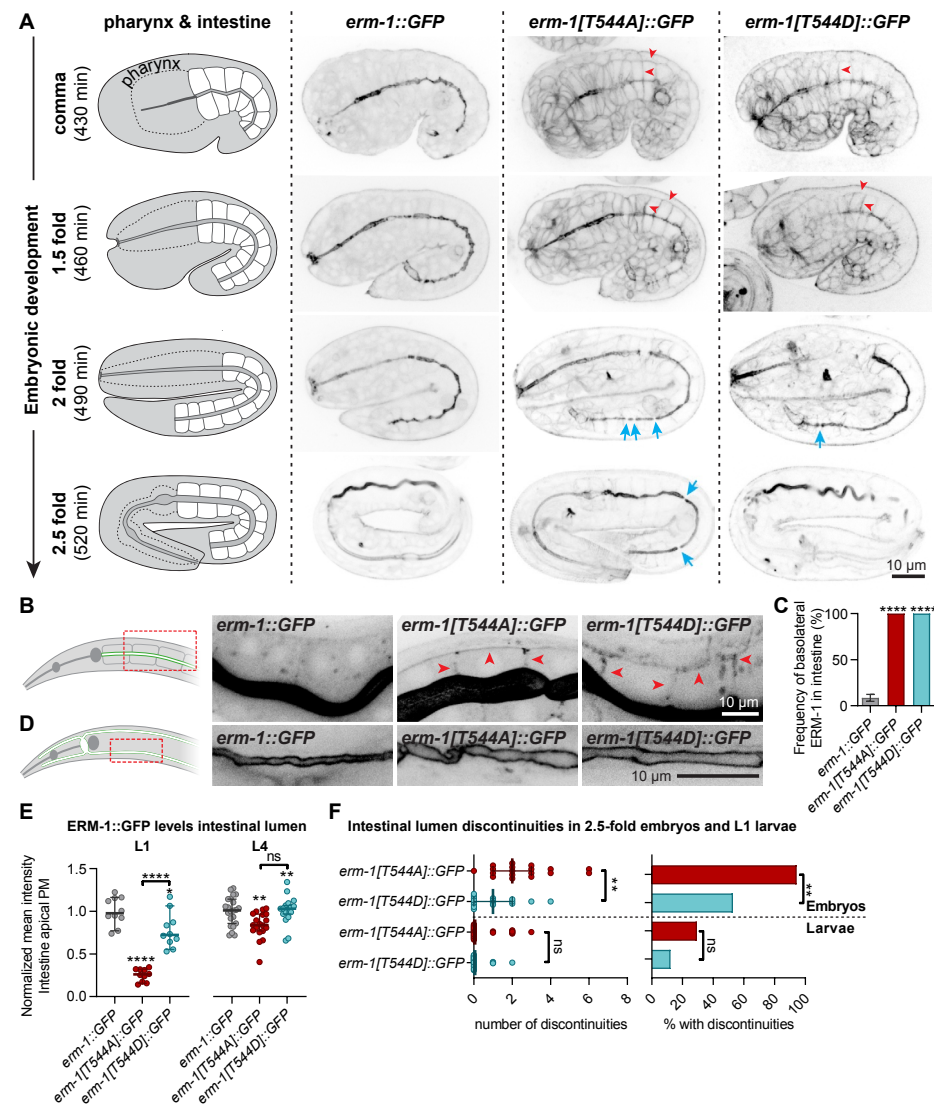


Figure 6: T544 phosphorylation cycling supports apical recruitment of ERM-1 and intestinal lumen formation. (A) Distribution of ERM-1::GFP variants in different embryonic stages. Blue arrows indicate lumen discontinuities, and red arrowheads indicate examples of ectopic basolateral ERM-1 localization. (B) Basolateral localization (red arrowheads) of ERM-1::GFP variants in the intestine of L1 larvae. Images are overexposed for clarity. (C) Frequency of animals with ERM-1::GFP detectable at the basolateral membrane (n = 58, 39 and 26). Statistical comparisons are with *erm-1::GFP*. (D) Apical localization of ERM-1::GFP variants in the excretory canal of L4 larvae. Red dashed rectangles in B and D indicate the area imaged. (E) Intensity of ERM-1::GFP variants at the apical intestinal membrane of L1 larvae. Each symbol represents an individual animal (n = 10 for L1, and n = 22, 19 and 17 for L4). Error bars are the median \pm 95 % CI. Statistical comparisons are with *erm-1::GFP* unless indicated otherwise. (F) Number of intestinal lumen discontinuities (median \pm 95 % CI) and fraction of animals with discontinuities in

~ Figure description continues on the next page ~

late embryos and L1 larvae (n = 34, 41, 18 and 16 from top to bottom). Tests of significance: Fisher's exact test for D and bar graph in F; Tukey's multiple comparisons test for E; and Dunn's multiple comparisons test for dot plot in F. ns, not significant. **P \leq 0.01, ****P \leq 0.0001.

(Supplementary figure 4B), presumably owing to a detrimental influence of the COOH-terminal GFP tag. These results further demonstrate the importance of ERM-1 phosphorylation in the early stages of intestinal lumenogenesis.

Mobility of ERM-1 at the membrane is modulated by T544 phosphorylation status

The altered distribution of ERM-1 T544 mutants might be attributable to changes in the dynamics of ERM-1 association with the membrane. To investigate this, we performed fluorescence recovery after photobleaching (FRAP) experiments using GFP tagged wild-type and T544 mutant strains. In the intestine, ERM-1::GFP was extraordinarily stable, with recovery of bleached areas averaging 15 % after 45 min (Figure 7A, B). However, the fraction and speed of recovery were dramatically increased for the ERM-1[T544A)::GFP and ERM-1[T544D)::GFP mutant forms (Figure 7A, B). Recovery profiles for wild-type and T544 mutants were best fitted with a two-component curve, suggesting the presence of two distinct populations (Supplementary table 1). We did not observe a noticeable difference in recovery of ERM-1[T544A)::GFP at the middle versus the borders of the bleached region (Supplementary figure 6A, B), which suggests that the increased recovery resulted from faster association/dissociation rates, rather than a change in lateral diffusion rate at the plasma membrane.

Recovery rates of wild-type ERM-1::GFP in the excretory canal were similar to those in the intestine (Figure 7C, D). However, in this tissue no changes in recovery rates were detected for T544 mutant forms (Figure 7C, D). To rule out the possibility that the disrupted canal morphology resulting from the COOH-terminal GFP tag affected the recovery of ERM-1, we also analyzed ERM-1::GFP fusions in heterozygous animals, which have morphologically normal canals. We observed no difference in recovery (Supplementary figure 6C). Finally, we analyzed the recovery of ERM-1::GFP in the adult germline. Challenges related to imaging depth and tissue movement prevented us from accurate prolonged analysis of recovery at the apical membrane, thus we focused on the more easily imaged basolateral membrane. ERM-1::GFP was much more dynamic in this tissue, with bleached areas recovering \pm 70 % after 10 min (Figure 7E, F). Surprisingly, both ERM-1[T544A)::GFP and ERM-1[T544D)::GFP had slower recovery profiles (Figure 7E, F; Supplementary table 1), suggesting that these forms are more stably associated with the basolateral membrane than ERM-1::GFP. Our data show that ERM-1 dynamics

are modulated by C-terminal phosphorylation and tissue-specific properties, potentially including different binding partners or differences in lipid membrane composition.

Phosphorylation of T544 controls apical actin enrichment and dynamics

C-terminal phosphorylation of ERM proteins has been reported to be required for apical actin enrichment in epithelial cells (ABBATTISCIANNI *et al.*, 2016; HIPFNER *et al.*, 2004; ROCH *et al.*, 2010). In *C. elegans*, loss of *erm-1* function results in reduced apical actin levels in the intestine and in the excretory canal, whereas overexpression of ERM-1 in the excretory canal leads to excessive accumulation of apical actin (BERNADSKAYA *et al.*, 2011; GÖBEL *et al.*, 2004; VAN FÜRDEN *et al.*, 2004). The apical actin network of tubular epithelia in *C. elegans* is mostly composed of the specialized actin ACT-5 (MACQUEEN *et al.*, 2005). To analyze ACT-5 in the canal, we generated a transgenic line expressing mCherry::ACT-5 from the *sulp-4* promoter. Consistent with our results using VHA-5::GFP, the excretory canals showed variable, but fully penetrant, morphological defects in both ERM-1 T544 mutants (Figure 8A). In canal regions with a widened lumen, apical ACT-5 coating was sparser and circumferential bundles were visible. The apical-to-cytoplasmic ratio of mCherry::ACT-5 was decreased in both *erm-1[T544A]* and *erm-1[T544D]* mutants, relative to control animals expressing wild-type *erm-1* (Figure 8A). This suggests that, in the excretory canal, cycling of T544 phosphorylation is important for recruitment of actin to the apical membrane.

To analyze ACT-5 distribution in intestinal cells, we used an integrated YFP::ACT-5 transgene (BOSSINGER *et al.*, 2004). In intestines of wild-type embryos, we detected a strong enrichment of ACT-5 at the apical domain of intestinal cells soon after polarization (Figure 8B). By contrast, apical enrichment of YFP::ACT-5 in comma-stage embryos of *erm-1[T544A]* and *erm-1[T544D]* mutants was not readily detected (Figure 8B), and YFP::ACT-5 was clearly detectable in the cytoplasm and along the basolateral membrane (Figure 8B). Similar to the distribution of ERM-1 T544 mutants during embryogenesis, we did observe apical enrichment of YFP::ACT-5 at later embryonic stages (Figure 8B, C). In larval stages, YFP::ACT-5 levels also followed the pattern we observed for ERM-1 in the T544 mutants (Figure 8D; compare with Figure 6E; Supplementary figure 7A). In *erm-1[T544D]* mutants, apical YFP::ACT-5 levels were normal throughout larval development. In *erm-1[T544A]* mutants, apical levels were reduced in L1 larvae, but partially recovered by the L4 stage.

We next investigated ACT-5 dynamics by FRAP. The effects on ACT-5 recovery by *erm-1[T544A]* and *erm-1[T544D]* mutations were consistent with the effects we observed on ACT-5 levels. In the excretory canal, recovery of mCherry::ACT-5 was slightly faster in both mutants than in *erm-1* wild-type animals, with the fastest recovery observed in the *erm-1[T544A]* background (Figure 8E). In the

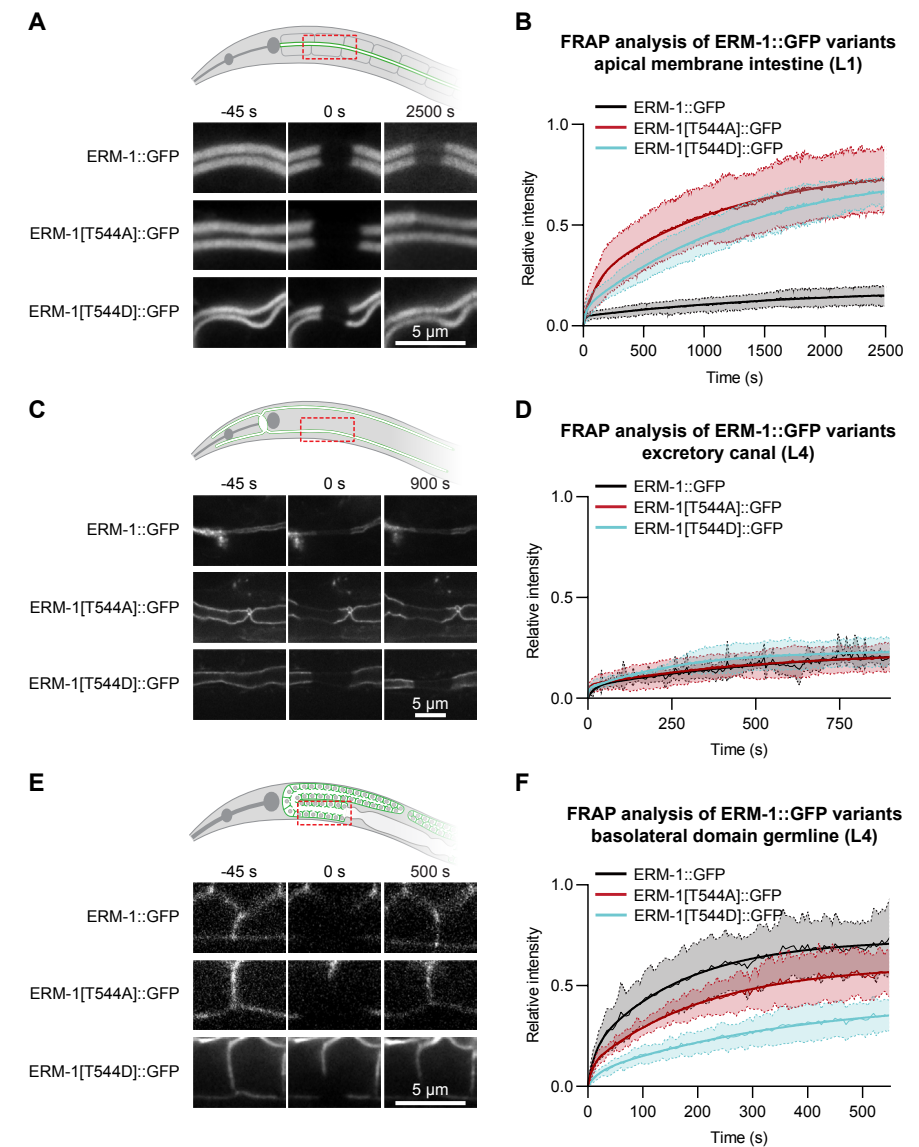


Figure 7: T544 phosphorylation cycling is required for stable ERM-1 localization in the intestine. Stills from time-lapse movies (A, C, E) and FRAP curves (B, D, F) of GFP-tagged ERM-1 variants at the apical membrane of the intestine of L1 larvae ($n = 7$ for ERM-1::GFP, $n = 8$ for ERM-1[T544A] and $n = 7$ for ERM-1[T544D]), the apical membrane of the excretory canal of L4 larvae ($n = 5$ for ERM-1::GFP, $n = 4$ for ERM-1[T544A] and $n = 4$ for ERM-1[T544D]), or the basolateral membrane of the germline of L4 larvae ($n = 10$ for ERM-1::GFP, $n = 7$ for ERM-1[T544A] and $n = 7$ for ERM-1[T544D]). Thin lines and shading represent the mean \pm s.d., and thick lines represent curve fitting of averaged FRAP data with a double exponential equation.

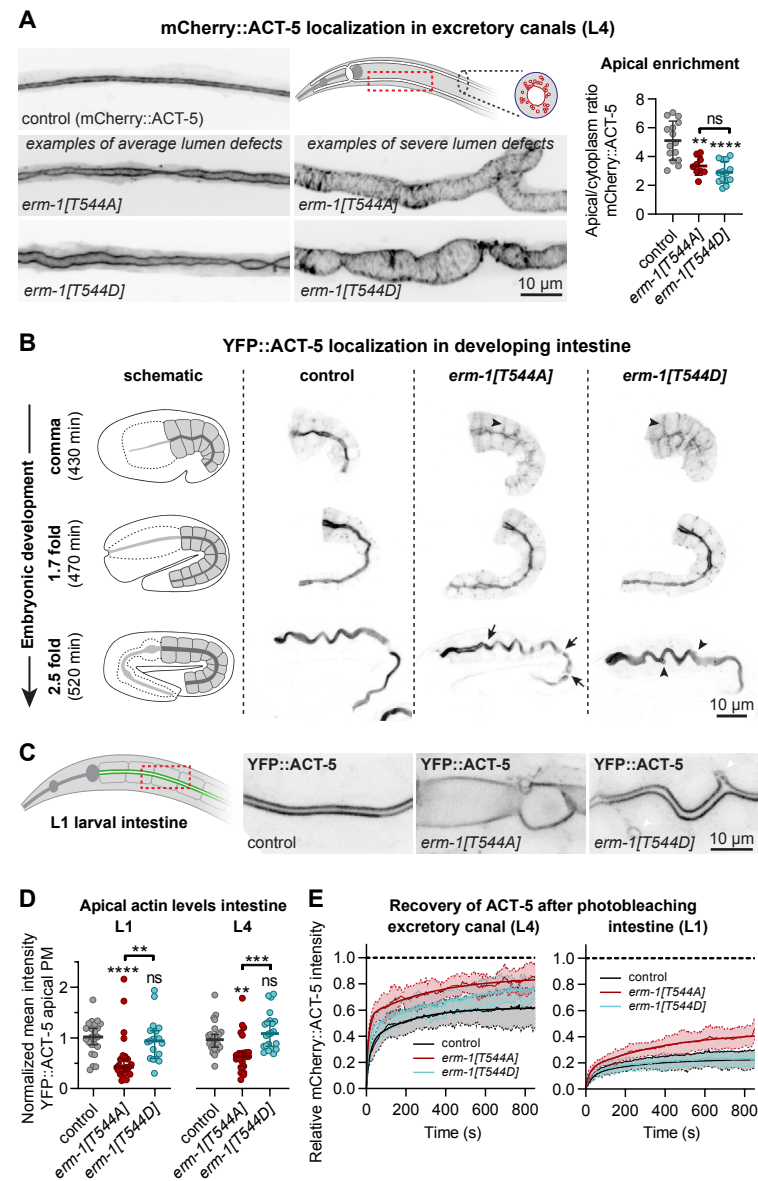


Figure 8: Phosphorylation of T544 controls apical actin recruitment and dynamics. (A) Lumen morphology and distribution of mCherry::ACT-5 in the excretory canal of L4 larvae. Canal widths vary (see Figure 3E), and examples of severely widened and less severely widened canals are shown. Graph shows apical-to-cytoplasmic ratio of mean intensity of mCherry::ACT-5. Each data point represents the average of three measurements in a single animal ($n = 15, 9$ and 14). Error bars are the mean \pm s.d. (B, C) Intestinal distribution of YFP::ACT-5. Arrows indicate discontinuities. Arrowheads in comma stage indicate basolateral YFP::ACT-5, and arrowheads in 2.5-fold stage indicate ectopic expansions of the cortical actin network. (D) Quantification of YFP::ACT-5 levels at the intestinal apical membrane. Each symbol represents a single animal ($n = 23, 26$ and

~ Figure description continues on the next page ~

19 for L1 and $n = 24, 21$ and 22 for L4). Error bars are the median \pm 95 % CI. Tests of significance: Dunnett's T3 multiple comparisons test for A; Dunn's multiple comparisons test for D. ns, not significant. ** $P \leq 0.01$, *** $P \leq 0.001$, **** $P \leq 0.0001$. Statistical comparisons are with control unless indicated otherwise. (E) FRAP curves of apical mCherry::ACT-5 in the excretory canal of L4 larvae ($n = 14$ for control, $n = 6$ for *erm-1[T544A]* and $n = 7$ for *erm-1[T544D]*) and apical YFP::ACT-5 in the intestine of L1 larvae ($n = 8$ for control, $n = 13$ for *erm-1[T544A]* and $n = 8$ for *erm-1[T544D]*). Thin lines and shading represent the mean \pm s.d., and thick lines were obtained by curve fitting averaged FRAP data with a double exponential equation.

intestine, recovery of YFP::ACT-5 in control animals was slow (± 23 % in 15 min) and similar to that of ERM-1::GFP (Figure 7A; Figure 8E). Recovery of apical YFP::ACT-5 in the intestine of *erm-1[T544A]* mutants was faster than in control animals (± 41 % in 15 min), whereas no difference was seen in *erm-1[T544D]* (Figure 8E; Supplementary figure 7B).

Collectively, our results show that T544 phosphorylation is important for cortical actin organization by ERM-1 in tubular epithelia. The similar delay in apical enrichment of ERM-1 and ACT-5 in the embryonic intestine, and the similar defects in ACT-5 and ERM-1 levels in larval intestines of *erm-1[T544A]* mutants, suggest that the presence of ERM-1 at the apical membrane is a major factor in ACT-5 recruitment.

Discussion

ERM proteins drive morphological specialization events required for the function of numerous cell types across animal species. Here, we characterized the contribution of the major conserved regulatory sites important for the activity of ERM proteins *in vivo* in *C. elegans*. The use of CRISPR/Cas9 allowed us to analyze the effects of PIP₂-binding and C-terminal phosphorylation mutants in the absence of wild-type product, without addition of any tags and at endogenous expression levels. This is especially relevant because ERM proteins are affected by fluorescent protein tags and often have dose-dependent effects (BERRYMAN *et al.*, 1995; CAO *et al.*, 2005; CHAMBERS & BRETSCHER, 2005; GAUTREAU *et al.*, 2000; KHAN *et al.*, 2013). In agreement with studies in *Drosophila* and mammalian cultured cells (FIEVET *et al.*, 2004; HAO *et al.*, 2009; ROCH *et al.*, 2010; YONEMURA *et al.*, 2002), we showed that the PIP₂-binding site is essential for ERM-1 activity. By contrast, our phosphorylation mutants demonstrate that phosphorylation is not essential for ERM activity in *C. elegans*, despite contributing to multiple aspects of ERM-1 function, often in a tissue-specific manner.

The similarity in phenotypes caused by the *erm-1[4KN]* mutation and the putative *erm-1(tm667)* null allele (GÖBEL *et al.*, 2004) demonstrates the essentiality of the PIP₂-binding site. Effects on protein localization were also largely consistent with an essential role for the PIP₂-binding site in localizing ERM-1 to the plasma membrane. Unexpectedly, however, we detected substantial amounts of ERM-1 at the plasma membrane of intestinal cells and the excretory canal in

heterozygous *erm-1[4KN]::GFP/+* animals and in first generation homozygous animals. Given that first generation *erm-1[4KN]::GFP* homozygous animals contain very low levels of wild-type ERM-1, it is unlikely that dimerization with wild-type ERM-1 can account for the significant plasma membrane localization of ERM-1[4KN]::GFP. An alternative model is the formation of higher order ERM-1 complexes, in which the presence of a small fraction of wild-type ERM-1 can mediate membrane localization of ERM-1[4KN]. Finally, wild-type ERM-1 might enact apical membrane modifications that promote ERM-1[4KN] recruitment.

To investigate the contribution of T544 phosphorylation, we mutated the endogenous *erm-1* locus to express either a non-phosphorylatable T544A variant or a phosphomimetic T544D variant. Our results show that non-phosphorylatable ERM-1 can support *C. elegans* development. Although T544 mutant embryos display intestinal lumenogenesis defects that resemble those we observed in *erm-1[4KN]* mutants and that have been described for *erm-1(RNAi)* (VAN FÜRDEN *et al.*, 2004), these defects largely resolve by the L1 stage, and both *erm-1[T544A]* and *erm-1[T544D]* mutants are homozygous viable. Perhaps most strikingly, both ERM-1 T544A and T544D animals develop intestines with a normal appearance and only a mildly reduced length of microvilli. These results contrast with the findings of studies in mammalian cell culture and *Drosophila* that non-phosphorylatable and phosphomimetic ERM variants cannot substitute for wild-type ERM proteins (KARAGIOSIS & READY, 2004; PARAMESWARAN *et al.*, 2011; POLESSELLO *et al.*, 2002; VISWANATHA *et al.*, 2012). However, one study in *Drosophila* showed that expression of a Moesin-T559A transgene (but not Moesin-T559D) could significantly rescue viability of a strong *moesin* allele (ROCH *et al.*, 2010), and two others demonstrated rescuing activity for Moesin-T559D, but not for Moesin-T559A (HIPFNER *et al.*, 2004; SPECK *et al.*, 2003). Moreover, phosphorylation of ERM proteins is not required for the formation of microvillus-like structures in A431 and MDCK II cells (YONEMURA *et al.*, 2002). Thus, non-phosphorylated ERM proteins can be active, and the importance of C-terminal phosphorylation is likely to depend on the biological setting and experimental system used.

One of the main functions of ERM proteins is to link the plasma membrane and the actin cytoskeleton. Binding to PIP₂ and C-terminal phosphorylation have been shown cooperatively to promote the actin-binding activity of ERM proteins (BOSK *et al.*, 2011; BRAUNGER *et al.*, 2014; HUANG *et al.*, 2007; MATSUI *et al.*, 1998; NAKAMURA *et al.*, 1999). In this process, phosphorylation does not appear to regulate the F-actin binding strength of individual ERM proteins directly, but instead increases the pool of ERM protein available for interaction with actin by promoting the open conformation (BOSK *et al.*, 2011; BRAUNGER *et al.*, 2014). Our results are consistent with this model because the levels of apical actin in the intestine and canal were correlated with the levels of apical ERM-1, and

not with the phosphorylation state. The fact that microvilli are formed in *erm-1[T544A]* mutants also indicates that ERM-1[T544A] can be active and capable of organizing apical actin. The close correlation between ERM-1 and ACT-5 levels in the intestine also highlights the important role of ERM-1 in organizing apical actin in this tissue.

Multiple aspects of the defects in *erm-1[T544A]* and *erm-1[T544D]* mutants were strikingly similar. This includes the lumen formation defects in the excretory canal and early intestine, the delayed apical accumulation in embryonic development, and the increased mobility in the larval intestine. These results are consistent with a model in which cycling between phosphorylated and non-phosphorylated states is crucial to controlling the activity of ERM-1, as has been proposed to account for ERM protein activity in activation of B and T cells, in secretion of gastric parietal cells, and in formation of microvilli in epithelial cells (PARAMESWARAN *et al.*, 2011; VISWANATHA *et al.*, 2012; ZHU *et al.*, 2007). This interpretation does rely on the assumption that phosphomimetic mutations mimic the phosphorylated state, which is supported by extensive characterization of phosphomimetic ERM mutants in other systems (BOSK *et al.*, 2011; CARRENO *et al.*, 2008; CHAMBERS & BRETSCHER, 2005; CHARRAS *et al.*, 2006; GAUTREAU *et al.*, 2000; HUANG *et al.*, 1999; KUNDA *et al.*, 2008; MATSUI *et al.*, 1998; NAKAMURA *et al.*, 1999; OSHIRO *et al.*, 1998; POLESSELLO *et al.*, 2002; SIMONS *et al.*, 1998; SPECK *et al.*, 2003).

How does the dynamic turnover of C-terminal phosphorylation regulate ERM activity? A previous study in cultured epithelial cells found that local phosphocycling by apical kinases restricts ezrin localization and activity to microvilli (VISWANATHA *et al.*, 2012). Similar polarized kinase activity was shown to restrict Moesin activity to the apical cortex of tracheal cells in *Drosophila* (UKKEN *et al.*, 2014). During embryonic intestinal development, we observed a delay in the apical enrichment of ERM-1 in *erm-1[T544A]* and *erm-1[T544D]* mutants, and in the larval intestine, both T544A and T544D substitutions greatly increased the mobility of ERM-1. These results indicate that in *C. elegans*, local phosphorylation cycling promotes the apical enrichment and basolateral exclusion of ERM-1. How phosphorylation cycling promotes the stable apical localization of ERM-1 is not clear. One possibility is that ERM-1 needs to cycle between different conformations in order to cope with a changing microenvironment, which presumably involves actin treadmilling and local changes in the concentration or availability of PIP₂ and protein binding partners. ERM-1 stability in the excretory canal was unaffected by the phosphorylation mutants, perhaps reflecting a difference in the dynamics of apical membrane components between tissues. Regardless of the underlying reason, ERM-1 turnover dynamics can vary greatly depending on the biological context and are subject to tissue-specific regulation. Finally, we note that although both mutant forms behave in a similar manner in many respects, apical ERM-1[T544A]::GFP levels are significantly lower than either ERM-1::GFP or ERM-1[T544D]::GFP

levels in the L1 intestine and never become completely normal. Thus, cycling-independent aspects of T544 phosphorylation presumably do play a role in regulating ERM-1.

Previous FRAP studies in microvilli of LLC-PK1 cells and in blebbing M2 melanoma cells indicate the presence of three pools of ezrin with recovery half-times in the range of seconds to minutes (COSCOY *et al.*, 2002; FRITZSCHE *et al.*, 2014). Our analysis of ERM-1::GFP protein dynamics by FRAP also supports the presence of at least two pools of ERM-1 in *C. elegans*, but reveals an unexpected stability for ERM-1 in the intestine and excretory canal. Similar results were obtained by A. Bidaud Meynard and G. Michaux (personal communication). Slow recovery of ERM-1 is consistent with a recent study which found that the ezrin FERM domain binds phosphoinositide-rich membranes with very high affinity and slow dissociation dynamics (SENJU *et al.*, 2017), whereas ERM-1::GFP levels at the basolateral domain of the gonad recovered more rapidly. Our results in the intestine might therefore reflect an inherent physiological difference from cells in culture and between tissues.

In contrast to the intestine, lumen formation and outgrowth of the excretory canal were severely affected in both *erm-1[T544A]* and *erm-1[T544D]* mutant animals throughout their lifespan. Surprisingly, however, neither localization nor mobility of ERM-1 in the canal was affected by altered T544 regulation. ERM proteins interact with and regulate the function of numerous proteins, including trafficking components, transmembrane channels or pumps, polarity determinants and junction proteins (BRYANT *et al.*, 2014; CHIRIVINO *et al.*, 2011; DERETIC *et al.*, 2004; KHAN *et al.*, 2013; KVALVAAG *et al.*, 2013; MÉDINA *et al.*, 2002; PILOT *et al.*, 2006; ZHU *et al.*, 2007). Moreover, several interaction partners have been shown to interact selectively with either non-phosphorylated or phosphorylated forms of ezrin (VISWANATHA *et al.*, 2013). It is possible that a difference in the subset of ERM-1 interaction partners involved in each tissue explains why effects on ERM-1 localization and mobility are not strictly correlated with the phenotypic defects at the tissue level. The absence of changes in ERM-1 protein behavior in the canal further indicate that C-terminal threonine phosphorylation is not the only mechanism that controls ERM-1 localization and stability. Binding to specific interaction partners might contribute to ERM-1 localization, but alternative mechanisms of regulation are also possible. For example, a recent study found that in breast epithelial cells, ezrin membrane association is regulated by acetylation of ezrin (SONG *et al.*, 2020). Overall, these results demonstrate that C-terminal phosphorylation is a versatile regulatory modification that modulates ERM-1 function in a context-dependent manner and underscore the importance of studying ERM regulation in different biological scenarios.

Methods

Caenorhabditis elegans strains and culture conditions

Caenorhabditis elegans strains were cultured in standard conditions (BRENNER, 1974). Only hermaphrodites were used, and all experiments were performed with animals grown at 20°C on nematode growth medium (NGM) agar plates. Supplementary table 2 contains a list of all the strains used.

CRISPR/Cas9 genome engineering

Endogenous eGFP protein fusions and point mutations were generated by homology-directed repair of CRISPR/Cas9-induced DNA double-strand breaks. *erm-1[T544A]* and eGFP protein fusions were generated in an N2 background, with the exception of *erm-1[4KN]::GFP*, in which *erm-1[KN]/+* was used as the starting genetic background; remaining point mutations were generated in a *pha-1(e2123ts)* background. In all cases, two single guide RNA (sgRNA) plasmids targeting each locus were used. The sgRNA plasmids were generated by ligation of annealed oligo pairs into the *pU6::sgRNA* expression vectors pMB70 (Addgene 47943) or pJIR50 (Addgene 75026) as previously described (WAAIJERS *et al.*, 2013; WAAIJERS *et al.*, 2016). To introduce point mutations, synthesized single-stranded oligodeoxynucleotides (ssODNs) with 33-45 bp homology arms were used as a repair template, and integration events were selected using either *dpy-10* (ARRIBERE *et al.*, 2014) or *pha-1* (WARD, 2015) co-CRISPR approaches. eGFP knock-ins were introduced using a plasmid-based repair template with 450-600 bp homology arms and containing a self-excising cassette (SEC) for selection, as previously described (DICKINSON *et al.*, 2015). To introduce eGFP, we created a custom SEC vector, pJIR82 (Addgene 75027), by replacing a fragment of pDD282 (Addgene 66823) comprising the GFP sequence with a similar fragment comprising a codon-optimized and synthetic intron-containing eGFP sequence using the flanking Bsu36I and BglII restriction sites. In all cases, correct genome editing was confirmed by Sanger sequencing (Macrogen Europe) of PCR amplicons encompassing the edited genomic region. The maternal-effect lethal *erm-1[KN]* and *erm-1[KN]::GFP* alleles were balanced with *dpy-5(e61); unc-29(e403)* I (strain DR102). In all cases, edited strains were backcrossed twice with N2 to eliminate any non-linked unspecific editing events, and one additional round of backcrossing was done for strains generated in a *pha-1(e2123ts)* background. The sequences of all oligonucleotides used (synthesized by Integrated DNA Technologies) are listed in Supplementary table 3.

Microscopy

Imaging of *C. elegans* was done by mounting embryos or larvae on a 5 % agarose pad in a 10 mM Tetramisole solution in M9 buffer (0.22 M KH₂PO₄, 0.42 M Na₂HPO₄, 0.85 M NaCl and 0.001 M MgSO₄) to induce paralysis. Spinning disk confocal imaging was performed using a Nikon Ti-U microscope

equipped with a Yokogawa CSU-X1 spinning disk and an Andor iXon+ EMCCD camera, using $\times 60$ and $\times 100$ 1.4 NA objectives. Time-lapse imaging for FRAP experiments was performed on a Nikon Eclipse-Ti microscope equipped with a Yokogawa CSU-X1-A1 spinning disk and a Photometrics Evolve 512 EMCCD camera, using a $\times 100$ 1.4 NA objective. Targeted photobleaching was done using an ILas system (Roper Scientific France/PICT-IBiSA, Institut Curie). Two epifluorescence microscopy set-ups were used. Digital interference contrast (DIC) imaging was done in an upright Zeiss Axioplan2 microscope using a $\times 63$ 1.4 NA objective, and imaging to quantify excretory canal outgrowth was done in an upright Zeiss Axio Imager 2 microscope using a $\times 20$ 0.5 NA objective. Microscopy data were acquired using MetaMorph Microscopy Automation & Image Analysis Software (spinning disk), Zeiss AxioVision (DIC) and Zeiss Zen (epifluorescence). All stacks along the *z*-axis were obtained at 0.25 μm intervals, and all images were analyzed and processed using ImageJ and Adobe Photoshop. For quantifications, the same laser power and exposure times were used within experiments.

Quantitative image analysis

Quantitative analysis of spinning disk images was done in ImageJ. In all quantifications, the mean background intensity was quantified by drawing a circular region of diameter 50 pixels in areas within the field of view that did not contain any animals, and values were normalized using the mean intensity of eGFP, YFP or mCherry at the apical membrane of the corresponding tissue in control animals. In the intestine, all measurements were done in cells forming int2 through int6, and the intensity of fluorescence at the apical membrane was quantified in regions where opposing apical membranes could be seen clearly as two lines. To quantify the intensity of fluorescence of ERM-1[4KN>::GFP in intestinal cells and mCherry::ACT-5 in the excretory canal, measurements were performed in maximum intensity projections of three consecutive *z*-slices showing the highest intensity at the apical membrane. The peak intensity at the apical membrane was calculated by averaging the peak values of intensity profiles from multiple 40-pixel-wide line scans perpendicular to the membrane per animal. The mean cytoplasmic intensity was obtained by averaging the mean intensity values of multiple elliptical regions within the cytoplasm. Each measurement was corrected for background noise and normalized as described above. Averaged apical and cytoplasmic intensity values were used to calculate the apical-to-cytoplasmic intensity ratio per animal. Distribution plots of the fluorescence intensity of GFP-tagged ERM-1 variants in the larval germline, and for PEPT-1::DsRed and GFP::RAB-11 in the intestine, were obtained using the same method. For GFP-tagged ERM-1 variants in the germline, three measurements were done per animal in single frames where both apical and basal membranes were clearly visible. For animals expressing both PEPT-1::DsRed and GFP::RAB-11 in the intestine, two measurements were

done per animal in maximum intensity projections of the three consecutive *z*-slices with the highest intensity of PEPT-1::DsRed at the apical membrane. Measurements from single animals were not averaged in either case. Intensity distribution profiles were obtained by tracing line scans (15 pixels wide for the germline and 40 pixels wide for the intestine) encompassing the entire germ cell compartments or intestinal cells along the apical-basal axis. Intensity profiles were trimmed manually to exclude values outside the cells/compartments of interest, and each value was corrected for background noise and normalized as described above. To make direct comparisons and plot intensity profiles despite differences in the distance between basal and apical membranes, a custom R script was made to interpolate intensity values linearly on the *y*-axis to a fixed distance along the *x*-axis for each intensity profile defined by the average apical-basal distance in control animals (script is available upon request). For the germline, apical-to-basal intensity ratios were calculated using the peak intensity values at the apical and basal membranes per intensity profile. To quantify the intensity of fluorescence of eGFP-tagged ERM-1 variants and YFP::ACT-5 in intestinal cells, a free-hand region was drawn either surrounding the apical membrane or in the cytoplasm, and mean intensity values were extracted for all *z*-slices in which apical membrane was visible. The background was subtracted per frame, and each value was normalized as described above. The mean intensity at the apical membrane and cytoplasm were calculated by averaging measurements through the *z*-axis of two intestinal cells per animal. Averaged intensity values were used to calculate the apical-to-cytoplasmic ratio per animal.

Brood size and lethality

Starting at the L4 stage, individual P0 animals were cultured at 20°C and transferred to a fresh plate every 24 h for 6 days. Hatched and unhatched progeny were scored 24 h after removal of the P0, and larval lethality was scored 48 h after removal of the P0.

Relative excretory canal outgrowth and canal width

To quantify relative canal outgrowth in the excretory canal cell, F1 progeny of L4 animals expressing the VHA-5::GFP transgene grown in standard or RNAi culture plates were scored at the L4 stage. The distance between the cell body and either the anterior or posterior distal body tips was determined by tracing a segmented line along the center of the animal. The length of each individual canal was measured with a segmented line from the anterior-posterior bifurcation points close to the cell body until the canal tip. Relative outgrowth was calculated as the fraction of canal length over the distance between the cell body and distal tips. Severe outgrowth defects were defined as canals that extend $\leq 35\%$ of the distance between the excretory canal cell body and either anterior or posterior tips. The frequency was calculated by the sum of both

anterior and posterior canals with severe defects over total canals quantified per genotype. For canal width, we measured the width at the three widest points, including at any cysts present, in the most severely affected posterior canal of an animal. The average measurement of these three points represents one data point.

FRAP experiments and analysis

For FRAP assays, the laser power was adjusted in each experiment to avoid complete photobleaching of the selected area. Photobleaching was performed on a circular region with a diameter of 30–100 pixels at the cortex, and recovery was followed at 5 s intervals for 15–45 min depending on the tissue. Time-lapse movies were analyzed in ImageJ. The size of the area for FRAP analysis was defined by the full width at half-maximum of an intensity plot across the bleached region in the first post-bleach frame. For each time-lapse frame, the mean intensity value within the bleached region was determined, and the background, defined as the mean intensity of a non-bleached region outside the animal, was subtracted. The mean intensities within the bleached region were corrected for acquisition photobleaching per frame using the background-subtracted mean intensity of a similar non-bleached region at the cortex, which was normalized to the corresponding pre-bleach mean intensity. FRAP recovery was calculated as the change in corrected intensity values within the bleach region from the first frame after bleach (set to zero) normalized to the mean intensity of the 10 frames before bleaching. Curve fitting was done on averaged recovery data per sample using the non-linear regression analysis in GraphPad. One- and two-phase association were tested, and in all cases the data were best fitted with a two-phase curve. Intensity distribution plots were obtained by performing a three-pixel-wide line scan perpendicular to the apical membrane.

Immunohistochemistry

Antibody stainings were performed in mixed-stage (anti-pERM) or synchronous (anti-ERM-1) populations. Synchronized animals were obtained from gravid adult animals by bleaching and allowed to develop in M9 for 4–6 h for embryonic stages, or in standard culture plates for 10 h for early larval stages. Mixed-stage or synchronous larval populations were collected from plates and were washed three times in M9 (for stainings of post-embryonic stages, samples were incubated for 30 min with gentle shaking before the last wash), washed once in water, and transferred to a poly-l-lysine-coated slide. Samples were permeabilized by freeze-cracking and fixed at -20°C with methanol for 5 min and acetone for 10 min for staining with the ERM-1 antibody, or with P buffer (3.7 % formaldehyde, 75 % methanol, 250 μM EDTA and 50 mM NaF) for 15 min and methanol for 5 min for the pERM antibody. Samples were rehydrated in an ethanol series (90, 60 and 30 %, for 10 min each at -20°C), rinsed three

times in PBS-Tween (PBST; 1.35 M NaCl, 27 mM KCl, 100 mM Na_2HPO_4 , 18 mM KH_2PO_4 and 0.05 % Tween-20), and blocked for 1 h with 1 % bovine serum albumin and 10 % serum in PBST at room temperature (RT). Samples were incubated with primary antibodies in blocking solution overnight at 4°C , washed four times for 15 min in PBST, and secondary antibodies in blocking solution were incubated for 2 h at RT. Finally, samples were washed three times in PBST and once in PBS, for 10 min each, and mounted with Prolong Gold Antifade (ThermoFisher). The following antibodies and dilutions were used: MH27 mouse monoclonal (Developmental Studies Hybridoma Bank, validated to have no immunoreactivity in mutant embryos), 1:20; ERM-1 rabbit polyclonal [gift from O. Bossinger, validated to have no immunoreactivity in *erm-1(RNAi)* embryos (VAN FÜRDEN *et al.*, 2004)], 1:100; pERM rabbit polyclonal (Cell Signaling Technology #3144, verified here to not stain ERM-1[T544A]), 1:100; Alexa-Fluor 488 goat anti-rabbit and Alexa-Fluor 568 goat anti-mouse (Life Technologies, A-11008 and A11004, respectively) 1:500.

Feeding RNAi

The *aqp-8* RNAi clone was obtained from the genome-wide Vidal full-length HT115 RNAi feeding library derived from the ORFeome v.3.1 collection (RUAL *et al.*, 2004). An HT115 bacterial clone expressing the L4440 vector lacking an insert was used as a control. For feeding RNAi experiments, bacteria were precultured in 2 ml lysogeny broth (LB) supplemented with 100 $\mu\text{g}/\text{ml}$ ampicillin (Amp) and 2.5 $\mu\text{g}/\text{ml}$ tetracyclin (Tet) at 37°C in an incubator rotating at 200 rpm for 6–8 h, then transferred to new tubes with a total volume of 10 ml for overnight culturing. To induce production of double-stranded RNA, cultures were incubated for 90 min in the presence of 1 mM isopropyl β -D-thiogalactopyranoside (IPTG). Bacterial cultures were pelleted by centrifugation at 4000 g for 15 min and concentrated five times. NGM agar plates supplemented with 100 $\mu\text{g}/\text{ml}$ Amp and 1 mM IPTG were seeded with 250 μl of bacterial suspension and kept at RT for 48 h in the dark. Six to eight L4 hermaphrodites per strain were transferred to individual NGM-RNAi plates against target genes, and phenotypes were analyzed in the F1 generation.

Transmission electron microscopy

For TEM, L4 animals were fixed by high-pressure freezing with the EMPACT-2 system (Leica Microsystems). Freeze-substitution (FS) was done in anhydrous acetone containing 1 % OsO_4 , 0.5 % glutaraldehyde and 0.25 % uranyl acetate for 60 h in an FS system (AFS-2; Leica Microsystems). Larvae were embedded in an Epon-Araldite mix (hard formula; EMS). Adhesive frames were used (Gene Frame 65 μl ; ThermoFisher) for flat-embedding, as previously described (KOLOTUEV *et al.*, 2012), to facilitate anterior-posterior orientation and sectioning. Ultrathin sections were cut on an ultramicrotome (UC7; Leica Microsystems) and collected on formvar-coated slot grids (FCF2010-CU; EMS). Each larva was

sectioned in five different places, with ≥ 10 μm between each grid to ensure that different cells were observed. Each grid contained ≥ 10 consecutive sections of 70 nm thickness. The TEM grids were observed using a JEM-1400 transmission electron microscope (JEOL) operated at 120 kV, equipped with a Gatan Orius SC200 camera (Gatan) and piloted by the Digital Micrograph program. The length of the microvilli was quantified using Fiji on TEM pictures of at least five sections per worm.

Excretory canal-specific mCherry::ACT-5 reporter

The *Psulp-4::mCherry::ACT-5* construct was cloned into the pBSK vector using Gibson Assembly (GIBSON *et al.*, 2009). A fragment containing 2.3 kb immediately upstream of the *sulp-4* coding sequence, and a fragment of 1.7 kb containing the entire genomic sequence of *act-5* and 215 bp of the 3' untranslated region, were amplified from *C. elegans* genomic DNA. The codon-optimized mCherry sequence with synthetic introns and a C-terminal linker was amplified from pJIR83 (Addgene 75028). Correct amplification and assembly were confirmed by Sanger sequencing. Primers used are listed in Supplementary table 3. Several stable transgenic lines were generated by microinjection of N2 young adult animals with 5 ng/ μl *Psulp-4::mCherry::ACT-5* and 10 ng/ μl *Plin-48::GFP* as a co-injection marker, which did not affect excretory canal development, and one was selected for further analysis.

Statistical analysis

All statistical analyses were performed using GraphPad Prism v.8. For population comparisons, a D'Agostino & Pearson test of normality was first performed to determine whether the data were sampled from a Gaussian distribution. For data drawn from a Gaussian distribution, comparisons between two populations were made using Student's unpaired t-test, with Welch's correction if the standard deviations of the populations differed significantly, and comparisons between more than two populations were made using a one-way ANOVA, or Welch's ANOVA if the standard deviations of the populations differed significantly. For data not drawn from a Gaussian distribution, a non-parametric test was used (Mann-Whitney U-test for two populations and Kruskal-Wallis test for more than two populations). ANOVA and non-parametric tests were followed up with multiple comparison tests of significance (Dunnett's, Tukey's, Dunnett's T3 or Dunn's). The tests of significance used and the sample sizes are indicated in the figure legends. No statistical method was used to predetermine sample sizes. No samples or animals were excluded from analysis. The experiments were not randomized, and the investigators were not blinded to allocation during experiments and outcome assessment.

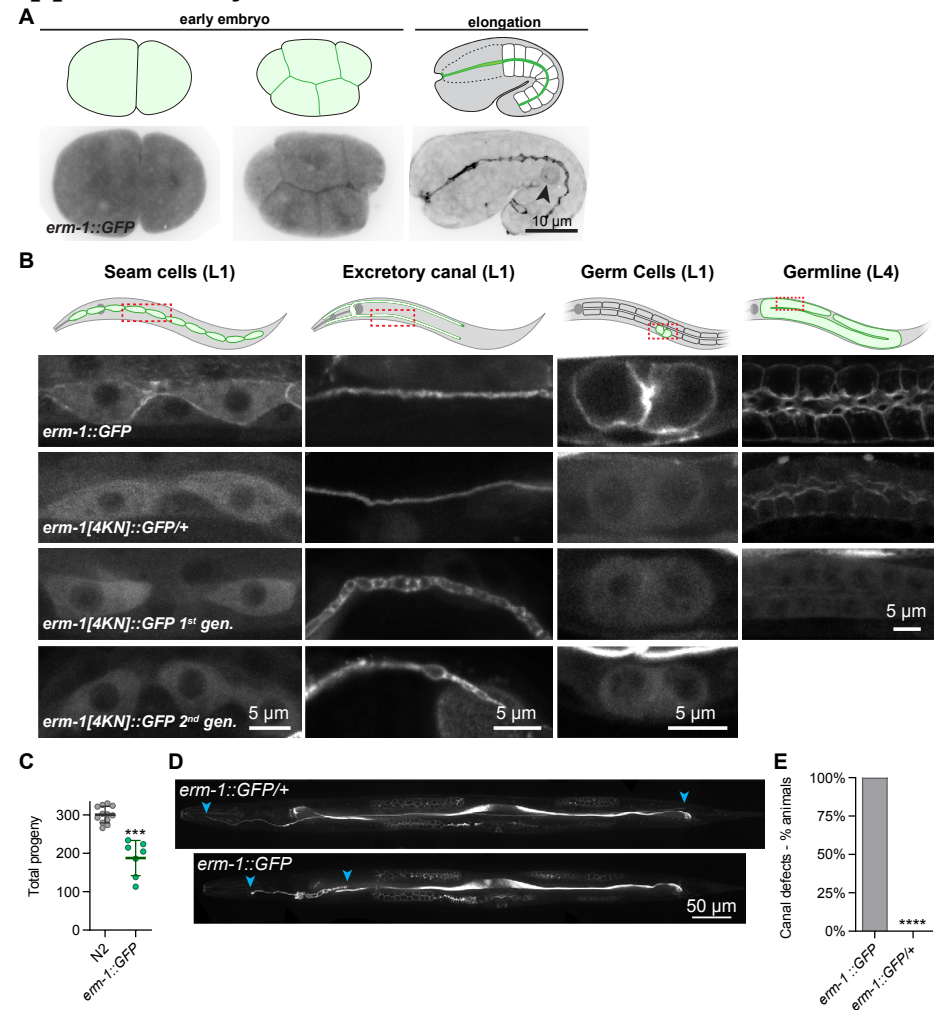
Acknowledgements

We thank J. Kerver-Stumpfova for technical assistance, H. R. Pires for the *dlg-1::mCherry* knock-in, O. Bossinger for providing the ERM-1 antibody and the BJ49 strain, M. Labouesse for sharing the ML846 strain, and M. Zerial for sharing the MZE1 strain. We also thank WormBase, the Biology Imaging Center Faculty of Sciences, Department of Biology, Utrecht University, and the electron microscopy facility of the Microscopy Rennes Imaging Center (MRIC). Some strains were provided by the *Caenorhabditis* Genetics Center, which is funded by the US National Institutes of Health (NIH) Office of Research Infrastructure Programs (P40 OD010440). The MH27 monoclonal antibody developed by R. Francis and R. H. Waterston was obtained from the Developmental Studies Hybridoma Bank, created by the National Institute of Child Health and Human Development of the NIH and maintained at The University of Iowa. We thank S. van den Heuvel, M. Harterink and members of the S. van den Heuvel, M.B. and R. Korswagen groups for helpful discussions.

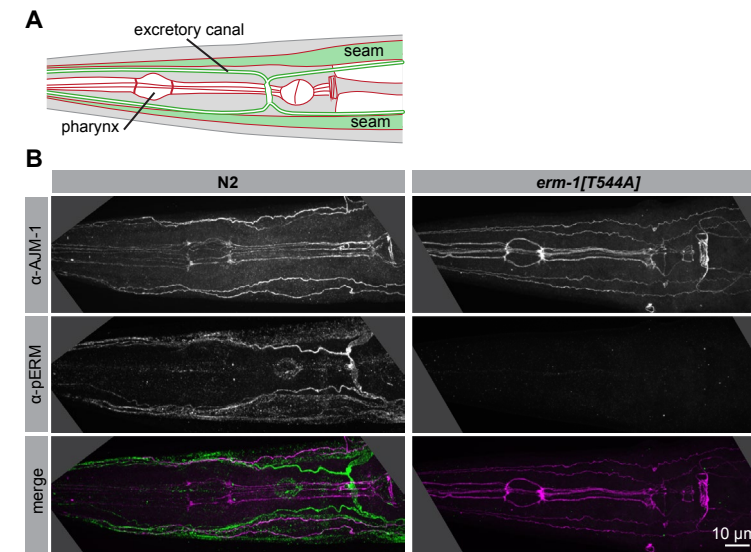
Author contributions

Conceptualization: J.J.R., M.B.; Methodology: J.J.R., J.J.S., O.N., R.S., J.C.; Formal analysis: J.J.R., J.J.S., O.N., R.S.; Investigation: J.J.R., J.J.S., O.N., R.S.; Writing - original draft: J.J.R., M.B.; Writing - review & editing: J.J.S., R.S., G.M., M.B.; Visualization: J.J.R., J.J.S., O.N., R.S., M.B.; Supervision: G.M., M.B.; Project administration: M.B.; Funding acquisition: G.M., M.B.

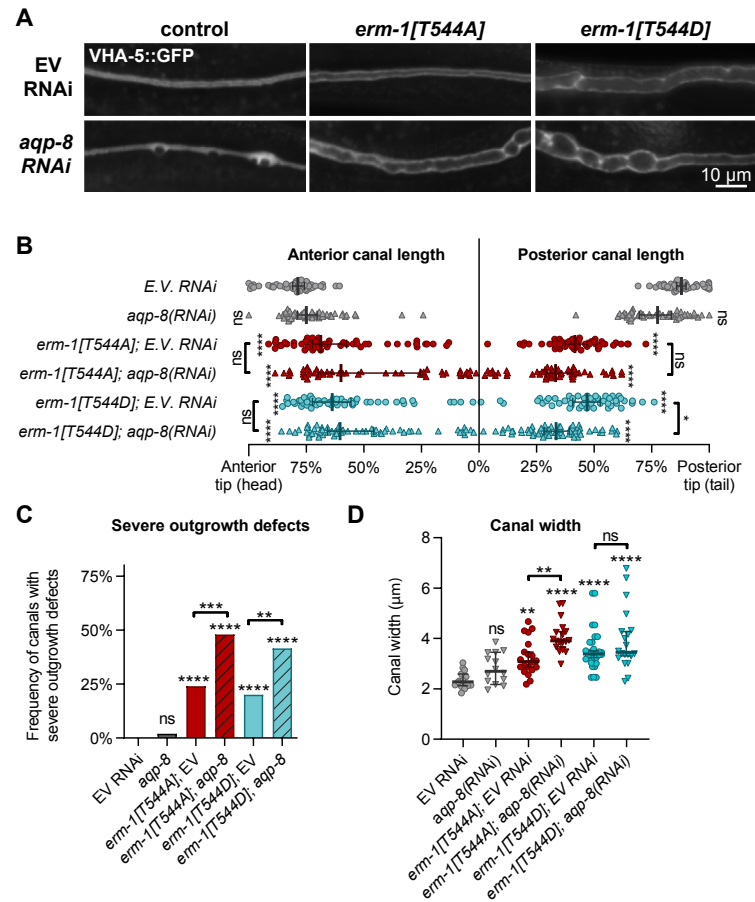
Supplementary material:



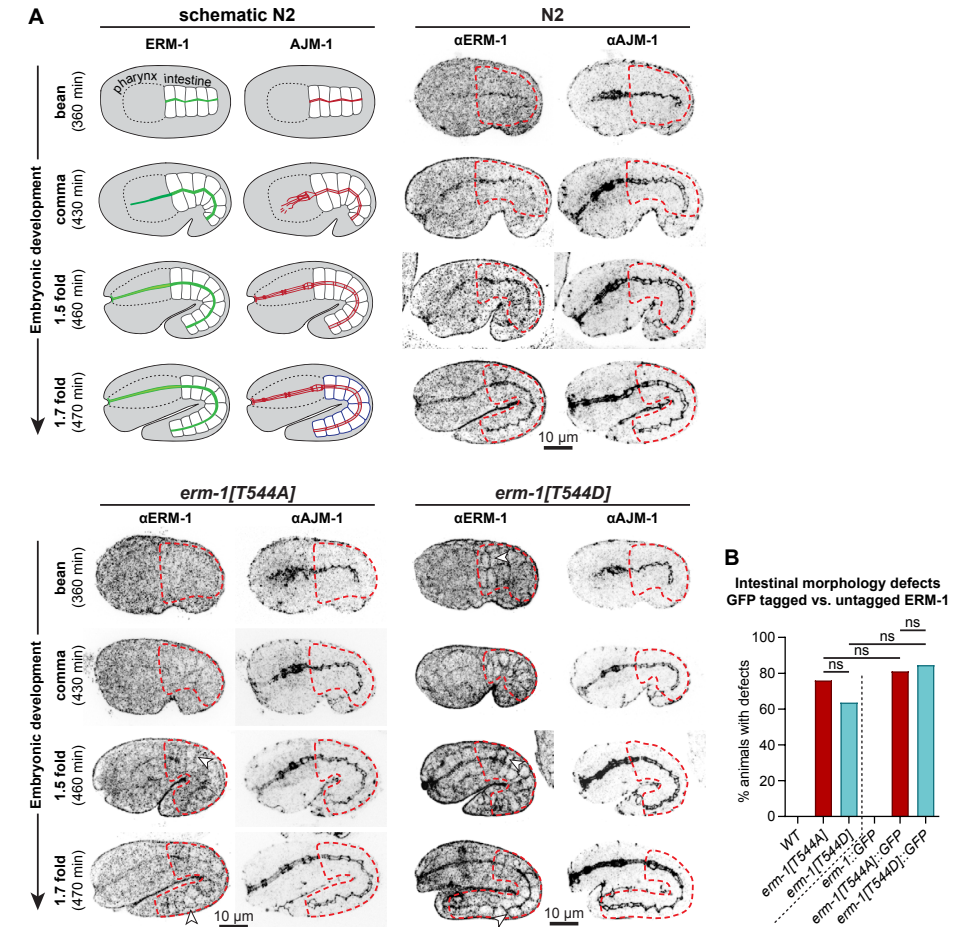
Supplementary figure 1: Distribution of ERM-1::GFP. (A) Localization of ERM-1::GFP in different embryonic stages. Arrowhead indicates a germ cell. **(B)** Localization of GFP-tagged wild-type and 4KN ERM-1 variants in different larval tissues. ERM-1[4KN]::GFP was imaged in 1st and 2nd generation homozygous and in heterozygous animals. Dashed rectangles in drawings indicate tissue and region imaged. **(C)** Quantification of total progeny. Each symbol represents the progeny of an individual animal ($n = 12, 7$). Error bars: mean \pm SD. Welch's Student t-test *** = $P \leq 0.001$. **(D)** Example of excretory canal outgrowth in heterozygous and homozygous *erm-1::GFP* animals. Arrowhead indicates posterior canal end. Images were computationally straightened. **(E)** Percentage of *erm-1::GFP* homozygous and heterozygous animals with excretory canal outgrowth defects ($n = 48, 40$). Fisher's exact test **** = $P \leq 0.0001$.



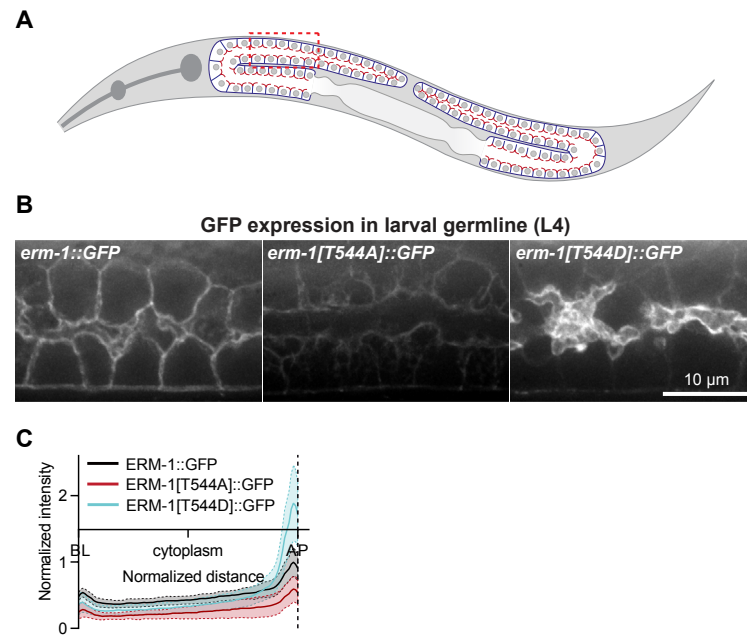
Supplementary figure 2. ERM-1[T544A] is not recognized by a phospho-ERM antibody. (A) Schematic representation of the head region imaged in adult animals in B. View is from the dorsal side and shows the lateral rows of fused seam cells, the pattern of cell junctions in the pharynx, and the excretory canal cell. Red indicates cell junctions visualized by AJM-1 staining in B, and green indicates structures where ERM-1 localizes (apical area of seam cells and excretory canal). **(B)** Fixed adults of indicated genotypes were stained with antibodies recognizing the junctional protein AJM-1 and phosphorylated ERM proteins. Images are maximum projections of a Z-stack taken through the entire width of the animal.



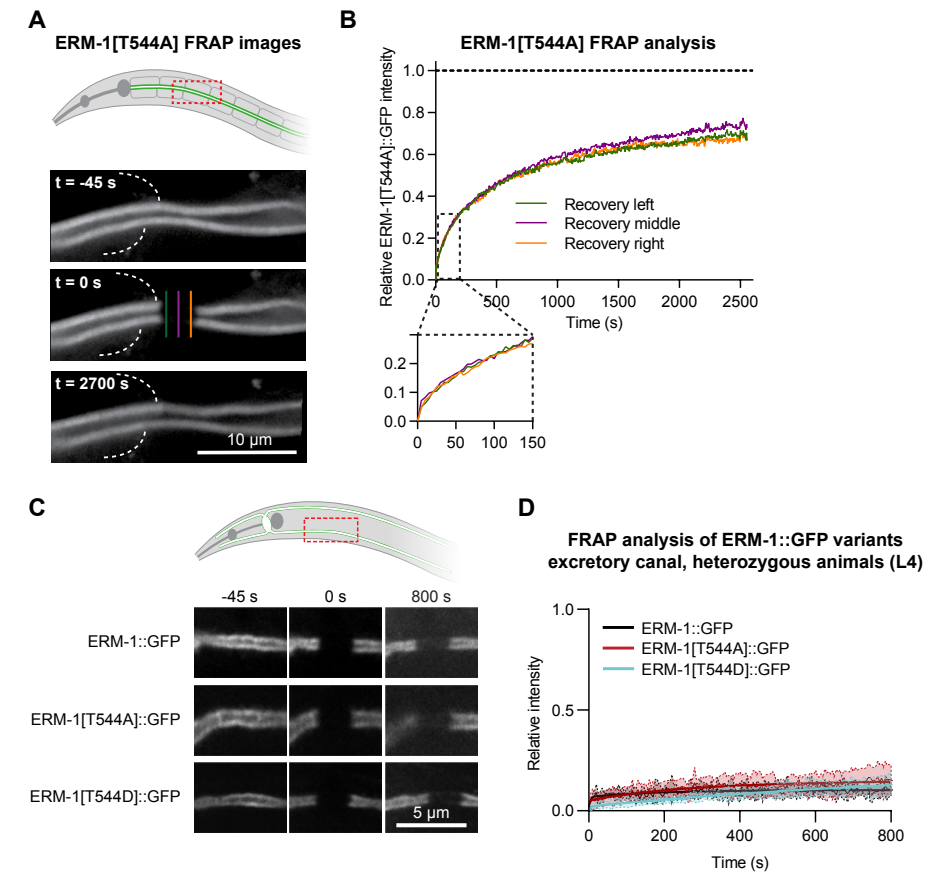
Supplementary figure 3: ERM-1 T544 phosphorylation in excretory canal lumenogenesis functions in parallel with aqp-8. (A) Excretory canal lumen morphology in L4 animals fed with empty vector (EV) or *aqp-8* RNAi clones, visualized by a VHA-5::GFP transgene using epifluorescence microscopy. Images are taken at the 1st half of a posterior canal. (B) Quantification of excretory canal outgrowth in L4 animals. All four canal branches were measured per animal, and each data point represents one branch ($n = 25, 26, 25, 25, 25, 29$ animals, from top to bottom). Error bars: median \pm 95 % CI. (C) Frequency of anterior and posterior canals from B extending less than 35 % of the distance between cell body and tips. (D) Quantification of canal width in L4 animals. Each data point represents the average of three measurements at the widest points of a single posterior canal. One canal was imaged per animal ($n = 15, 17, 13, 18, 13$ animals). Error bars: median \pm 95 % CI. Unless indicated otherwise by a connecting line, statistical comparisons are with EV RNAi. Tests of significance used: Dunn's multiple comparison test for B and D, Fisher's exact test for C. ns = not significant, * = $P \leq 0.05$, ** = $P \leq 0.01$, *** = $P \leq 0.001$, **** = $P \leq 0.0001$.



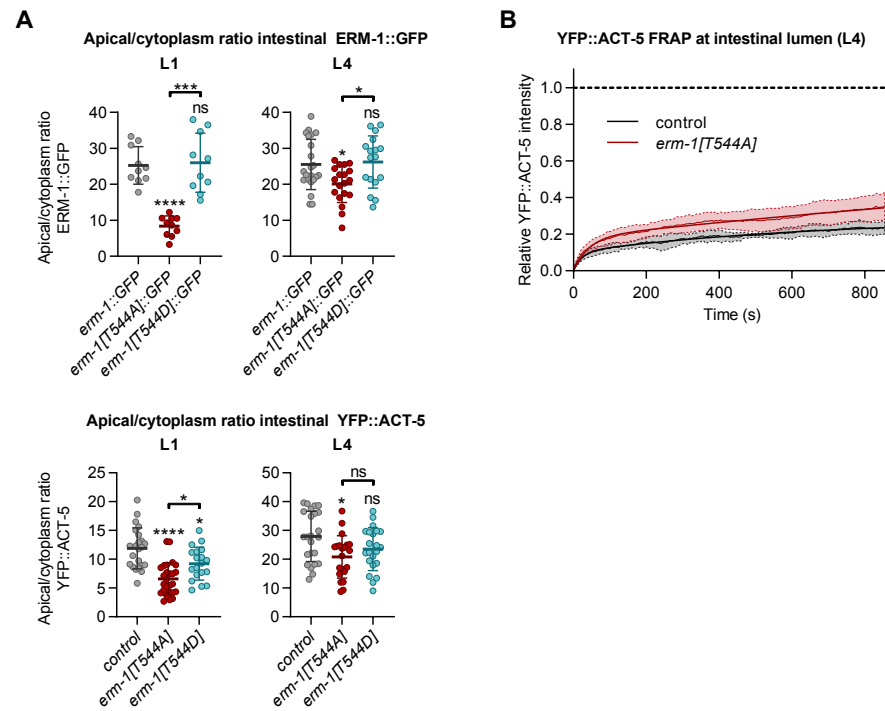
Supplementary figure 4. (A) Distribution of endogenous ERM-1 and the junctional protein AJM-1 in embryos. ERM-1 and AJM-1 were visualized by antibody staining of fixed embryos of indicated genotypes at different embryonic stages. Intestine is outlined by red dashed line. Schematic drawings show the localization of ERM-1 (green) and AJM-1 (red) in intestinal cells of wild-type embryos. Grey outlines of intestinal cells indicate the basolateral domain. Arrowheads point to examples of ectopic basolateral ERM-1 localization. (B) Comparison of intestinal morphology defects in animals expressing GFP tagged vs. untagged ERM-1[T544A] or ERM-1[T544D]. Frequency of animals with intestinal morphology defects ($n = 30, 25, 33, 71, 37, 26$). Fisher's exact test. ns = not significant.



Supplementary figure 5: Distribution of ERM-1 variants in the germline. (A) Schematic representation of the L4 germline. Dark blue represents basolateral membranes, and dark red apical membranes. Imaged region is indicated by the red dashed rectangle. (B) Distribution of GFP-tagged ERM-1 variants in the germline of live L4 larvae. Images are maximum intensity projections and were acquired and displayed with the same settings for comparison. (C) Distribution plot of GFP mean fluorescence intensity \pm S.D. along the apical-basolateral axis in the germline of L4 larvae. Intensity was normalized to the average peak intensity of wild-type animals at the apical membrane, and length was normalized between the basolateral (BL) and apical (AP) membranes. $n = 27$ animals for ERM-1::GFP, 16 for ERM-1[T544A]::GFP, 22 for ERM-1[T544D]::GFP.



Supplementary figure 6: (A) Stills from time-lapse movie of ERM-1[T544A]::GFP fluorescence recovery after photobleaching in the intestinal lumen of an L1 animal. Dotted curved lines indicate lateral membranes separating neighbor and bleached cells. **(B)** Recovery of ERM-1[T544A] at three different positions along the bleached region, as indicated by the colored lines in A. Small graph below shows the recovery within in the first 150s in greater detail. **(C)** Stills from time-lapse movies of fluorescence recovery of GFP-tagged ERM-1 variants in the excretory canal of L4 larvae. **(D)** 2500 FRAP curves of GFP-tagged ERM-1 variants at the apical membrane in the excretory canals of L4 larvae ($n = 3$ for ERM-1::GFP, 8 for ERM-1[T544A]::GFP, and 5 for ERM-1[T544D]::GFP). Animals in C and D are heterozygous, carrying one wild-type (untagged) *erm-1* copy.



Supplementary figure 7: Distribution and mobility of ACT-5 in the intestine of *erm-1* phosphorylation mutants. (A) Apical levels of ERM-1::GFP and YFP::ACT-5 in the intestines of L1 and L4 larvae. Data shown is identical to Figures 6E and 8D, but expressed as apical/cytoplasm ratio to account for variability in expression of the Pges-1::YFP::ACT-5 transgene. Each data point represents the apical/cytoplasmic ratio of the fluorescence intensity of a single animal ($n = 10$ for ERM-1::GFP in L1; 22, 19 and 17 for ERM-1::GFP L4; 23, 26 and 19 for YFP::ACT-5 in L1; and 24, 21 and 22 for YFP::ACT-5 in L4). Error bars: mean \pm SD for ERM-1::GFP and median \pm 95 % CI for YFP::ACT-5. Unless indicated otherwise by a connecting line, statistical comparisons are with control. Tests of significance: Dunnett's T3 multiple comparisons test for ERM-1::GFP quantification and Dunn's multiple comparisons test for YFP::ACT-5. ns = not significant, * = $P \leq 0.05$, ** = $P \leq 0.01$, *** = $P \leq 0.001$, **** = $P \leq 0.0001$. (B) FRAP curves of apical YFP::ACT-5 in the intestine of L4 larvae. Thin lines and shading represent the mean \pm SD, and thick lines were obtained by curve fitting averaged FRAP data with a double exponential equation. $n \geq 8$ animals.

Tissue	ERM-1 variant	Plateau	Fast half-time (s)	Slow half-time (s)	Goodness of fit R2
Intestine AP	ERM-1::GFP	19 %	8.3	1276.0	0.991
	ERM-1[T544A]::GFP	80 %	61.1	822.6	0.997
	ERM-1[T544D]::GFP	79 %	17.3	986.1	0.999
Excretory canal (homozygous)	ERM-1::GFP	25 %	12.6	429.4	0.918
	ERM-1[T544A]::GFP	24 %	2.8	386.2	0.992
	ERM-1[T544D]::GFP	24 %	1.3	196.7	0.991
Excretory canal (heterozygous)*	ERM-1::GFP/+	10 %	2.6	128.0	0.490
	ERM-1[T544A]::GFP/+	15 %	1.5	197.5	0.871
	ERM-1[T544D]::GFP/+	23 %	2.6	766.1	0.976
Germline BL	ERM-1::GFP	73 %	8.4	117.2	0.992
	ERM-1[T544A]::GFP	60 %	5.2	143.9	0.995
	ERM-1[T544D]::GFP	44 %	12.1	260.0	0.994

Supplementary table 1: Two-component association curve fit analysis of FRAP data (GraphPad Prism 8). *Data from heterozygous animal are shown for completeness, but due to poor goodness of fit no firm conclusions can be drawn.

Strain	Genotype
N2	Wild-type
GE24	<i>pha-1(e2123ts) III</i>
BOX166	<i>erm-1(mib11[erm-1[4KN]]) I / dpy-5(e61); unc-29(e403) I</i>
BOX213	<i>erm-1(mib15[erm-1::eGFP]) I</i>
BOX233	<i>erm-1(mib21[erm-1[4KN]::GFP]) I / dpy-5(e61); unc-29(e403) I</i>
BOX165	<i>erm-1(mib10[erm-1[T544A]]) I</i>
BOX163	<i>erm-1(mib9[erm-1[T544D]]) I</i>
ML846	<i>vha-5(mc38) IV; mcEx337[vha-5(+):GFP; rol-6(su1006)]</i>
BOX167	<i>erm-1(mib10[erm-1[T544A]]) I; vha-5(mc38) IV; mcEx337[vha-5(+):GFP; rol-6(su1006)]</i>
BOX168	<i>erm-1(mib9[erm-1[T544D]]) I; vha-5(mc38) IV; mcEx337[vha-5(+):GFP; rol-6(su1006)]</i>
BOX566	<i>hmr-1(he298[hmr-1::eGFP]) I; dlg-1(mib23[dlg-1::mCherry]) X</i>
BOX297	<i>erm-1(mib9[erm-1[T544D]]) I; hmr-1(he298[hmr-1::eGFP]) I; dlg-1(mib23[dlg-1::mCherry]) X</i>
BOX324	<i>erm-1(mib10[erm-1[T544A]]) I; hmr-1(he298[hmr-1::eGFP]) I; dlg-1(mib23[dlg-1::mCherry]) X</i>
MZE1	<i>unc-119(ed3) III; cbgIs91[pPept-1:PEPT-1::DsRed;unc-119(+)]; cbgIs98[pPept-1:GFP::RAB-11.1;unc-119(+)]</i>
BOX183	<i>erm-1(mib10) I; unc-119(ed3) III; cbgIs91[pPept-1:PEPT-1::DsRed;unc-119(+)]; cbgIs98[pPept-1:GFP::RAB-11.1;unc-119(+)]</i>
BOX179	<i>erm-1(mib9) I; unc-119(ed3) III; cbgIs91[Ppemt-1::PEPT-1::dsREsD, unc-119(+)]; cbgIs98[Ppemt-1::GFP::RAB-11.1, unc-119(+)]</i>
BOX218	<i>erm-1(mib19[erm-1[T544A]::GFP]) I</i>
BOX215	<i>erm-1(mib16[erm-1[T544D]::GFP]) I</i>
BOX369	<i>erm-1(mib19[erm-1[T544A]::GFP]) I; dlg-1(mib23[dlg-1::mCherry]) X</i>
BOX261	<i>mibEx55[Psulp-4::mCherry::ACT-5; Plin-48::GFP]</i>
BOX265	<i>erm-1(mib10[erm-1[T544A]]) I; mibEx55[Psulp-4::mCherry::ACT-5; Plin-48::GFP]</i>
BOX266	<i>erm-1(mib9[erm-1[T544D]]) I; mibEx55[Psulp-4::mCherry::ACT-5; Plin-48::GFP]</i>
JM125	<i>Is[Pges-1::YFP::ACT-5]</i>
BOX196	<i>erm-1(mib10[erm-1[T544A]]) I; Is[Pges-1::YFP::ACT-5]</i>
BOX197	<i>erm-1(mib9[erm-1[T544D]]) I; Is[Pges-1::YFP::ACT-5]</i>
Bj49	<i>kcls6[Pifb-2::IFB-2::CFP]</i>
BOX256	<i>erm-1(mib9[erm-1[T544D]]) I; kcls6[Pifb-2::IFB-2::CFP]</i>
BOX571	<i>erm-1(tm677)/tmC18 [dpy-5(tm1s1200) + myo-2p::Venus] I</i>

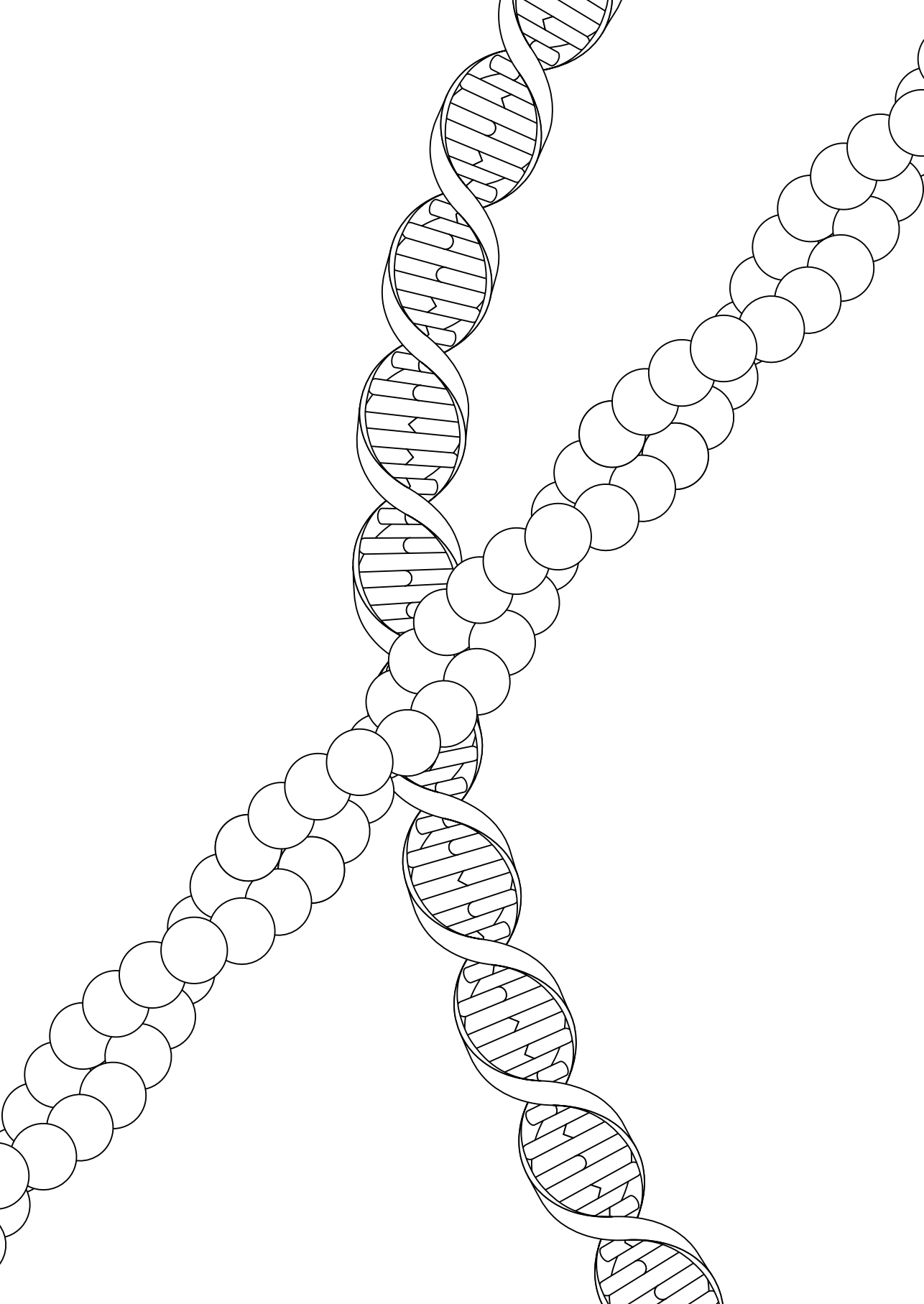
Supplementary table 2: List of strains used.

Reagents to generate the <i>Psulp-4::mCherry::ACT-5</i> construct	
<i>Psulp-4</i> left primer	CGGGCCCCCTCGAGGTCGACGGTATCGATAAGCTTGA TTGGATTCCGCAATGCTTTGA
<i>Psulp-4</i> right primer	TTTGAATACTGGAAAAATAGTTGC
mCherry left primer	CTTTTAAAATAATATGCAACTATTTTCCAGTATTCAA AATGTCCAAGGGAGAGGAGGA
mCherry right primer	CATCGATGCTCCTGAGGCTCCCGATGCTCCCTGTAGAG CTCGTCCATTCC
ACT-5 left primer	GGAGCATCGGGAGCCTCAGGAGCATCGATGGAAGAAGAA ATCGCCGCC
ACT-5 right primer	TAGTGGATCCCCGGGCTGCAGGAATTCGATAATTATAT TTTAAAAAATGAGGGGAAATAATACACAAGT
Reagents to generate <i>erm-1[4KN]</i>	
sgRNA 1 left primer	AATTACATGAGCCTTCTTATCAAT
sgRNA 1 right primer	AAACATTGATAAGAAGGCTCATGT
sgRNA 2 left primer	TCTTGATCAAACCAATTGATAAGA
sgRNA 2 right primer	AAACTCTTATCAATTGGTTTGATC
ssODN repair template	GGATTCCCATGGTCGGAGATTGTAATATATCATTCAAC GACAATAATTTTGTATCAAGCCGATCGACAATAATGCT CATGTAAGTGATTACTGTACACACAGTTTGTCTGGCA TCA
integration check left primer	CATCAAGCCGATCGACAATAAT
integration check right primer	GTAGTTACCGTTGAGCTGATTTG
Reagents to generate <i>erm-1[T544A]</i> , <i>erm-1[T544D]</i>	
sgRNA 1 left primer	AATTAAGACTCTCCGTCAAATCCG
sgRNA 1 right primer	AAACCGGATTTGACGGAGAGTCTT
sgRNA 2 left primer	TCTTACTCTCCGTCAAATCCGTGG
sgRNA 2 right primer	AAACCCACGGATTTGACGGAGAGT
ssODN repair template T544A	GCCCGATTCCAAATTTTAAATTTTTCAGAACAAAAAGGC CGGACGGGATAAATATAAAGCTCTGCGACAGATCCGTGG AGGAAACACAAAACGAAGAATCGATCAATACGAAAAAT
ssODN repair template T544D	GCCCGATTCCAAATTTTAAATTTTTCAGAACAAAAAGGC CGGACGGGATAAATATAAAGATCTGCGACAGATCCGTGG AGGAAACACAAAACGAAGAATCGATCAATACGAAAAAT
integration check left primer A	GCCGGACGGGATAAATATAAAG
integration check left primer D	GCCGGACGGGATAAATATAAAGA
integration check right primer	CCCGAGGAGAAGCACACATG

~ Table continues on the next page ~

Reagents to generate <i>erm-1::GFP</i> , <i>erm-1[4KN)::GFP</i> , <i>erm-1[T544A)::GFP</i> , <i>erm-1[T544D)::GFP</i>	
sgRNA 1 left primer	AATTAAGACTCTCCGTCAAATCCG
sgRNA 1 right primer	AAACCGGATTTGACGGAGAGTCTT
sgRNA 2 left primer	TCTTACTCTCCGTCAAATCCGTGG
sgRNA 2 right primer	AAACCCACGGATTTGACGGAGAGT
LH arm left primer	ACGTTGTAAAACGACGGCCAGTCGCCGCGAGAGGTTCCG TATTTTAAAAAACTCG
LH arm right primer step 1	TGATCGATTCTTCGTTTTGTGTTTCCTCCCCTAATCTGC CGGAGAGTCTTGTACTTGTCG
LH arm right primer step 1 A	TGATCGATTCTTCGTTTTGTGTTTCCTCCCCTAATCTGC CGCAGAGCCTTGTACTTGTCGCGTCCGG
LH arm right primer step 1 D	TGATCGATTCTTCGTTTTGTGTTTCCTCCCCTAATCTGC CGCAGATCCTTGTACTTGTCGCGTCCGG
LH arm right primer step 2	GATGCTCCTGAGGCTCCCGATGCTCCCATATTTTCGTAT TGATCGATTCTTCGTTTTGTG
RH arm left primer	CGTGATTACAAGGATGACGATGACAAGAGATAATTATTT GTTCTATCGTATTTTCCTTT
RH arm right primer	GGAAACAGCTATGACCATGTTATCGATTTTCGCTCCATCG AAACCCTTGGA
integration check left primer	CTGTCACTGACTACGACGTTCTG
integration check right primer	CCCAGGAGAAGCACACATG

Supplementary table 3: List of oligonucleotides used.



Chapter 3

ERM-1 phosphorylation and NRFL-1
redundantly control lumen formation in
the *C. elegans* intestine

Jorian J. Sepers*, João J. Ramalho*, Jason R. Kroll,
Ruben Schmidt & Mike Boxem

Division of Developmental Biology, Institute of Biodynamics and Biocomplexity, Department of
Biology, Faculty of Science, Utrecht University, Utrecht, The Netherlands

*These authors have contributed equally to this work.

This chapter is an adapted version of the following publication:

Sepers, J.J., Ramalho, J.J., Kroll, J.R., Schmidt, R. and Boxem, M., 2022. ERM-1 phosphorylation and NRFL-1 redundantly control lumen formation in the *C. elegans* intestine. *Frontiers in Cell and Developmental Biology*, 10, 769862.

Reorganization of the plasma membrane and underlying actin cytoskeleton into specialized domains is essential for the functioning of most polarized cells in animals. Proteins of the ezrin-radixin-moesin (ERM) and Na⁺/H⁺ exchanger 3 regulating factor (NHERF) family are conserved regulators of cortical specialization. ERM proteins function as membrane-actin linkers and as molecular scaffolds that organize the distribution of proteins at the membrane. NHERF proteins are PDZ-domain containing adapters that can bind to ERM proteins and extend their scaffolding capability. Here, we investigate how ERM and NHERF proteins function in regulating intestinal lumen formation in the nematode *Caenorhabditis elegans*. *C. elegans* has single ERM and NHERF family proteins, termed ERM-1 and NRFL-1, and ERM-1 was previously shown to be critical for intestinal lumen formation. Using CRISPR/Cas9-generated *nrfl-1* alleles we demonstrate that NRFL-1 localizes at the intestinal microvilli, and that this localization is depended on an interaction with ERM-1. However, *nrfl-1* loss of function mutants are viable and do not show defects in intestinal development. Interestingly, combining *nrfl-1* loss with *erm-1* mutants that either block or mimic phosphorylation of a regulatory C-terminal threonine causes severe defects in intestinal lumen formation. These defects are not observed in the phosphorylation mutants alone, and resemble the effects of strong *erm-1* loss of function. The loss of NRFL-1 did not affect the localization or activity of ERM-1. Together, these data indicate that ERM-1 and NRFL-1 function together in intestinal lumen formation in *C. elegans*. We postulate that the functioning of ERM-1 in this tissue involves actin-binding activities that are regulated by the C-terminal threonine residue and the organization of apical domain composition through NRFL-1.

Introduction

The establishment of molecularly and functionally distinct apical, basal, and lateral domains is a key feature of polarized epithelial cells. The outside-facing apical domain has a different lipid and protein composition than the basal and lateral domains and is often decorated by microvilli. The specialization of the apical domain and microvilli formation requires the activities of the ezrin/radixin/moesin (ERM) family of proteins. ERM proteins consist of an N-terminal band Four-point-one/ezrin/radixin/moesin (FERM) domain that mediates binding to the plasma membrane and membrane-associated proteins, a C-terminal tail that mediates actin binding, and a central α -helical linker region (FEHON *et al.*, 2010; McCLATCHEY, 2014). In the cytoplasm, ERM proteins are kept in an inactive, closed, conformation that masks most of regulatory and protein interaction motifs due to an intramolecular interaction between the N- and C-terminal domains (GARY & BRETSCHER, 1995; LI *et al.*, 2007; MAGENDANTZ *et al.*, 1995; PEARSON *et al.*, 2000). Binding to the plasma membrane lipid phosphatidylinositol-(4,5) bisphosphate (PIP₂) as well as phosphorylation of a

conserved C-terminal threonine residue (T567 in ezrin) promote the transition to an open and active conformation that can link the plasma membrane to the underlying actin cytoskeleton and control the spatial distribution of protein complexes at the membrane (BARRET *et al.*, 2000; COSCOY *et al.*, 2002; FIEVET *et al.*, 2004; HAO *et al.*, 2009; NAKAMURA *et al.*, 1999; ROCH *et al.*, 2010; SIMONS *et al.*, 1998; YONEMURA *et al.*, 2002).

The ability of ERM proteins to associate with other proteins can be extended by binding to the scaffolding proteins NHERF1 and NHERF2 (Na⁺/H⁺ exchanger regulatory factors 1 and 2). NHERF1/2 were identified as co-regulators of the Na⁺/H⁺ exchanger NHE3 in kidney epithelial cells (LAMPRECHT *et al.*, 1998; WEINMAN *et al.*, 1993; YUN *et al.*, 1997). Independently, NHERF1 was identified as the ERM-binding phosphoprotein 50 (EBP50), based on its ability to interact with activated ezrin and moesin (RECZEK *et al.*, 1997). NHERF1/2 are closely related proteins that contain two postsynaptic density 95/disks large/zona occludens-1 (PDZ) domains and an ERM-binding (EB) C-terminal tail that can bind to the FERM domain of active ERM proteins. Since their discovery, a large variety of NHERF1/2 interactors have been identified, including transporters like the cystic fibrosis transmembrane conductance regulator (CFTR) (SEIDLER *et al.*, 2009), growth factor receptors including EGFR and PDGFR (LAZAR *et al.*, 2004; MAUDSLEY *et al.*, 2000), and other scaffold proteins such as the NHERF family member PDZK1 (PDZ domain containing 1) (LALONDE & BRETSCHER, 2009).

The functional significance of the interaction of NHERF1/2 with ERM proteins is best understood for NHERF1/EBP50. In JEG3 cells, NHERF1/EBP50 promotes microvilli formation or stability by acting as a linker between ezrin and PDZK1, and mice lacking either ezrin or NHERF1/EBP50 show similar defects in microvilli formation and organization in the intestine (GARRETT *et al.*, 2010; LALONDE *et al.*, 2010; MORALES *et al.*, 2004; SAOTOME *et al.*, 2004). In a model of MDCK cells developing into 3D cysts, a complex of NHERF1/EBP50, ezrin, and Podocalyxin promotes apical identity and is required for lumen formation (BRYANT *et al.*, 2014). In a different 3D cyst model grown from Caco-2 colorectal cells, NHERF1/EBP50 is similarly required for apical-basal polarization and lumen formation, but in conjunction with moesin rather than ezrin (GEORGESCU *et al.*, 2014).

In addition to extending the scaffolding capacity of ERM proteins, NHERF proteins have also been reported to regulate the activity of ERM proteins. In NHERF1/EBP50 knockout mice, levels of ERM proteins in membrane fractions of kidney and intestinal epithelial cells are decreased, suggesting that NHERF1/EBP50 stabilizes ERM proteins at the plasma membrane (MORALES *et al.*, 2004). In *Drosophila* follicle cells, the single NHERF1/2 ortholog Sip1 is thought to promote phosphorylation and activation of Moesin through recruitment of the Ste20-family kinase Slik (HUGHES *et al.*, 2010). In an ovarian cancer cell line, depletion of NHERF1/EBP50 led to reduced levels of phosphorylated ERM

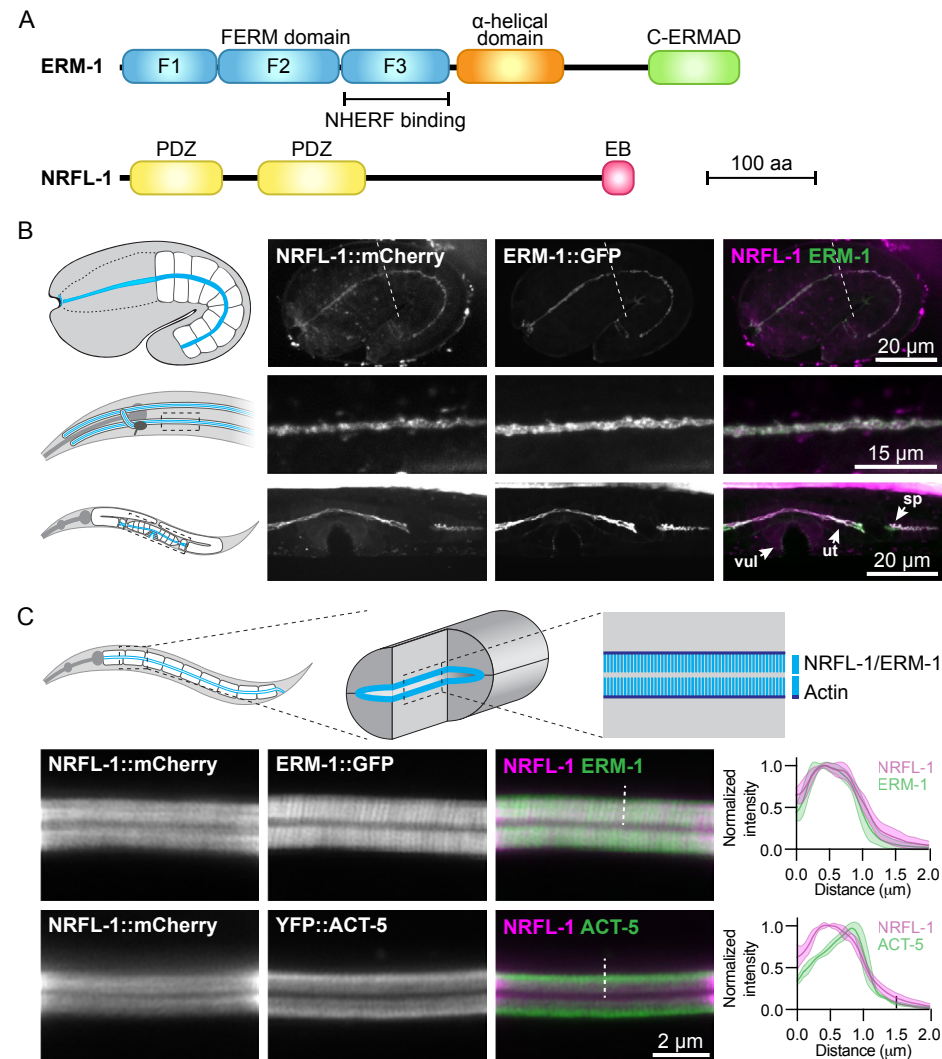


Figure 1: NRFL-1::mCherry localizes to the apical microvilli of intestinal cells. **(A)** Schematic representation of the domain organization of ERM-1 and NRFL-1. F1-F3 correspond to the three structural modules making up the FERM domain. FERM Four-point-one, ezrin, radixin, moesin; C-ERMAD C-terminal ezrin Radixin moesin (ERM) association domain; PDZ Post-synaptic density-95, disks-large and zonula occludens-1; EB ERM binding. **(B)** Distribution of NRFL-1::mCherry and ERM-1::GFP in embryos (top panels), the excretory canal in L1 larvae (middle panels), and the vulva (vul), uterus (ut) and spermatheca (sp) in L4 larvae (bottom panels). Dashed line in the embryo panels separates the pharynx (left) from the intestine (right). **(C)** Distribution of NRFL-1::mCherry relative to ERM-1::GFP and YFP::ACT-5 at the apical membrane of L4 larval intestines. Dashed line serves as an example of the line scan position used for the graphs on the right. Graphs plot the relative fluorescence intensity from the intestinal lumen to the cytoplasm. Solid line represents the mean and the shading lines the \pm SD. $n = 6$ animals for both graphs. Images were taken using spinning-disk (B) and Airyscan confocal microscopes (C), and maximum

~ Figure description continues on the next page ~

intensity projections (B) or a single plane (C) are presented. Note that due to the longer wavelength emitted by mCherry compared to GFP, the microvilli are better resolved using ERM-1::GFP than using NRFL-1::mCherry.

(pERM) upon stimulation with lysophosphatidic acid (LPA) (Oh *et al.*, 2017). Similarly, NHERF2 was found to promote the phosphorylation of ERM in bovine pulmonary artery endothelial cells, possibly through an interaction with Rho kinase 2 (ROCK2) (BORATKÓ & CSORTOS, 2013). Finally, NHERF1/EBP50 may also indirectly affect the localization of ERM proteins, by promoting the local accumulation of PIP₂ through recruitment of lipid phosphatases or kinases (GEORGESCU *et al.*, 2014; IKENOUCI *et al.*, 2013). Thus, NHERF proteins may function both as ERM effectors and regulators.

Here, we make use of the nematode *Caenorhabditis elegans* to better understand how NHERF and ERM proteins function together to promote apical domain identity. The *C. elegans* genome encodes single orthologs of each protein family, termed NRFL-1 and ERM-1, that are highly similar in sequence and domain composition to their counterparts in other organisms (Figure 1A; Supplementary figure 1A). ERM-1 localizes to the apical surface of several epithelial tissues and is essential for apical membrane morphogenesis in the intestine (GÖBEL *et al.*, 2004; VAN FÜRDEN *et al.*, 2004). Loss of *erm-1* in the intestine causes constrictions, loss of microvilli, severe reduction in the levels of apical actin, and defects in the accumulation of junctional proteins (BERNADSKAYA *et al.*, 2011; GÖBEL *et al.*, 2004; VAN FÜRDEN *et al.*, 2004). Recently, we demonstrated that the functioning of ERM-1 critically depends on its ability to bind membrane phospholipids, while phosphorylation of a C-terminal regulatory threonine residue modulates ERM-1 apical localization and dynamics (CHAPTER 2).

In contrast to ERM-1, little is known about the functioning of NRFL-1. A yeast-two hybrid screen identified the amino acid transporter (AAT) family protein AAT-6 as an interactor of NRFL-1 (HAGIWARA *et al.*, 2012). However, the effects of NRFL-1 loss are minor. In aging adults, AAT-6 is no longer retained at the luminal membrane of the intestine in *nrfl-1* mutants, while younger *nrfl-1* mutants show increased mobility of AAT-6 by fluorescence recovery after photobleaching (FRAP). Moreover, *nrfl-1* mutants are homozygous viable, demonstrating that NRFL-1 is not critical for intestinal development (HAGIWARA *et al.*, 2012).

To investigate the relationship between ERM-1 and NRFL-1, we used CRISPR/Cas9 engineering to generate an *nrfl-1* deletion mutant, a mutant lacking the ERM-1 binding domain, and fluorescently tagged NRFL-1 variants. We show that NRFL-1 localizes to the apical microvillar domain of the intestine, and that this localization depends on the ability of NRFL-1 to bind to ERM-1 via the C-terminal ERM-1 binding domain. The loss of *nrfl-1* did not affect the localization, phosphorylation status, or protein dynamics of ERM-1, indicating that *C. elegans* NRFL-1 does not control the activity of ERM-1. However, when

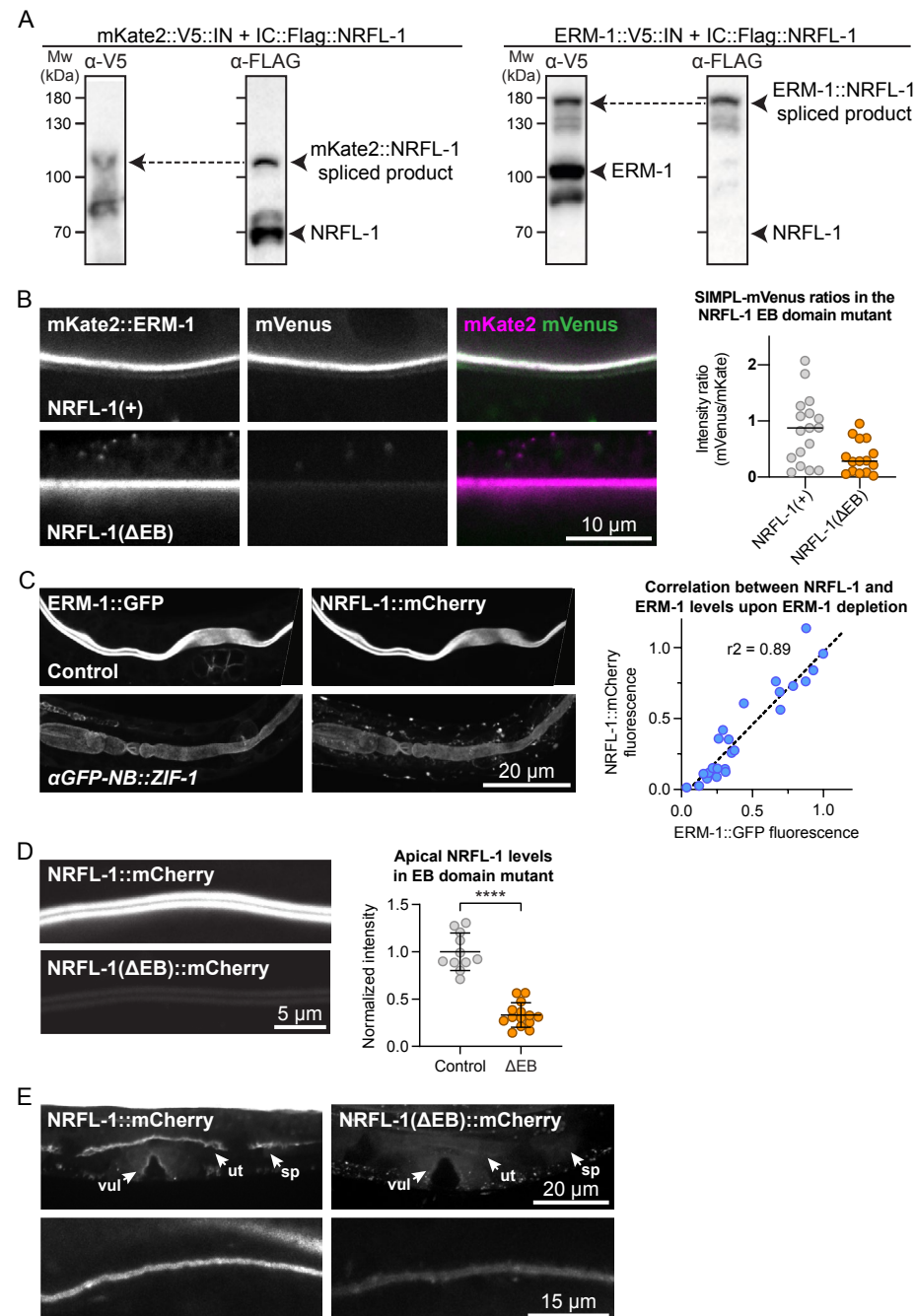


Figure 2: NRFL-1 localizes to the apical domain through ERM-1 binding. (A) Detection of an ERM-1–NRFL-1 interaction using the SIMPL system. V5 and FLAG epitopes are detected by western blot. Arrowheads indicate both unspliced proteins and the higher molecular weight covalently linked fusion proteins, generated by Intein splicing activity. Little splicing

~ Figure description continues on the next page ~

of NRFL-1 is observed with the control mKate2::V5::IN protein, while all NRFL-1 is spliced to ERM-1 in animals expressing ERM-1::V5::IN. (B) Detection of an interaction of ERM-1 with wild-type NRFL-1, but not with NRFL-1(ΔEB), using the SIMPL-mVenus system. NRFL-1a::InteinC-3xFLAGVC155 [NRFL-1(+)] or NRFL-1a(ΔEB)::InteinC-3xFLAG-VC155 [NRFL-1(ΔEB)] are expressed with mKate2::ERM-1::VN155-HA-V5-InteinN (mKate2::ERM-1). Fluorescence micrographs show representative examples. Graphs show quantification of apical mVenus levels, expressed as a ratio over mKate2::ERM-1 to account for varying expression levels of the extrachromosomal array. Each data point represents a single intestinal cell. Lines indicate median. $n = 17$ cells for NRFL-1(+) and 15 cells for NRFL-1(ΔEB). (C) Quantification of apical levels of NRFL-1::mCherry vs. ERM-1::GFP in L1 larval intestines upon different levels of ERM-1::GFP depletion by expression of an anti-GFP nanobody::ZIF-1 fusion protein. Fluorescence micrographs show representative examples, graph shows quantification of signal intensity at the apical membrane. Each data point in the graph represents a single animal, and the line a linear regression. Values are normalized to the mean intensity in control animals. $n = 25$ animals. (D) Quantification of apical levels of NRFL-1(ΔEB)::mCherry relative to NRFL-1::mCherry at the apical membrane of L1 larval intestines. Fluorescence micrographs show representative examples, and the graph the quantification. Each data point in the graph represents a single animal, and values are normalized to the mean intensity in control animals. Error bars: mean \pm SD; Statistical test: Welch's Student's t-test; **** $p \leq 0.0001$. $n = 10$ animals for NRFL-1::mCherry and 14 animals for NRFL-1(ΔEB)::mCherry. (E) Localization of NRFL-1::mCherry and NRFL-1(ΔEB)::mCherry in the vulva (vul), uterus (ut) and spermatheca (sp) in L4 larvae (top panels), and the excretory canal in L1 larvae (bottom panels). Images of the same tissue were acquired and displayed with the same settings for comparison. All images were taken using a spinning disk confocal microscope, and a single plane (B) or maximum intensity projections (C,D, E) are presented.

we combined the *nrfl-1* null mutant with *erm-1* mutants that block or mimic phosphorylation of the C-terminal threonine 544 residue, we observed severe intestinal defects, resembling the effects of strong loss of *erm-1* function. In mice, ezrin was shown to form distinct complexes with NHERF1/EBP50 and actin. As the ERM-1 phosphorylation mutants affect the ability of ERM-1 to interact with actin, we postulate that the activities of ERM-1 in the intestine redundantly involve actin binding and the organization of apical domain composition through NRFL-1.

Results

NRFL-1 localizes to the apical domain through ERM-1 binding

To investigate the relationship between NRFL-1 and ERM-1, we first examined if NRFL-1 colocalizes with ERM-1. We used CRISPR/Cas9 to engineer an endogenous C-terminal NRFL-1::mCherry fusion, which tags all predicted isoforms. Animals homozygous for the *nrfl-1::mCherry* knock-in are viable and have a wild-type appearance. We detected expression of NRFL-1 in multiple epithelia including the intestine, excretory canal, pharynx, uterus, and spermatheca (Figures 1B, C). In each of these tissues, NRFL-1::mCherry co-localized with an endogenous ERM-1::GFP fusion protein at the cortex (Figures 1B, C). In the embryo, NRFL-1 localized to the nascent apical domain of intestinal cells, overlapping with ERM-1 (Figure 1B). Confocal super resolution

imaging of the intestine in larval stages showed co-localization of NRFL-1 with ERM-1::GFP and YFP::ACT-5 at microvilli, apical to the more intense belt of YFP::ACT-5 at the terminal web (Figure 1C). The observed distribution of NRFL-1::mCherry is consistent with previous observations in *C. elegans* (HAGIWARA *et al.*, 2012), as well as with localization of EBP50 in mammalian epithelial tissues (INGRAFFEA *et al.*, 2002; KREIMANN *et al.*, 2007; MORALES *et al.*, 2004).

We previously showed that ERM-1 and NRFL-1 interact in a yeast two-hybrid assay and in pull-downs from mammalian cultured cells (KOORMAN *et al.*, 2016). To determine if these proteins interact in a more physiological setting, we used the recently developed split intein-mediated protein ligation (SIMPL) system that relies on protein splicing by split intein domains to detect protein-protein interactions (YAO *et al.*, 2020). We ubiquitously expressed ERM-1 fused to the intein N-terminal fragment (IN) and the V5 epitope, and NRFL-1 fused to the C-terminal fragment (IC) and the FLAG epitope. We observed full splicing of NRFL-1 to ERM-1 by western blot of *C. elegans* lysates, apparent as a high molecular weight band that stains with both V5 and FLAG antibodies (Figure 2A). In contrast, a negative control pair consisting of IC-tagged NRFL-1 and IN-tagged mKate2 showed only limited splicing of NRFL-1 to mKate2 (Figure 2A). To visualize if splicing occurs *in vivo* in the intestine, we modified the SIMPL system by including a split mVenus tag. We added the mVenus N-terminal fragment (VN155) to ERM-1::V5-IN and mVenus C-terminal fragment (VC155) to IC-FLAG::NRFL-1, such that upon intein splicing the reconstituted mVenus becomes linked to NRFL-1 (KODAMA & HU, 2010). We readily observed localization of mVenus at the apical domain of intestinal cells, indicating that NRFL-1 and ERM-1 interact in this tissue (Figure 2B).

We next investigated whether NRFL-1 distribution to the apical plasma membrane is dependent on ERM-1, by analyzing NRFL-1::mCherry upon tissue-specific depletion of ERM-1. To deplete ERM-1 in intestinal cells, we introduced an anti-GFP-nanobody::ZIF-1 fusion driven by the intestine-specific *elt-2* promoter as an extrachromosomal array in animals expressing endogenous ERM-1::GFP and NRFL-1::mCherry (WANG *et al.*, 2017). Expression of the nanobody::ZIF-1 fusion resulted in variable levels of ERM-1::GFP depletion. The apical levels of ERM-1::GFP and NRFL-1::mCherry showed a linear correlation, indicating that apical recruitment of NRFL-1 in the intestine directly depends on ERM-1 (Figure 2C).

The interaction between mammalian EBP50 and ezrin requires the C-terminal EB domain (FINNERTY *et al.*, 2004; RECZEK & BRETSCHER, 1998; RECZEK *et al.*, 1997), which is conserved in NRFL-1 (Figures 1A; Supplementary figure 1A). To determine if the NRFL-1 EB domain is required for the interaction with ERM-1, we repeated the SIMPL-mVenus experiment using an NRFL-1(Δ EB) mutant that lacks the C-terminal 28 amino acids of NRFL-1. Compared to wild-type NRFL-1,

we observed only residual apical localization of mVenus in intestinal cells, indicating that the interaction of NRFL-1 with ERM-1 depends on the presence of the EB domain (Figure 2B).

To determine if the EB domain is necessary for the apical localization of NRFL-1, we used CRISPR/Cas9 to engineer the 28 aa EB deletion in the *nrfl-1::mCherry* strain. The resulting *nrfl-1(Δ EB)::mCherry* animals are homozygous viable, consistent with the lack of severe defects in previously described *nrfl-1* mutants (HAGIWARA *et al.*, 2012; NA *et al.*, 2017). We detected a dramatic reduction in apical levels of NRFL-1(Δ EB)::mCherry in intestinal cells when compared with NRFL-1::mCherry (Figure 2D). NRFL-1(Δ EB)::mCherry also failed to localize at the cortex in the uterus and spermatheca, while apical levels in the excretory canal were reduced (Figure 2E). These results indicate that apical recruitment of NRFL-1 is mediated by the EB domain. However, the presence of some residual apical NRFL-1(Δ EB)::mCherry in the intestine and excretory canal suggests the existence of alternative membrane-targeting mechanisms. Collectively, our results show that the interaction between ERM and NHERF proteins is conserved in *C. elegans*, and that the localization of NRFL-1 is largely mediated by its interaction with ERM-1.

NRFL-1 cooperates with ERM-1 phosphorylation in regulating intestinal lumen formation

We next wanted to investigate the effects of loss of NRFL-1 on intestinal lumen formation. Previous studies using partial deletion alleles of *nrfl-1* indicated that loss of NRFL-1 alone does not cause defects in the formation of the intestine (HAGIWARA *et al.*, 2012; NA *et al.*, 2017). To rule out the possibility that the lack of severe defects is due to the production of truncated NRFL-1 proteins, we used CRISPR/Cas9 genome engineering to generate the *nrfl-1(mib59)* deletion allele. This allele lacks almost the entire *nrfl-1* locus and additionally causes a frameshift in the first exon of the long isoforms (Figure 3A). Hence, we refer to *mib59* as *nrfl-1(null)*. The *mib59* deletion also removes a candidate non-coding RNA and overlapping 21U-RNA located in the large 3rd exon of *nrfl-1a*. Animals homozygous for the *nrfl-1(null)* allele are viable, have a healthy appearance, and normal brood sizes, confirming that NRFL-1 is not essential for *C. elegans* development (Figure 3B, C).

One of the possible reasons for the lack of a severe intestinal phenotype in *nrfl-1(null)* animals is that NRFL-1 may only mediate part of the functions of ERM-1 in the intestine. To investigate this possibility, we made use of the non-phosphorylatable *erm-1[T544A]* and phosphomimetic *erm-1[T544D]* alleles we generated previously (CHAPTER 2). Both mutants cause a delay in the apical recruitment of ERM-1 and actin during embryogenesis, and the appearance of constrictions along the course of the lumen that only occasionally persist to the L1 stage. In contrast to *erm-1* RNAi or strong loss-of-function alleles, however,

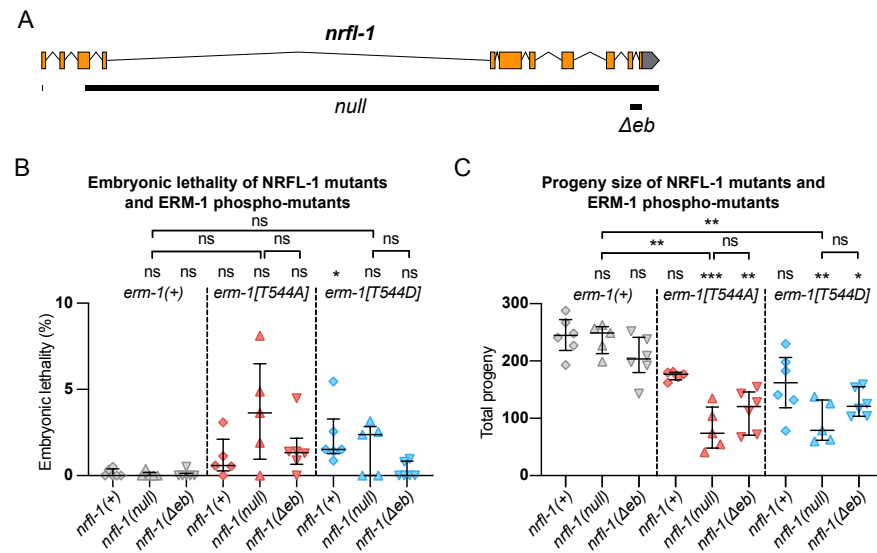


Figure 3: NRFL-1 cooperates with ERM-1 C-terminal phosphorylation. (A) Gene model for *nrfl-1a*. Orange boxes represent exons and lines represent introns. Grey box represents 3' untranslated region. Black bars denote the regions deleted in null and Δeb alleles. (B, C) Quantification of embryonic lethality (B) and total progeny (C) from parents of indicated genotypes. Each data point represents the embryonic lethality (B) or progeny (C) of a single animal; $n = 5$ or 6 . Error bars: mean \pm SD. Statistical test: Kruskal-Wallis test with Dunn's multiple comparison correction.

these animals are viable. Thus, *erm-1[T544A]* and *erm-1[T544D]* represent partial loss-of-function alleles that may act as a sensitized background to reveal the contribution of NRFL-1 to ERM-1 functioning. We therefore generated double mutants that carry the *nrfl-1(null)* allele and either of the *erm-1[T544A]* or *erm-1[T544D]* alleles. As a first indicator of synthetic defects, we examined the double mutant strains for embryonic lethality or an increase in the mild brood size defect observed in *erm-1[T544A]* and *erm-1[T544D]* mutants. We did not observe strong embryonic lethality in any mutant combination ($< 5\%$, Figure 3B). However, combining *nrfl-1(null)* with either *erm-1* phosphorylation mutant resulted in a strongly reduced brood size (Figure 3C). In addition, many larvae in the double mutant combination had a sick appearance and developed slowly. Nevertheless, both double mutants can be maintained as homozygotes, unlike strong *erm-1* loss of function mutants.

We next examined the formation of the intestinal lumen and actin distribution using YFP::ACT-5 as a marker. We did not detect any defects in apical enrichment of ACT-5 or intestinal morphology in *nrfl-1(null)* embryos and larvae (Figures 4A–C). Combining the *erm-1[T544A]* and *erm-1[T544D]* alleles with the *nrfl-1(null)* allele significantly increased the frequency of intestinal constrictions and their persistence until larval development (Figures 4A, C). Intestines of early larval *nrfl-1(null); erm-1[T544A]* and *nrfl-1(null);*

erm-1[T544D] animals were characterized by a cystic appearance and multiple constrictions that block intestinal flow as seen in feeding assays with fluorescent membrane-impermeable dextran (Supplementary figure 2A). In surviving L2 or older animals, we only observed morphological defects but no lumen discontinuities, indicating that the early larval arrest in double mutants is due to a block of flow of food through the intestine (Supplementary figure 2B). In addition to the increase in intestinal constrictions, we also observe that loss of *nrfl-1* caused a further decrease in the apical levels of YFP::ACT-5 in *erm-1[T544A]* and *erm-1[T544D]* mutant animals (Figure 4B).

Finally, as the EB domain is essential for the apical localization of NRFL-1 and its interaction with ERM-1, we determined if loss of the EB domain results in similar synergistic phenotypes with the ERM-1 phosphorylation mutants as complete loss of NRFL-1. We used CRISPR/Cas9 genome engineering to generate a second *nrfl-1(Δeb)* allele, also removing the final 28 aa but lacking the mCherry tag used above (Figure 3A). Similar to our observations for the mCherry-tagged variant, homozygous *nrfl-1(Δeb)* mutants are viable and show no significant defects in brood size, intestinal development, or apical ACT-5 enrichment (Figures 3B, C; Figures 4A–C). However, when combined with *erm-1[T544A]* or *erm-1[T544D]*, the resulting double mutants showed similar defects in viability, growth, brood size, intestinal development, and ACT-5 enrichment as observed using the *nrfl-1(null)* allele (Figures 3B, C; Figures 4A–C). Thus, the *nrfl-1(Δeb)* allele behaves like a null allele of *nrfl-1*. Taken together, our data show that NRFL-1 and ERM-1 function together in promoting lumen formation in the *C. elegans* intestine, and the binding to ERM-1 is essential for the functioning of NRFL-1 in the intestine.

NRFL-1 does not directly regulate ERM-1 activity

NRFL-1 could function together with ERM-1 in at least two ways. It could act as a scaffold protein that is required for ERM-1 to organize protein complexes at the membrane, or it could regulate the activity of ERM-1 itself. To distinguish between these possibilities, we investigated whether loss of NRFL-1 affects the distribution, mobility, or T544 phosphorylation status of ERM-1. We first analyzed the distribution of ERM-1::GFP in larval *nrfl-1(null)* mutants. We did not detect any change in ERM-1::GFP subcellular localization or levels at the apical membrane in the intestine (Figure 5A). Moreover, FRAP analysis demonstrated that the mobility of ERM-1::GFP at the apical intestinal membrane was not significantly altered in *nrfl-1(null)* larvae (Figure 5B). We next investigated whether NRFL-1 regulates ERM-1 C-terminal phosphorylation by staining *nrfl-1(null)* mutants with an antibody specific for the C-terminal phosphorylated form of ERM proteins (pERM). The residues used to raise this antibody are fully conserved between mammals and *C. elegans* (CHAPTER 2). Nevertheless, we first confirmed the specificity of the antibody for T544

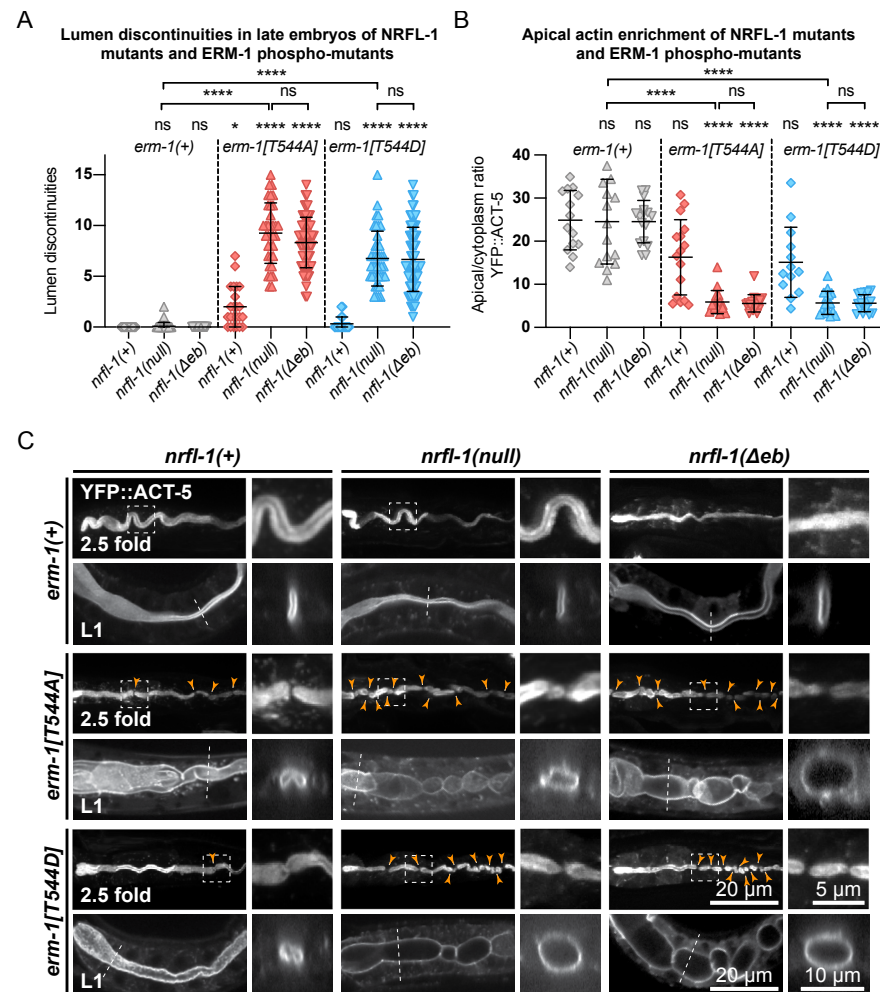


Figure 4: ERM-1 phosphorylation and NRFL-1 redundantly contribute to intestinal morphology. (A) Quantification of lumen discontinuities in 2.5-fold stage embryos of indicated genotypes expressing YFP::ACT-5. Each data point represents a single animal. Error bars: mean \pm SD. Statistical test: Kruskal-Wallis test with Dunn's multiple comparison correction. *nrfl-1(+); erm-1(+)* n = 19, *nrfl-1(null); erm-1(+)* n = 35, *nrfl-1(Δ eb); erm-1(+)* n = 48, *nrfl-1(+); erm-1[T544A]* n = 23, *nrfl-1(null); erm-1[T544A]* n = 35, *nrfl-1(Δ eb); erm-1[T544A]* n = 61, *nrfl-1(+); erm-1[T544D]* n = 28, *nrfl-1(null); erm-1[T544D]* n = 41, *nrfl-1(Δ eb); erm-1[T544D]* n = 69. (B) Quantification of the apical-cytoplasm ratio of YFP::ACT-5 in L1 larvae of indicated genotypes. Each data point represents a single animal. Error bars: mean \pm SD. Statistical test: Kruskal-Wallis test with Dunn's multiple comparison correction. *nrfl-1(+); erm-1(+)* n = 14, *nrfl-1(null); erm-1(+)* n = 15, *nrfl-1(Δ eb); erm-1(+)* n = 16, *nrfl-1(+); erm-1[T544A]* n = 16, *nrfl-1(null); erm-1[T544A]* n = 16, *nrfl-1(Δ eb); erm-1[T544A]* n = 16, *nrfl-1(+); erm-1[T544D]* n = 13, *nrfl-1(null); erm-1[T544D]* n = 16, *nrfl-1(Δ eb); erm-1[T544D]* n = 16. (C) Representative images of intestinal defects in 2.5-fold stage embryos and L1 larvae of indicated genotypes, expressing YFP::ACT-5 as an apical marker. Images of the 2.5-fold stage embryos were computationally straightened, and the

~ Figure description continues on the next page ~

orange arrowheads indicate the constrictions in the lumen. Small panels to the right of each embryo panel show an enlargement of the region indicated by the dashed box, and small panels to the right of each L1 larva show a crosssection view of the intestine at the position indicated by the dotted line. All images are taken using a spinning-disk confocal microscope, and maximum intensity projections are presented.

phosphorylated ERM-1 by immunostaining of ERM-1[T544A] mutant animals. We readily detected pERM staining of the intestinal lumen in wild-type larvae, while no staining was observed in ERM-1[T544A] animals (Supplementary figure 3A). Moreover, treatment of embryos with a phosphatase abolished staining with the pERM antibody (Supplementary figure 3B). Thus, the pERM antibody is specific for T544 phosphorylated ERM-1. We then stained *nrfl-1(+)* and *nrfl-1(null)* animals with the pERM antibody. In both backgrounds, the pERM antibody stained the lumen of the intestine, indicating that loss of *nrfl-1* does not significantly alter the phosphorylation status of the C-terminal regulatory threonine of ERM-1 (Figure 5C). Taken together, our results show that NRFL-1 does not regulate the distribution, dynamics, or phosphorylation of ERM-1, and therefore does not seem to directly regulate ERM-1.

Discussion

ERM and NHERF proteins function together in the specialization of polar membrane domains in several mammalian cell types. Here, we show that this cooperation is conserved in *C. elegans*, and that ERM-1 and NRFL-1 function together in lumen formation in the intestine. NRFL-1 physically interacts with ERM-1 through its C-terminal EB domain. The interaction with ERM-1 is responsible for the apical localization of NRFL-1 in the intestine, as depletion of ERM-1 or deletion of the EB domain results in a loss of NRFL-1 apical localization.

Loss of *nrfl-1* by itself did not cause overt defects in intestinal formation, animal development, or viability. Three previous partial deletion alleles of *nrfl-1* have been described: *ok2292*, *tm3501*, and *ok297* (HAGIWARA *et al.*, 2012; NA *et al.*, 2017). No severe defects in animal development were reported for *ok2292* or *tm3501* (HAGIWARA *et al.*, 2012). However, *nrfl-1(ok297)* animals were reported to have ruptured vulva and sterile phenotypes (NA *et al.*, 2017). Given that neither of the other two previously characterized alleles nor our newly generated *nrfl-1* deletion allele display these phenotypes, we think it is likely that the *ok297* strain analyzed either contains additional background mutations or that *ok297* represents a neomorphic allele of *nrfl-1*. The non-essential role of *nrfl-1* contrasts with data in mice, where NHERF1/EBP50 loss causes defects in intestinal microvilli formation (MORALES *et al.*, 2004), and in *Drosophila*, where *Sip1* mutants cause morphological defects in the follicle cells surrounding the oocytes and late embryonic lethality (HUGHES *et al.*, 2010).

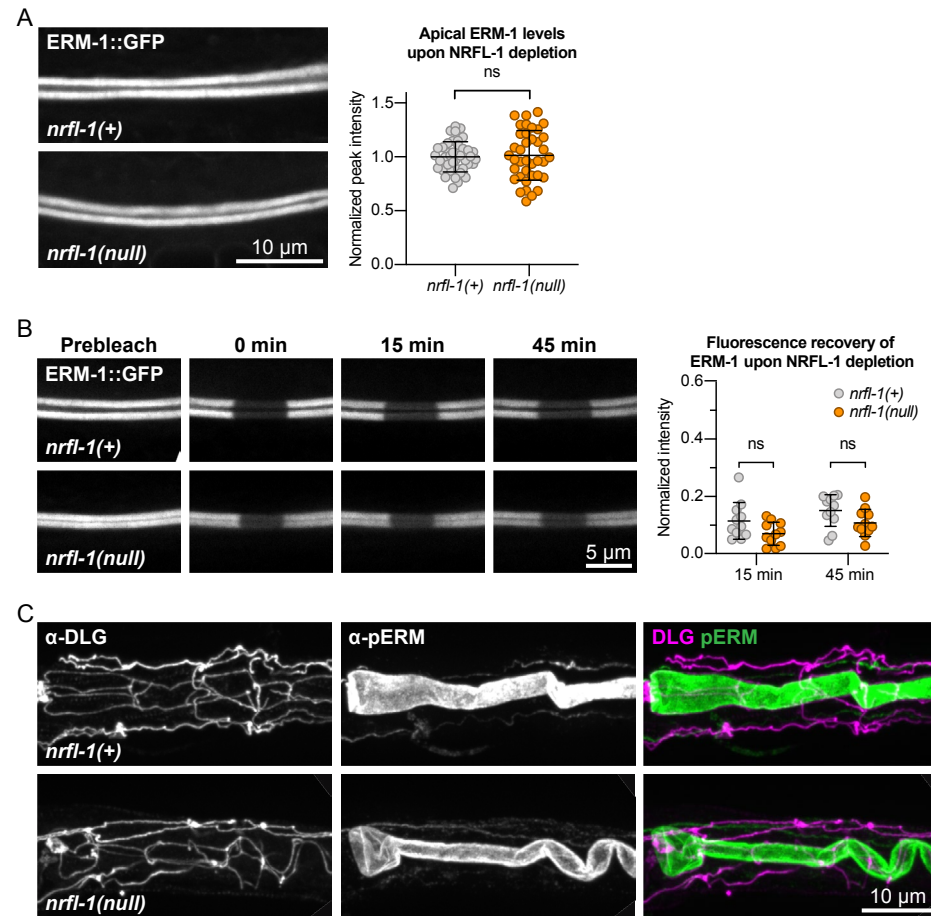


Figure 5: NRFL-1 does not regulate ERM-1 apical accumulation, dynamics, or phosphorylation status. (A) Representative images and quantification of ERM-1::GFP levels at the apical membrane of intestines in *nrfl-1(+)* and *nrfl-1(null)* L4 larvae. Each data point represents a single animal, and values are normalized to the mean intensity in control animals. Error bars: mean \pm SD. Statistical test: Unpaired Student's t-test. *nrfl-1(+)* n = 40, *nrfl-1(null)* n = 38. (B) FRAP analysis of apical ERM-1::GFP in the intestine of *nrfl-1(+)* and *nrfl-1(null)* L4 larvae. Fluorescence micrographs show representative examples. Graph shows the fluorescence intensity of ERM-1 in the photobleached region at the apical intestinal domain during recovery. Each data point represents a single animal, and values are relative to prebleach levels. Error bars: mean \pm SD. Statistical test: Unpaired Student's t-test. n = 11 for both genotypes and both timepoints. (C) Representative images of fixed *nrfl-1(+)* and *nrfl-1(null)* larvae stained with antibodies recognizing the junctional protein DLG-1 (α -DLG) and phosphorylated ERM-1 (α -pERM).

Combining the *nrfl-1(null)* deletion mutant with phosphorylation-defective *erm-1[T544A]* or *erm-1[T544D]* mutants resulted in severe defects in intestinal lumen formation. Double mutant animals have a cystic intestinal lumen, characterized by distended regions and severe constrictions. These animals develop slowly or arrest during early larval development, likely due at least

in part to the inability of luminal contents to travel through the digestive system. The double mutant intestinal phenotype is similar to that described for *erm-1(RNAi)* and the *erm-1(tm677)* deletion allele (GÖBEL *et al.*, 2004; VAN FÜRDEN *et al.*, 2004), and to an ERM-1 mutant unable to bind to the plasma membrane (ERM-1[4KN]) (CHAPTER 2). Nevertheless, complete loss of *erm-1* functioning causes maternal effect L1 lethality, while *erm-1[T544A]; nrfl-1* and *erm-1[T544D]; nrfl-1* double mutant strains can be maintained homozygously despite the developmental defects.

In many other systems, the loss of NHERF proteins results in similar phenotypes as loss of ERM proteins. NHERF1/EBP50 and ezrin are both required for microvilli formation in mouse intestinal cells as well as in cultured epithelial cells (BONILHA *et al.*, 1999; GARBETT *et al.*, 2010; LALONDE *et al.*, 2010; MORALES *et al.*, 2004; SAOTOME *et al.*, 2004; VISWANATHA *et al.*, 2012), and loss of NHERF1/EBP50 or moesin causes similar defects in the morphogenesis of 3D cysts grown from Caco-2 cells (GEORGESCU *et al.*, 2014). This is likely due to positive effects of NHERF proteins on the localization, stability, or activity of ERM proteins (BORATKÓ & CSORTOS, 2013; HUGHES *et al.*, 2010; MORALES *et al.*, 2004; OH *et al.*, 2017). In *C. elegans* we found no evidence for such a role towards wild-type ERM-1. The loss of NRFL-1 did not cause any noticeable defects in the localization or levels of ERM-1 at the apical membrane, in the mobility of ERM-1 as examined by FRAP, or in the phosphorylation of T544. We also did not observe a decrease in apical actin levels in *nrfl-1* mutant animals. In organisms where NHERF loss affects the localization or activity of ERM proteins, the loss of NHERF would result in both a lack of protein scaffolding by NHERF and a reduction in actin organizing ability of ERM. Thus, the lack of a reciprocal relationship in *C. elegans* make it a unique model in which these different aspects of ERM protein function can be observed separately.

To explain our observations, we considered two possible models for the roles of ERM-1 and NRFL-1. In the first, the functioning of *C. elegans* ERM-1 involves at least two separable activities: one regulated by the phosphorylation of the C-terminal T544 residue, and one mediated via the recruitment of NRFL-1. The exact consequences of altering T544 phosphorylation are not known, but apical enrichment of the intestinal actin ACT-5 is clearly disrupted (CHAPTER 2). This is in agreement with findings in other systems that C-terminal phosphorylation of ERM proteins is required for apical recruitment of actin (ABBATTISCIANNI *et al.*, 2016; HIPFNER *et al.*, 2004; ROCH *et al.*, 2010). Interestingly, fractionation experiments from kidney epithelial cells indicated that ERM proteins interact with actin and NHERF1/EBP50 in distinct complexes (MORALES *et al.*, 2004). Together with the lack of ACT-5 defects in *nrfl-1* mutants, this presents a possible model in which T544 phosphorylation regulates actin binding, while the scaffolding activities of NRFL-1 mediate recruitment or local distribution of membrane-associated proteins by ERM-1. This model can, however, not account for the observation

that loss of *nrfl-1* causes a further decrease of apical actin levels in *erm-1*[T544A] or *erm-1*[T544D] mutant animals, which indicates that NRFL-1 can contribute to the actin organizing activities of ERM-1.

In the second model, both the T544 phosphorylation cycle and binding of NRFL-1 promote an open, active, ERM-1 configuration. A redundant role for T544 phosphorylation and NRFL-1 binding in ERM-1 activation would account for the lack of effects of *nrfl-1* loss on wild-type ERM-1, and for our previous observations that T544 mutations in *C. elegans* have a relatively mild effect on ERM-1 activity compared to similar mutations in mammalian ERM proteins (CHAPTER 2). Support for this model comes from the wedge mechanism that has been proposed for the mammalian kinase LOK, in which the C-terminal domain of LOK wedges apart the FERM and F-actin-binding domains of ezrin to gain access to the regulatory T567 site (PELASEYED *et al.*, 2017). A chimeric kinase in which the LOK C-terminal domain was replaced with the NRFL-1 ortholog EBP50t was able to phosphorylate ezrin, indicating that EBP50t harbors a similar wedging activity as the LOK C-terminal domain. However, the existence of a wedging mechanism has not been investigated in *C. elegans* nor independently confirmed in mammalian systems. Moreover, loss of *nrfl-1* alone did not affect apical actin levels. Together with the lack of effects of *nrfl-1* loss on ERM-1 localization and stability, this argues against this second model: if T544 phosphorylation and NRFL-1 performed similar roles in ERM-1 activation, their loss would be expected to result in similar defects as well.

Most likely, the activities of NRFL-1 and ERM-1 in *C. elegans* involve a combination of these two models. NRFL-1 may primarily mediate the scaffolding activities of ERM-1 but also promote the open and active conformation of ERM-1, while T544 phosphorylation is the dominant mechanism regulating actin organization by ERM-1. Only when T544 phosphorylation is disrupted does the positive effect of NRFL-1 binding on promoting an open ERM-1 conformation capable of actin binding become apparent. Regardless of the exact mechanism, our results demonstrate that ERM-1 phosphorylation and NRFL-1 redundantly control lumen formation in the *C. elegans* intestine.

There are important differences between our studies in *C. elegans* and studies of ERM proteins in other organisms. The first is that phosphorylation of the C-terminal threonine residue is generally considered to be a critical step in the activation of ERM proteins, while T544A and T544D mutations are tolerated in *C. elegans*. Importantly, the requirement for phosphorylation is not universal. Several studies have observed rescuing activity of Moesin-T559A or Moesin-T559D transgenes in *Drosophila* (HIPFNER *et al.*, 2004; ROCH *et al.*, 2010; SPECK *et al.*, 2003), and phosphorylation of ERM proteins is not required for the formation of microvilli-like structures in A431 and MDCK II cells (YONEMURA *et al.*, 2002). The second major difference is that loss of *nrfl-1* by itself causes no severe defects in *C. elegans*, while loss of NHERF1/EBP50 causes intestinal

abnormalities in mice (BROERE *et al.*, 2009; MORALES *et al.*, 2004) and flies lacking the NHERF ortholog Sip1 are not viable (HUGHES *et al.*, 2010). We think it is most likely that the activities and regulation of ERM proteins are conserved between organisms—involving lipid binding, regulatory phosphorylation on the C-terminal threonine residue, and the binding to adapter proteins—but that the relative importance of these events depends on the biological setting and experimental system used.

Methods

C. elegans strains and culture conditions

C. elegans strains were cultured under standard conditions (BRENNER, 1974). Only hermaphrodites were used, and all experiments were performed with animals grown at 15 °C or 20 °C on standard Nematode Growth Medium (NGM) agar plates seeded with OP50 *Escherichia coli*. Supplementary table 1 contains a list of all the strains used.

Cloning and strain generation for the SIMPL system

Bait and prey SIMPL constructs were generated using the SapI-based cloning strategy, as previously described (YAO *et al.*, 2020). For the conventional SIMPL system, previously described intein inserts were used (YAO *et al.*, 2020). For the SIMPL-mVenus system, the InteinC-3xFLAG-VC155 and VN155-HA-V5-InteinN inserts were codon-optimized for *C. elegans*, flanked by SapI sites and ordered as gBlocks (IDT). Primers containing the appropriate SapI overhangs were used to amplify *erm-1*, *nrfl-1* and *nrfl-1*(Δ eb) from a cDNA library, InteinC-3xFLAG-VC155 from the ordered gBlock and mKate from pDD375 (Addgene #91825). All gBlocks and PCR products were blunt-end cloned into the plasmid pHSG298. Bait or prey, intein, the *rps-0* promoter and the *unc-54* 3' UTR fragments were combined and inserted into the pMLS257 plasmid (Addgene #73716) using the SapTrap assembly method (SCHWARTZ & JORGENSEN, 2016; YAO *et al.*, 2020). Finally for the SIMPL-mVenus system, an mKate2 sequence was integrated into the newly generated *Prps-0::erm-1::VN155-HA-V5-InteinN::unc-54* plasmid. The mKate2 sequence and the *Prps-0::erm-1::VN155-HA-V5-InteinN::unc-54* plasmid were amplified using primers with the appropriate overhangs to incorporate the mKate2 into the plasmid between the promoter and *erm-1* coding sequence using Gibson Assembly (GA). Constructs were verified by Sanger sequencing before injection (Macrogen Europe). Plasmids used for injection were purified using the PureLink HQ Mini Plasmid DNA Purification Kit (Thermo Fisher) using the extra wash step and buffer recommended for endA + strains.

Transgenic animals expressing bait and prey constructs were generated by microinjection in the gonads of young adult N2 animals using an inverted microinjection setup (Eppendorf) with 20 ng/ μ L of bait and prey plasmids, as well as the pDD382 plasmid (Addgene #91830) containing a visible dominant

Rol marker and an hygromycin selection cassette. The DNA mix was spun at max speed on a tabletop centrifuge for 15 min prior to injection. Injected animals were incubated for 2–3 days at 20°C before addition of hygromycin B (250 µg/ml) to the plates. After 1–2 days, surviving Rol animals were singled, allowed to develop, and F2 progeny was screened for successful transmission of the transgenic extrachromosomal array. Multiple lines with successful transmission were saved and used for analysis.

Western blot SIMPL analysis

Animals were grown on NGM plates supplemented with hygromycin B (250 µg/ml) until plates were full, washed off with M9 buffer (0.22 M KH₂PO₄, 0.42 M Na₂HPO₄, 0.85 M NaCl, 0.001 M MgSO₄), washed three times with M9 buffer, and incubated at room temperature (RT) for 20 min. Samples were then pelleted and resuspended in 100–200 µL of lysis buffer (25 mM Tris-HCl pH 7.5, 150 mM NaCl, 1 mM EDTA, 0.5 % IGEPAL CA-630 (Sigma-Aldrich), 1 tablet/50 ml cOmplete protease inhibitor cocktail (Sigma-Aldrich)), and sonicated with a Diagenode BioRupter Plus for 10 min with the high setting and on/off cycles of 30 s in a 4 °C water bath. The lysates were spun at max speed for 15 min, an equal volume of 2 × SDS buffer (100 mM Tris-HCl, 4 % SDS, 0.2 % bromophenol blue, 20 % glycerol, and 10 % β-mercaptoethanol) was added, and boiled 10 min. Depending on the experiment, 5–12 µL of protein lysate was loaded into pre-cast protein gels (4–12 % Bolt Bis Tris Plus, ThermoFisher) together with 10 µL of the molecular marker (PageRuler prestained, ThermoFisher). Gels were run for 30–45 min at 200 V in NuPAGE MOPS SDS Running buffer (ThermoFisher), and transferred onto a PVDF membrane (Immobilon-P 0.45 µm, Millipore) at 4°C and 30 V overnight in Bolt transfer buffer (Thermo Fisher). For staining, membranes were rinsed in TBST (50 mM Tris-Cl, 150 mM NaCl, 0.1 % Tween-20), blocked with 4 % milk in TBST for 1 h at RT, and incubated with primary antibodies in milk for 1 h at RT. Membranes were washed three times for 10 min in TBST, incubated with secondary antibodies in milk for 1 h at RT, and washed again three times for 10 min in TBST before exposure using ECL (SignalFire Plus, Cell signaling). The following antibodies and concentrations were used: rabbit anti-V5, 1:1000 (Cell Signaling #13202); mouse anti-FLAG, 1:10000 (Sigma #F1804); goat anti-Rabbit and donkey anti-mouse HRP conjugates, 1:5000.

CRISPR/Cas9 genome engineering

The *nrfl-1::mCherry*, *nrfl-1(Δeb)* and *nrfl-1(Δeb)::mCherry* strains were engineered by homology-directed repair of CRISPR/Cas9-induced DNA double-strand breaks (DSBs), while the *nrfl-1(null)* deletion was generated by imprecise repair of CRISPR/Cas9-induced DSBs. Delivery of components for CRISPR/Cas9 editing was done by microinjection in the gonads of young adult animals of different genetic backgrounds: *nrfl-1(Δeb)* and *nrfl-1(mib59)* were

generated in an N2 background; *nrfl-1::mCherry* was generated in BOX273 background, and *nrfl-1(Δeb)::mCherry* in a BOX422 background. All sequences of the oligonucleotides and crRNAs used (synthesized by IDT) are listed in Supplementary table 2.

For the *nrfl-1::mCherry*, two plasmid-based sgRNAs were used, generated by ligation of annealed oligo pairs into the *pU6::sgRNA* expression vector pJIR50 (Addgene #75026) as previously described (WAAIJERS *et al.*, 2016). To generate the *nrfl-1::mCherry* repair template we created a custom SEC vector, pJIR83 (Addgene #75028), by replacing a fragment of pDD282 (Addgene #66823) containing the GFP sequence with a similar fragment containing a codon optimized mCherry sequence with synthetic introns using the flanking Bsu36I and BglII restriction sites. Homology arms of about ± 750 bp, flanking the DSB site, were amplified from genomic DNA and introduced into pJIR83 as previously described (DICKINSON *et al.*, 2015). The sgRNA (100 ng/µL) and SEC repair template (20 ng/µL) plasmids combined with *Peft-3::Cas9* (60 ng/µL; Addgene #46168) and *Pmyo-2::mCherry* co-injection marker (2.5 ng/µL; pCFJ90, Addgene #19327) were micro-injected in the gonad of young adults. Two injected animals were pooled per plate, incubated for 3 days at 20°C, 500 µL of 5 mg/ml hygromycin was added per plate, and non-transgenic Rol animals were selected after 4–5 days. These selected animals were lysed and genotyped with primers flanking the homology arms and confirmed by Sanger sequencing. To eliminate the SEC selection cassette L1 progeny of homozygous Rol animals was heat shocked in a water-bath at 34°C for 1 h.

To generate the *nrfl-1(null)* deletion allele a mix containing *Peft-3::Cas9* (Addgene #46168; 50 ng/µL), two pairs of sgRNA plasmids targeting the 5' or 3' ends of the *nrfl-1* open reading frame (75 ng/µL each), and a *dpy-10* sgRNA plasmid (50 ng/µL) for co-CRISPR selection (ARRIBERE *et al.*, 2014) were micro-injected in the gonad of young adults. To select for deletions, injected animals were transferred to individual plates, incubated for 3–4 days at 20°C, and 96 non-transgenic F1 animals (wild-type, Dpy, or Rol) from 2–3 plates containing high numbers of Dpy and Rol animals were selected and transferred to individual plates. After laying eggs, F1 animals were lysed and genotyped with primers flanking the *nrfl-1* ORF. In all cases, deletions were confirmed by Sanger sequencing. Sanger sequencing was also used to determine the precise molecular lesion in selected animals. The *nrfl-1(null)* allele used in this paper, *nrfl-1(mib59)*, consists of a 9 bp deletion starting 1 bp before the initial base of the start codon of long *nrfl-1* isoforms (a, c, d, h, j), and a second 11,537 bp deletion spanning part of the third exon (791 bp from start of *nrfl-1a*) until the downstream intergenic region, which includes the entire ORFs of the small *nrfl-1* isoforms (left flank 5' atgcttgatctctgaagaaggag, right flank 5' aat

atcacgaacaacttctaggagc). The *mib59* allele also deleted an ncRNA (C01F6.16) and three piRNAs (C01F6.10, F32B2.25, and F23B2.28) located within *nrfl-1* introns.

The NRFL-1 EB domain deletions were generated using the Alt-R CRISPR/Cas9 system (IDT). A single-stranded oligodeoxynucleotide with about 35 bp homology arms was used as a repair template to fuse the flanks of a deletion spanning nucleotides 1390–1473 of *nrfl-1h*, as previously described (DOKSHIN *et al.*, 2018). A mix of 250 ng/μL Cas9 protein, 2 μM repair template, 4.5 μM each *nrfl-1* crRNAs, 10 μM tracrRNA, as well as 1 μM *dpy-10* crRNA and ssODN repair for co-CRISPR selection (ARRIBERE *et al.*, 2014) was micro-injected into the gonads of young adults. Animals were selected as described above for the *nrfl-1(null)* allele and genotyped using two primers flanking the deletion.

Microscopy and image analysis

Imaging of *C. elegans* was done by mounting embryos or larvae on a 5 % agarose pad in 20 mM Tetramisole solution in M9 to induce paralysis. Spinning disk confocal imaging was performed using a Nikon Eclipse Ti-U manual microscope equipped with a Yokogawa CSU-X1 spinning disk using a 60× 1.4 NA objective, 488 and 561 nm lasers, Semrock 488 long-pass, 525/30 (green), 617/73 (red) & 512/630 (dual) emission filters, 600 Texas Red (EX540-580/DM595/BA600-660) filter blocks, and Andor iXON DU-885 camera. Imaging for FRAP and immunohistochemistry experiments was performed on a Nikon Eclipse-Ti with Perfect Focus System microscope equipped with a Yokogawa CSU-X1-A1 spinning disk using 60× and 100× 1.4 NA objectives, Chroma ET-DAPI (49000), ET-GFP (49002), ET-mCherry (49008) emission filters, 355 nm, 488 nm, 491 nm, and 561 nm lasers, and a Photometrics Evolve 512 EMCCD camera. Targeted photobleaching was done using an ILas system (Roper Scientific France/PICT-IBiSA, Institut Curie). Spinning disk images were acquired using MetaMorph Microscopy Automation and Image Analysis Software. All stacks along the z-axis were obtained at 0.25 μm intervals. Super resolution images of the microvilli were obtained using a Zeiss AxioObserver 7 SP microscope with Definite Focus 2 operated by Zeiss ZEN software with an Airyscan 32-channel GaAsP-PMT area detector using a 100× 1.46 NA objective, and Laser Argon Multiline and 561 nm lasers. Maximum intensity Z projections were done in ImageJ (Fiji) software (RUEDEN *et al.*, 2017; SCHINDELIN *et al.*, 2012). For quantifications, the same laser power and exposure times were used within experiments. Image scales were calibrated for each microscope using a micrometer slide. For display in figures, level adjustments, false coloring, and image overlays were done in Adobe Photoshop. Image rotation, cropping, and panel assembly were done in Adobe Illustrator. All edits were done

non-destructively using adjustment layers and clipping masks, and images were kept in their original capture bit depth until final export from Illustrator for publication.

Quantitative image analysis

Quantitative analysis of spinning disk images was done in Fiji. All values were corrected for background levels by subtracting the average of three regions within the field of view that did not contain any animals. For quantification of apical protein levels, measurements were done in intestinal cells forming int2 through int6, and where the opposing apical membranes could be clearly seen as two lines. Levels were obtained by averaging the peak values of intensity profiles from three 25 px-wide (10 px-wide for the SIMPL-mVenus system) line scans perpendicular to the membrane per animal. For YFP::ACT-5, which is expressed from a transgene with variable expression levels, we express apical enrichment as the ratio of apical/cytoplasmic. Cytoplasmic levels were measured by averaging three regions within the cytoplasm of intestinal cells. Intensity distribution profiles to analyze co-distribution of NRFL-1 with ERM-1 and ACT-5 were obtained by taking three 25 px-wide line scans perpendicular to the apical membrane in each animal. Before averaging these three values, they were aligned and normalized to the peak value. Measurements of multiple animals were again aligned based on the peak value. All presented graphs were made using GraphPad Prism and Adobe Illustrator.

Protein degradation

For protein degradation using the anti-GFP-nanobody::ZIF-1 approach (WANG *et al.*, 2017), gonads of young adult BOX428 animals were microinjected with 30 ng/μL *Pelt-2::α-GFP-NB::ZIF-1* and 2.5 ng/μL *Pmyo-2::GFP* (#Addgene 26347) as a co-injection marker. Transgenic F1 animals were transferred to individual plates, F2 progeny was screened for successful transmission of the extrachromosomal array and imaged using spinning disk microscopy.

Brood size

L4 animals were put on individual plates at 20°C and transferred to a new plate daily until they died. After the parent was removed from a plate, hatched animals and the unhatched eggs were counted 2–4 days later. The number of animals and unhatched eggs combined constitutes the total progeny size. The graph presented was made using GraphPad Prism and Adobe Illustrator.

Texas red-dextran assay

Mixed stage populations were collected in M9 and washed two times in M9. Animals were then pelleted, concentrated, resuspended in 1 mg/ml Texas Red-dextran 40,000 MW (ThermoFisher D1829) in egg buffer (118 mM NaCl, 48 mM KCl, 2 mM MgCl₂, 2 mM CaCl₂, 25 mM HEPES pH 7.3), and incubated for

60 min on a shaker at 500 rpm. The dye in solution was removed by washing the samples with M9 two times. Animals were paralyzed in 10 mM Tetramisole, transferred to an agarose pad on a glass slide, and imaged using spinning disk microscopy.

FRAP experiments and analysis

For FRAP assays, laser power was adjusted in each experiment to avoid complete photobleaching of the selected area, as the time scale of experiments prevented assessment of photo-induced damage. Photobleaching was performed on a circular region with a diameter of 30 or 40 px at the cortex, and images were taken just before bleaching, directly after, after 15 min, and after 45 min. These images were analyzed using ImageJ. The size of the area for FRAP analysis was defined by the full width at half maximum of an intensity plot across the bleached region. For each time point, the mean intensity value within the bleached region was determined, and the background, defined as the mean intensity of a non-bleached region outside the animal, was subtracted. The mean intensities within the bleached region were corrected for acquisition photobleaching per frame using the background-subtracted mean intensity of a similar non-bleached region at the cortex, which was normalized to the corresponding pre-bleach mean intensity. FRAP recovery was calculated as the change in corrected intensity values within the bleached region from the first image after bleaching normalized to the mean intensity just before bleaching.

Immunohistochemistry

For the staining of larval stages, embryos were obtained from gravid adults by bleaching and allowed to hatch and develop on plates at 15 °C for 24 h. Animals were collected from plates and washed three times with M9 and once with MQ H₂O before being transferred to poly-L-lysine-coated frosted slides. For the staining of embryos, embryos were obtained from gravid adults by dissection in MQ H₂O on poly-L-lysine-coated frosted slides and allowed to develop at RT for 4 h. A coverslip (Carl Roth, #1) was lowered on top of larvae/embryos, followed by freezing in liquid nitrogen and snapping off of the coverslip. Fixation was performed in formaldehyde solution with phosphatase inhibitors (3,7 % formaldehyde (Sigma-Aldrich), 250 μM EDTA and 50 mM NaF in PBS (1,35 M NaCl, 27 mM KCl, 100 mM Na₂HPO₄, 18 mM KH₂PO₄)) at RT for 10 min. Samples were rinsed in PBS, permeabilized (PBS + 0,5 % triton X-100 (Sigma-Aldrich)) for 30 min, washed four times in wash buffer (0,1 % Triton X-100, 250 μM EDTA and 50 mM NaF in PBS) for 10 min each and then blocked (1 % bovine serum albumin (Sigma-Aldrich) and 10 % goat serum (Sigma-Aldrich)) for 1 h at RT. For the staining with protein phosphatase treatment, samples were treated with Lambda Protein phosphatase (NEB) for 30 min at 30°C followed with an additional four times washing step before they were blocked. Primary antibodies (anti-phospho-ezrin (Thr567)/radixin (Thr564)/moesin (Thr558)

(48G2) rabbit mAb #3726 (Cell Signaling Technologies) 1:200 and mouse anti-DLG (Hybridoma bank) 1:50) in blocking solution were applied overnight at 4°C. Samples were then washed four times in wash buffer for 10 min each and stained with secondary antibodies (Alexa-Fluor 488 goat anti-rabbit and Alexa-Fluor 568 goat anti-mouse (Life Technologies, A-11008 and A11004), both 1:500) in blocking solution for 1 hour at RT. Samples were then washed four times in wash buffer and once in PBS for 10 min each and finally mounted with Prolong Gold Antifade with DAPI (ThermoFisher) under a coverslip and sealed with nail polish.

Statistical analysis

All statistical analyses were performed using GraphPad Prism 8. For population comparisons, a D'Agostino and Pearson test of normality was first performed to determine if the data was sampled from a Gaussian distribution. For data drawn from a Gaussian distribution, comparisons between two populations were done using an unpaired t-test, with Welch's correction if the SDs of the populations differed significantly, and comparisons between > 2 populations were done using a one-way ANOVA, or a Welch's ANOVA if the SDs of the populations differed significantly. For data not drawn from a Gaussian distribution, a non-parametric test was used (Mann-Whitney for 2 populations and Kruskal-Wallis for > 2 populations). ANOVA and non-parametric tests were followed up with multiple comparison tests of significance (Dunnett's, Tukey's, Dunnett's T3 or Dunn's). Tests of significance used and sample sizes are indicated in the figure legends. No statistical method was used to pre-determine sample sizes. No samples or animals were excluded from analysis. The experiments were not randomized, and the investigators were not blinded to allocation during experiments and outcome assessment.

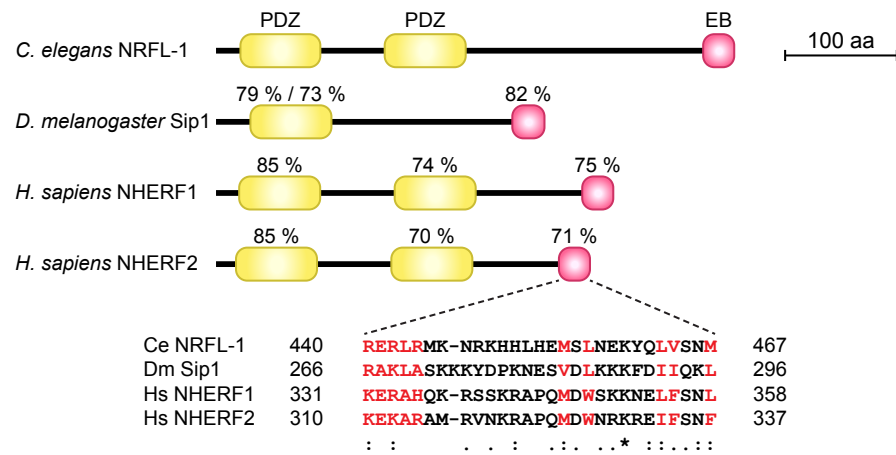
Author contributions

Conceptualization: JS, JR, MB; Methodology: JS, JR, JK, RS; Formal analysis: JS, JR, JK; Investigation: JS, JR, JK, RS; Writing—original draft: JS, JR, MB; Writing—review and editing: JK, RS; Visualization: JS, JR; Supervision: MB; Project administration: MB; Funding acquisition: MB.

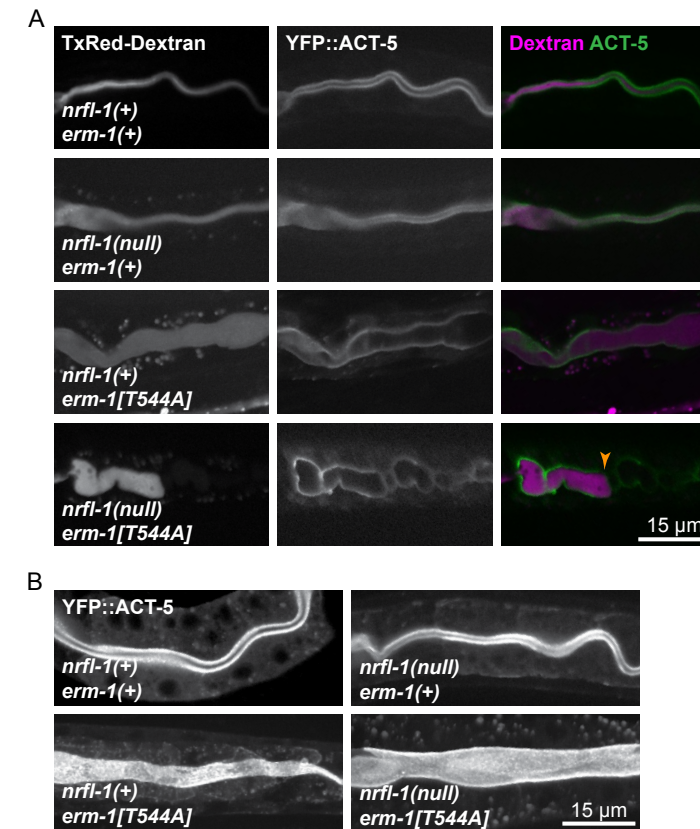
Acknowledgments

We thank V. Portegijs and S. van den Heuvel for the *Pelt-2::αGFP-NB::ZIF-1* plasmid, H.R. Pires for strain BOX273, and members of the S. van den Heuvel, S. Ruijtenberg, and MB groups for helpful discussions. We also thank Wormbase (HARRIS *et al.*, 2020) and the Biology Imaging Center, Faculty of Sciences, Department of Biology, Utrecht University.

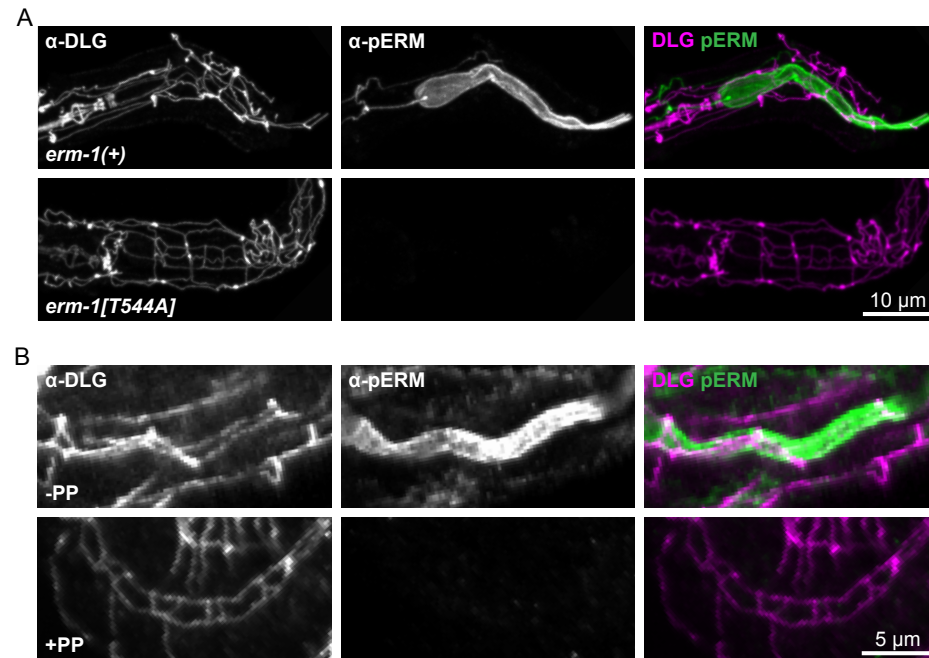
Supplementary material:



Supplementary figure 1: NRFL-1 is recruited to the apical domain by ERM-1 in different tissues. Schematic representation of the domain organization of *C. elegans* NRFL-1, *D. melanogaster* Sip1 and *H. sapiens* NHERF1/EBP50 and NHERF2. Percentages above the domains represent the similarity between that domain and the corresponding domain of NRFL-1. For the single PDZ domain of Sip1, two percentages are presented corresponding to each NRFL-1 PDZ domain. In the EB domain alignment, amino acids that are important for the interaction with ERM proteins are shown in red (TERAWAKI *et al.*, 2006). PDZ = Post-synaptic density-95, disks-large and zonula occludens-1; EB = ERM binding.



Supplementary figure 2: Lumen discontinuities in *nrfl-1* and *erm-1* single and double mutants. (A) Representative images of the intestine in L2 larvae of the indicated genotypes expressing YFP::ACT-5 as an apical marker. (B) L1 larvae carrying the apical marker YFP::ACT-5 of the indicated genotypes fed with Texas-Red Dextran. The orange arrowhead indicates the constriction that prevents the flow of fluorescent dye along the intestine. All images are taken using a spinning-disk confocal microscope, and a single focal plane is shown.



Supplementary figure 3: Validation of the specificity of the α -pERM for T544 phosphorylated ERM-1. (A, B) Representative images of fixed animals stained with antibodies recognizing the junctional protein DLG-1 (α -DLG) and phosphorylated ERM-1 (α -pERM). (A) shows *erm-1(+)* and *erm-1[T544A]* larvae and (B) shows the intestine of wild-type 2.5-fold embryos that are untreated (-PP) and treated with protein phosphatase (+PP). All images are taken using a spinning-disk confocal microscope, and maximum intensity projections are presented.

Strain	Genotype
N2	Wild-type
JM125	<i>calS107[Pges-1::act-5::YFP]</i>
BOX163	<i>erm-1(mib9[erm-1[p. T544D]]) I</i>
BOX165	<i>erm-1(mib10[erm-1[p. T544A]]) I</i>
BOX196	<i>erm-1(mib10[erm-1[p. T544A]]) I; calS107[Pges-1::act-5::YFP]</i>
BOX197	<i>erm-1(mib9[erm-1[p. T544D]]) I; calS107[Pges-1::act-5::YFP]</i>
BOX273	<i>mibIs48[Pelt-2::TIR-1::tagBFP2-Lox511::tbb-2-3'UTR, IV:5014740-5014802 (cxTi10816 site))] IV</i>
BOX404	<i>nrfl-1(mib59[nrfl-1a(null = c.-1_8del; c.287_1404+703)]) IV</i>
BOX422	<i>nrfl-1(mib73[nrfl-1::mCherry]) IV; mibIs48[Pelt-2::TIR-1::tagBFP2-Lox511::tbb-2-3'UTR, IV:5014740-5014802 (cxTi10816 site))] IV</i>
BOX428	<i>erm-1(mib15[erm-1::eGFP]) I; nrfl-1(mib73[nrfl-1::mCherry]) IV; mibIs48[Pelt-2::TIR-1::tagBFP2-Lox511::tbb-2-3'UTR, IV:5014740-5014802 (cxTi10816 site))] IV</i>
BOX429	<i>nrfl-1(mib73[nrfl-1::mCherry]) IV; mibIs48[Pelt-2::TIR-1::tagBFP2-Lox511::tbb-2-3'UTR, IV:5014740-5014802 (cxTi10816 site))] IV; calS107[Pges-1::act-5::YFP]</i>
BOX440	<i>nrfl-1(mib75[nrfl-1a(Δeb = c.1318_1401del)::mCherry]) IV; mibIs48[Pelt-2::TIR-1::tagBFP2-Lox511::tbb-2-3'UTR, IV:5014740-5014802 (cxTi10816 site))] IV; calS107[Pges-1::act-5::YFP]</i>
BOX597	<i>nrfl-1(mib104[nrfl-1a(Δeb = c.1318_1401del)]) IV</i>
BOX670	<i>erm-1(mib10[erm-1[p. T544A]]) I; nrfl-1(mib59[nrfl-1a(null = c.-1_8del; c.287_1404+703)]) IV</i>
BOX671	<i>erm-1(mib9[erm-1[p. T544D]]) I; nrfl-1(mib59[nrfl-1a(null = c.-1_8del; c.287_1404+703)]) IV</i>
BOX672	<i>nrfl-1(mib59[nrfl-1a(null = c.-1_8del; c.287_1404+703)]) IV; calS107[Pges-1::act-5::YFP]</i>
BOX673	<i>erm-1(mib10[erm-1[p. T544A]]) I; nrfl-1(mib59[nrfl-1a(null = c.-1_8del; c.287_1404+703)]) IV; calS107[Pges-1::act-5::YFP]</i>
BOX674	<i>erm-1(mib9[erm-1[p. T544D]]) I; nrfl-1(mib59[nrfl-1a(null = c.-1_8del; c.287_1404+703)]) IV; calS107[Pges-1::act-5::YFP]</i>
BOX675	<i>erm-1(mib10[erm-1[p. T544A]]) I; nrfl-1(mib104[nrfl-1a(Δeb = c.1318_1401del)]) IV</i>
BOX676	<i>erm-1(mib9[erm-1[p. T544D]]) I; nrfl-1(mib104[nrfl-1a(Δeb = c.1318_1401del)]) IV</i>
BOX677	<i>nrfl-1(mib104[nrfl-1a(Δeb = c.1318_1401del)]) IV; calS107[Pges-1::act-5::YFP]</i>
BOX678	<i>erm-1(mib10[erm-1[p. T544A]]) I; nrfl-1(mib104[nrfl-1a(Δeb = c.1318_1401del)]) IV; calS107[Pges-1::act-5::YFP]</i>
BOX679	<i>erm-1(mib9[erm-1[p. T544D]]) I; nrfl-1(mib104[nrfl-1a(Δeb = c.1318_1401del)]) IV; calS107[Pges-1::act-5::YFP]</i>

Supplementary table 1: List of *C. elegans* strains used

SIMPL system	
<i>erm-1</i> SapI forward	CTGCTCTTCGAAGATGTCGAAAAAGCGATCAA
<i>erm-1</i> SapI reverse	CTGCTCTTCGCGTCATATTTTCGTATTGATCGA
<i>nrfl-1</i> SapI forward	CTGCTCTTCGAAGATGGTGCACATTCGAGCGA
<i>nrfl-1</i> SapI reverse	CTGCTCTTCGCGTCATGTTGCTGACCAATTGAT
<i>nrfl-1(Δeb)</i> SapI reverse	AGGCTCTTCGCGTAGCTTCTCTTGTGACAFAAAT
InteinC-3xFLAG-VC155 SapI forward	GAGCTCTTCGACGATGGACGAGCGTGAGCTTA
InteinC-3xFLAG-VC155 SapI reverse	GAGCTGCTCTTCGGCACTTGTAGAGCTCATCCATTC
InteinC-3xFLAG-VC155 GA forward	TCGGACACCGTATGTCGAAAAAGCGATC
InteinC-3xFLAG-VC155 GA reverse	TCGGAGACCATATTACCTTAAAATTCAAAAATTAATTCAG
mKate2 GA forward	TTTTAAGGTAATATGGTCTCCGAGCTCATTAAAGAAAA C
mKate2 GA reverse	TTTTTTCGACATACGGTGTCCGAGCTTGATG
<i>nrfl-1(null)</i>	
<i>nrfl-1</i> sgRNA 5' forward oligo 1	TCTTGTGCTCGGAATGTGCACCA
<i>nrfl-1</i> sgRNA 5' reverse oligo 1	AAACTGGTGCACATTCGAGCGAC
<i>nrfl-1</i> sgRNA 5' forward oligo 2	TCTTGTCAACGACACAAAGTCTTGG
<i>nrfl-1</i> sgRNA 5' reverse oligo 2	AAACCAAGACTTTGTGTCGTTGAC
<i>nrfl-1</i> sgRNA 3' forward oligo 1	TCTTGCCTTAACGAGAAGTATCAAT
<i>nrfl-1</i> sgRNA 3' reverse oligo 1	AAACATTGATACTTCTCGTTAAGGC
<i>nrfl-1</i> sgRNA 3' forward oligo 2	TCTTGCCAATTGATACTTCTCGTTA
<i>nrfl-1</i> sgRNA 3' reverse oligo 2	AAACTAACGAGAAGTATCAATTGGC
Deletion forward primer	TGGACAGTTCGTTGGTACCG
Deletion reverse primer	TACACGCGCAAAGTGACCTA
<i>nrfl-1::mcherry</i> - Combined with both <i>nrfl-1</i> sgRNAs 3' of <i>nrfl-1(null)</i>	
LH arm forward primer	ACGTTGTAAAACGACGGCCAGTCGCCGGCATTTAATGC GCATTGGTCTGC
LH arm reverse primer step 1	GACTAATTGATACTTCTCGTTAAGACTCATCTCGTGCC TACAATT
LH arm reverse primer step 2	CCTGAGGCTCCCGATGCTCCCATGTTGCTGACTAATTG ATACTTCTCGT
RH arm forward primer	AGGATGACGATGACAAGAGATAATCTTTTGCAACTTCT TCTTATTTTCTTC
RH arm reverse primer	GGAAACAGCTATGACCATGTTATCGATTTACCTTCCA ATGTCAGGTTCCC
Integration forward primer	TCAGGGAGCCGGATCTGATT
Integration reverse primer	CGGCTGAACAAAAGGAGCAG

~ Table continues on the next page ~

<i>nrfl-1(Δeb)</i>	
<i>nrfl-1</i> EB sgRNA 5'	UUUAAUCUUCAUGCUGAACG
<i>nrfl-1</i> EB sgRNA 3'	AUUGAUACUUCUGUUAAGG
ssODN repair template	ACGATGATATCTATCATTTGTGTCAGCAAGAGAAGCTACG ATGATATCTATCATTTGTGTCAGCAAGAGAAGCT
Integration forward primer	ATGCATCACCTCGAGGCTG
Integration reverse primer	TGAGCGATTGTGAAATGGAAGG
<i>nrfl-1(Δeb)::mcherry</i> - Combined with <i>nrfl-1</i> EB sgRNA 5' of <i>nrfl-1(Δeb)</i>	
<i>nrfl-1</i> EB mCherry sgRNA	TCATAACATTGCATATTCAT
ssODN repair template	CCCCAGATCAAGAATTTGGTTTTAATCTTCATGCTGTT GATAAGTATCATAAAGATCATAACATGCTTACAGCTG GGATAATGTTGAAAGAGTTGATACTCGTCCA
Integration forward primer	GATTTGGCGGGTTTTTCGAGG
Integration reverse primer	CGGCTGAACAAAAGGAGCAG

Supplementary table 2: List of DNA and RNA sequences used



Chapter 4

Regulation of *Caenorhabditis elegans*
intestinal lumen formation by the
Ste20-family kinase GCK-4^{Lok/Slk}

Jorian J. Sepers¹, João J. Ramalho¹, Savvas Tzavellas¹,
Mark Roosjen², Jason R. Kroll¹, Ruben Schmidt¹, Dolf
Weijers² & Mike Boxem¹

1. Division of Developmental Biology, Institute of Biodynamics and Biocomplexity, Department of Biology, Faculty of Science, Utrecht University, Utrecht, The Netherlands
2. Laboratory of Biochemistry, Wageningen University and Research, Wageningen, The Netherlands

Many vital organs in the body are composed of tubular structures responsible for transporting nutrients, waste, liquids, and gases. The development of a tube involves the formation of a lumen, a process regulated by various intracellular networks including cell polarity, the cytoskeleton, and cell-cell junctions. The precise molecular mechanisms and interactions among these networks remain poorly understood. Here, we make use of the *C. elegans* intestine as a model system to delve into the molecular mechanisms underlying lumen formation. We identify the germinal center kinase family member GCK-4, an ortholog of mammalian LOK and SLK, as a novel regulator of lumen formation in the *C. elegans* intestine. Depletion of GCK-4 causes a widened lumen and multiple constrictions in the intestine, and the affected animals arrest as young larvae probably due to an inability to feed. In addition, loss of GCK-4 results in alterations in the apical actin network and adherens junctions. GCK-4 localizes to the tips of the intestinal microvilli and its kinase domain is essential for its activity. However, in contrast to its orthologs, GCK-4 is not responsible for phosphorylation of the microvillar proteins of the ERM protein family. We hypothesize that GCK-4 is an essential regulator of intestinal lumen formation by organizing the apical actin network. Finally, we combined two distinct proteomic approaches to find candidate GCK-4 interactors, which will play a crucial role in the future identification of GCK-4 kinase substrates.

Introduction

Many organs in the body are composed of tubular structures responsible for transporting nutrients, waste, liquids, and gases. Tubulogenesis entails the transformation of a tissue into a tubular shape. A pivotal aspect of this process is lumen formation, which involves creating a cavity either between cells or within a single cell. This phenomenon can occur through various mechanisms. For instance, cells within a tissue may be eliminated to form a cavity, or two or more cells may detach from one another and fill the space between them with liquid. *De novo* lumen formation typically proceeds in three stages: initiation, membrane growth, and maturation (SIGURBJÖRNSDÓTTIR *et al.*, 2014).

In the initiation step, the tissue establishes the starting point for lumen formation. This is achieved by establishing apical-basolateral polarity, with the apical membrane serving as the site for future lumen development (DATTA *et al.*, 2011; SIGURBJÖRNSDÓTTIR *et al.*, 2014). The initial cue for this polarization typically originates externally. For example, in zebrafish angiogenesis, the apical membrane of newly formed endothelial cells aligns with the polarity of neighboring cells through cell-cell junctions (HERWIG *et al.*, 2011). Additionally, Madin-Darby canine kidney (MCDK) cells determine their basal membrane

through an interaction with the extracellular matrix (O'BRIEN *et al.*, 2001; YU *et al.*, 2008).

During the membrane growth stage, cells transport the necessary membrane material to the developing lumen. This necessitates a reorganization of the trafficking machinery to facilitate polarized transport of the required material to the apical domain. In this step, apical polarity organizers serve not only as guidance cues but also actively regulate the intracellular trafficking (DATTA *et al.*, 2011; SIGURBJÖRNSDÓTTIR *et al.*, 2014). For example, in both MCDK cells and the *Caenorhabditis elegans* excretory canal, the apical PAR proteins are responsible for recruiting the exocyst to the apical membrane, facilitating lumen formation (ABRAMS & NANCE, 2021; BRYANT *et al.*, 2010).

The lumen attains its final shape and size during the maturation phase (DATTA *et al.*, 2011; SIGURBJÖRNSDÓTTIR *et al.*, 2014). This is generally a result of a delicate equilibrium between outward forces from the lumen and inward forces exerted by the apical membrane wrapping around it (SCHOTTENFELD-ROAMES & GHABRIAL, 2013). The outward force originates from content secreted into the lumen and osmotic pressure. For instance, the lumen of the *Drosophila* trachea, where the loss of COPII-dependent secretion or disruption of osmotic pressure, regulated by the Na⁺/K⁺ ATPase channel, causes the lumen to shrink (PAUL *et al.*, 2003; TSAROUHAS *et al.*, 2007). Conversely, the inward force is typically facilitated by the apical cytoskeleton network. For example, the absence of the intermediate filament protein IFB-1 results in an enlargement of the luminal diameter in the *C. elegans* excretory canal (KOLOTUEV *et al.*, 2013).

In this study, we make use of the *C. elegans* intestine as a model system to investigate the mechanisms underlying lumen formation. The *C. elegans* intestine, although simple in structure, has proven to be a robust system for investigating organ development (MCGHEE, 2007). The earliest signs of lumen formation become apparent at the (lima) bean stage (DEPPE *et al.*, 1978). At this stage, the intestinal primordium is comprised of 16 daughter cells that align in eight pairs adjacent to each other. During this E16 stage, these cells are polarizing, with early apical markers becoming enriched at the midline between the pairs (LEUNG *et al.*, 1999). Subsequently, the cells initiate lumen formation through a process known as cord hollowing. This involves the creation of small luminal pockets between the opposing cell pairs, which eventually coalesce into a single continuous lumen (LEUNG *et al.*, 1999; SIGURBJÖRNSDÓTTIR *et al.*, 2014). By the 1.5-fold stage, cell rearrangements and four additional cell divisions have transpired, resulting in the formation of nine rings comprising a total of 20 cells, all encircling a continuous lumen (LEUNG *et al.*, 1999). As the intestine matures, the lumen becomes oval-shaped lined with a brush border. The first intestinal ring, composed of four cells, connects to the pharynx, the organ responsible for

food intake. The final ring connects to the rectum, serving as the passageway from the intestine to the external environment (DEPPE *et al.*, 1978; SULSTON *et al.*, 1983).

In the nematode intestine, lumen formation depends on conserved organizers, such as the apical PAR proteins and HMR-1, the E-Cadherin ortholog. Depletion of these proteins leads to a failure in correct polarity establishment, resulting in a non-contiguous lumen (NATURALE *et al.*, 2022; SALLEE *et al.*, 2021; SEGBERT *et al.*, 2004). The cytoskeleton also plays a crucial role, as depletion of both actin and intermediate filament (IF) components causes lumen defects. Depletion of intestinal actin isoform ACT-5 leads to a widened lumen accompanied by constrictions (MACQUEEN *et al.*, 2005). Depleting the IF regulators SMA-5 or BBLN-1 results in small invaginations of the lumen into the cytoplasm, possibly due to weak spots in the terminal web, a network of actin and IF surrounding the intestinal lumen (GEISLER *et al.*, 2016; REMMELZWAAL *et al.*, 2021). In order to gain deeper insights into intestinal lumen formation, our aim is to identify additional regulators of lumen formation.

In this study, we identify the Sterile 20-family kinase GCK-4 as a novel regulator of intestinal lumen formation in *C. elegans*. Depletion of GCK-4 leads to the widening of the intestinal lumen along with constrictions, and the affected animals arrest at an early larval stage. Furthermore, we observe a decrease in the levels of apical actin, and the morphology of the adherens junctions is altered. We show that GCK-4 is localized to the apical membranes of most epithelial tissues and is enriched at the tip of the microvilli of the larval intestine. We and others previously observed similar phenotypes for inactivation of the actin membrane linker ERM-1, the sole ezrin-radixin-moesin (ERM) family ortholog (GÖBEL *et al.*, 2004; VAN FÜRDEN *et al.*, 2004). Moreover, the GCK-4 orthologs LOK and SLK are known to phosphorylate a key regulatory site in the C-terminus of ERM proteins (BELKINA *et al.*, 2009; HIPFNER *et al.*, 2004; VISWANATHA *et al.*, 2012). Nevertheless, loss of GCK-4 did not result in loss of ERM-1 phosphorylation and a physical interaction between the two proteins could not be detected. Thus, GCK-4 likely controls intestinal tubulogenesis through mechanisms other than ERM-1 regulation. To identify candidates for such mechanisms, we attempt to identify interactors and kinase substrates of GCK-4 by combining phosphoproteomics and proximity-labeling approaches.

Results

GCK-4 is essential for intestinal lumen formation

To uncover novel regulators of intestinal morphology and tubulogenesis in *C. elegans*, we conducted a small-scale genetic screen. In this screen, we employed feeding RNAi to efficiently knockdown candidate kinases that could potentially regulate intestinal lumen formation (RUAL *et al.*, 2004; TIMMONS & FIRE, 1998). These kinases were selected based on the role of their orthologs

in regulating the apical actin network in other model systems. We identified GCK-4, a serine-threonine kinase, ortholog of the mammalian LOK and SLK. Upon depleting of GCK-4 via RNA injection, the intestinal lumen has a cystic appearance and multiple constrictions (Figure 1A). In addition, seemingly all the affected animals arrest as young L1 larvae, probably due to their inability to feed.

In order to ascertain the underlying molecular cause of the defects in lumen formation resulting from GCK-4 depletion, we investigated the cytoskeleton, apical-basolateral polarity and *C. elegans* apical junctions (CeAJ) of intestinal cells. Each of these cellular structures play a crucial role in the tubulogenesis of this organ, and the depletion of any of these components leads to alterations in the intestinal morphology. These networks operate synergistically, as they interact with one another and are interdependent for their localization and function (MADURO, 2017; MCGHEE, 2007).

Initially, we examined the various cytoskeletal components in the intestine of *gck-4* RNAi-treated animals. Using YFP::ACT-5 as marker for the apical actin cytoskeleton, we observed a nearly 6-fold decrease in apical ACT-5, along with a 1.5-fold increase both at the basolateral membrane and in the cytoplasm (Figure 1A; Supplementary figure 1A). Additionally, while ACT-5 typically becomes enriched at the apical membrane as early as the comma stage, in *gck-4* RNAi embryos, we only observed clear enrichment from the 1.5-fold stage onward (Figure 1A) (BIDAUD-MEYNARD *et al.*, 2021). Thus, apical enrichment of ACT-5 is delayed in the embryo and reduced throughout development upon GCK-4 depletion. For the microtubule (MT) cytoskeleton, we made use of an endogenous fusion of GFP with the MT binding protein MAPH-1.1 as a marker (WAAIJERS *et al.*, 2016). We did not observe discernible differences in the subcellular-location of GFP::MAPH-1.1 between control and *gck-4* RNAi animals (Figure 1B). However, the cytoplasmic GFP::MAPH-1.1 levels were higher upon GCK-4 knockdown, most-likely due to a decrease in the cytoplasmic volume caused by the widened lumen (Supplementary figure 1B). To visualize apical MT minus ends, we examined GIP-1, a core component of the apical non-centrosomal MT-organizing center (JANSKI *et al.*, 2012; SALLEE *et al.*, 2018). Here, we found no overt differences between control and the GCK-4 depleted animals (Figure 1B). Lastly, we examined the subapical intermediate filament (IF) network using an IFB-2::GFP fusion (REMMELZWAAL *et al.*, 2021). Both apical localization and levels of IFB-2::GFP were unaltered upon GCK-4 knockdown (Figure 1B). In summary, GCK-4 appears to be crucial for the organization of the apical actin network in the intestine, while the MT and IF organization are unaffected following GCK-4 depletion.

To investigate apical-basolateral polarity, we employed a *C. elegans* strain in which the apical protein PAR-6 and the basolateral protein LET-413 are endogenously tagged by GFP and mCherry, respectively (CASTIGLIONI *et al.*, 2020;

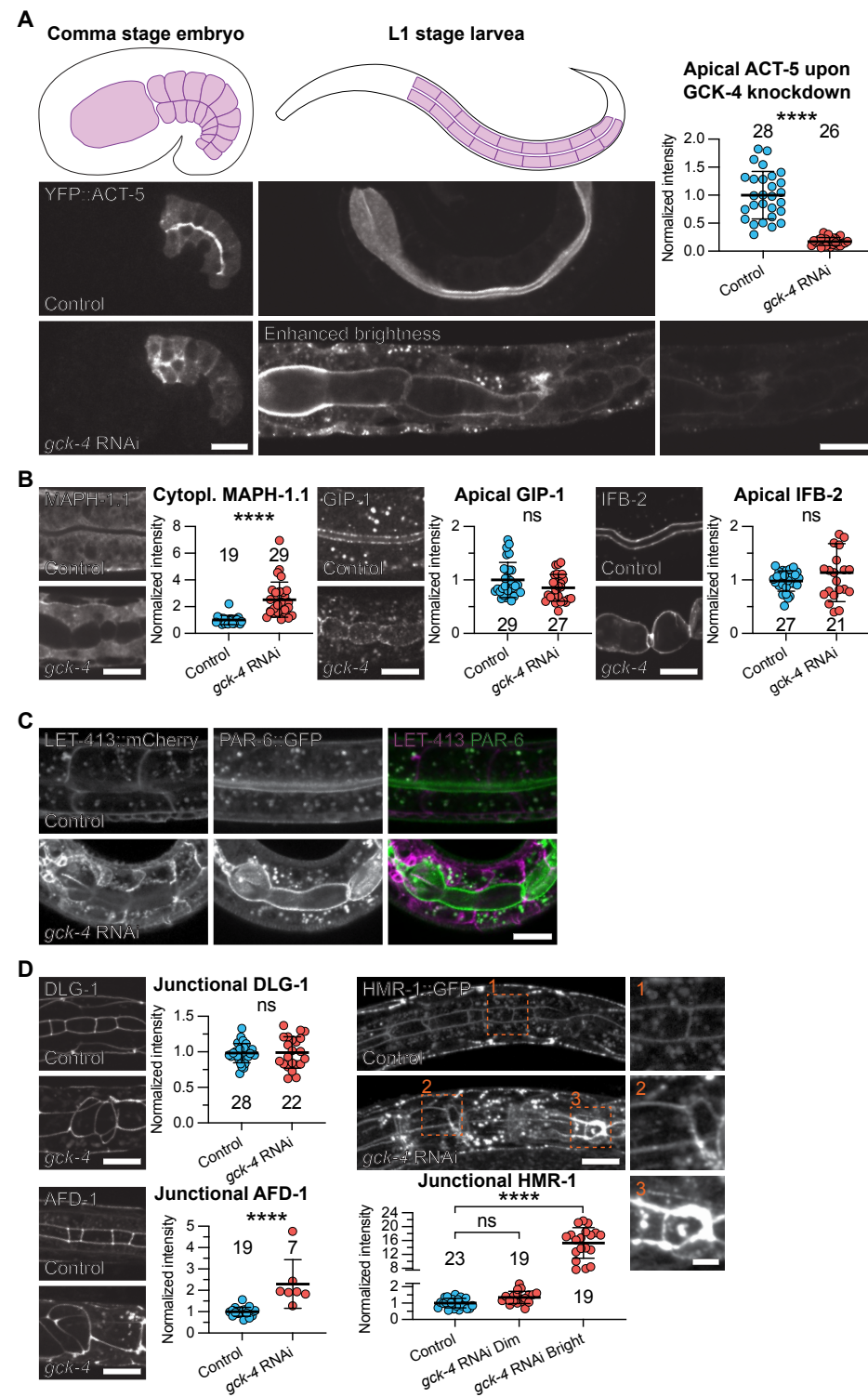


Figure 1: GCK-4 is essential for the intestinal morphogenesis and lumen formation.

Spinning disk microscopy images of control and *gck-4* RNAi animals with complementary quantifications. **(A)** YFP::ACT-5 in both comma stage embryos and L1 stage larvae with complementary illustrations of the respective developmental stages. In the “Enhanced brightness” image, the YFP::ACT-5 levels were enhanced to show the *gck-4* phenotype more clearly, while the image to the right shows part of the same image using the same settings as the control larvae to compare YFP::ACT-5 levels. Quantifications of apical YFP::ACT-5 levels were done in L1 larvae. **(B)** The cytoskeletal components GFP::MAPH-1.1, GIP-1::RFP and IFB-2::GFP in L1 larvae. **(C)** The apical-basolateral components PAR-6::GFP and LET-413::mCherry within one L1 larvae. **(D)** The cell junction components DLG-1::AID*::mCherry, AFD-1::GFP and HMR-1::GFP in L1 larvae. For HMR-1::GFP, the small panels to the right shows an enlargement of the region indicated by the orange boxes and numbers. All images shown are representative maximum intensity projections, and within one experiment the images are acquired and displayed with the same settings for comparison except for the “Enhanced brightness” image in A. All scale bars are 10 μ m, except for the enlarged images of HMR-1 for which the scale bars are 3 μ m. For all quantifications, each data point in the graphs represents a single animal, *n* values are indicated in the graphs, data is normalized to the control conditions, and the error bars show mean \pm standard deviation (SD). For the statistical analysis, an unpaired t-test was performed, except for the HMR-1 quantifications for which an ANOVA with Šidák correction for multiple testing was performed.

RIGA *et al.*, 2021). Upon *gck-4* RNAi, PAR-6 and LET-413 still localize to their respective subcellular domains (Figure 1C). However, surprisingly, the cortical levels of both proteins are upregulated, particularly in the case of LET-413 (Supplementary figure 1C). In a previous publications from our lab, we utilized overexpression lines of PAR-6 and LET-413, deliberately elevating their cortical levels (KROLL *et al.*, 2021; WAAIJERS *et al.*, 2016). Notably, these animals did not exhibit any phenotypes resembling the *gck-4* RNAi phenotype, suggesting that the increased cortical levels are not the cause of the observed defects. So, loss of GCK-4 does not affect the establishment or maintenance of apical-basolateral polarity, however it does impact the cortical levels of these polarity regulators.

Finally, we investigated the CeAJ in the intestine upon GCK-4 knockdown. The *C. elegans* intestine has three junctional complexes: DLG-1/AJM-1 complex (DAC), SAX-7/MAGI-1/AFD-1 complex (SMAC) and Cadherin/Catenin complex (CCC) (LABOUESSE, 2006; MCGHEE, 2007; PÁSTI & LABOUESSE, 2018). Therefore, to examine all three complexes, we made use of the endogenous *dlg-1::AID*::mCherry*, *afd-1::GFP* and *hmr-1::GFP* alleles (CHAPTER 2; RIGA *et al.*, 2021). DLG-1 and AFD-1 appeared largely unaffected by the loss of GCK-4, retaining their localization to the CeAJ and exhibiting uniform distribution throughout the intestine (Figure 1D). However, junctional AFD-1::GFP levels were about twice as high upon GCK-4 depletion. Notably, the AFD-1::GFP animals also carry the LET-413::AID*::GFP allele, which may interfere with the quantifications. However, LET-413 is not enriched at the CeAJ in either wild-type or GCK-4-depleted conditions (Figure 1C). Furthermore, LET-413 levels are relatively low compared to AFD-1, rendering LET-413::AID*::GFP virtually negligible in comparison to AFD-1::GFP (Supplementary figure 1D).

To conclude, it appears that GCK-4 has no major impact on the organization of DAC or SMAC. Using HMR-1::GFP, we analysed the CCC in both control and *gck-4* RNAi backgrounds. Normally, HMR-1 exhibits homogeneous distribution throughout the junctions in the intestine. However, this pattern is disrupted upon GCK-4 depletion, which resulted in varying junctional levels throughout the intestine (Figure 1D). In the majority of the intestines in GCK-4 knockdown animals, the average HMR-1 levels are comparable to control animals, however brighter foci can be observed (Figure 1D – HMR-1, box 2). In small sections of the intestine, junctional HMR-1 levels are approximately 15 times higher compared to control animals (Figure 1D – HMR-1, box 3). In these areas, the junctions deviate from the typical ladder-like pattern, with the two parallel lines that run from anterior to posterior intersecting. To conclude, GCK-4 does not appear to exert an influence on the organization of the DAC and SMAC, but it plays a crucial role in the proper formation of the CCC. Although the adherens junctions are formed, it is not uniform, exhibiting small foci as well as seemingly aggregated regions with altered morphology.

To summarize, GCK-4 plays an indispensable role in the regulation of intestinal morphogenesis and facilitating lumen formation. The absence of GCK-4 leads to changes in cytoskeletal, junctional, and polarity networks. Among these, the most significant alterations are in the organization of the apical actin network and adherens junctions. Nevertheless, it is yet to be determined whether these changes arise directly from GCK-4 depletion or if they represent downstream responses to the altered intestinal morphology.

GCK-4 localizes to the tip of the intestinal microvilli

To gain a better insight in the function of GCK-4, we next investigated its localization pattern. We inserted the sequences encoding mCherry in combination with an auxin inducible degron (AID*) or green fluorescent protein (GFP) into the endogenous locus using CRISPR/Cas9 genome engineering. GCK-4::GFP is expressed and apically enriched in the intestine from the bean stage onwards, shortly after polarization of the intestinal cells (Figure 2A). This apical localization in the intestine persists throughout embryonic development, and subsequently, GCK-4 becomes expressed and apically enriched in the pharynx as well (Figure 2A). After hatching, GCK-4 is present in several different epithelial tissues, primarily localizing at the apical domain. These tissues include the intestine, excretory canal, hypodermis (including the seam cells), spermatheca, uterus, and vulva (Figure 2B). GCK-4 is also present in the pharynx, where it appears to be expressed in the muscle cells. Interestingly, GCK-4 does not localize to the cortex in the pharynx, but rather is found in the cytoplasm (Figure 2B).

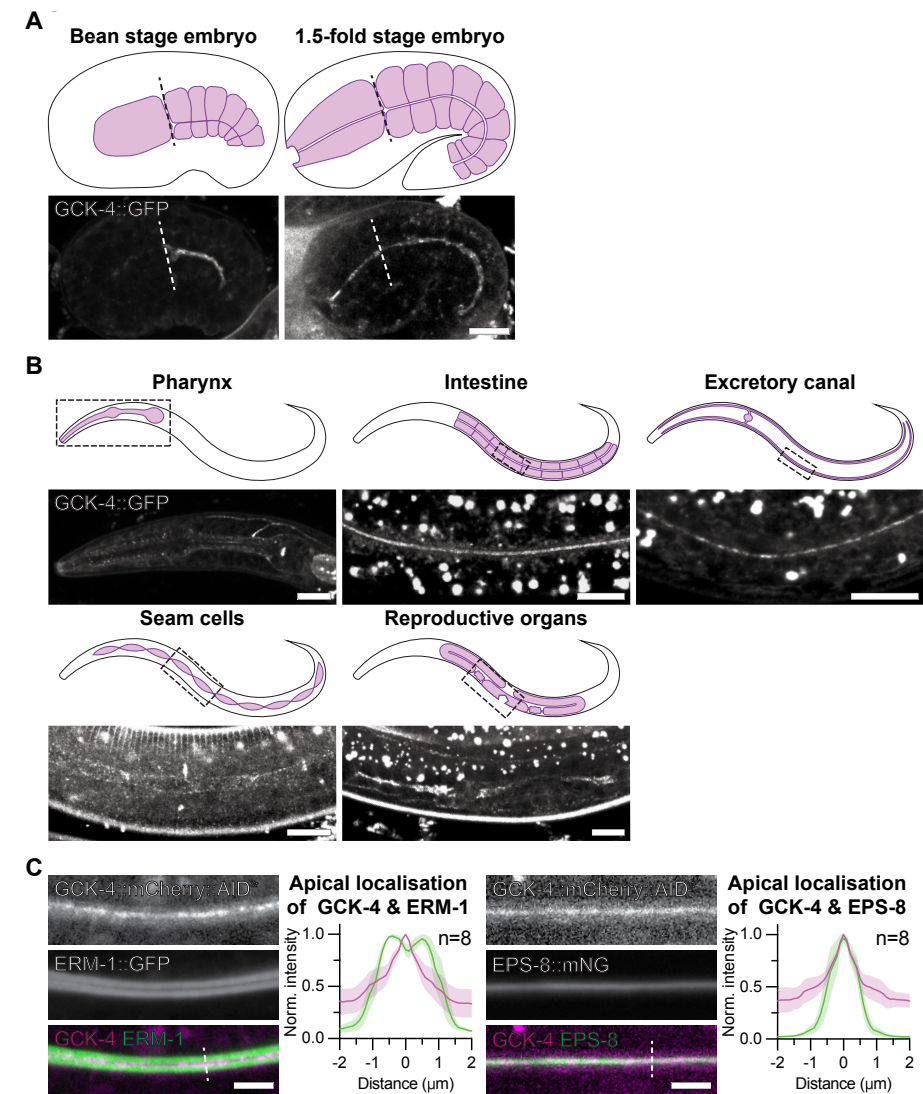


Figure 2: GCK-4 localizes to the tip of the microvilli in the intestine. (A, B) Spinning disk microscopy images of GCK-4::GFP in embryos and various organs in the larvae, respectively, with complementary illustrations of the respective developmental stages and organs. In A, the dashed line separates the pharynx (left) from the intestine (right). Scale bars are 10 μ m. (C) Spinning disk microscopy image of the GCK-4::mCherry:AID* distribution relative to ERM-1::GFP and EPS-8::mNeonGreen at the apical membrane of L4 larval intestines with complementary quantifications. Dashed line serves as an example of the line scan position used for the graphs on the right. Scale bars are 3 μ m. Graphs plot the relative fluorescence intensity across the opposing brush borders for which zero is the intestinal lumen. The indicated n values indicate animals used, data is normalized to the maximum value of the measured protein in the same animal, and solid line represents the mean and the shading the \pm SD. All Images shown are representative maximum intensity projections.

Upon closer inspection of the larval intestine, GCK-4 appeared to strictly localize to the tip of the apical microvilli (Figure 2B). In order to validate this, we compared the localization of GCK-4::mCherry::AID* to ERM-1::GFP, which localizes along the entire length of microvilli, and EPS-8::mNeonGreen, which localizes to the microvillar tips (CHAPTER 2; CROCE *et al.*, 2004). GCK-4 localized apical to ERM-1 overlapping with EPS-8 in the microvillar tips (Figure 2C). To conclude, GCK-4 resides at the apical domain of various epithelial tissues, and in the intestine specifically localizes to the tips of microvilli.

GCK-4 is not the sole ERM-1 T544 kinase

Orthologs of GCK-4 in mammals and *Drosophila* largely act through phosphorylation of substrates by the kinase domain. However, kinase-independent functions have also been reported (CONWAY *et al.*, 2017; HIPFNER *et al.*, 2004; PANNETON *et al.*, 2015; PELASEYED *et al.*, 2017). To determine if the contribution of GCK-4 to lumen formation is mediated through phosphorylation by its kinase domain, we employed CRISPR/Cas9 technology to generate an endogenous kinase-dead allele of GCK-4 by introducing a mutation in the ATP binding site (K64R) (SABOURIN & RUDNICKI, 1999). This kinase dead allele of GCK-4 is not homozygous viable and causes phenotypes that are highly similar to those observed in *gck-4* RNAi animals. These homozygous animals derived from heterozygous parents arrest at the L1 larval stage, display reduced levels of apical YFP::ACT-5, and show a cystic intestinal lumen accompanied by multiple constrictions (Figure 3A). Furthermore, all the homozygous animals displayed these defects, validating that the *gck-4* phenotype is 100 % penetrant. Therefore, we conclude that the kinase domain is essential for GCK-4 activity and that most or all GCK-4 activity requires presence of a functional kinase domain.

Next, we wanted to identify the kinase substrate(s) of GCK-4. Orthologs of GCK-4 are kinases of the ERM protein family, phosphorylating a conserved residue on the C-terminal tail responsible for actin binding (BELKINA *et al.*, 2009; HIPFNER *et al.*, 2004; VISWANATHA *et al.*, 2012). The sole *C. elegans* ERM ortholog, ERM-1, is an important actin regulator in the intestine, and loss of the protein causes seemingly identical morphological and luminal defects as loss of GCK-4 (Figure 1A) (GÖBEL *et al.*, 2004; VAN FÜRDEN *et al.*, 2004). In addition, the conserved C-terminal T544 phosphosite is important for fine-tuning ERM-1 activity. The absence of T544 phosphorylation leads to tubulogenesis defects in both the intestine and excretory canal, although these are less severe compared to the complete loss of ERM-1 as the affected animals remain viable (CHAPTER 2). Taken together, we hypothesize that GCK-4 functions as an ERM-1 T544 kinase, thereby partially explaining the phenotype observed upon GCK-4 depletion.

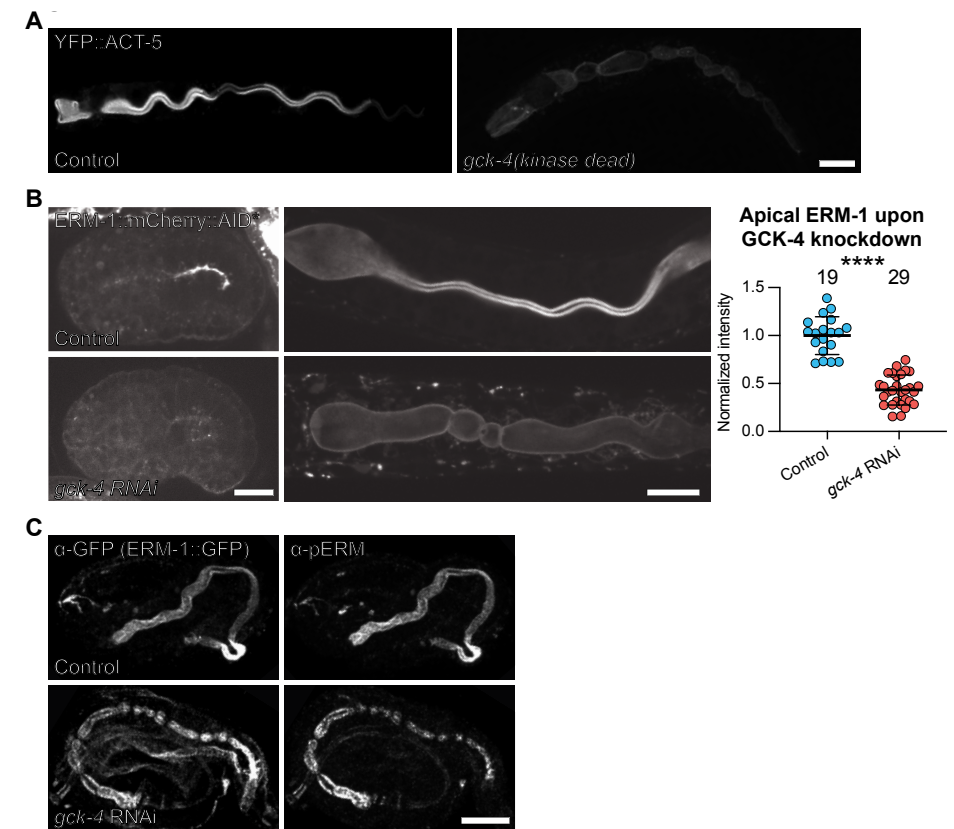


Figure 3: GCK-4 is not the sole ERM-1 T544 kinase. (A) Spinning disk microscopy images of control and *gck-4(kinase dead)* L1 stage larvae expressing YFP::ACT-5. **(B)** Spinning disk microscopy images of control and *gck-4* RNAi animals expressing ERM-1::GFP in both a bean stage embryos and L1 stage larvae with complementary quantifications. Quantifications of apical ERM-1::GFP levels were done in L1 larvae. For the quantifications, each data point in the graph represents a single animal, n values are indicated in the graph, data is normalized to the control condition, the error bars show mean \pm SD, and an unpaired t-test was performed. **(C)** Spinning disk microscopy images of control and *gck-4* RNAi embryos stained with antibodies recognizing the ERM-1::GFP (α -GFP) and phosphorylated ERM-1 T544 residue (α -pERM). All Images shown are representative maximum intensity projections, and all scale bars are 10 μ m. Within one experiment the images are acquired and displayed with the same settings for comparison, except for C due to a substantial variation in staining efficiency.

To investigate the relationship between GCK-4 and ERM-1, we first examined ERM-1::GFP localization upon depletion of GCK-4. Like GCK-4, ERM-1 becomes enriched at the apical membrane shortly after polarization during embryonic development in the intestine (Figure 1A) (CHAPTER 2; BIDAUD-MEYNARD *et al.*, 2021). However, upon *gck-4* RNAi, the apical enrichment of ERM-1 is delayed (Figure 3B). Furthermore, ERM-1 levels exhibit a 2-fold reduction at the apical domain in arrested larvae and are around 1.5-fold increased at the basolateral membrane and in the cytoplasm (Figure 3B; Supplementary figure 2A). These

findings are consistent with observations in T544A phosphonull mutant animals (CHAPTER 2). In addition, the ERM-1 interacting protein NRFL-1 displayed a similar localization defect as ERM-1 in *gck-4* RNAi animals (Supplementary figure 2B) (CHAPTER 3).

The data above support the notion that GCK-4 is an ERM-1 T544 kinase. However, reduced levels of ERM-1 and NRFL-1 may also be a secondary consequence of reduced apical actin levels or other changes to the apical surface caused by GCK-4 inactivation. We therefore more directly examined ERM-1 T544 phosphorylation levels using an antibody specific for the phosphorylated form of the conserved C-terminal residue of ERM proteins (pERM). Previously, we showed that this pERM antibody does not stain the ERM-1 phosphonull allele or wild-type ERM-1 of a sample treated with a phosphatase (CHAPTER 3). We depleted GCK-4 by RNAi in ERM-1::GFP expressing animals, and stained embryos with the pERM-specific antibody as well as an anti-GFP antibody to visualize total ERM-1 protein. Depletion of GCK-4 did not cause a loss of pERM staining, showing that the T544 residue is still phosphorylated in the absence of GCK-4 (Figure 3C). In addition, we also failed to detect a physical interaction between ERM-1 and GCK-4 using the CeLINC assay, which is designed to identify binary interactions *in vivo* (Supplementary figure 2C) (KROLL *et al.*, 2021). These experiments demonstrate that GCK-4 is not the kinase, or at least not the only kinase, that phosphorylates the T544 residue of ERM-1 in the intestine.

Proteomic approaches to identify candidate GCK-4 substrates

As the *gck-4* phenotype is not explained by a loss of ERM-1 T544 phosphorylation (Figure 3C), we set out to experimentally identify candidate substrates of GCK-4 by combining two proteomic approaches: phosphoproteomics and proximity-labeling. Using phosphoproteomics, we can detect differences in phosphorylation status of proteins upon GCK-4 depletion. However, phosphoproteomic approaches often yield hundreds or thousands of candidate sites, and it is not possible to distinguish phosphorylation changes that are a direct consequence of GCK-4 loss from secondary consequences. Proximity-labeling allows us to detect proteins in close-proximity to GCK-4, but does not inform about the nature of an interaction or if there is a direct physical interaction at all. The combination of both techniques allows us to detect proteins that are both in close-proximity of GCK-4 and lose phosphorylation upon GCK-4 depletion, and should therefore yield a shortlist of candidate kinase substrates.

For the phosphoproteomics, we employed the auxin-inducible degradation (AID) system to deplete GCK-4 specifically in the intestine, preventing us from picking up GCK-4 targets in other tissues (ZHANG *et al.*, 2015). In addition, the AID system provides temporal control, allowing us to deplete GCK-4 for a short period, which should enhance the sensitivity of our data to phosphorylation

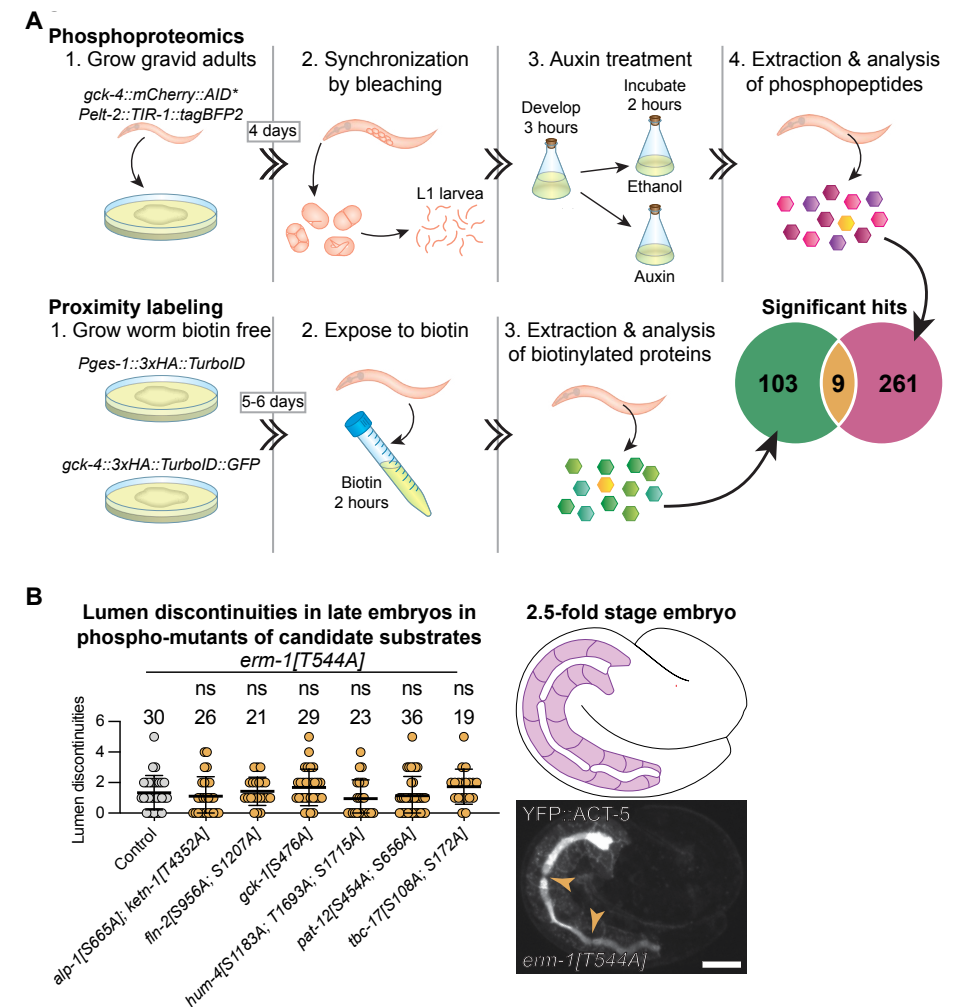


Figure 4: Proteomic approaches to find GCK-4 kinase substrate candidates. (A) A schematic illustration of the phosphoproteomics and proximity-labeling approaches used to find potential substrates of GCK-4. The green part of the Venn-diagram represents the significant hits of the PL, the pink part the significant hits of the PP, and the yellow part represents the common hits between the two approaches. **(B)** Quantification of lumen discontinuities in late embryos of the different GCK-4 substrate candidates in an *erm-1[T544A]* background expressing YFP::ACT-5. The image on the right is a spinning disk microscopy image of an *erm-1[T544A]* embryo to demonstrate the counted gaps in the intestine, indicated with the orange arrowhead, with a complementary illustration. The image shown is a representative maximum intensity projection, and the scale bar is 10 μm. For the quantification, each data point in the graph represents a single animal, n values are indicated in the graph, the error bars show mean ± SD, and an ANOVA with Šidák correction for multiple testing was performed.

changes directly linked to GCK-4 depletion. For the procedure, we obtained a synchronized L1 population expressing endogenous GCK-4::mCherry::AID* and TIR1 from the *elt-2* intestinal promoter. These synchronized animals were treated with either ethanol as a control or auxin (dissolved in ethanol) for GCK-4 depletion (Figure 4A - “Phosphoproteomics”). Although we were unable to detect GCK-4 after just 15 minutes of auxin exposure, we chose to treat the animals for 2 hours as phosphorylation is lost over time (Supplementary figure 3A). From these treated animals, phosphopeptides were extracted and analyzed using mass spectrometry.

For the proximity-labeling, we made use of a TurboID-based approach following previously established protocols for *C. elegans* (ARTAN *et al.*, 2021; BRANON *et al.*, 2018). We generated a CRISPR/Cas9 engineered endogenous *gck-4::3xHA::TurboID::GFP* allele, and made use of an existing intestinal cytoplasmic TurboID, *Pges-1::3xHA::TurboID*, line as a control (BRANON *et al.*, 2018). In a biotin-free environment, we cultured these strains to minimize biotinylation, thereby reducing the occurrence of false positive hits (Figure 4A - “Proximity labeling”). Following this, we administered biotin treatment to these animals for 2 hours, and then we conducted protein extraction on these worms. Subsequently, we enriched the protein extract for biotinylated proteins and subjected them to analysis using mass spectrometry.

For both the phosphoproteomics and proximity-labeling we observed clear differences between control and the GCK-4 samples. Phosphoproteomics identified 285 phosphorylated sites in 261 proteins that were significantly enriched in control vs. GCK-4 depleted animals (i.e. sites that lost phosphorylation upon GCK-4 loss). Proximity-labeling identified 103 proteins that were significantly enriched in *gck-4::3xHA::TurboID::GFP* animals compared to controls (Figure 4A, “Significant hits”; Supplementary figure 3B). Combining the two approaches, we found nine common hits: ALP-1, FLN-2, GCK-1, HUM-4, KETN-1, PAT-12, RPS-19, TBC-17 and UNC-15 (Supplementary table 1). RPS-19 is a ribosomal protein not likely to be specifically related to the *gck-4* phenotype, and UNC-15 is expressed solely in muscle cells (KAGAWA *et al.*, 1989). We therefore regarded these proteins as likely false positives. Most of the remaining hits have been linked to actin organization and are expressed in the intestine (BAKER & TITUS, 1997; DEMASO *et al.*, 2011; HAN & BECKERLE, 2009; HETHERINGTON *et al.*, 2011; MCKEOWN *et al.*, 2006; ONO *et al.*, 2006; PAL *et al.*, 2017; ROSE & BAILLIE, 1980).

Since the phenotype caused by GCK-4 depletion is likely due to loss of phosphorylation of target proteins, we next generated phosphonull mutants of candidate target proteins. The serine or threonine residues with altered phosphorylation levels were changed into non-phosphorylatable alanines using CRISPR/Cas9 genome engineering. For some proteins we mutated more than one phosphosite, as phosphorylation of multiple sites was significantly reduced upon GCK-4 degradation. It is possible that GCK-4 has multiple kinase substrates

and that the *gck-4* phenotype is due to loss of phosphorylation of multiple proteins. To increase our chances of identifying relevant target proteins, we therefore generated the phosphomutants in the sensitized background of the *erm-1[T544A]* allele, which predisposes animals to intestinal defects when combined with other mutations. We also combined the *alp-1[S665A]* and *ketn-1[T4352A]* phosphomutants since *alp-1* and *ketn-1* are genetic interactors (HAN & BECKERLE, 2009). In a previous study, we found that counting the number of constrictions in late-embryos (post 2-fold embryos) is an accurate prediction of the severity of the *erm-1* and related phenotypes (CHAPTER 3). Therefore, we used the same assay to investigate the effects of the phosphomutants of candidate substrates on intestinal morphogenesis. Unfortunately, none of the phosphomutant combinations we investigated resulted in a change in the number of gaps in the late-embryonic intestine compared to the single *erm-1[T544A]* mutant alone. Thus, the tested phosphosite combinations are not responsible for the *gck-4* phenotype.

Discussion

In this study, we identified the *C. elegans* ortholog of LOK and SLK, GCK-4, as an essential regulator of lumen formation in the intestine. Loss GCK-4 results in a widened lumen accompanied by multiple constrictions, and the animals arrest as L1 larvae presumably because they are unable to feed. Depletion of GCK-4 notably affects both the apical actin network and adherens junctions. In most tissues, GCK-4 localizes to the apical membrane, and in the intestine GCK-4 localizes to the tips of the microvilli. Furthermore, we showed that the kinase domain of GCK-4 is essential for its activity. Surprisingly, GCK-4 does not seem to act through phosphorylation of ERM-1, despite the similarity between *gck-4* and *erm-1* phenotypes and the GCK-4 orthologs acting as ERM kinases (BELKINA *et al.*, 2009; GÖBEL *et al.*, 2004; HIPFNER *et al.*, 2004; VAN FÜRDEN *et al.*, 2004; VISWANATHA *et al.*, 2012). To identify the GCK-4 kinase substrates critical for intestinal lumen formation, we combined phosphoproteomics and proximity-labeling approaches. However, our initial short list of phosphosite candidates did not yield any essential targets.

GCK-4 seems to be a regulator of the apical actin cytoskeleton

What role does GCK-4 play in lumen formation in the *C. elegans* intestine? Our research indicates that GCK-4 influences various aspects of the intestine, however we posit that its primary function lies in regulating the actin cytoskeleton, supported by three key observations. First, the *gck-4* phenotype mimics the *act-5* and *erm-1* phenotypes and the phenotype of animals with combined phosphonull *erm-1* and *nrfl-1* mutants, all conditions showing multiple constrictions and a widened lumen (CHAPTER 3; GÖBEL *et al.*, 2004; MACQUEEN *et al.*, 2005; VAN FÜRDEN *et al.*, 2004). In addition, loss of the microvillar actin plus-end capping protein EPS-8 results in widening of the lumen, similar

to GCK-4 depletion (CROCE *et al.*, 2004). In these conditions severe microvilli defects were observed, strongly indicating that the brush border is affected in GCK-4 depleted animals as well (CHAPTER 2; CROCE *et al.*, 2004; MACQUEEN *et al.*, 2005). Second, GCK-4 resides strictly to the microvilli in the intestine, which are greatly enriched with and supported by the actin cytoskeleton. Third, hits in the proteomic analyses are enriched for proteins binding and regulating actin (Supplementary figure 3C). Some of these proteins may function in muscle sarcomeres rather than the intestine, suggesting a broader role for GCK-4 in the actin organization in the pharyngeal muscles. This aligns with findings in mammals and *Drosophila*, where the GCK-4 orthologs have been demonstrated to be pivotal for muscle development (KATZEMICH *et al.*, 2019; SABOURIN & RUDNICKI, 1999). To conclude, GCK-4 is closely linked to the actin cytoskeleton network and is most likely an actin regulator.

The orthologs of GCK-4 are primarily believed to regulate actin by phosphorylating members of the ERM protein family (BELKINA *et al.*, 2009; HIPFNER *et al.*, 2004; VISWANATHA *et al.*, 2012). We showed that loss of GCK-4 does not cause a loss of ERM-1 T544 phosphorylation, and neither ERM-1 nor the ERM-1 T544 phosphosite were hits in the proximity-labeling and phosphoproteomic screens (Figure 3C; Supplementary figure 3B). These findings strongly suggest that GCK-4 does not function as an ERM-1 kinase, or at least not as the sole one. This raises the question of how GCK-4 regulates the apical actin network in the intestine? Besides ERM proteins, the GCK-4 orthologs are known to be involved in signaling pathways, such as the MAPK and FAK pathways, and various cellular processes, such as apoptosis, proliferation, migration and tissue repair (GARLAND *et al.*, 2021). Generally, the orthologs modulate these pathways and processes by regulating the actin cytoskeleton, often through proteins like RhoA, Dynactin, or Paxillin (BAGCI *et al.*, 2020; GUILLUY *et al.*, 2008; QUIZI *et al.*, 2013; ZHAPPAROVA *et al.*, 2013). However, none of these proteins were identified in the phosphoproteomics and proximity-labeling approaches, suggesting that GCK-4 may contribute to lumen formation through a novel substrate.

In addition to the observed actin defects, the adherens junctions are altered in the intestine as well. Bright HMR-1 foci are present in the CeAJ throughout the intestine, and in certain areas HMR-1 levels are approximately 15 times higher and HMR-1 has an altered morphology (Figure 1D). This raises questions about how GCK-4 influences the CCC and how this contributes to lumen formation. If they do interact directly, it is likely that GCK-4's influence on HMR-1 occurs early in intestinal development, immediately following polarization. This is because both proteins are apically localized during this developmental stage, and they assume distinct positions in later stages of development. (LEUNG *et al.*, 1999). In non-transformed mouse mammary gland epithelial cells, SLK localizes to adherens junctions, and the absence of SLK prevents these junctions from breaking down during epithelial-mesenchymal transition (CONWAY *et al.*,

2017). Additionally, lymphocytes of LOK knockout mice exhibit enhanced cell adhesion through LFA-1/ICAMs (ENDO *et al.*, 2000). This demonstrates that the GCK-4 orthologs can localize to cell-cell junctions and have the capacity to destabilize junctions through phosphorylation. Potentially, GCK-4 depletion enhances CCC stability in the *C. elegans* intestine, leading to their maintenance at the apical side, ultimately resulting in constrictions. This aligns with previous observations, as *erm-1* exhibits a genetic interaction with *hmr-1* and *hmp-1*, the β -catenin ortholog, leading to gaps in the CeAJ network, which are not observed upon knockdowns of any of the individual genes alone (SEGBERT *et al.*, 2004; VAN FÜRDEN *et al.*, 2004). According to the phosphoproteomics analysis, HMP-1 displays approximately three-fold reduced phosphorylation upon GCK-4 knockdown at the S308 site (Supplementary table 1). This suggests that GCK-4 may influence the CCC through HMP-1 phosphorylation.

Alternatively, the disturbance in the adherens junctions may be a consequence of the disruption of the apical actin network downstream of GCK-4. Apical actin and CeAJ assembly have a reciprocal dependency, where disruption in one leads to maturation defects in the other. For instance, loss of the WAVE/SCAR actin regulator complex causes increased HMR-1 levels at the CeAJ during embryonic development (CORDOVA-BURGOS *et al.*, 2021; SASIDHARAN *et al.*, 2018). In addition, the *erm-1* phosphomutants displays an altered CeAJ morphology and local enrichments of HMR-1 in the larval intestine similar to what we observed for GCK-4 (CHAPTER 2). In *erm-1* phosphomutants, the local enrichment of HMR-1 corresponded with the presence of the constrictions, indicating that this adherens junctions defect may be accountable for the non-continuous lumen. Taken together, these findings strongly suggest that the changes in adherens junctions levels and morphology observed in the GCK-4 knockdown background stem from the disruption of the apical actin cytoskeleton rather than direct regulation of GCK-4 upon the CCC.

Improving the proteomics to find GCK-4 interactors

We performed the phosphoproteomics and proximity-labeling approaches to identify candidate substrates for GCK-4. Unfortunately, none of the significant phosphorylation sites for which we generated mutants appear to have an impact on lumen formation in the intestine. What should be our next step in uncovering GCK-4 kinase substrates?

One way would be to focus mainly on the proximity-labeling data to first find proteins related to GCK-4 and lumen formation. The phosphoproteomics data could then highlight potential GCK-4 phosphosites in these proteins. The advantage of this approach is that it would circumvent the problem that we may have identified only a subset of phosphorylation sites in particular proteins. In this regard, from the seven tested candidates, HUM-4 and FLN-2 stand out as particularly promising. HUM-4, an unconventional myosin and

founding member of class XII myosins, is of interest due to its possession of a FERM domain, like members of the ERM family (BAKER & TITUS, 1997; JOHNSON *et al.*, 2022). FLN-2 is a filamin, which are involved in anchoring, organizing and maintaining actin networks by crosslinking F-actin and are essential for brush border maintenance (DEMASO *et al.*, 2011; NAKAMURA *et al.*, 2007; ZHOU *et al.*, 2014). Additionally, FLN-2 is enriched at the apical membranes shortly after intestinal polarization, mirroring the localization of GCK-4 (BIDAUD-MEYNARD *et al.*, 2021). Three other hits found by proximity-labeling are the before mentioned proteins NRFL-1 and EPS-8, and the apical polarity protein PAR-3 (Supplementary table 1). These proteins are important for lumen formation, and depletion of these genes contributes to phenotypes similar to GCK-4 knockdown (CHAPTER 3; CROCE *et al.*, 2004; NATURALE *et al.*, 2022; PICKETT *et al.*, 2022). To conclude, the proximity-labeling data alone provides a valuable set of proteins that can be further investigated as potential GCK-4 interactors. However, the precise nature of these interactions remains uncertain, as these proteins either did not have any significant phosphosites according the phosphoproteomic analysis, or the significant ones were tested and did not yield any striking results.

An alternative way to find GCK-4 kinase substrates would be to optimize the phosphoproteomics approach to reduce the number of candidate hits. One potential improvement is to shorten the depletion time of GCK-4 to reduce the duration in which downstream phosphorylation effects of GCK-4 depletion can occur. Alternatively, we should incorporate controls for auxin treatment, as recent studies have shown that auxin can influence the physiology of *C. elegans* (BHOI *et al.*, 2021; HILLS-MUCKEY *et al.*, 2022; LOOSE & GHAZI, 2021). Given that the GCK-4 knockdown animals were treated with auxin while the control animals were not, it is likely that some changes in phosphorylation may be attributed to the auxin treatment itself. We should therefore analyze control animals that have been treated with auxin, but without protein depletion. A third improvement that is more difficult to implement is to conduct the experiment with embryos instead of L1 larva. The *gck-4* phenotype manifests during embryonic stages, as depletion of GCK-4 in L1 larvae using AID does not result in intestinal defects. In addition, apical polarity proteins play a crucial role in intestinal lumen formation, but their impact is only significant when depleted during the polarization phase of the intestine. Given that the luminal abnormalities observed in apical polarity protein depletions closely resemble the phenotypes of *gck-4* and *erm-1*, it is plausible that a similar developmental timeline applies to GCK-4 (NATURALE *et al.*, 2022; PICKETT *et al.*, 2022; SALLEE *et al.*, 2021). Unfortunately, AID-mediated depletion is difficult in embryos due to the inability of auxin to penetrate the eggshell (NEGISHI *et al.*, 2019). Alternative depletion approaches, such as ZIF-1 mediated degradation, are also impractical as loss of GCK-4 is lethal and homozygous depletion lines cannot be established (SALLEE *et al.*, 2021).

Methods

C. elegans strains and culture conditions

C. elegans strains were cultured under standard conditions (BRENNER, 1974). Only hermaphrodites were used, and all experiments were performed with animals grown at 15 °C or 20 °C on standard Nematode Growth Medium (NGM) agar plates seeded with OP50 *Escherichia coli*, unless indicated otherwise. Supplementary table 2 contains a list of all the strains used.

RNA injection

Young adults were injected with double stranded RNA targeting *gck-4* (FIRE *et al.*, 1998) derived from L4440 plasmid (Addgene #1654) based RNAis available from a library (RUAL *et al.*, 2004) and one generated in this study. For the newly generated RNAi clone, GCK-4 cDNA was amplified using primers (IDT, Supplementary table 3) with overhangs for AgeI (NEB) digestion. Both the PCR product and L4440 plasmid were digested by AgeI, and the cut plasmid was dephosphorylated. Finally, the PCR product was sticky-end ligated into the cut L4440 plasmid, and the resulting plasmid was verified by Sanger sequencing. dsRNA was obtained by amplifying the RNAi plasmids using the T7 primers and *in vitro* double-stranded RNA synthesis using the MEGAscript T7 transcription kit (Thermo Fisher Scientific). The dsRNA was injected into the gonads of young adults (FIRE *et al.*, 1998).

CRISPR/Cas9 genome editing

All alleles were made using the homology-directed repair of the CRISPR/Cas9-induced DNA double-strand breaks, for which the reagents were micro-injected into the gonad of young adults. If appropriate, repair templates included silent mutations to prevent recutting of repaired loci by Cas9. To verify the edits, the insertion sites were PCR amplified and sequenced by Sanger sequencing. Supplementary table 3 contains a list of all CRISPR/Cas9 edits made with the respective oligo sequences (IDT).

The *gck-4::mCherry::AID** and *afd-1::GFP* alleles were made using plasmid based expression of Cas9, sgRNA and a plasmid repair template (RT) contain a self-excising cassette for selection of candidate integrants (DICKINSON *et al.*, 2015). The *gck-4::mCherry::AID** plasmid RT was designed and assembled using Gibson Assembly strategy, and *afd-1::GFP* plasmid RT was assembled using the SapTrap cloning strategy, both as described previously (DICKINSON *et al.*, 2015; SCHWARTZ & JORGENSEN, 2016). The *gck-4[K64R]::mCherry::AID** allele was generated by introducing the K64R mutation in the excising *gck-4::mCherry::AID** allele, using Cas9 and sgRNA plasmids and a DNA oligo RT with \pm 35 bp homology arms. Integration events were selected using *dpy-10* co-CRISPR (ARRIBERE *et al.*,

2014). For all three CRISPR/Cas9 modifications described in this paragraph, one or two single guide RNA (sgRNA) plasmids targeting each locus were used as previously described (WAAIJERS *et al.*, 2013; WAAIJERS *et al.*, 2016).

The *gck-4::GFP*, *gck-4::TurboID::GFP* and phosphonull alleles were made using the Alt-R CRISPR/Cas9 system (IDT), as previously described (GHANTA *et al.*, 2021). RTs for the *gck-4::GFP* and *gck-4::TurboID::GFP* alleles were amplified using primers with 5' SP9 modifications (IDT) from the PJJ5001 (Chapter 6, Addgene #188324) and pRS183 (pBSK based plasmid with 3xHA::TurboID::GFP) plasmids. DNA oligos were used as RTs for the phosphonull alleles. In order to alter multiple phosphosites within one animal, reagents for generating phosphonull alleles of multiple phosphosites were injected at the same time. For these injections, the total amount of Cas9, tracrRNA, crRNA and RT used was the same as for a single CRISPR/Cas9 modification, but the amount of crRNA and RT for each phosphosite was half for two modifications, or one-third for three modifications.

Immunohistochemistry

For the staining of embryos, embryos were obtained from gravid adults by dissection in MQ H₂O on poly-L-lysine-coated frosted slides and allowed to develop at room temperature for 4 h. A coverslip (Carl Roth, #1) was lowered on top of larvae/embryos, followed by freezing in liquid nitrogen and snapping off the coverslip. Fixation was performed in formaldehyde solution with phosphatase inhibitors (3,7 % formaldehyde (Sigma-Aldrich), 250 μM EDTA and 50 mM NaF in PBS (1,35 M NaCl, 27 mM KCl, 100 mM Na₂HPO₄, 18 mM KH₂PO₄)) at room temperature for 10 min. Samples were rinsed in PBS, permeabilized (PBS + 0,5 % triton X-100 (Sigma-Aldrich)) for 30 min, washed four times with wash buffer (0,1 % Triton X-100, 250 μM EDTA and 50 mM NaF in PBS) for 10 min each and then blocked (1 % bovine serum albumin (Sigma-Aldrich) and 10 % goat serum (Sigma-Aldrich)) for 1 h at room temperature. For the staining with protein phosphatase treatment, samples were treated with Lambda Protein phosphatase (NEB) for 30 min at 30 °C followed with an additional four times washing step before they were blocked. Primary antibodies (anti-phospho-ezrin (Thr567)/radixin (Thr564)/moesin (Thr558) (48G2) rabbit mAb #3726 (Cell Signaling Technologies) 1:200 and mouse anti-GFP mAb #11814460001 (Roche) 1:100 in blocking solution were applied overnight at 4°C. Samples were then washed four times with wash buffer for 10 min each and stained with secondary antibodies (Alexa-Fluor 488 goat anti-rabbit and Alexa-Fluor 568 goat anti-mouse (Life Technologies, A-11008 and A11004), both 1:500) in blocking solution for 1 hour at room temperature. Samples were then washed four times with wash buffer and once in PBS for 10 min each and finally mounted with Prolong Gold Antifade with DAPI (Thermofisher) under a coverslip and sealed with nail polish.

CeLINC

For CeLINC, the strains were generated, the experiments were performed, and the data was analyzed as described previously (KROLL *et al.*, 2021). Young animals of the *erm-1(mib15[erm-1::GFP]); mib1s48[Pelt-2::TIR-1::tagBFP2::tbb-2-3'UTR]; gck-4(mib37[gck-4::mCherry::AID])* (BOX327) strain were micro-injected in the gonad with pJRK136 (Addgene #173744), pJRK248 (Addgene #173755) and a complementary CRY2-nanobody plasmid. In addition to those plasmids, for the experiments in which GCK-4 was the bait the pJRK249 plasmid (anti-mCherry nanobody, Addgene #173747), and for ERM-1 as bait the pJRK252 (anti-GFP nanobody, Addgene #173749) were injected. Animals were exposed to ambient light overnight before imaging to ensure aggregation and recruitment of the bait protein.

Spinning disk microscopy

Imaging of living animals was performed by mounting the larvae and embryos on a 5 % agarose pad in 20 mM tetramisole solution in M9 (0.22 M KH₂PO₄, 0.42 M Na₂HPO₄, 0.85 M NaCl, 0.001 M MgSO₄). Spinning disk confocal imaging was performed using a Nikon Ti-U microscope equipped with a Yokogawa CSU-X1 spinning disk using a 60×-1.4 NA objective, and an Andor iXON DU-885 or Prime BSI Express Scientific CMOS camera. Spinning disk images were acquired using MetaMorph Microscopy Automation & Image Analysis Software. All stacks along the z-axis were obtained at 0.25-μm intervals, and maximum intensity Z projections were done in Fiji 1.0 software. Imaging for immunohistochemistry experiments was performed on a Nikon Eclipse-Ti with Perfect Focus System microscope equipped with a Yokogawa CSU-X1-A1 spinning disk using 60× and 100× 1.4 NA objectives, and a Photometrics Evolve 512 EMCCD camera. Image scales were calibrated using a micrometer slide. For display in Figures, level adjustments, false coloring, and image overlays were done in Adobe Photoshop 24.1.0. Image rotation, cropping, and panel assembly were done in Adobe Illustrator 27.1.1. All edits were done nondestructively using adjustment layers and clipping masks, and images were kept in their original capture bit depth until final export from Illustrator for publication.

Quantitative microscopy imaging analysis

Quantitative analysis of spinning disk images was done in Fiji 1.0 and Python 3. All measurement values were first corrected for imaging system background levels by subtracting the average of a region within the field of view that did not contain any animals. Three measurements were taken per animal on a maximum projection of 3 slices, and the final value is the average of these three measurements. For the apical membrane, lateral membrane and junction measurements the max value of a 25, 10 or 25, respectively, pixel wide line perpendicular to the cellular structure was taken. For the HMR-1::GFP junction measurements, only 2 measurements were performed per worm, since the

parts with brighter junctions were usually not occurring more than two times per animal. Cytoplasmic protein levels were measured by taking the average of a region within the cytoplasm. The width of the lumen and intestine was obtained using the *par-6::GFP; let-143::mCherry* (BOX251) strain. A single line scan was taken from a single slice across an L1 larva, resulting in two peaks for both PAR-6 and LET-413 corresponding to the apical and basal membranes, respectively. The space between the max value of the two peaks was used to determine the luminal and intestinal width. Intensity distribution profiles to analyze co-distribution of ERM-1::GFP, EPS-8::mNG and GCK-4::mCherry::AID* in the microvilli were obtained by taking 25-px-wide line scans perpendicular to the apical membrane. Lines scans within one animal were aligned and normalized based on their peaks value and averaged. Measurements of multiple animals were again aligned based on the peak value.

PL sample preparation

Approximately 500 animals were allowed to produce progeny on NGM plates seeded with MG1655 *E. coli* for at least 5 days at 20 °C. The progeny was harvested and washed with M9 buffer, and incubated in M9 with MG1655 *E. coli* and 1 mM of biotin for 2 h at room temperature. Animals were washed with M9, and the M9 was aspirated after allowing the worms to settle on ice. Two volumes of RIPA buffer (50 mM Tris pH 8, 150 mM NaCl, 0.1 % SDS, 0.5 % sodium deoxycholate, 1 % Triton X-100, 1 mM PMSF) supplemented with complete protease inhibitor EDTA-free (Sigma Aldrich) were added to one volume of packed worms. Lysate were snap frozen in liquid nitrogen and stored at -80 °C until further processing.

Lysates were ground into powder in liquid nitrogen. After rethawing, DDT and SDS was added for a final concentration of 1 mM and 1 %, respectively. Lysates were then incubated at 95 °C for 5 min and sonicated for 10 min using a Diagenode Bioruptor at max setting in 30 s ON/ 30 s OFF bursts at 4 °C. Urea was added for a final concentration of 2 M. After centrifuging the lysates for 45 min at 4 °C using a tabletop centrifuge at the max speed, the clear supernatant between the pellet and surface lipid layer was transferred to a new tube. The lysates were desalted (Zepha spin Desalting Columns and Plates, 7K MWCO) to remove free biotin, and the protein concentrations were measured using the BCA Assay Kit (Thermo Scientific).

MyOne streptavidin beads (Invitrogen) were used for the biotinylated protein purification. The beads were equilibrated by washing with RIPA buffer containing 2 % SDS and 2 M urea. Then, 5 mg of total protein lysate was transferred to 110 µl of streptavidin beads and incubated overnight at 4 °C. The unbound lysate was removed, and beads were washed with 2 % SDS wash buffer (150 mM NaCl, 1 mM EDTA, 2 % SDS, 50 mM Tris-HCl pH 7.4), 1 M KCl and with 50 mM ammonium bicarbonate. Streptavidin beads were

resuspended in 50 mM ammonium bicarbonate with 50 mM acrylamide and incubated for 30 min at room temperature, after which the supernatant was replaced by 50 mM ammonium bicarbonate and 0.5 µg Trypsin (Sigma Aldrich) and incubated overnight at 20 °C. The supernatant was transferred to new tube, and samples were acidified using 10 % TFA until pH reached a value of 2-3. Lysate were stored at room temperature until mass spectrometry analysis. For the mass spectrometry analysis, nano liquid chromatography–tandem mass spectrometry (LC–MS/MS) was performed as described previously, with the exception that a 30 min linear gradient was used for the liquid chromatography (Roosjen *et al.*, 2022).

Phosphoproteomics sample preparation

Approximately 2500 animals were allowed to produce progeny on NGM plates seeded with OP50 *E. coli* for 4 days at 20 °C. The progeny was used to obtain developmentally synchronized L1 population by hypochlorite bleaching of gravid adults to release embryos, which were hatched overnight in M9 buffer. Synchronized L1 larvae were initially incubated in S medium liquid culture at 20 °C with OP50 *E. coli* and allowed to develop for 3 h. Then 1/1000 part (v/v) of ethanol and 1 M auxin (Alfa Aesar) dissolved in ethanol was added to the control and GCK-4 depletion samples, respectively. Animals were incubated for another 2 h at 20 °C, and then harvested and washed with M9 buffer. The M9 was completely aspirated, and worm pellets were snap frozen in liquid nitrogen and stored at -80 °C until further processing. The protein extraction, enrichment for phosphorylated proteins and LC–MS/MS was performed as described previously, with the exception that a 60 min linear gradient was used for the liquid chromatography (Roosjen *et al.*, 2022).

Mass spectrometry data analysis

Data handling and manipulation was performed using Python, and the statistical analysis using Perseus 2.0.7.0. For the proximity-labeling analysis the label-free quantitation (LFQ) intensity values were used, and the average LFQ values of a wild-type samples were subtracted to correct for the endogenous biotinylated proteins. For the phosphoproteomics analysis the intensity values were used for analysis. For both analyses, protein groups that contain more than two invalid measurements (equal to 0) in both conditions were excluded. After log2 transforming of the intensity values, invalid measurements were imputed according to a 1.8 down shifted normal distribution with 0.3-fold width from the distribution of the valid measurements. For statistical testing, an unpaired t-test with a Benjamini-Hochberg correction was performed. Proteins groups were considered significant hits if they had an over 2-fold change compared to the control sample, and an adjusted p value below 0.05. The presented volcano graphs were made using R 4.2.2, using the ggplot 3.4.1

package (WICKHAM, 2016). Gene Ontology Enrichment Analysis was performed using WormBase (ANGELES-ALBORES *et al.*, 2018), and the presented bar plot was made using GraphPad Prism, and Adobe Illustrator.

Statistical analysis

All statistical analyses were performed using GraphPad Prism 9. The location of the sample sizes and statistical test for population comparisons are indicated in the Figure legends. No statistical method was used to pre-determine sample sizes. No samples or animals were excluded from analysis. The experiments were not randomized, and the investigators were not blinded to allocation during experiments and outcome assessment. All presented graphs were made using GraphPad Prism and Adobe Illustrator. ns is $P > 0.05$, * is $P \leq 0.05$, ** is $P \leq 0.01$, *** is $P \leq 0.001$, and **** is $P \leq 0.0001$.

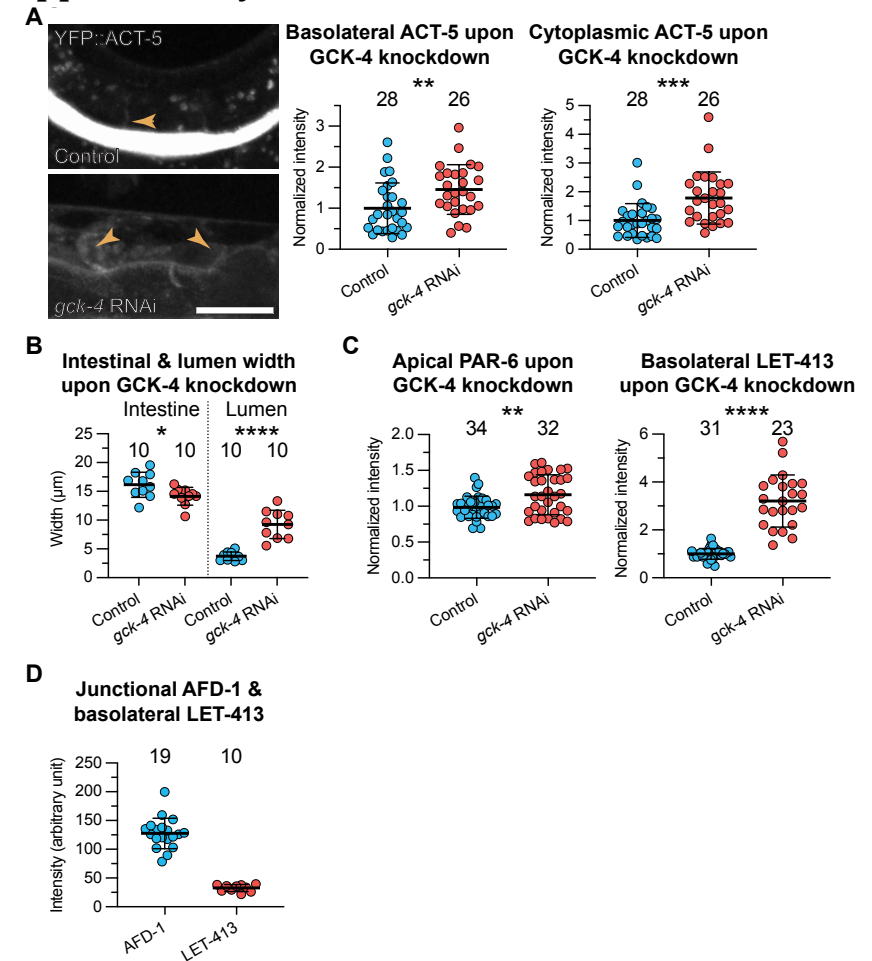
Acknowledgments

We thank Amalia Riga for the *afd-1(mib34[afd-1::GFP])* I allele (BOX314), and the Gregoire Michaux group for the *eps-8(bab140[eps-8::mNG])* IV allele (BOX669). We also thank Wormbase (HARRIS *et al.*, 2020) and the Biology Imaging Center, Faculty of Sciences, Department of Biology, Utrecht University. The *tmC24[F23D12.4(tmIs1233)]* allele (BOX499) was provided by the *Caenorhabditis* Genetics Center, which is funded by the US National Institutes of Health (NIH) Office of Research Infrastructure Programs (P40 OD010440). We thank members of the S. van den Heuvel, S. Ruijtenberg, S.J.E. Suijkerbuijk, and M.B. groups for helpful discussions.

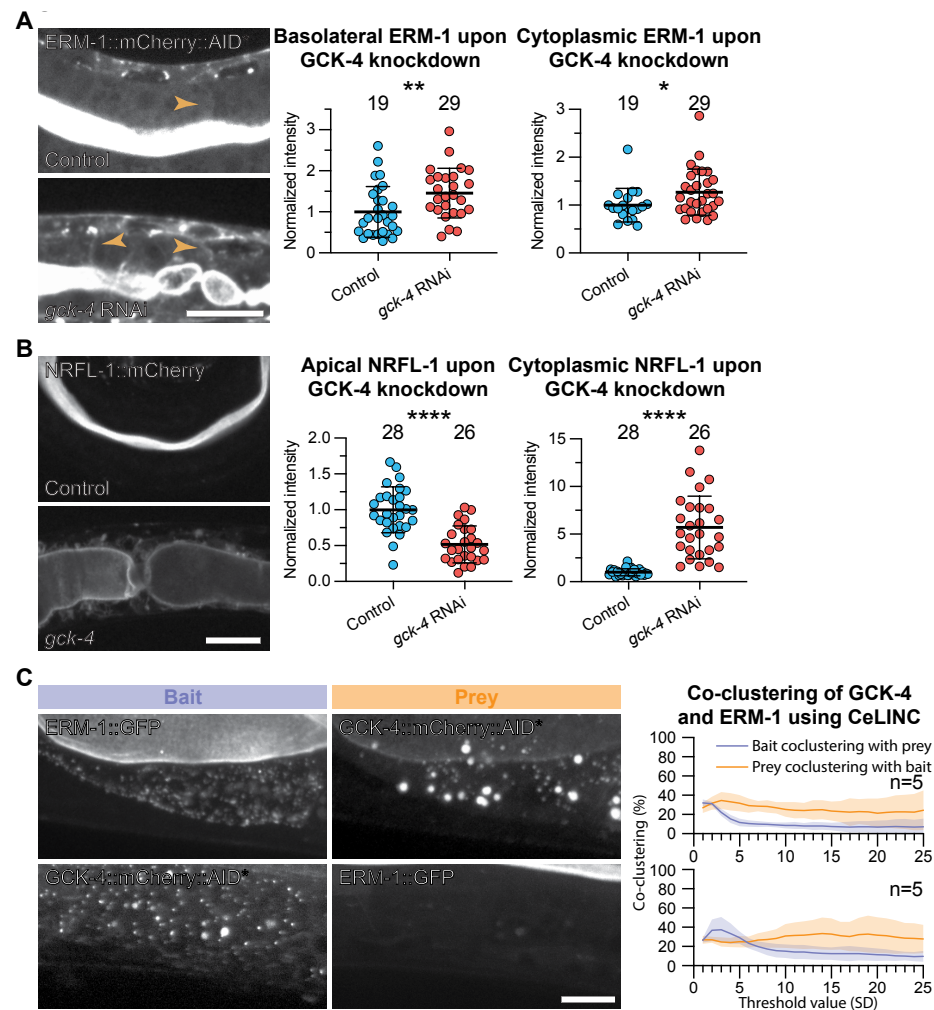
Author contributions

Conceptualization: J.J.S., J.J.R., M.B.; Methodology: J.J.R., J.J.S., S.T., M.J., J.R.K., R.S.; Formal analysis: J.J.S., J.J.R., M.J.; Investigation: J.J.R., J.J.S., S.T., M.J., J.R.K., R.S.; Writing - original draft: J.J.S.; Writing - review & editing: M.B.; Visualization: J.J.S.; Supervision: J.J.S., D.W., M.B.; Project administration: M.B.; Funding acquisition: D.W., M.B.

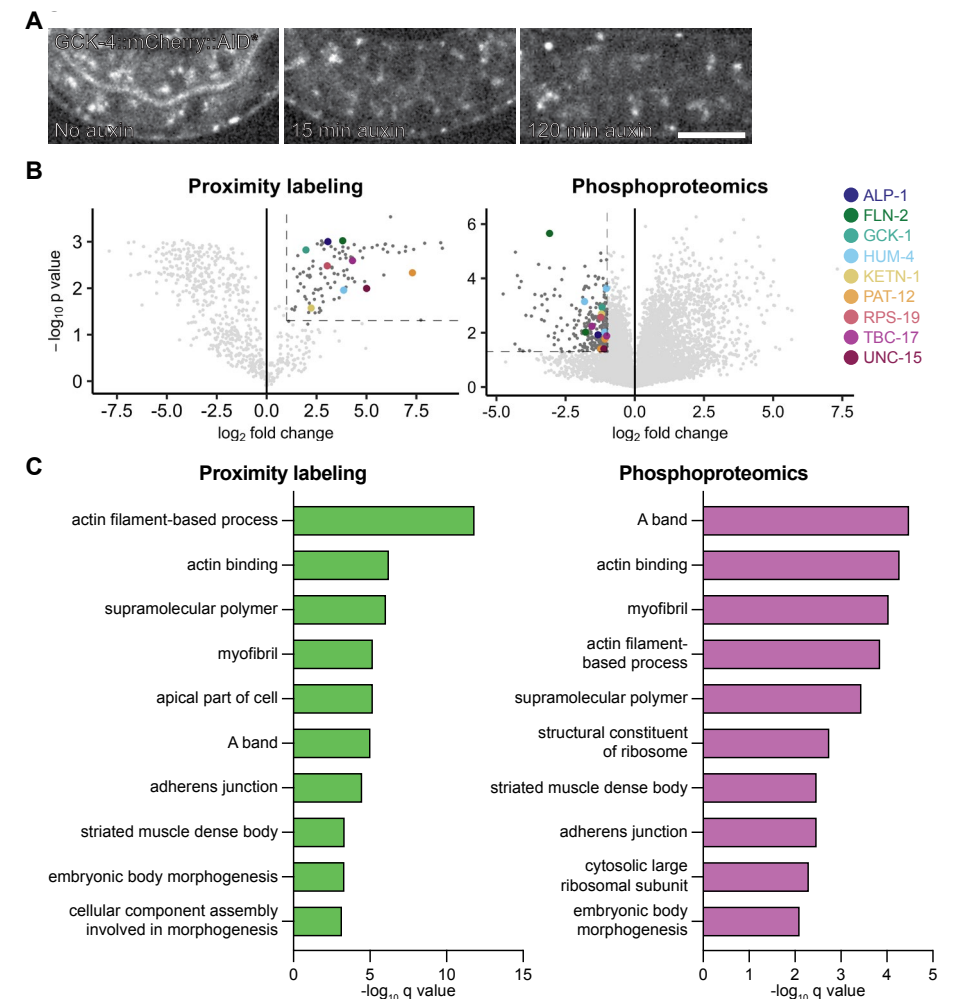
Supplementary material:



Supplementary figure 1: GCK-4 is vital for proper intestinal morphology. (A) Spinning disk microscopy image of intestines from control and *gck-4* RNAi L1 larvae expressing YFP::ACT-5 with complementary quantifications. Images shown are representative maximum intensity projections, are acquired and displayed with the same settings for comparison, and scale bars are 10 μm . (B) Quantification of the width of the intestine and lumen of control and *gck-4* RNAi L1 larvae. (C) Quantification of the intestinal apical PAR-6::GFP and basolateral LET-413::mCherry levels of control and *gck-4* RNAi L1 larvae. (D) Quantification of the intestinal junctional AFD-1::GFP and basolateral LET-413::AID*::GFP levels of control L1 larvae. For all quantifications, each data point in the graphs represents a single animal, n values are indicated in the graphs, the error bars show mean \pm SD, and an unpaired t-test was performed. In A and D, the data is normalized to the control conditions.



Supplementary figure 2: GCK-4 affects ERM-1 and NRFL-1 localization, but does not seem to physically interact with ERM-1. (A, B) Spinning disk microscopy images of intestines from control and *gck-4 RNAi* L1 larvae expressing ERM-1::GFP (A) and NRFL-1::mCherry (B) with complementary quantifications. In A, the orange arrow heads point to the lateral membranes. Images shown are representative maximum intensity projections and are acquired and displayed with the same settings for comparison, and scale bars are 10 μ m. For the quantifications, each data point in the graphs represents a single animal, n values are indicated in the graphs, the data is normalized to the control conditions, the error bars show mean \pm SD, and unpaired t-tests was performed. (C) Spinning disk microscopy images and quantifications of CeLINC with ERM-1 and GCK-4 in the intestine. Images shown are representative maximum intensity projections, and scale bars are 10 μ m. Graphs plot the co-clustering of bait with prey foci and vice versa with increasing intensity SD threshold. The indicated n values indicate animals used, and solid line represents the mean and the shading the \pm SD.



Supplementary figure 3: Combined phosphoproteomics and proximity-labeling analysis to discover substrate candidates of GCK-4. (A) Spinning disk microscopy images in L1 larvae upon depletion of GCK-4::mCherry::AID* in the intestine using various time points of auxin exposure. The images shown are a representative single slice images and are acquired and displayed with the same settings for comparison, and the scale bar is 5 μ m. (B) Volcano plots of both the phosphoproteomics and proximity-labeling data. For the PL, each data point in the graphs represents a protein group, and for the PP, each data point represents a phosphosite. The light and dark gray data points represent non-significant and significant, respectively, changed protein groups or phosphosites between the control and GCK-4 samples. The colored dots are proteins that are significant in both proteomic approaches, see legend on the right. The dotted lines mark the thresholds for what is considered significant. (C) Quantification of top ten most significantly enriched GO-terms in the significant protein groups or phosphosites of the proximity-labeling and phosphoproteomics, respectively, analyses.

Gene	PL log2 FC	PL p-value	PP log2 FC	PP p-value	Phosphosite
<i>alp-1</i>	3,07	0,0012	-1,33	0,0119	S665
<i>fln-2</i>	3,81	0,0012	-1,78 -3,08	0,0095 0,000002	S956 S1207
<i>gck-1</i>	1,97	0,0016	-1,18	0,0012	S476
<i>hum-4</i>	3,86	0,0126	-1,82 -1,08 -1,02	0,0007 0,0095 0,0002	S1183 T1693 S17215
<i>ketn-1</i>	2,23	0,0277	-1,20	0,0020	T4352
<i>pat-12</i>	7,30	0,0050	-1,08 -1,23	0,0170 0,0340	S454 S646
<i>rps-19</i>	3,03	0,0033	-1,23	0,0027	S6
<i>tbc-17</i>	4,30	0,0022	-1,55 -1,02	0,0058 0,0132	S108 S172
<i>unc-15</i>	5,00	0,0123	-1,11	0,0393	S16
<i>eps-8</i>	6,32 4,39	0,0013 0,0010	No significant phosphosites		
<i>nrf1-1</i>	1,56	0,0016	No significant phosphosites		
<i>par-3</i>	7,91 2,15	0,0012 0,0060	No significant phosphosites		
<i>hmp-1</i>	Not significant		-1,65	0,0036	S308

Supplementary table 1: Relevant results of the proximity-labeling and phosphoproteomics analysis.

Strain	Genotype	Origin
BOX213	<i>erm-1(mib15[erm-1::GFP]) I</i>	Ramalho <i>et al.</i> , 2020
BOX251	<i>par-6(mib24[par-6::eGFP]) I</i> <i>let-413(mib29[let-413::mCherry]) V</i>	Castiglioni <i>et al.</i> , 2021, Riga <i>et al.</i> , 2021
BOX314	<i>afd-1(mib34[afd-1::GFP]) I</i> <i>let-413(mib32[let-413::AID::eGFP]) V</i>	Riga <i>et al.</i> , 2021, This study
BOX327	<i>erm-1(mib15[erm-1::GFP]) I</i> <i>mibIs48[Pelt-2::TIR-1::tagBFP2::tbb-2-3'UTR] IV</i> <i>gck-4(mib37[gck-4::mCherry::AID]) X</i>	This study
BOX377	<i>erm-1(mib40[erm-1::mCherry::AID]) I</i> <i>maph-1.1(mib12[GFP::maph-1.1]) I</i>	Remmelzwaal <i>et al.</i> , 2021, Waaier <i>et al.</i> , 2016
BOX417	<i>mibIs48[Pelt-2::TIR-1::tagBFP2::tbb-2-3'UTR] IV</i> <i>gck-4(mib37[gck-4::mCherry::AID]) X</i> <i>Is[Pges-1::act-5::YFP]</i>	Castiglioni <i>et al.</i> , 2021, This study
BOX429	<i>nrf1-1(mib73[nrf1-1::mCherry]) IV</i> <i>mibIs48[Pelt-2::TIR-1::tagBFP2::tbb-2-3'UTR] IV</i> <i>Is[Pges-1::act-5::YFP]</i>	Chapter 3
BOX475	<i>ifb-2(mib101[ifb-2::egfp] II)</i>	Remmelzwaal <i>et al.</i> , 2021
BOX499	<i>mibIs48[Pelt-2::TIR-1::tagBFP2::tbb-2-3'UTR] IV</i> <i>gck-4(mib89[gck-4[K64R]::mCherry::AID]) X /</i> <i>tmC24[F23D12.4(tmIs1233); unc-9(tm9718)] X</i> <i>Is[Pges-1::act-5::YFP]</i>	Dejima <i>et al.</i> , 2018, This study
BOX568	<i>par-6(mib30[par-6::aid::GFP]) I</i> <i>gip-1(wow25[tagRFP-t::3xMyc::gip-1]) III</i> <i>mibIs49[Pwrt-2::TIR-1::tagBFP2::tbb-2-3'UTR] IV</i>	Castiglioni <i>et al.</i> , 2021
BOX669	<i>eps-8(bab140[eps-8::mNG]) IV</i> <i>gck-4(mib37[gck-4::mCherry::AID]) X</i>	Lab of Gregoire Michaux, This study
BOX804	<i>hmr-1(he298[hmr-1::GFP]) I</i> <i>mibIs49[Pwrt-2::TIR-1::tagBFP2::tbb-2-3'UTR] IV</i> <i>dlg-1(mib128[dlg-1::AID::mCherry]) X</i>	Riga <i>et al.</i> , 2021
BOX909	<i>gck-4(mib210[gck-4::GFP]) X</i>	This study
BOX963	<i>erm-1(mib10[erm-1[T544A]]) I</i> <i>fln-2(mib243[fln-2[S956A; A1207S]]) X</i> <i>Is[Pges-1::act-5::YFP]</i>	Ramalho <i>et al.</i> , 2020, This study
BOX965	<i>erm-1(mib10[erm-1[T544A]]) I</i> <i>gck-1(mib245[gck-1[S476A]]) V</i> <i>Is[Pges-1::act-5::YFP]</i>	This study
BOX972	<i>erm-1(mib10[erm-1[T544A]]) I</i> <i>tbc-17(mib253[tbc-17[S108A; S172A]]) II</i> <i>Is[Pges-1::act-5::YFP]</i>	This study
BOX985	<i>erm-1(mib10[erm-1[T544A]]) I</i> <i>hum-4(mib248[hum-4[S1183; T1693A; S1715]]) X</i> <i>Is[Pges-1::act-5::YFP]</i>	This study

~ Table continues on the next page ~

Strain	Genotype	Origin
BOX986	<i>erm-1(mib10[erm-1[T544A]]) I</i> <i>pat-12(mib249[pat-12[S454A; S646A]]) III</i> <i>Is[Pges-1::act-5::YFP]</i>	This study
BOX987	<i>erm-1(mib10[erm-1[T544A]]) I</i> <i>alp-1(mib238[alp-1[S665A]]) IV</i> <i>ketn-1(mib240[ketn-1[T4352A]]) V</i> <i>Is[Pges-1::act-5::YFP]</i>	This study

Supplementary table 2: List of *C. elegans* strains used.

<i>gck-4</i> RNAi	
cDNA For.	ATCGACCGGTAGATGGATGCTATGGAACGC
cDNA Rev.	ATCGACCGGTAGACGAAGTGTACGACATTC
<i>afd-1::GFP</i>	
crRNA For.	TTGGAATTATGGCTTTTGCGGGG
crRNA Rev.	AACCCCGCAAAGCCATAATTC
Repair Template LHA For.	GGCTGCTCTTCGTGGCATCTCGATGCACCAAGATTGAC
Repair Template LHA Rev.	GGGTGCTCTTCGCGCTGGCTTTTGCGGGGTGGCGG
Repair Template RHA For.	CTGCTCTTCGACGTAATTCTTATGTATTTTTAAAGAAAATTGTTT TTTCAC
Repair Template RHA Rev.	GTGCTCTTCGTACGATCTCCGAACCCTAAGAAATTGTCC
Genotyping For.	CGAATTCGCTGAGGTGAAATC
Genotyping Rev.	CCTCTCAAACATGACCGCGTA
<i>gck-4::mCherry::AID*</i>	
crRNA 1 For.	TCTTAGAGCGTTCAAGGCATGTGA
crRNA 1 Rev.	AAACTCACATGCCTTGAACGCTCT
crRNA 2 For.	TCTTGTGAGAAGCATAGAGCGTTCA
crRNA 2 Rev.	AAACTGAACGCTCTATGCTTCTGAC
Repair Template LHA For.	GGCTGCTCTTCGTGGCGCGAAATGCAAGAACGAA
Repair Template LHA Rev.	GGGTGCTCTTCGCGCAGGCATGTGACGGCCAGA
Repair Template RHA For.	GGCTGCTCTTCGACGTGAACGCTCTATGCTTCTGACT
Repair Template RHA Rev.	GGGTGCTCTTCGTACTGGTTGAATCGGGATAAAACGT
Genotyping For.	TGCGAATCAGTGCAGTGGTA
Genotyping Rev.	ACAGTAAGATGGTTGAATCGGGA
<i>gck-4::GFP</i> – Same genotyping primers as <i>gck-4::mCherry::AID*</i>	
crRNA	TCAGAAGCATAGAGCGTTCA
Repair Template For.	CTCAGGCCTCAACGCTGTCTGGCCGTACATGCCTGGCAGCGGTG GCAGTGGTA
Repair Template Rev.	GAACGTAGAAATGAGTCAGAAGCATAGAGCGTTCACTTGTAGAGC TCGTCCATTC

~ Table continues on the next page ~

<i>gck-4[K64R]::mCherry::AID*</i>	
crRNA 1 For.	TCTTAATTTCAATAGACTTTGATG
crRNA 1 Rev.	AAACCATCAAAGTCTATTGAAATT
crRNA 2 For.	TCTTAAGTCTATTGAAATTCAGA
crRNA 2 Rev.	AAACTCTTGAATTTCAATAGACTT
Repair Template	CAGTGTACGGACGGATCCCAAACCTTTTGGCCGCTAGTCGAAGTA TCGAAATTCAGAAGGGCAAGAAGCTGGAAGATTTT
Genotyping For. Wild Type	TGCCGCATCAAAGTCTATTGA
Genotyping For. K64R	TTGCCGCTAGTCGAAGTATC
Genotyping For. Sequencing	TGTTTCGTGCCAATCAAGCG
Genotyping Rev.	AGCCACTTGAGTGCATCACA
<i>gck-4::TurboID::GFP</i> – Same genotyping primers as <i>gck-4::mCherry::AID*</i> and crRNA as <i>gck-4::GFP</i>	
Repair Template For.	CTCAGGCCTCAACGCTGTCTGGCCGTCACATGCCTTACCCATACG ACGTCCCAGAC
Repair Template Rev.	GAACGTAGAAATGAGTCAGAAGCATAGAGCGTTCAGTAGAGCTCG TCCATTCCGT
<i>alp-1[S665A]</i>	
crRNA	GGTGAATGCTGAGGTGATCG
Repair Template	TCCGTTGGTCTCAAAGATGTACATGCTCCAGTACCTCTTCCAAGA GCTCCGCAGCACTCACCTCAACCAGTGCAGAGCTACATTGTTCCG AG
Genotyping For. Wild Type	GTACCACTTCTCGATCACC
Genotyping For. S665A	CCTCTTCCAAGAGCTCCG
Genotyping For. Sequencing	TCCCTGAAAGCAATGGTGTAG
Genotyping Rev.	GTGATGGTCCAGTAGGTTTCATG
<i>fln-2[S956A]</i>	
crRNA	CAATTCTGAGTAGTAGGACA
Repair Template	GTAACAACACATGTGATTTTTTTTCCAGAACCATGGCATATTATT CTGAATTGTCCGGACCTGGACTGGTACGAGCACCCGT
Genotyping For. Wild Type	CAGAACCATGTCTACTACTCAG
Genotyping For. S956A	CAGAACCATGGCATATTATTCTG
Genotyping For. Sequencing	ACAAACTACTCGAGTGCATCC
Genotyping Rev.	TTGTCTAGGCTTGCTCTATTACC

~ Table continues on the next page ~

<i>fln-2[S1207A]</i>	
crRNA	CTAGATTCTCTGAGAAGTTG
Repair Template	AACGCAGTGAAGAGACAATGCTCCGAAGCCACAACCTCCTTCGTG AAGCTAGAAAAGCAGATAAGCCTTGCAATCGGTAAGC
Genotyping For.	CAACCGCCATTTTCAGCAG
Genotyping Rev. Wild Type	CTGCTTTTCTAGATTCTCTGAGAAG
Genotyping Rev. S1207A	GCTTTTCTAGCTTCACGAAGG
Genotyping Rev. Sequencing	CAATGGCTGACAGATCTTTGAAC
<i>gck-1[S476A]</i>	
crRNA	GTGTTGGTTATATTTTCGACG
Repair Template	ATCGACCTATGAGCGAACGGGTATCATCGCAAGTAGCACCAGTA AATATAATCAACACAGGACATCATCGCAATGGTGTGCAAGG
Genotyping For.	CGCTATCGCATGTTAGAAGC
Genotyping Rev. Wild Type	GTGTTGGTTATATTTTCGACGGG
Genotyping Rev. S476A	CTGTGTTGATTATATTTACTCGGTGC
Genotyping Rev. Sequencing	ACGATGTCGGAACATGGC
<i>hum-4[S1183A]</i>	
crRNA	TAAGTTTTTCTTGGGAGAAC
Repair Template	ATGGAGACCATAACAAGATCATTCTCATATTTTAAAGGCACCAGTT TTGCCAAGAAAACCTTATTCGAAGTGGGTAGTTCCCAT
Genotyping For. Wild Type	ATTTTAAAATCGCCAGTTCTCCC
Genotyping For. S1183A	TTAAAGGCACCAGTTTTGGC
Genotyping For. Sequencing	GCAAGCTGTTGAAGATAACGG
Genotyping Rev.	CCAATGTGAAGAATGGCGG
<i>hum-4[T1693A]</i>	
crRNA	GGAGGCTGTGCTGGTGTAT
Repair Template	AAACTACCACCACCAGTAGACAATGTGAGACTTATCAGGCCAATA GCTCCTGCCAGCCACCAATAACACAGTACCTGTTCCATCCGAA CCAGT
Genotyping For.	TTCTAGTGAGTTCTCTTGGTGC
Genotyping Rev. Wild Type	TGCTGGTGTATTGGCCG
Genotyping Rev. T1693A	GCAGGAGCTATTGGCCTG
Genotyping Rev. Sequencing	TGTGGAACGAGTGGTTCTTC

~ Table continues on the next page ~

<i>hum-4</i>[S1715A] – Same “Genotyping Rev. Sequencing” as <i>hum-4</i>[T1693A]	
crRNA	GTGGAGTTGGCTGTGGTACA
Repair Template	AGATGTTTAAATGGGATTTAACAAGCATTTTTTCAGGCACCAGTGC CTCAGCCAACACCACCTCCACCACCACCACCAGTCCGTGAAGAAT G
Genotyping For.	TTCCACCACCACCATCAAG
Genotyping Rev. Wild Type	TGGCTGTGGTACAGGGCT
Genotyping Rev. S1715A	TGGCTGAGGCACTGGTGC
<i>ketn-1</i>[T4352A]	
crRNA	TCGAGCTCTGGCGCTGGAGT
Repair Template	CAGGAGCCGATGAAGGTCGCTTCAAGAACTTCCAGCCCCAGCGC CAGAATTGGACGTTCCAGCCAGAGATCAAGTTAAGCTTAAGAC
Genotyping For. Wild Type	ACTCCAGCGCCAGAGCTC
Genotyping For. T4352A	GCCCCAGCGCCAGAATTG
Genotyping For. Sequencing	GAATGGAGCTCGAGGAAGTC
Genotyping Rev.	TGAGGCGACTCTGATTTCG
<i>pat-12</i>[S454A]	
crRNA	CGTCCCGTCATCACTCCGGA
Repair Template	GAGAAGAAAGAACGTCGTAGCCGTCATCACTCCTCCTCGCGTCAC CATGCAGGATGGGAGGGTCATACTGGTGGATATCAAGGTAA
Genotyping For.	AGCCTGCAACTAGGTTATTCAG
Genotyping Rev. Wild Type	CATCCGGAGTGATGACGG
Genotyping Rev. S454A	CATCCTGCATGGTGACGC
Genotyping Rev. Sequencing	AAGGAGGATGTGATTGCTCC
<i>pat-12</i>[S646A]	
crRNA	TTGGCATCAAAAGCGAATCA
Repair Template	ATGACATGAGCCGACTCGAGGCAGAGTCCGTGATGCCTTGCTTA TGCCAATGCCAGCTGGTAATATGTAAGTGACGGA
Genotyping For.	TTGAATTTTCGAGGTCGGTGG
Genotyping Rev. Wild Type	TGGCATTTGGCATCAAAAGC
Genotyping Rev. S646A	CTGGCATTGGCATAAGCAAG
Genotyping Rev. Sequencing	TCAACTGGCTTTCCGTCAC

~ Table continues on the next page ~

<i>tbc-17</i> [S108A]	
crRNA	GATTCTCGGTCACGTGACGG
Repair Template	AAACATCCTCACCGTCCCAATATCCGCGTCCCCGGCTCGAGACC GTGAAAGTCAGCCACCACCCACACAGCCACGTACCACCATCA
Genotyping For. Wild Type	CGTCACGTGACCGAGAATC
Genotyping For. S108A	GGCTCGAGACCGTGAAAG
Genotyping For. Sequencing	AAAACACAACCTTAGACGAA
Genotyping Rev.	TCCAGCAATTTGCCAATTCG
<i>tbc-17</i> [S172A] – Same “Genotyping For. Sequencing” as <i>tbc-17</i>[S108A]	
crRNA	GACGAGCTTCATAAGTCGCC
Repair Template	ATTGGCTCATCAGCCGGATTTCCGGAAGCAGGAGCTTGACGAACTC CACAAGGCCCTTGAAGTCGGTGGGCGGCTCGCGGAGCACAACA
Genotyping For. Wild Type	TCGACGAGCTTCATAAGTCG
Genotyping For. S172A	GACGAACTCCACAAGGCC
Genotyping Rev.	AATTCAGCAATTTGCCGG

Supplementary table 3: List of DNA and RNA sequences used.

A decorative graphic on the left side of the page. It features a DNA double helix structure with vertical hatching on the base pairs, and a protein chain represented by a series of circles connected by a line, forming a vertical stem. The DNA helix is positioned around the protein chain, with some strands overlapping it.

Chapter 5

The mIAA7 degron improves
auxin-mediated degradation in
Caenorhabditis elegans

Jorian J. Sepers¹, Noud H.M. Verstappen¹, An A. Vo²,
James Matthew Ragle², Suzan Ruijtenberg¹, Jordan D.
Ward² & Mike Boxem¹

1. Division of Developmental Biology, Institute of Biodynamics and Biocomplexity, Department of Biology, Faculty of Science, Utrecht University, Utrecht, The Netherlands
2. Department of Molecular, Cell, and Developmental Biology, University of California-Santa Cruz, Santa Cruz, USA

This chapter is an adapted version of the following publication:

Sepers, J.J., Verstappen, N.H., Vo, A.A., Ragle, J.M., Ruijtenberg, S., Ward, J.D. and Boxem, M., 2022. The mIAA7 degron improves auxin-mediated degradation in *Caenorhabditis elegans*. *G3 Genes|Genomes|Genetics*, 12(10), jkac22.

Auxin-inducible degradation is a powerful tool for the targeted degradation of proteins with spatiotemporal control. One limitation of the auxin-inducible degradation system is that not all proteins are degraded efficiently. Here, we demonstrate that an alternative degron sequence, termed mIAA7, improves the efficiency of degradation in *Caenorhabditis elegans*, as previously reported in human cells. We tested the depletion of a series of proteins with various subcellular localizations in different tissue types and found that the use of the mIAA7 degron resulted in faster depletion kinetics for 5 out of 6 proteins tested. The exception was the nuclear protein HIS-72, which was depleted with similar efficiency as with the conventional AID* degron sequence. The mIAA7 degron also increased the leaky degradation for 2 of the tested proteins. To overcome this problem, we combined the mIAA7 degron with the *C. elegans* AID2 system, which resulted in complete protein depletion without detectable leaky degradation. Finally, we show that the degradation of ERM-1, a highly stable protein that is challenging to deplete, could be improved further by using multiple mIAA7 degrons. Taken together, the mIAA7 degron further increases the power and applicability of the auxin-inducible degradation system. To facilitate the generation of mIAA7-tagged proteins using CRISPR/Cas9 genome engineering, we generated a toolkit of plasmids for the generation of dsDNA repair templates by PCR.

Introduction

Perturbing the functioning of proteins is essential to decipher their biological roles and can be accomplished using a wide variety of approaches (HOUSDEN *et al.*, 2017). The desire to investigate the functioning of proteins in specific cell or tissue types or at specific developmental stages has led to the development of several methods that offer spatial or temporal control over protein expression. In *Caenorhabditis elegans*, tissue-specific RNA interference (RNAi) and conditional loss-of-function alleles utilizing targeted nucleases or recombinase strategies can conditionally interfere with protein functioning at the level of the corresponding mRNA or genetic locus (CHENG *et al.*, 2013; DAVIS *et al.*, 2008; HOIER *et al.*, 2000; MUÑOZ-JIMÉNEZ *et al.*, 2017; QADOTA *et al.*, 2007; RUIJTENBERG & HEUVEL, 2015; SHEN *et al.*, 2014). To target proteins directly, several conditional protein depletion systems have been developed that mark proteins of interest for degradation by the 26S proteasome through ubiquitination (ARMENTI *et al.*, 2014; CHO *et al.*, 2013; WANG *et al.*, 2017; WU & GRIFFIN, 2017). The best-known of these systems are the ZF1-mediated degradation, nanobody-mediated degradation, and auxin-inducible degradation (AID) systems. ZF1-mediated degradation and nanobody-mediated degradation repurpose the endogenous E3 ubiquitin ligase substrate-recognition subunit ZIF-1 (ARMENTI *et al.*, 2014; WANG *et al.*, 2017). The ZF1-mediated degradation system targets proteins that are tagged with the ZF1 zinc-finger domain by ectopic expression of ZIF-1 and

can be combined with a *zif-1* loss-of-function background to avoid undesired degradation from endogenously expressed ZIF-1 (ARMENTI *et al.*, 2014; SALLEE *et al.*, 2021). Nanobody-mediated degradation targets proteins that are tagged with a fluorescent protein by exogenously expressing ZIF-1 fused to a nanobody that targets the fluorescent protein (WANG *et al.*, 2017). Finally, in the AID system, a protein of interest is tagged with an AID degron sequence derived from indole-3-acetic acid (IAA) proteins and combined with the expression of the plant-derived F-box protein transport inhibitor response 1 (TIR1) (NISHIMURA *et al.*, 2009; ZHANG *et al.*, 2015). TIR1 forms a functional SKP-1-Cullin-F-box protein (SCF) E3 ubiquitin ligase complex with endogenous SCF proteins. In the presence of auxin (IAA), TIR1 associates with the AID degron resulting in polyubiquitination of the target protein (NISHIMURA *et al.*, 2009; ZHANG *et al.*, 2015).

Most of the systems described above allow for spatial or temporal control, but not both simultaneously, by placing components of the system under control of tissue-specific or -inducible promoters. Combined spatial and temporal control could, however, be accomplished by incorporating bipartite expression systems (NANCE & FRØKJÆR-JENSEN, 2019). In contrast, in the AID system, expression of TIR1 from tissue-specific promoters confers spatial control while timing the addition of auxin offers temporal control over protein degradation.

The AID system has rapidly gained in popularity within the *C. elegans* community and various resources to facilitate its usage have been generated. For example, several strains are available that express TIR1 from different tissue-specific promoters (e.g. ASHLEY *et al.*, 2021; ZHANG *et al.*, 2015)) and cloning vectors are available that facilitate the generation of repair templates for genome editing (ASHLEY *et al.*, 2021; KROLL *et al.*, 2021; NEGISHI *et al.*, 2019). Several improvements or alterations to the AID system have also been generated. These include synthetic auxin analogs that may cause less cytotoxicity or are more soluble in aqueous buffers (MARTINEZ *et al.*, 2020), and an auxin modification that is more effective at promoting protein degradation in embryos, presumably by better permeating the eggshell (NEGISHI *et al.*, 2019).

Most recently, an improved AID system (AID2) was adapted for *C. elegans* that addresses 2 caveats of AID: leaky degradation that is observed for a subset of proteins and impact on the physiology of *C. elegans* caused by exposure to auxin (HILLS-MUCKEY *et al.*, 2022; NEGISHI *et al.*, 2019; YESBOLATOVA *et al.*, 2020). Ideally, auxin-induced protein degradation should occur strictly upon the addition of auxin, and the addition of auxin should not cause effects other than the degradation of the target protein. However, the AID system does suffer from leaky or basal degradation of at least a subset of target proteins in the absence of auxin, which can result in undesired phenotypes (HILLS-MUCKEY *et al.*, 2022; LI *et al.*, 2019; MARTINEZ *et al.*, 2020; MENDOZA-OCHOA *et al.*, 2019; NATSUME *et al.*, 2016; NEGISHI *et al.*, 2019; SATHYAN *et al.*, 2019; SCHIKSNIS *et al.*, 2020; YESBOLATOVA *et al.*, 2019; YESBOLATOVA *et al.*, 2020). In addition, the millimolar concentrations of auxin needed for

maximum degradation efficacy increase the lifespan of worms and activate unfolded protein response pathways resulting in an enhanced protection against ER stress (BHOI *et al.*, 2021; HILLS-MUCKEY *et al.*, 2022; LOOSE & GHAZI, 2021). The improved AID2 system relies on a TIR1 mutation (F79G in *Arabidopsis* TIR1) that alters the auxin-binding interface to fit the bulky auxin-derivative 5-phenyl-indole-3-acetic acid (5-Ph-IAA) (HILLS-MUCKEY *et al.*, 2022; NEGISHI *et al.*, 2019). The use of this TIR1 variant greatly reduces leaky degradation while requiring low micromolar concentrations of 5-Ph-IAA that are less likely to affect the physiology of exposed animals.

One caveat of the AID system that has not yet been addressed in *C. elegans* is that some target proteins demonstrate slow degradation kinetics, incomplete depletion, or both, complicating their functional analysis (DUONG *et al.*, 2020; PATEL & HOBERT, 2017; RIGA *et al.*, 2021; SERRANO-SAZIZ *et al.*, 2018). Here, we adapt an alternative AID degnon sequence (mIAA7) that was shown to result in faster and more complete protein degradation in cultured human cells for use in *C. elegans* (LI *et al.*, 2019). We show that the mIAA7 degnon improves degradation for a panel of proteins with different subcellular locations, expressed across different tissues. While the mIAA7 degnon did enhance the leaky degradation of 2 out of 4 proteins tested, we show that it can be effectively combined with the *C. elegans* AID2 system (*C.e.*AID2) to achieve more complete protein depletion without detectable leaky degradation. Finally, we demonstrate that using 2 or more degnons could improve degradation of ERM-1, the most challenging protein to degrade that we have encountered to date. Thus, the mIAA7 degnon further expands the usefulness of the AID system to determine the biological functioning of proteins in *C. elegans*.

Results

The mIAA7 degnon improves AID-mediated degradation

AID degnons are derived from IAA proteins and consist of the conserved domain required for TIR1 recognition (Domain II) and flanking sequences (GRAY *et al.*, 2001; RAMOS *et al.*, 2001). The two most commonly used degnon sequences, termed AID* and mAID, are based on the IAA17 protein (Figure 1A) (KUBOTA *et al.*, 2013; MORAWSKA & ULRICH, 2013). An alternative degnon sequence derived from IAA7 was recently shown to result in faster and more complete protein degradation in cultured human cells, compared to the mAID degnon (LI *et al.*, 2019). This degnon, termed mIAA7, contains the IAA7 Domain II and includes a longer N-terminal flanking region than AID* or mAID (Figure 1A).

To assess the effectiveness of the mIAA7 degnon in *C. elegans*, we selected the Discs large ortholog DLG-1 as an initial test protein to degrade. DLG-1 is a cell polarity regulator that is involved in the formation of cell-cell junctions and is essential for embryonic development (BOSSINGER *et al.*, 2004; FIRESTEIN & RONGO, 2001; KÖPPEN *et al.*, 2001; MCMAHON *et al.*, 2001). Previously, we found that

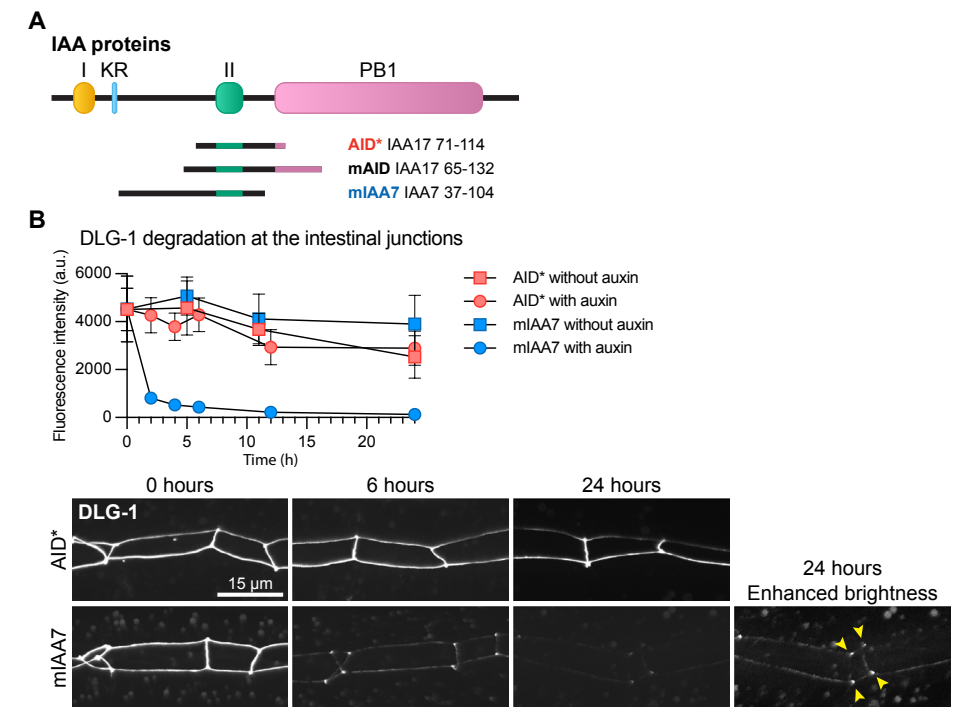
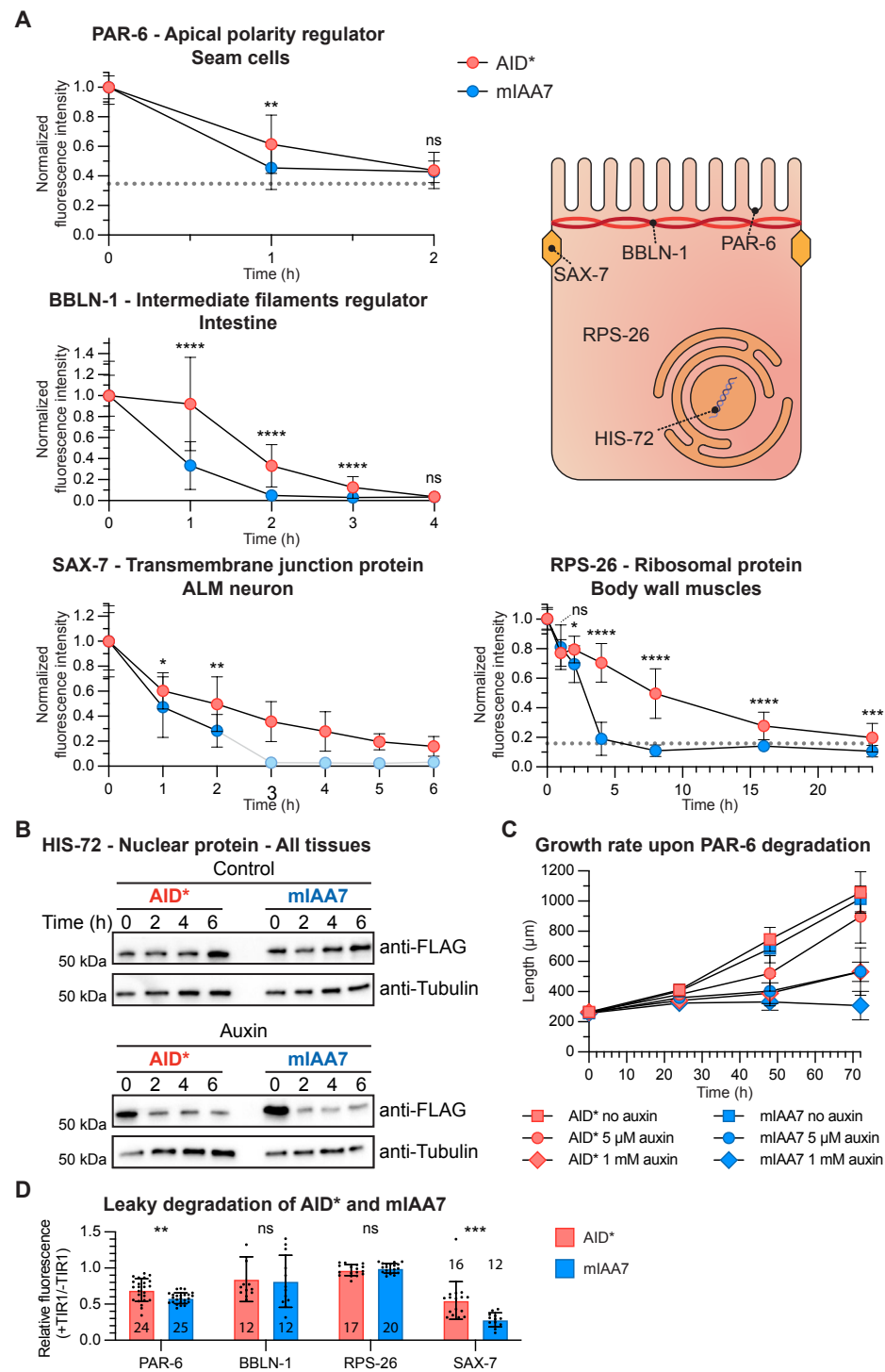


Figure 1: The mIAA7 degnon improves auxin-mediated degradation of DLG-1. (A) Schematic overview of IAA proteins and the different AID degnons that have been derived from them. I = domain I; II = domain II; KR = conserved lysine and arginine residue; PB1 = Phox and Bem1p domain. (B) Comparison between AID*- and mIAA7-mediated degradation kinetics of intestinal DLG-1 in L3 larvae using 1 mM auxin. Values in the graph are arbitrary units and each data point represents the average intensity at intestinal cell junctions for the given condition and timepoint. Error bars: mean \pm SD; n = 7–20 animals. Images shown are representative maximum intensity projections that were acquired and displayed with the same settings for comparison, except for the indicated panel with enhanced brightness to show residual DLG-1. Arrowheads point to the apical junctional sites where 3 intestinal cells meet.

the conventional AID* degnon was ineffective at mediating the degradation of DLG-1 (RIGA *et al.*, 2021). To determine if use of the mIAA7 degnon results in more effective degradation, we tagged the endogenous *dlg-1* locus with codon optimized mIAA7 and GFP sequences by homology-directed repair of CRISPR/Cas9-induced DNA double-strand breaks, using the same insertion site and tag order used previously to generate the *dlg-1::AID*::GFP* locus. We then compared the degradation kinetics of AID* and mIAA7 tagged DLG-1 in the intestine, using a single-copy integrated transgene expressing TIR1 from the intestine specific *elt-2* promoter. We exposed synchronized larvae to auxin from the L3 stage and quantified the levels of DLG-1 at apical junctions of intestinal cells at various timepoints over a 24-h time period. Consistent with our previous observations, depletion of DLG-1 tagged with AID* was inefficient, with junctional fluorescence levels similar to controls not exposed



~ Figure description on the next page ~

Figure 2: The mIAA7 degron robustly increases the efficiency of AID-induced protein degradation for several proteins across multiple tissues and cellular compartments.

(A) Comparison between AID*- and mIAA7-mediated degradation for indicated proteins and tissues. Drawing represents a generic polarized cell with the subcellular localization of the proteins investigated indicated. PAR-6 was measured at the apical domain of seam cells in L2 larvae on 5 μM auxin, BBLN-1 was measured at the apical domain in the intestine of L3 larvae treated with 50 μM auxin, SAX-7 was measured at the plasma membrane in the ALM neuron cell body of L3 larvae treated with 5 μM auxin, and RPS-26 was measured in the cytoplasm of body wall muscles of L2 larvae treated with 1 mM auxin. Values are normalized to the mean intensity levels at 0 h of auxin exposure, and each data point represents the average intensity for the given condition and timepoint. Due to the nature of the quantification for PAR-6 and RPS-26, the fluorescence levels did not reach zero as they did for the other targets. Nonzero baseline level values of wild-type animals are indicated, resembling a completely degraded protein pool. For SAX-7 degradation using the mIAA7 degron, exposure to auxin of 3 h or longer resulted in complete depletion and an inability to locate the ALM cell body. For these timepoints, values were plotted at 0 and no statistics were performed (light shaded dots). Error bars: mean \pm SD; Statistical test: Mann-Whitney U test; n = 9–29 animals. **(B)** Western blots detecting HIS-72: AID*::3xFLAG and HIS-72::mIAA7::3xFLAG in synchronized control or 4 mM auxin-treated L1 larvae. An anti-alpha-tubulin loading control and protein size standard markers in kilodaltons are provided. Time in hours in control media or 4 mM auxin containing media is indicated. **(C)** Comparison of Larval growth between AID*- and mIAA7-mediated PAR-6 degradation in the epidermis using 5 μM and 1 mM auxin. **(D)** Comparison of leaky degradation between AID* and mIAA7 degrons for the indicated proteins. Measurements for each protein were done as in panel A. Values are normalized to the mean intensity levels of animals expressing the same degrotagged protein but not expressing TIR1. Each data point in the graph represents a single animal. Error bars: mean \pm SD; statistical test: Mann-Whitney U test; n values are indicated in or above the bars.

to auxin for the complete duration of the experiment (Figure 1B). In contrast, DLG-1 tagged with mIAA7 was depleted to 4.8 % of starting levels after 12 h of auxin exposure (Figure 1B). Degradation was not fully complete, as low levels of DLG-1 remained detectable even after 24 h of exposure to auxin, particularly at the apical junctional sites where 3 intestinal cells meet (Figure 1B). Nevertheless, the use of the mIAA7 degron dramatically improved the efficiency of auxin-mediated degradation of DLG-1 in *C. elegans*.

To evaluate the effectiveness of the mIAA7 degron more systematically, we next investigated the degradation kinetics of a variety of proteins using both AID* and mIAA7. The proteins were chosen to represent distinct subcellular localizations and their degradation was investigated in different tissue types. We investigated degradation of the apical polarity regulator PAR-6 in larval seam cells, of the intermediate filament regulator BBLN-1 in intestinal cells, of the adhesion protein SAX-7 in the ALM neurons, and of the ribosomal protein RPS-26 in body wall muscle cells. For SAX-7, measurements were taken in the ALM cell body, since degradation in neurites was ineffective in most if not all neurons. For each of these proteins, endogenous lines expressing the protein tagged with AID* and a fluorescent protein had previously been generated in our groups. We generated mIAA7-tagged variants keeping the tag order

and orientation (N- or C-terminal) and introducing as few other changes to the protein amino acid sequence as possible. We then performed timecourse experiments with synchronized animals to compare the degradation efficiencies, adding auxin at the L2- (PAR-6 and RPS-26) or L3 stage (BBLN-1 and SAX-7) and quantifying fluorescence levels at indicated intervals (Figure 2). PAR-6 levels were measured at seam–hyp7 junctions, BBLN-1 levels at the apical intermediate filament layer, SAX-7 levels at the cell wall of the ALM cell body, and RPS-26 in the cytoplasm of body wall muscle cells. PAR-6, BBLN-1, and SAX-7 are already highly efficiently degraded using the AID* degron. For these proteins, we lowered the auxin concentration from 1 mM to 5 or 50 μ M to increase the time needed for degradation. Under these conditions, for each of these proteins, maximum depletion was achieved twice as fast with the mIAA7 degron compared to the AID* degron (Figure 2A; Supplementary figure 1A). More strikingly, mIAA7-mediated degradation of the ribosomal protein RPS-26 in the body wall muscle cells resulted in complete degradation in 6 h compared to 24 h with the AID* degron (Figure 2A; Supplementary figure 1A). Thus, for all 4 proteins, use of mIAA7 increases the degradation efficiency.

Finally, we tested the ability of the IAA7 degron to improve the degradation of the nuclear histone protein HIS-72, as several nuclear proteins showed only a modest increase in degradation efficiency with the mIAA7 degron in human cells (Li *et al.*, 2019). We previously observed that the degradation efficiency of HIS-72 tagged with AID* varied between cell types, making this protein a good test case to detect a potential difference in degradation kinetics (our unpublished data). To be able to monitor HIS-72 levels in individual cells by immunofluorescence as well as measure overall HIS-72 levels by Western blot, we inserted sequences encoding GFP, the AID* or mIAA7 degron, and a triple FLAG tag at the start codon of the *his-72* locus. We exposed synchronized L1 animals ubiquitously expressing TIR1 to auxin and analyzed HIS-72 levels by fluorescence microscopy and Western blot analysis over a 6-h period at 2-h intervals. Control animals were not exposed to auxin. By Western blot analysis, HIS-72 levels were reduced but not absent after 2 h of exposure to auxin using both the AID* and mIAA7 degrons. HIS-72 levels did not decrease further upon prolonged auxin exposure and using either degron. These findings were corroborated by the fluorescence microscopy analysis. At 2 h of auxin exposure, HIS-72 levels in cells in the central region of the body were sharply reduced, while HIS-72 levels in cells in the head and tail regions appeared unaffected (Supplementary figure 2A). Further exposure to auxin up to 6 h did not appear to decrease HIS-72 levels in the head and tail regions. Thus, the mIAA7 degron does not appear to improve the efficiency of HIS-72 depletion, but does function comparably to the AID* degron for this protein.

Improved protein degradation kinetics are ultimately expected to yield stronger loss-of-function phenotypes or a more rapid onset of phenotypes upon addition of auxin. To test this, we measured larval growth upon degradation of PAR-6 in the epidermis from hatching. We recently showed that full depletion of epidermal PAR-6 causes a severe growth defect, in which larvae do not grow beyond L1 size (CASTIGLIONI *et al.*, 2020). We therefore exposed animals to two auxin concentrations: a conventional 1 mM concentration that we had previously found to result in an incomplete growth arrest using the AID* degron, and the 5 μ M concentration used to quantify PAR-6 protein levels above. Animals with mIAA7-tagged PAR-6 on 1 mM auxin have a full growth arrest, while the other conditions resulted in a partial growth defect (Figure 2C). Importantly, at both concentrations the growth defect was stronger for PAR-6 tagged with the mIAA7 degron than for AID*-tagged PAR-6, with the mIAA7 degron yielding a growth defect at 5 μ M that was very similar to that obtained with the IAA7 degron at 1 mM auxin (Figure 2C). These results illustrate that the mIAA7 degron can induce stronger knockdown phenotypes than the AID* degron.

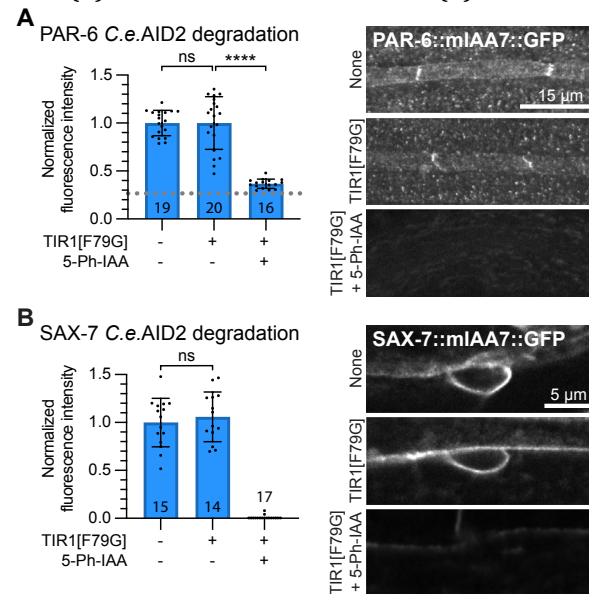
Taken together, our data demonstrate that the mIAA7 degron robustly increases the efficiency of AID-induced protein degradation across multiple tissues and cellular compartments, except for the nuclear protein HIS-72. The latter result might suggest that the degradation speed of nuclear proteins is mainly limited by the accessibility of TIR1 to the nuclear proteins rather than the degron sequence, though more nuclear proteins will need to be tested to assess the generalizability of this hypothesis. However, this assertion is in line with mIAA7-mediated degradation data in human cells, where improved degradation of nuclear proteins was achieved by expressing TIR1 with a nuclear localization signal (NLS) sequence (Li *et al.*, 2019).

mIAA7 can increase leaky degradation of target proteins

The increase in degradation efficiency conferred by the mIAA7 degron raises the possibility that leaky degradation levels are similarly increased. To investigate this possibility, we determined depletion levels of PAR-6, BBLN-1, SAX-7, and RPS-26 tagged with the AID* or mIAA7 degron as above in strains lacking or expressing TIR1. For RPS-26, we did not observe significant leaky degradation with either degron (Figure 2D; Supplementary figure 2A). For BBLN-1, we observed moderate leaky degradation, with a ± 17 % decrease in fluorescence intensity using the AID* degron upon TIR1 expression in the intestine (Figure 2D; Supplementary figure 2A). However, use of the mIAA7 degron did not increase the leaky degradation of BBLN-1 (Figure 2D; Supplementary figure 2A). For PAR-6 and SAX-7, we observed more severe levels of leaky degradation that were significantly increased using the mIAA7 degron compared to the AID* degron. For PAR-6, leaky degradation was increased from 31 % to 42 % in the seam cells, and for SAX-7 leaky degradation increased from 45 % to 72 % in

Figure 3: The mIAA7 degron is compatible with the *C.e.*AID2 system. mIAA7-mediated degradation of PAR-6 in the seam cells (A) and of SAX-7 in the ALM neuron (B) of L2 larvae using the *C.e.*AID2 system.

Values are normalized to the mean intensity levels of animals expressing the same degron-tagged proteins but not expressing TIR1 and not treated with 5-Ph-IAA (i.e. the first bar). Each data point in the graph represents a single animal. Error bars: mean \pm SD; statistical test: 1-way ANOVA with Šidák multiple testing correction; n values are indicated in or above the bars. Images shown are representative maximum intensity projections that were acquired and displayed with the same settings for comparison.



the ALM neuron cell body (Figure 2D; Supplementary figure 2A). Despite these reduced protein levels, no overt phenotypes were observed for any of these proteins. Together, these data corroborate that for some target proteins leaky degradation is a potential caveat of the AID system. In addition, the use of a more effective degron, such as mIAA7, can increase leaky degradation.

The mIAA7 degron is compatible with the *C.e.*AID2 system

Recently, the AID2 system utilizing a TIR1 variant altered to fit the bulky auxin-derivative 5-Ph-IAA was adapted for *C. elegans* and shown to sharply reduce or eliminate leaky degradation while requiring low micromolar concentrations of 5-Ph-IAA (HILLS-MUCKEY *et al.*, 2022; NEGISHI *et al.*, 2019). Given these advantages, we set out to test whether the *C.e.*AID2 system is compatible with the novel mIAA7 degron. We used CRISPR/Cas9 genome editing to introduce the F79G mutation into the TIR1 transgene in our PAR-6 and SAX-7 mIAA7 strains. Protein fluorescence levels were measured in these strains comparing animals not expressing TIR1, animals expressing TIR1[F79G] in the absence of auxin analog, and animals expressing TIR1[F79G] in the presence of 1 μ M 5-Ph-IAA. Protein levels of PAR-6 in the seam cells and SAX-7 ALM neuron cell body were not affected by the presence of TIR1[F79G], demonstrating that the mIAA7 degron does not induce leaky degradation when combined with TIR1[F79G]. Importantly, exposure to 1 μ M 5-Ph-IAA yielded complete degradation of the target proteins (Figure 3A, B). Thus, similar to the AID* and mAID degrons that were previously tested (HILLS-MUCKEY *et al.*, 2022; NEGISHI *et*

al., 2019), the mIAA7 degron is compatible with the AID2 TIR1[F79G] variant, resulting in effective degradation at low auxin analog concentrations and no observable leaky degradation.

The use of multiple degrons can improve the efficacy of the AID system

As a final test of the efficacy of the mIAA7 degron, we tagged the ezrin/radixin/moesin ortholog ERM-1 with mIAA7. ERM-1 is highly expressed in the intestine, where it is required for microvilli formation and patterning of the lumen. The ERM-1 protein appears highly stable and shows little turnover at the apical domain (CHAPTER 2; CHAPTER 3). Previously, we have tested both AID- and ZIF-1-mediated depletion approaches, neither of which resulted in full depletion of intestinal ERM-1 (CHAPTER 2; CHAPTER 3). Therefore, we wanted to test if the novel mIAA7 degron could improve ERM-1 degradation. We tagged the endogenous *erm-1* locus with mCherry and mIAA7 or AID* degron coding sequences using CRISPR/Cas9 genome engineering. We then compared ERM-1 degradation in the intestine using TIR1[F79G] and 1 μ M 5-Ph-IAA, measuring fluorescence levels at the apical domain of the intestine throughout larval development in synchronized animals. Whereas the AID* degron did not yield any detectable degradation, the use of the mIAA7 degron caused significant depletion of ERM-1, again confirming that mIAA7 improves the efficacy of the AID system (Figure 4A). However, \pm 76 % of ERM-1 remained after 24 h and fluorescence levels did not further decrease in the following days. Thus, mIAA7-mediated degradation of ERM-1 in the intestine is still inefficient.

In yeast, it has been shown that addition of multiple degrons to a protein can improve the AID-mediated degradation rate (KUBOTA *et al.*, 2013; ZHANG *et al.*, 2022). In addition, in human cell lines, the degradation rate has been shown to be affected by the localization of the degron tag (LI *et al.*, 2019). We therefore investigated whether altering the number or position of degrons could improve ERM-1 degradation. Originally, ERM-1 was C-terminally tagged with mCherry followed by the mIAA7 degron (Figure 4B – “C-terminal”). To test the effect of multiple degrons, we engineered similar alleles with double and triple mIAA7 degrons (Figure 4B – “C-term 2 \times ,” “C-term 3 \times ”). To test the influence of the degron position we also generated an allele with mIAA7 located internally between the ERM-1 and mCherry coding sequences (Figure 4B – “Internal”) and an allele combining the internal and C-terminal mIAA7 tags (Figure 4B – “Inter + C-term”).

Synchronized animals carrying the different mIAA7 *erm-1* alleles and expressing TIR1[F79G] in the intestine were exposed to 5-Ph-IAA for 24 h and apical ERM-1 fluorescence levels were measured. Adding an additional degron to the ERM-1 C-terminus significantly improved the degradation, depleting \pm 3.5 times more protein than a single degron. Nevertheless, \pm 50 % of ERM-1 protein remained present. Adding a third degron to the C-terminus did not

result in a further increase in degradation. We did not observe a significant difference in depletion levels between ERM-1 variants with different locations of the mIAA7 tags. Both single mIAA7 tagged alleles showed similar levels of ERM-1 depletion, as did the double ERM-1 tags “C-term 2x” and “Inter + C-term.” This suggests that the positioning of the degron does not greatly alter AID-mediated degradation efficacy. In addition, when using multiple degrons in ERM-1, it is irrelevant whether they are placed in tandem or at distinct positions. In summary, AID-mediated protein degradation of ERM-1 can be further improved by using multiple degrons tags, while the position of the degrons has no significant effect on degradation efficiency.

Plasmid toolkit

To facilitate CRISPR/Cas9-mediated tagging of target proteins with the mIAA7 degron and commonly used fluorescent proteins we generated a plasmid toolkit (Supplementary figure 3). The plasmids encode 1 of 5 different fluorescent proteins flanked by the mIAA7 degron on either the N- or C-terminal side, and by a 12-amino acid glycine-rich linker on the opposing side. In addition, we generated a plasmid with GFP and 3 FLAG epitope tags for detection and analysis of a target protein using an antibody. Using these plasmids to generate dsDNA repair templates allows for tagging of a protein of interest both N- and C-terminally with a choice of positioning the mIAA7 degron between the fluorescent protein and the protein of interest, or at the exposed terminus of the fluorescent protein. By designing primers with homology arms as overhangs according to established CRISPR/Cas9 protocols (DOKSHIN *et al.*, 2018; PAIX *et al.*, 2015) this plasmid toolkit greatly facilitates the generation of double-stranded DNA repair templates for CRISPR/Cas9 genome engineering of fluorescently tagged AID alleles.

Discussion

The AID system is becoming increasingly popular in the *C. elegans* field due to its ability to degrade target proteins with both spatial and temporal control (ASHLEY *et al.*, 2021; HILLS-MUCKEY *et al.*, 2022; NEGISHI *et al.*, 2019; ZHANG *et al.*, 2015). However, the degradation efficiency varies between proteins, and not all proteins are depleted to the extent that expected phenotypes are observed (DUONG *et al.*, 2020; PATEL & HOBERT, 2017; RIGA *et al.*, 2021; SERRANO-SAIZ *et al.*, 2018). Here, we demonstrated that an alternative degron sequence, termed mIAA7, improves the efficiency of degradation in *C. elegans*, as previously reported in human cell culture (Li *et al.*, 2019).

The improvements to degradation efficiency appear to be applicable to most proteins, as we observed increased depletion efficiency for 6 proteins tested, each with different subcellular localizations and investigated in different tissue types. The only exception was the nuclear protein HIS-72, which was depleted with similar efficiency. In human cells, mIAA7 did not improve the depletion

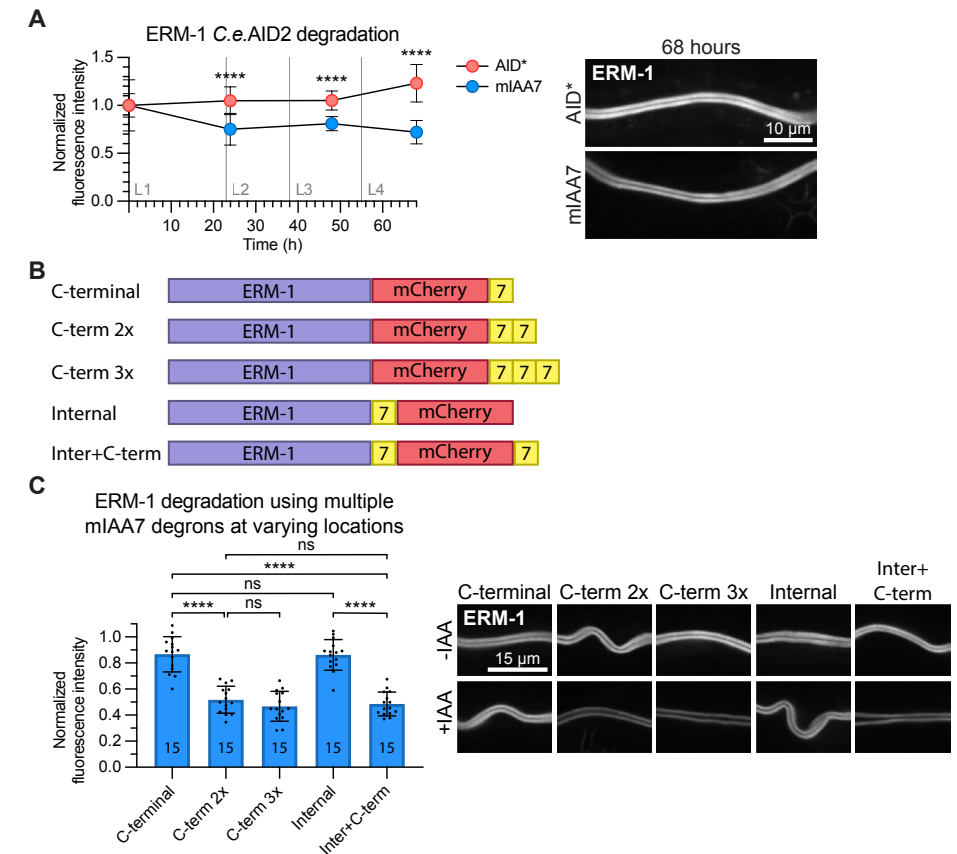


Figure 4: Tagging ERM-1 with multiple mIAA7 degrons improves auxin-mediated degradation. (A) Comparison between AID*- and mIAA7-mediated degradation of intestinal ERM-1 throughout larval development using the *C.e.AID2* system. Data points represent the mean intensity normalized to the mean intensity levels of animals with the same genotype and age that were not exposed to 5-Ph-IAA. Error bars: mean \pm SD; Statistical test: MannWhitney U test; n = 12–16 animals. Images shown are representative maximum intensity projections that were acquired and displayed with the same settings for comparison. (B) Schematic overview of the different ERM-1 alleles used for testing the effect of multiple degrons and degron location on auxin-mediated degradation efficiency. (C) Comparison of intestinal degradation of ERM-1 tagged with 1 or multiple mIAA7 degrons at varying locations in L3 larvae using the *C.e.AID2* system. Values are normalized to the mean intensity levels of animals with the same genotype that were not exposed to 5-Ph-IAA, and each data point represents a single animal. Images shown are representative maximum intensity projections that were acquired and displayed with the same settings for comparison. Error bars: mean \pm SD; statistical test: 1-way ANOVA with Šidák multiple testing correction; n values are indicated in the bars.

of the highly expressed nuclear proteins LMNA and LMNB1 (Li *et al.*, 2019). However, depletion of these proteins was strongly increased when using an auxin receptor F-box protein targeted to the nucleus. A similar modification may therefore improve the depletion of nuclear proteins in *C. elegans* as well.

There are two main differences between mIAA7 and AID* that could contribute to the difference in degradation efficiency. First, mIAA7 is derived from IAA7 instead of IAA17, and hence differs in exact primary sequence. Second, the 2 degrons contain different parts of the IAA protein. While both degrons contain IAA Domain II, mIAA7 has a longer N-terminal extension and shorter C-terminal extension than AID* (Figure 1A). A degron derived of IAA17 using the same protein region as mIAA7 resulted in a degradation speed close to mIAA7 in human cell culture (Li *et al.*, 2019), which suggests that it is the region of the IAA protein used rather than the primary sequence that determines degradation efficiency. In support of this hypothesis, the region N-terminal to domain II was shown to be required for TIR1-mediated degradation in plants (DREHER *et al.*, 2006; MOSS *et al.*, 2015). However, replacing the mIAA7 sequence downstream of domain II with the same region from IAA12 lowered the degradation speed, indicating that primary sequence can affect degradation efficiency as well (NIEMEYER *et al.*, 2020). One way the primary sequence could affect degradation efficiency is by providing lysine residues that can be ubiquitinated. However, the conserved KR sequence, hypothesized to be important for degradation plants (DREHER *et al.*, 2006; MOSS *et al.*, 2015), is absent from the mIAA7 degron and including it did not improve degradation in human cell culture (Li *et al.*, 2019). Moreover, all IAA7 ubiquitination sites that were found using mass spectrometry or are bioinformatically predicted are absent from the mIAA7 degron sequence (NIEMEYER *et al.*, 2020; WANG *et al.*, 2021). Finally, IAA1 has been reported to be ubiquitinated and degraded without any lysine residues (GILKERSON *et al.*, 2015). These data suggest that the degron itself is not ubiquitinated by the TIR1-SCF complex or that IAA proteins can be ubiquitinated in a noncanonical manner. An alternative explanation for the effects of primary sequence on degradation efficiency is offered by a recent model based on crosslinking proteomics, in which the regions flanking domain II contribute to the stability of the interaction between TIR1/Auxin Signaling F-Box (AFB) proteins, IAA proteins, and auxin (NIEMEYER *et al.*, 2020). While IAA7 showed the strongest interaction with TIR1 out of 8 IAA proteins by yeast 2-hybrid (CALDERÓN VILLALOBOS *et al.*, 2012; NIEMEYER *et al.*, 2020), *Arabidopsis* alone encodes 29 IAA proteins and 6 AFBs (LISCUM & REED, 2002; LUO *et al.*, 2018; MORFFY & STRADER, 2022; PARRY *et al.*, 2009). Therefore, even more effective IAA-AFB combinations may be discovered.

One of the drawbacks of the AID system is the potential for degradation in the absence of auxin. In our experiments, RPS-26 and BBLN-1 showed little leaky degradation with either degron, but leaky degradation for PAR-6 and SAX-7 was relatively high for AID* and was enhanced by use of the mIAA7 degron. Importantly, when combining the mIAA7 degron with the *C.e.*AID2 system that utilizes TIR1[F79G] and the auxin-derivative 5-Ph-IAA, we observed no leaky degradation of PAR-6 and SAX-7 in the absence of auxin/5-Ph-IAA. Thus, the benefits of the mIAA7 degron can be realized without the drawback of increased

leaky degradation. Additional measures that users could take to address leaky degradation include reducing the expression levels of TIR1, using AFB2 instead of TIR1 (Li *et al.*, 2019), or re-engineering the degron sequence to include the PB1 domain of Auxin Response Factor plant proteins, which was shown to reduce leaky degradation of AID degron-tagged proteins in human cell culture (SATHYAN *et al.*, 2019).

Despite the improvements in degradation kinetics conferred by the mIAA7 degron, some proteins remain refractive to full depletion. For difficult to degrade proteins, the addition of multiple degron sequence can further increase the degradation efficiency. In our hands, auxin-mediated degradation of ERM-1 was improved when tagged with two mIAA7 degrons compared to a single degron. This finding is in line with previous results in yeast, in which using multiple degrons improved degradation (KUBOTA *et al.*, 2013; ZHANG *et al.*, 2022). However, in contrast to results in yeast, we did not observe a further improvement in the depletion efficiency when using three degrons. This difference may be specific to ERM-1, which associates very stably with the apical domain of intestinal cells (CHAPTER 2; CHAPTER 3). It is possible, therefore, that a fraction of ERM-1 is not accessible to the SCF complex or the proteasome and that all accessible ERM-1 is degraded after 24 h using two degrons. Alternatively, the ubiquitination or degradation machinery may be rate limiting due to the high expression levels of ERM-1.

Interestingly, the position of the degrons did not seem to affect the degradation rate of ERM-1. Two degrons in tandem resulted in similar depletion levels as two degrons flanking the mCherry sequence on both sides. We did not test an N-terminal placement of the degron as the two predicted splice variants of ERM-1 do not share the same N-terminus, resulting in the degradation of only a subpopulation of ERM-1. Our results contrast with data from human cell culture in which degron position did influence the degradation rate for 2 proteins tested (Li *et al.*, 2019). For the protein SEC61B degradation was higher when mIAA7 was positioned at the extreme N-terminus compared to an internal position between a fluorescent protein and SEC61B. For the protein Seipin, a C-terminal degron performed better than an N-terminal degron, and including a fluorescent protein downstream of the C-terminal degron further increased degradation efficiency. Given the low number of proteins tested in *C. elegans* and human cells, the exact influence of degron position requires further investigation (Li *et al.*, 2019).

In summary, the mIAA7 degron further extends the usability of the AID system in *C. elegans*, improving degradation efficiency while, particularly in combination with *C.e.*AID2, not affecting the steady-state level of proteins in the absence of auxin.

Methods

C. elegans strains and culture conditions

C. elegans strains were cultured under standard conditions (BRENNER, 1974). Only hermaphrodites were used. All experiments were performed with animals grown at 15°C or 20°C on standard Nematode Growth Medium (NGM) agar plates seeded with OP50 *Escherichia coli*. The HIS-72 timecourse experiment was performed in liquid culture (see below). Supplementary table 1 contains a list of all the strains used and their source.

Cloning of the mIAA7 repair template plasmids

The mIAA7 repair templates were cloned into pBSK+ (Addgene #212207) using the Gibson assembly cloning strategy (GIBSON *et al.*, 2009). Linear DNA molecules were generated by PCR using Q5 polymerase (NEB) using primers (IDT) containing overhangs with the appropriate Gibson assembly sequences and, if applicable, the 12-amino acid glycine-rich linker. The mIAA7 sequence, based on Li *et al.* (2019), was codon-optimized for *C. elegans* with a synthetic intron and ordered as a gBlock Gene Fragment (IDT). The pJJS001–pJJS004 plasmids were assembled by inserting the mIAA7 and GFP or mCherry sequences directly into pBSK+. The pJJS005–pJJS012 plasmids were assembled by substituting the GFP of pJJS001 and pJJS002 plasmids with the respective fluorescent protein sequences. All assembly products were verified by Sanger sequencing (Macrogen Europe). pJW2341 was assembled by Gibson cloning a mIAA7 fragment into pJW2086 (ASHLEY *et al.*, 2021). Cloning details are available upon request. Supplementary table 2 contains a list of all plasmids made with the respective primer sequences and origin of the fluorescent protein sequence.

CRISPR/Cas9 genome editing

All alleles were made using the homology-directed repair of the CRISPR/Cas9-induced DNA double-strand breaks. Repair templates included, when appropriate, silent mutations to prevent recutting of repaired loci by Cas9. To verify the edits, the insertion sites were PCR amplified and sequenced by Sanger sequencing. Supplementary table 3 contains a list of all CRISPR/Cas9 edits made with the respective primer sequences.

The *sax-7::AID*::GFP* allele was made using plasmid based expression of Cas9 and sgRNA and a plasmid repair template contain a self-excising cassette for selection of candidate integrants (DICKINSON *et al.*, 2015). Repair template and sgRNA plasmid were designed and assembled using the SapTrap cloning strategy (DICKINSON *et al.*, 2015; SCHWARTZ & JORGENSEN, 2016). Reagents were injected and knock-in animals were recovered as previously described.

All other alleles were generated using microinjected Cas9 ribonucleoprotein complexes and linear repair templates, similar to the approach described by (GHANTA *et al.*, 2021). We used a Cas9 amount of 250–700 ng/μl, a Cas9/

crRNA ratio of 3.0–4.5, and a pSEM229 (*Pmlc-1::mNeonGreen*) or pRF4 (*rol-6(su1006)*) coinjection marker (EL MOURIDI *et al.*, 2020; MELLO *et al.*, 1991). For tagging endogenous loci with a single AID* or mIAA7 degron and fluorescent protein, dsDNA repair templates were amplified using primers with 5' SP9 modifications (IDT) from the pJRK86 plasmid (AID*::GFP, Addgene #173743) and mIAA7 repair template plasmids in Supplementary table 1. For *his-72* editing, GFP::AID*::3xFLAG repair templates were generated by PCR using a pJW2086 template and GFP::mIAA7::3xFLAG repair templates were generated by PCR using a pJW2341 repair template (Supplementary table 1). For tagging ERM-1 with 2 degrons, a second mIAA7 degron was inserted into the existing ERM-1::mCherry::mIAA7 allele using similar dsDNA repair templates amplified from an mIAA7 repair template plasmids in Supplementary table 1. The C-term 3× ERM-1 allele was generated using the same reagents as the C-term 2× allele but was the result of a fortuitous incorrect repair event. The TIR1[F79G] alleles were generated using a ssDNA oligo repair template (IDT).

Auxin treatment of synchronized worms

Animals were developmentally synchronized by hypochlorite bleaching of gravid adults to release embryos, which were hatched overnight in M9 buffer. For HIS-72, depletion experiments were performed in liquid culture. Approximately 14,000 synchronized L1 animals were resuspended in 6 ml of M9 + 0.025 % gelatin supplemented with 13.3 % (v/v) concentrated OP50 and either 4 % ethanol (control) or 4 mM IAA (or auxin) in ethanol. All other depletion experiments were performed on agar plates. Synchronized L1 larvae were first placed on NGM plates seeded with *E. coli* OP50 and allowed to develop for 24–48 h. Animals were then transferred to NGM plates seeded with *E. coli* OP50 and containing 1 mM, 50 μM, or 5 μM IAA, or 1 μM 5-Ph-IAA. Auxin NGM plates were prepared by diluting 1M IAA (Alfa Aesar) or 1 mM 5-Ph-IAA (BioAcademia) dissolved in 100 % ethanol into NGM agar that was cooled down to ± 50°C prior to plate pouring.

Western blot analysis

At each timepoint, 500 μl of animals in solution was removed (± 1,160 larvae), and samples for western blotting were generated similar to Vo *et al.* (2021), except samples were resuspended in 100 μl of M9 + 0.025 % gelatin and freeze-cracked twice on dry ice before Laemmli sample buffer was added to 1× and samples were boiled for 5 min. Five microliters of lysate was resolved on precast 4–20 % Mini-Protean TGX Stain Free Gels (Bio-Rad) before being transferred to a polyvinylidene difluoride membrane by semi-dry transfer with a TransBlot Turbo (Bio-Rad). Blots were probed with 1:2,000 horseradish peroxidase (HRP)-conjugated anti-FLAG M2 (Sigma-Aldrich, A8592-5x1MG, Lot # SLCB9703) or 1:2,000 mouse anti-α-Tubulin 12G10 concentrated supernatant (Developmental Studies Hybridoma Bank). For the anti-α-tubulin

blot, we used 1:10,000 Digital anti-mouse HRP conjugate (Kindle Biosciences LLC, R1005) secondary antibody. Blots were developed similar to Johnson *et al.* (2023) using Supersignal West Femto Maximum Sensitivity Substrate (Thermo Fisher Scientific, 34095) and the high-resolution setting on a ChemiDoc MP system (Bio-Rad).

Epifluorescence microscopy

At each HIS-72 depletion, timepoint images were collected by removing 100 μ l of culture of the indicated genotype and treatment, adding 1 ml of M9 + 0.025 % gelatin, pelleting at 700 g, washing twice in M9 + 0.025 % gelatin, and then transferring animals to a 2 % agarose pad. Ten microliters of 5 mM levamisole was added to immobilize animals and a cover slip was placed on top. Images were acquired on an AxioImager M2 microscope (Carl Zeiss Microscopy, LLC) equipped with a Colibri 7 LED light source and an AxioCam 506 mono camera using a Plan-Apochromat 63x/1.40 Oil DIC lens. Acquired images were processed through Fiji software version: 2.3.0/1.53q (SCHINDELIN *et al.*, 2012).

Spinning disk confocal microscopy

Larvae were mounted on a 5 % agarose pad in 20 mM tetramisole solution in M9 to induce paralysis. Spinning disk confocal imaging was performed using a Nikon Ti-U microscope equipped with a Yokogawa CSU-X1 spinning disk using a 60 \times -1.4 NA objective, 488- and 561-nm lasers, Semrock “530” GFP-L and “600” TxRed emission filters, and an Andor iXON DU-885 camera. Spinning disk images were acquired using MetaMorph Microscopy Automation & Image Analysis Software. Image scales were calibrated using a micrometer slide. All stacks along the z-axis were obtained at 0.25- μ m intervals, and maximum intensity Z projections were done in Fiji software. For display in figures, level adjustments, false coloring, and image overlays were done in Adobe Photoshop. Image rotation, cropping, and panel assembly were done in Adobe Illustrator. All edits were done nondestructively using adjustment layers and clipping masks, and images were kept in their original capture bit depth until final export from Illustrator for publication.

Quantitative image analysis

Quantitative analysis of spinning disk images was done in Fiji and Python. All measurement values were first corrected for imaging system background levels by subtracting the average of a region within the field of view that did not contain any animals. For the measurements of the intestinal apical junctions (DLG-1) and membrane (BBLN-1 and ERM-1), analyses were done on intestinal cells forming int2 through int6, at the center of the intestinal lumen. A maximum projection of 5 slices was made, and 3 25-px-wide line scans perpendicular to the apical junction or membrane were taken per animal. For

the measurements of the cortex of the cell body of the ALM neuron (SAX-7), 2 10-px-wide line scans using a maximum projection of 3 slices were taken perpendicular to the membrane per animal. For each line scan, the peak value and cytoplasmic value were determined using the peak finding tools of the Scipy Signal Python datapack with *rel_height* of 1.0 (VIRTANEN *et al.*, 2020). Cytoplasmic values were subtracted from the corresponding peak values, and the resulting final junctional or membrane intensity values were averaged per animal. For SAX-7, exposure to auxin of 3 h or longer resulted in complete depletion and an inability to locate the ALM cell body. For these timepoints, values were plotted at 0 and no statistics were performed. For the measurement of PAR-6 at the apical domain of the seam cells and RPS-26 in the body wall muscle cytoplasm, averages of 3 regions were determined using a max projection of 3 slices (PAR-6) or a single slice (RPS-26).

C. elegans growth curves

To measure growth curves, L1 animals synchronized as described above were placed on NGM plates seeded with *E. coli* OP50 prepared as described above. Images were taken at 24-h intervals up to 72 h, using a Zeiss Axio Imager 2 equipped with a \times 20-0.5 NA objective and AxioCam MRm CCD (charge-coupled device) monochrome camera, driven by Zen Pro software. Animal length was quantified in FIJI software by drawing a line along the center line of the animal.

Statistical analysis

All statistical analyses were performed using GraphPad Prism 8. For population comparisons, a D’Agostino and Pearson test of normality was first performed to determine if the data were sampled from a Gaussian distribution. For data drawn from a Gaussian distribution, comparisons between 2 populations were done using an unpaired t-test, with Welch’s correction if the SDs of the populations differ significantly, and comparisons between > 2 populations were done using a 1-way ANOVA if the SDs of the populations differ significantly. For data not drawn from a Gaussian distribution, a nonparametric test was used (Mann–Whitney for 2 populations and Kruskal–Wallis for > 2 populations). ANOVA and nonparametric tests were followed up with multiple comparison tests of significance (Dunnett’s, Tukey’s, Dunnett’s T3, or Dunn’s). Tests of significance used and sample sizes are indicated in the figure legends. No statistical method was used to predetermine sample sizes. No samples or animals were excluded from analysis. The experiments were not randomized, and the investigators were not blinded to allocation during experiments and outcome assessment. All presented graphs were made using GraphPad Prism and Adobe Illustrator. ns is $P > 0.05$, * is $P \leq 0.05$, ** is $P \leq 0.01$, *** is $P \leq 0.001$, and **** is $P \leq 0.0001$.

Acknowledgments

We thank members of the S. van den Heuvel and M. Boxem groups for helpful discussions. We thank A. Riga for providing BOX523 and BOX857, D.J. Dolfin for providing SUR5 and SUR23, and V.C. Portegijs for providing the codon optimized wrmScarlet gBlock. We also thank Wormbase (HARRIS *et al.*, 2020) and the Biology Imaging Center, Faculty of Sciences, Department of Biology, Utrecht University. Some strains were provided by the *Caenorhabditis* Genetics Center, which is funded by NIH Office of Research Infrastructure Programs (P40 OD010440). The anti- α tubulin 12G10 monoclonal antibody developed by J. 438 Frankel and E.M. Nelson of the University of Iowa was obtained from the Developmental Studies Hybridoma Bank, created by the NICHD of the NIH and maintained at The University of Iowa, Department of Biology, Iowa City, IA 52242.

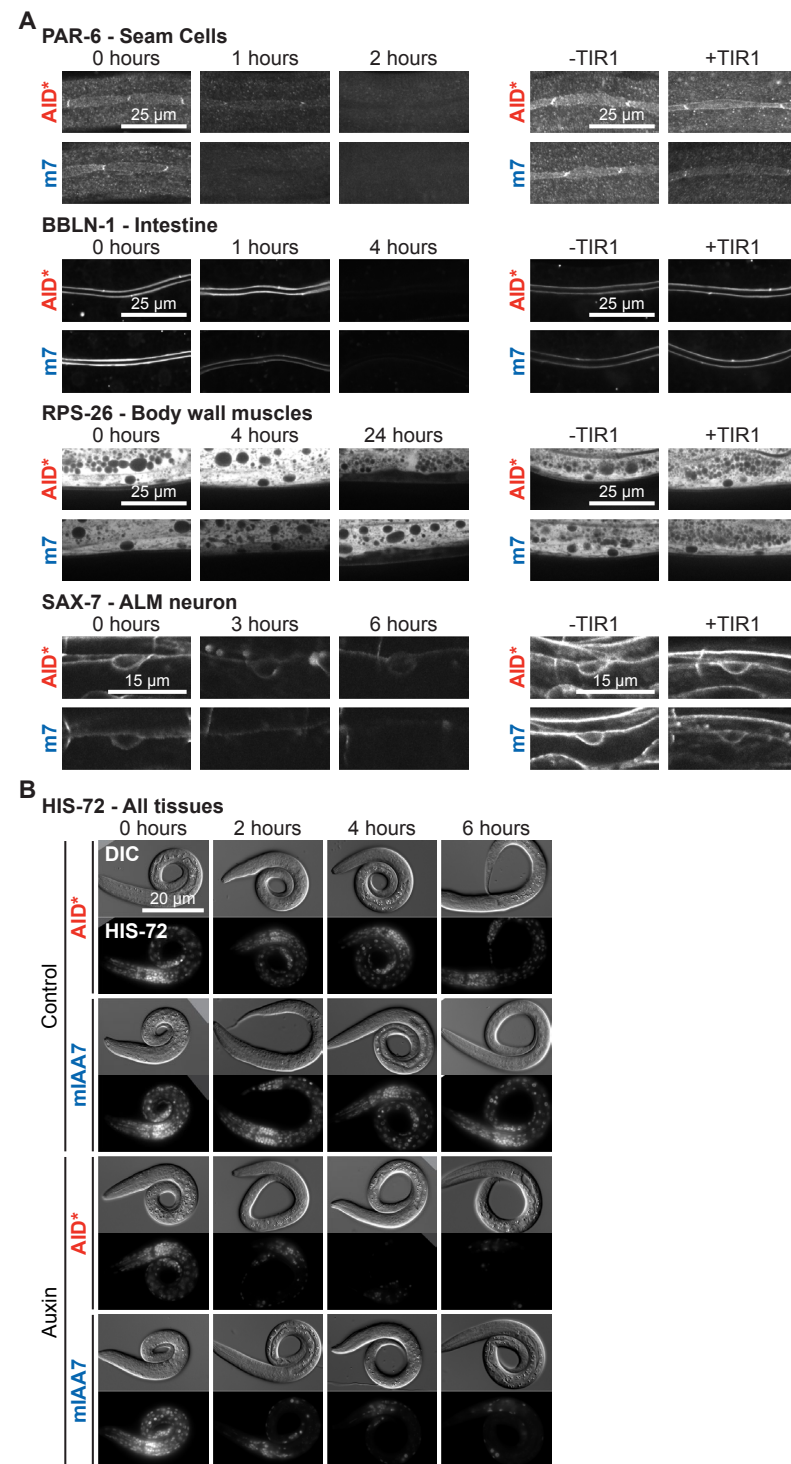
Author contributions

Conceptualization: JJS and MB; Formal analysis: JJS, NHMV, and JDW; Investigation: JJS, NHMV, AAV, SR, and JDW; Resources: JJS, NHMV, JMR, SR, JDW, and MB; Writing–original draft: JJS and NHMV; Writing–review and editing: SR, JDW, and MB; Visualization: JJS; Supervision: JJS, JDW, and MB; Project administration: JDW and MB; and Funding acquisition: JDW and MB.

Supplementary material:

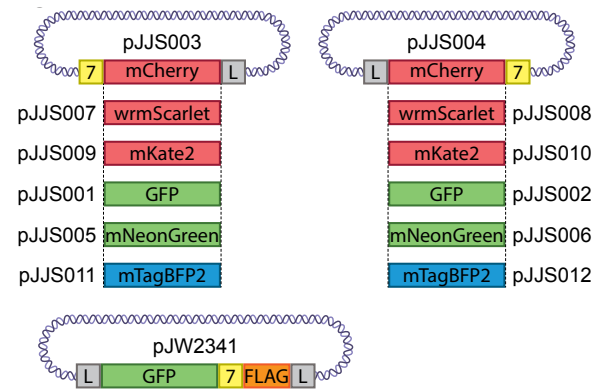


Supplementary figure 1: Schematic overview of the IAA proteins and the sequences of the different AID degrons that have been derived from them. Amino acids in bold are part of the degron sequences. IAA = Indole-3-acetic acid; AID = auxin inducible degron; I = domain I; KR = conserved lysine and arginine residue; II = domain II; PB1 = Phox and Bem1p domain.



~ Figure description on the next page ~

Supplementary figure 2: The mIAA7 degron robustly increases the efficiency of AID-induced protein degradation for several proteins across multiple tissues and cellular compartments. (A) Comparison between AID*- and mIAA7-mediated degradation for indicated proteins and tissues. PAR-6 was measured at the apical domain of seam cells in L2 larvae on 5 μ M auxin, BBLN-1 was measured at the apical domain in the intestine of L3 larvae treated with 50 μ M auxin, SAX-7 was measured at the plasma membrane in the ALM neuron cell body of L3 larvae treated with 5 μ M auxin, and RPS-26 was measured in the cytoplasm of body wall muscles of L2 larvae treated with 1 mM auxin. m7 = mIAA7. **(B)** Comparison between AID*- and mIAA7-mediated degradation for HIS-72 in all tissues of synchronized control or 4 mM auxin-treated L1 larvae. Images shown are representative maximum intensity projections that were acquired and displayed with the same settings for comparison, except for RPS-26 and HIS-72 for which a single plane is presented.



Supplementary figure 3: Schematic overview of the mIAA7 repair template plasmids.
7 = mIAA7 degron; L = linker sequence; GFP = green fluorescent protein; BFP = blue fluorescent protein; FLAG = 3x FLAG-tag.

Strain	Genotype	Source
Bristol N2	Wild type	CGC
PD1074	Wild type	CGC
BOX246	<i>par-6(mib30[par-6::AID*::GFP-LoxP]) I</i>	Castiglioni <i>et al.</i> (2020)
BOX273	<i>mibIs48[Pelt-2::TIR1::tagBFP2-Lox511::tbb-2-3'UTR, IV:5014740-5014802 (cxTi10816 site))] IV</i>	Castiglioni <i>et al.</i> (2020)
BOX408	<i>mibIs49[Pwrt-2::TIR1::tagBFP2-Lox511::tbb-2-3'UTR, IV:5014740-5014802 (cxTi10816 site))] IV</i>	Castiglioni <i>et al.</i> (2020)
BOX409	<i>par-6(mib30[par-6::aid::GFP-loxp]) I; mibIs49[Pwrt-2::TIR1::tagBFP2-Lox511::tbb-2-3'UTR, IV:5014740-5014802 (cxTi10816 site))] IV</i>	Castiglioni <i>et al.</i> (2020)
BOX523	<i>ieSi57 [Peft-3::TIR1::mRuby::unc-54 3'UTR + Cbr-unc-119(+)] II; sax-7(mib45[sax-7::AID*::GFP])</i>	This study
BOX526	<i>mibIs48[Pelt-2::TIR1::tagBFP2-Lox511::bb-2-3'UTR, IV:5014740-5014802 (cxTi10816 site))] IV; dlg-1(mib35[dlg-1::AID*::GFP-LoxP]) X</i>	Riga <i>et al.</i> (2021)
BOX623	<i>bbln-1(mib111[GFP::AID*::bbln-1]) X</i>	Rommelzwaal <i>et al.</i> (2021)
BOX632	<i>mibIs48[Pelt-2::TIR1::tagBFP2-Lox511::tbb-2-3'UTR, IV:5014740-5014802 (cxTi10816 site))] IV; bbln-1(mib111[GFP::AID*::bbln-1]) X</i>	Rommelzwaal <i>et al.</i> (2021)
BOX784	<i>mibIs48[Pelt-2::TIR1::tagBFP2-Lox511::tbb-2-3'UTR, IV:5014740-5014802 (cxTi10816 site))] IV; dlg-1(mib152[dlg-1::mIAA7::GFP]) X</i>	This study
BOX817	<i>mibIs48[Pelt-2::TIR1::tagBFP2-Lox511::tbb-2-3'UTR, IV:5014740-5014802 (cxTi10816 site))] IV; bbln-1(mib171[GFP::mIAA7::bbln-1]) X</i>	This study
BOX822	<i>bbln-1(mib172[GFP::mIAA7::bbln-1]) X</i>	This study
BOX823	<i>par-6(mib173[par-6::mIAA7::GFP]) I; mibIs49[Pwrt-2::TIR1::tagBFP2-Lox511::tbb-2-3'UTR, IV:5014740-5014802 (cxTi10816 site))] IV</i>	This study
BOX829	<i>par-6(mib174[par-6::mIAA7::GFP]) I</i>	This study
BOX838	<i>ieSi57 [Peft-3::TIR1::mRuby::unc-54 3'UTR + Cbr-unc-119(+)] II</i>	Zhang <i>et al.</i> (2015)
BOX847	<i>ieSi57 [Peft-3::TIR1::mRuby::unc-54 3'UTR + Cbr-unc-119(+)] II; sax-7(mib185[sax-7::mIAA7::GFP]) IV</i>	This study
BOX856	<i>sax-7(mib185[sax-7::mIAA7::GFP]) IV</i>	This study
BOX857	<i>sax-7(mib45[sax-7::AID*::GFP-loxP]) IV</i>	This study
BOX871	<i>erm-1(mib40[erm-1::mCherry::AID*]) I; mibIs50[Pelt-2::TIR1[F79G]::tagBFP2-Lox511::tbb-2-3'UTR, IV:5014740-5014802 (cxTi10816 site)] *mibIs48] IV</i>	Rommelzwaal <i>et al.</i> (2021) and this study

~ Table continues on the next page ~

Strain	Genotype	Source
BOX872	<i>erm-1(mib153[erm-1::mCherry::mIAA7]) I</i> ; <i>mibIs51[Pelt-2::TIR1[F79G]::tagBFP2-Lox511::tbb-2-3'UTR, IV:5014740-5014802 (cxTi10816 site)*mibIs48] IV</i>	This study
BOX873	<i>erm-1(mib175[erm-1::mIAA7::mCherry::mIAA7]) I</i> ; <i>mibIs52[Pelt-2::TIR1[F79G]::tagBFP2-Lox511::tbb-2-3'UTR, IV:5014740-5014802 (cxTi10816 site)*mibIs48] IV</i>	This study
BOX874	<i>erm-1(mib184[erm-1::mCherry::3x-mIAA7]) I</i> ; <i>mibIs53[Pelt-2::TIR1[F79G]::tagBFP2-Lox511::tbb-2-3'UTR, IV:5014740-5014802 (cxTi10816 site)*mibIs48] IV</i>	This study
BOX875	<i>mibIs54[Peft-3::TIR1[F79G]::mRuby::unc-54 3'UTR + Cbr-unc-119(+)*ieSi57] II</i> ; <i>sax-7(mib185 [sax-7::mIAA7::GFP]) IV</i>	This study
BOX879	<i>erm-1(mib187[erm-1::mCherry::2x-mIAA7]) I</i> ; <i>mibIs56[Pelt-2::TIR1[F79G]::tagBFP2-Lox511::tbb-2-3'UTR, IV:5014740-5014802 (cxTi10816 site)*mibIs48] IV</i>	This study
BOX880	<i>erm-1(mib191[erm-1::mIAA7::mCherry::]) I</i> ; <i>mibIs57[Pelt-2::TIR1[F79G]::tagBFP2-Lox511::tbb-2-3'UTR, IV:5014740-5014802 (cxTi10816 site)*mibIs48] IV</i>	This study
BOX882	<i>par-6(mib173[par-6::mIAA7::GFP]) I</i> ; <i>mibIs58[Pwrt-2::TIR1[F79G]::tagBFP2-Lox511::tbb-2-3'UTR, IV:5014740-5014802 (cxTi10816 site)*mibIs49] IV</i>	This study
SUR5	<i>rubSi4[rps-26::AID*::GFP]</i>	This study
SUR23	<i>rubSi4[rps-26::AID*::GFP]; Pmyo-3::TIR1::mRuby</i>	This study
SUR31	<i>rubSi10[rps-26::mIAA7::GFP]</i>	This study
SUR32	<i>rubSi11[rps-26::mIAA7::GFP]; Pmyo-3::TIR1::mRuby</i>	This study
IFM160	<i>bchSi59[Pmyo-3::TIR1::mRuby::tbb-2utr]II</i>	Venz <i>et al.</i> (2021)
JDW225	<i>wrdSi23[Peft-3::TIR1::F2A::mTagBFP2::AID*::NLS ::tbb-2 3'UTR, I:-5.32]</i>	Ashley <i>et al.</i> (2021)
JDW430	<i>wrdSi23[Peft-3::TIR1::F2A::mTagBFP2::AID*::NLS ::tbb-2 3'UTR, I:-5.32] I</i> ; <i>his-72(wrd100[GFP::AID*::3xFLAG::his-72]) III</i>	This study
JDW431	<i>wrdSi23[Peft-3::TIR1::F2A::mTagBFP2::AID*::NLS ::tbb-2 3'UTR, I:-5.32] I</i> ; <i>his-72(wrd101[GFP::mIAA7::3xFLAG::his-72]) III</i>	This study

Supplementary table 1: List of strains used.

pJJS001 <i>mIAA7::GFP::Linker</i> GFP origin: pJJR82 (Addgene #75027)	
pBSK For.	TGGCAGTGGAGGTACCGCGGAAGCGGTGCGGTGGAGCTCCAGCTTTTGTTTC
pBSK Rev.	CCAATTTCGCCCTATAGTGAGTTCG
mIAA7 For.	CTCACTATAGGGCGAATTGGATGGGATTCTCCGAGACC
mIAA7 Rev.	CCTTGGACATGGAGGAGGTCTTTTGTGTTG
GFP For.	GACCTCCTCCATGTCCAAGGGAGAGGAAC
GFP Rev.	CGCCGGTACCTCCACTGCCACCGCTGCCCTTGTAGAGCTCGTCCATTC
pJJS002 <i>Linker::GFP::mIAA7</i>	
pBSK For.	GCGGTGGAGCTCCAGCTTTTGTTTC
pBSK Rev.	CGCCGGTACCTCCACTGCCACCGCTGCCCAATTCGCCCTATAGTGAGTTCG
mIAA7 For.	GCTCTACAAGGGATTCTCCGAGACCGTC
mIAA7 Rev.	AAAAGCTGGAGCTCCACCGCGGAGGAGGTCTTTTGTGTTG
GFP For.	TGGCAGTGGAGGTACCGCGGAAGCGGTATGTCCAAGGGAGAGGAAC
GFP Rev.	CGGAGAATCCCTTGTAGAGCTCGTCCATTCCTGTTG
pJJS003 <i>mIAA7::mCherry::Linker</i> mCherry origin: pJJR83 (Addgene #75028)	
pBSK For.	TGGCAGTGGAGGTACCGCGGAAGCGGTGCGGTGGAGCTCCAGCTTTTGTTTC
pBSK Rev.	CCAATTTCGCCCTATAGTGAGTTCG
mIAA7 For.	CTCACTATAGGGCGAATTGGATGGGATTCTCCGAGACC
mIAA7 Rev.	CCTTGGACATGGAGGAGGTCTTTTGTGTTG
mCherry For.	GACCTCCTCCATGTCCAAGGGAGAGGAGGACAAC
mCherry Rev.	CGCCGGTACCTCCACTGCCACCGCTGCCCTTGTAGAGCTCGTCCATTC
pJJS004 <i>Linker::mCherry::mIAA7</i>	
pBSK For.	GCGGTGGAGCTCCAGCTTTTGTTTC
pBSK Rev.	CCAATTTCGCCCTATAGTGAGTTCG
mIAA7 For.	GCTCTACAAGGGATTCTCCGAGACCGTC
mIAA7 Rev.	AAAAGCTGGAGCTCCACCGCGGAGGAGGTCTTTTGTGTTG
mCherry For.	CTCACTATAGGGCGAATTGGGCGAGCGGTGGCAGTGGA
mCherry Rev.	CGGAGAATCCCTTGTAGAGCTCGTCCATTCCTCCG
pJJS005 <i>mIAA7::mNG::Linker</i> mNG origin: pDD346 (Addgene #133311)	
pJJS001 For.	GCTCTACAAGGGCAGCGGTGGCAGT
pJJS001 Rev.	TGGAGACCATGGAGGAGGTCTTTTGTGTTGGG
mNG For.	GACCTCCTCCATGGTCTCCAAGGGAGAGG
mNG Rev.	CACCGCTGCCCTTGTAGAGCTCGTCCATTC

~ Table continues on the next page ~

pJJS006	Linker::mNG::mIAA7
pJJS002 For.	GCTCTACAAGGGATTCTCCGAGACCGTC
pJJS002 Rev.	TGGAGACCATAACCGCTTCCGCCGGTA
mNG For.	CGGAAGCGGTATGGTCTCCAAGGGAGAGGAG
mNG Rev.	CGGAGAATCCCTTGTAGAGCTCGTCCATTCC
pJJS007	mIAA7::wrmScarlet::Linker wrmScarlet origin: Codon optimized gBlock
pJJS001 For.	GCTCTACAAGGGCAGCGGTGGCAGT
pJJS001 Rev.	TGCTGACCATGGAGGAGGTCTTTTGTGGG
mScarlet For.	GACCTCCTCCATGGTCAGCAAGGGAGAGG
mScarlet Rev.	CACCGCTGCCCTTGTAGAGCTCGTCCATTCC
pJJS008	Linker::wrmScarlet::mIAA7
pJJS002 For.	GCTCTACAAGGGATTCTCCGAGACCGTC
pJJS002 Rev.	TGCTGACCATAACCGCTTCCGCCGGTA
mScarlet For.	CGGAAGCGGTATGGTCAGCAAGGGAGAGG
mScarlet Rev.	CGGAGAATCCCTTGTAGAGCTCGTCCATTCTC
pJJS009	mIAA7::mKate2::Linker mKate2 origin: pDD375 (Addgene #91825)
pJJS001 For.	ACACCGTAAGGGCAGCGGTGGCAGT
pJJS001 Rev.	CGGAGACCATGGAGGAGGTCTTTTGTGGG
mKate2 For.	GACCTCCTCCATGGTCTCCGAGCTCATTAAAGAA
mKate2 Rev.	CACCGCTGCCCTTACGGTGTCCGAGCTTG
pJJS010	Linker::mKate2::mIAA7
pJJS002 For.	ACACCGTAAGGGATTCTCCGAGACCGTC
pJJS002 Rev.	CGGAGACCATAACCGCTTCCGCCGGTA
mKate2 For.	CGGAAGCGGTATGGTCTCCGAGCTCATTAAAGA
mKate2 Rev.	CGGAGAATCCCTTACGGTGTCCGAGCTTG
pJJS011	mIAA7::mTagBFP2::Linker TagBFP2 origin: JDW233 (Ashley <i>et al.</i> 2021)
pJJS001 For.	CAAGCTCAACGGCAGCGGTGGCAGT
pJJS001 Rev.	CCGAAACCATGGAGGAGGTCTTTTGTGGG
mTagBFP2 For.	GACCTCCTCCATGGTTTCGGAATTGATTAAGGAA
mTagBFP2 Rev.	CACCGCTGCCGTTGAGCTTGTGTCCGAGC
pJJS012	Linker::mTagBFP2::mIAA7
pJJS002 For.	CAAGCTCAACGGATTCTCCGAGACCGTC
pJJS002 Rev.	CCGAAACCATACCGCTTCCGCCGGTA
mTagBFP2 For.	CGGAAGCGGTATGGTTTCGGAATTGATTAAGGAA
mTagBFP2 Rev.	CGGAGAATCCGTTGAGCTTGTGTCCGAGC

~ Table continues on the next page ~

pJW2341	Linker::GFP::mIAA7::3xFLAG::Linker
pJW2086 For.	GAGCATGAGGTGACGGTCTCGGAGAATCCCCGCCACCTCCGGATCCGGATTG AAAG
pJW2086 Rev.	AACATGATGACCAACAAAAGACCTCCTCCGGTGGTGGCGTTCTGGCTCAGG
mIAA7 For.	GGATTCTCCGAGACCGTCGACCTC
mIAA7 Rev.	GGAGGAGGTCTTTTGTGGGTTCATC

Supplementary table 2: Primer sequences for plasmids.

<i>dlg-1::mIAA7::GFP</i>	
crRNA	GCCACGTCATTAGATGAAAT
Repair template For.	GTGAATCGCAGACGCCAATTTGGGTGCCACGTCATGGATTCTCCGAGACCGT
Repair template Rev.	GAGACAATTGAGAATATTGTTTAAAAAATAAAAGAAAATACGATAGAACAAATAATTAGGAGGAGGTCTTTTGTGGG
Genotyping For.	AGTGGCGAAGAAGCTCAAGC
Genotyping Rev.	CCACAATCACTGCCAGAAAACGG
<i>par-6::mIAA7::GFP</i>	
crRNA	AAATGATTTCGGACAGTGGAG
Repair template For.	TCCGAAACAGCAGCAGCCAAATGATTTCGGACAGTGGAGAAGACGGATTCTCCGAGACCGT
Repair template Rev.	AAAATCGAGGAAAAATGGCTGAAAAGAGTTTTTCACTTGTAGAGCTGTCCATTC
Genotyping For.	ACGAGGACCGTCACAACAAG
Genotyping Rev.	AGTATGGGCTCAGAGAGCTCTG
<i>GFP::mIAA7::bbln-1</i>	
crRNA	CTCATTTCAGTTGAACACAA
Repair template For.	TCTTTTTCTCCATTTCCCTCATTTTCAGTTGAACACAATGTCCAAGGGA GAGGAAC
Repair template Rev.	ACAATAGGCTCTTGCTCTTCTGCTCAACGACCATGGAGGAGGTCTTTGTTGG
Genotyping For.	ATCATCACCATCATCATCACC
Genotyping Rev.	GTCACCTCTCCTTCGTTGAG
<i>rps-26::AID*::GFP</i>	
crRNA	GAACAAACAACCTTATGGACG
Repair template For.	CTGCTGCTCGTCCAGGAGCTCCAGGACCACGTCCAATGCCTAAAGATCCAGCCAA
Repair template Rev.	AAAAAGGTTTATAATTTCAAAGAACAACAACCTTAGTAGAGCTCGTCCATTCCGT
Genotyping For.	ATCCACAGCAAGGTCGTCAG
Genotyping Rev.	GAGCAACACAATTCAGTTCGGG
<i>rps-26::mIAA7::GFP – same genotyping primers as <i>rps-26::AID*::GFP</i></i>	
crRNA	GAACAAACAACCTTATGGACG
Repair template For.	CCGCTGCTGCTCGTCCAGGAGCTCCAGGACCACGTCCAATGGGATTC TCCGAGACCGTC
Repair template Rev.	AAAAAGGTTTATAATTTCAAAGAACAACAACCTTAGTAGAGCTCGTCCATTCCGT

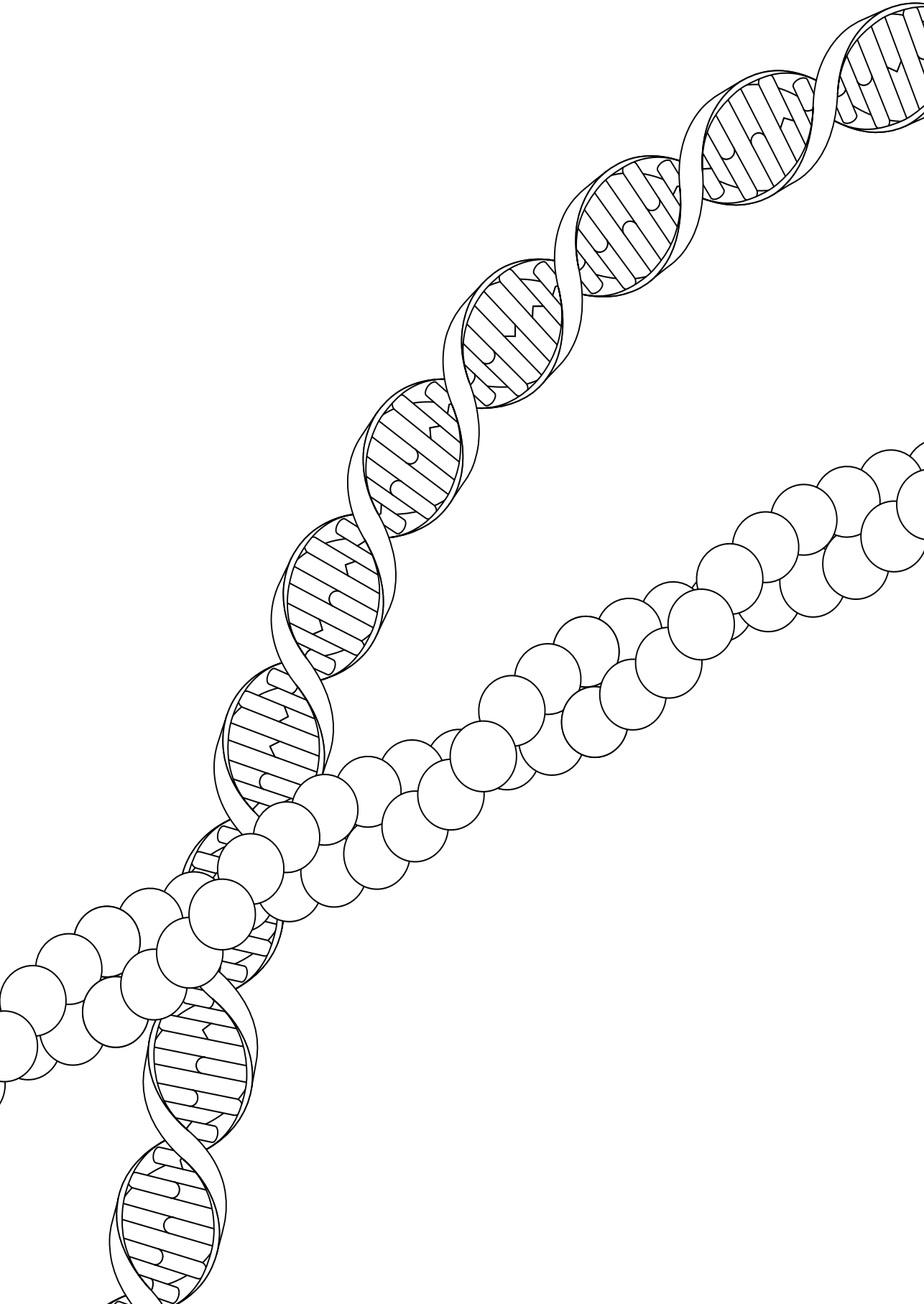
~ Table continues on the next page ~

<i>sax-7::AID*::GFP*</i>	
sgRNA 1 For.	TTGCCGGCCGAACGGCCCCGAGAA
sgRNA 1 Rev.	AACTTCTCGGGCCGTTTCGGCCGG
sgRNA 2 For.	TCTTCCGGCCGAACGGCCCCGAGAA
sgRNA 2 Rev.	AAACTTCTCGGGCCGTTTCGGCCGG
sgRNA 3 For.	TCTTGTCCACAAAAGAGCTTGATGC
sgRNA 3 Rev.	AAACGCATCAAGCTCTTTTGTGGAC
Left homology arm For.	CTGCTCTTCGTGGCTATCCAGTATCACAGCGTGAGCG
Left homology arm Rev.	GTGCTCTTCGCGGACAAACGTCGACGTTGATCCTTTTTTCTGGACGCTCGGCTG
Right homology arm For.	CTGCTCTTCGACGTAGAAGACTATCCACGTGTTTCCTTC
Right homology arm Rev.	GTGCTCTTCGTACGTCACCTACCCACATGGTTATCCG
Genotyping For.	GCCACAAGATGCTGATGAATGG
Genotyping Rev.	GGTAAAAGCTCTGGCAAACGTC
<i>sax-7::mIAA7::GFP</i>	
crRNA	GTCGACGTTGATCCTTTCTC
Repair template For.	TCTTTTTCTCCATTTCCCTCATTTTCAGTTGAACACAATGTCCAAGGGA GAGGAAC
Repair template Rev.	ACAATAGGCTCTTGCTCTTCTGCTCAACGACCATGGAGGAGGTCTTTGTTGG
Genotyping For.	ATCATCACCATCATCATCACC
Genotyping Rev.	GTCACCTCTCCTTCGTTGAG
<i>GFP::AID*::3xFLAG::his-72 and GFP::mIAA7::3xFLAG::his-72</i>	
crRNA	GGTACGAGCCATTGTTGTTTC
Repair template For.	TCCAACCATTTCTCAATTTCTCAATTTCCAGAACAACAATGAGTAAAGGAGAAGAATTGTTCACTGG
Repair template Rev.	CCGGTGGATTTACGAGCGGTTTGCTTGGTACGAGCTGAGGCTCCCGATGCTCCCTTG
Genotyping For.	CGATCGATAGTGACACGCGA
Genotyping Rev.	CACAGGTTGGTGTCTCGAA
<i>TIR1[F79G]</i>	
crRNA	AGGTTGAAGTCGGCGAAGTG
Repair template	AAGGTCGGTTCGCTCGAGCTCAAGGAAAGCCACATGGAGCCGATTTCAATCTTGTCCAGACGGATGGGGAGGATACGTCTACCCATG
Genotyping For.	AGAAGAAGTACTCGAGCACG
Genotyping WT Rev.	AGGTTGAAGTCGGCGAAG
Genotyping F79G Rev.	GACAAGATTGAAATCGGCTCC
Sequence Rev.	TTGAGCTTGAGGGACTTGAG

~ Table continues on the next page ~

<i>erm-1::mCherry::mIAA7</i>	
crRNA	ATATTGTTTAAAAAATAAA
Repair template For.	ACACAAAACGAAGAATCGATCAATACGAAAATATGGGCAGCGGTGGC AGTGGA
Repair template Rev.	GAGACAATTGAGAATATTGTTTAAAAAATAAAAGAAAAATACGATA GAACAAATAATTAGGAGGAGGTCTTTTGTGGG
Genotyping For.	AACTCGGTATTCCTTTACG
Genotyping Rev.	ATTGTAAAAGGCACTGATGG
<i>erm-1::mCherry::2x-mIAA7</i> – same genotyping primers as <i>erm-1::mCherry::mIAA7</i>	
crRNA	AGGAATGGACGAGCTCTACA
Repair template For.	GGGACGTCACCTCCACCGGAGGAATGGACGAGCTCTACAAAGGATTCT CCGAGACCGT
Repair template Rev.	AGGTTGAGCATGAGGTCGACGGTCTCGGAGAATCCGGAGGAGGTCTT TTGTTGG
<i>erm-1::mIAA7::mCherry</i> – same genotyping primers as <i>erm-1::mCherry::mIAA7</i>**	
crRNA 1	ATATTGTTTAAAAAATAAA
crRNA 2	AAGACTCTCCGTCAAATCCG
Repair template For. 1	TTGAGACAAATTCGCGGAGGAAACACGAAGAGGCGCATCGACCAATA CGAGAACATGGGATTCTCCGAGACCGT
Repair template For. 2	AGAACA AAAAGGCCGACGCGACAAGTACAAGACTTTGAGACAAATT CGCGGAGG
Repair template Rev.	AGACAATTGAGAATATTGTTTAAAAAATAAAAGTAAATACGATAGA ACAAATAATTACTTGTAGAGCTCGTCCATTC
<i>erm-1::mIAA7::mCherry::mIAA7</i> – same genotyping primers as <i>erm-1::mCherry::mIAA7</i>	
crRNA	AGCGGTGGCAGTGGAGGTAC
Repair template For.	AATACGAAAATATGGGCAGCGGTGGCAGTGGAGGTGGATTCTCCGAG ACCGT
Repair template Rev.	TCCTCCTCTCCCTTGGACATACCGCTCCGCCGGTGGAGGAGGTCTT TTGTTGG

Supplementary table 3: Genome engineering reagents. *Three crRNAs were used since 1 was not efficient enough. **Two crRNAs were used since 1 was not efficient enough. In addition, due to a size limitation of the primer oligo, the repair template was generated using 2 PCRs. An initial PCR using “repair template For. 1,” and a second reaction using “Repair template For. 2” and the product of the first reaction as template.



Chapter 6

General discussion

Jorian J. Sepers

Division of Developmental Biology, Institute of Biodynamics and Biocomplexity, Department of
Biology, Faculty of Science, Utrecht University, Utrecht, The Netherlands

Most organs in the body consist of tubular structures responsible for transporting nutrients, waste, liquids, and gases. Tubulogenesis refers to the process of the morphological transformation of a tissue into a tube shape. Defects in tubulogenesis have been associated with various diseases, such as polycystic kidney disease (LITTLE *et al.*, 2010). Additionally, certain cancers exploit the tubulogenesis mechanism to become more invasive or even metastatic (CARMELIET & JAIN, 2000; NAGLE & CRESS, 2011). In this thesis, I employed the *Caenorhabditis elegans* model organism to investigate tubulogenesis with a specific focus on the importance of the actin cytoskeleton during lumen formation.

In Chapter 2, we studied ERM-1, the single *C. elegans* ortholog of the ezrin/radixin/moesing (ERM) protein family. ERM proteins are conserved regulators of cortical specialization, that function as a membrane-actin linkers and organizers of molecular hubs. Previously, it was shown that ERM-1 in the *C. elegans* intestine is essential for lumen formation, as depletion of the protein results in a loss of microvilli and a widened lumen accompanied by constrictions (GÖBEL *et al.*, 2004; VAN FÜRDEN *et al.*, 2004). We investigated ERM-1 regulation by examining the conserved PIP₂ binding domain and phosphorylation of the C-terminal T544 residue. We generated endogenous mutants that eliminate the PIP₂ binding site, alongside phosphonull and phosphomimicking T544 mutants. PIP₂ binding mutants resemble the *erm-1* null phenotype, demonstrating that this domain is essential for ERM-1 function. The phosphomutants on the other hand have milder defects as they have a reduced fitness, but animals are viable. The phosphosite contributes to tubulogenesis, as the mutants prevent the excretory canal from fully extending to its intended length and leads to widening of the intestinal lumen often accompanied by constrictions. In contrast to ERM proteins from other species, both phosphonull and phosphomimetic alleles of the T544 site result in a similar fitness reduction. Therefore, both phospho-states of ERM-1 are important, and we postulate that phosphocycling contributes to modulation of ERM-1 activity. Collectively, the work in Chapter 2 highlights how ERM proteins can be fine-tuned for various tissues, as the removal of the PIP₂ binding site and the mutations of the T544 phosphosite result in differential alterations in ERM-1 activity across different tissues.

In Chapter 3, we worked on the role of the sole *C. elegans* NHERF ortholog, named NRFL-1, in the intestinal lumen formation. Typically, members of the NHERF family can bind ERM proteins and act as scaffolding proteins by revealing multiple PDZ domains. We showed that this holds true for NRFL-1 as well, as it is recruited to the microvilli by ERM-1 through the conserved C-terminal ERM binding domain, and that this is vital for NRFL-1 activity. NRFL-1 depletion does not result in any overt defects. However, loss of NRFL-1 and ERM-1 T544 phosphorylation combined closely mimics the *erm-1* null phenotype. We

did not find any indication that NRFL-1 regulates ERM-1 directly, so NRFL-1 likely acts downstream of ERM-1, in accordance with the postulated role of NHERF proteins as molecular hubs extending the scaffolding capability of ERM proteins. We hypothesize that ERM-1 activity in the intestine involves actin binding modulated by phosphocycling of the C-terminal threonine residue and the organization of the apical domain composition through NRFL-1

In Chapter 4, we set out to identify novel regulators of intestinal lumen formation and found the kinase GCK-4, ortholog of mammalian LOK and SLK, in a small candidate RNAi screen. Loss of GCK-4 causes a widened and round lumen accompanied by constrictions and the affected animals arrest as young larvae, mimicking the *erm-1* null phenotype. In addition, GCK-4 depletion results in a reduction of the apical actin network and a distorted localization of the Cadherin/Catenin complex (CCC), part of the *C. elegans* apical junctions (CeAJ). In an effort to decipher the role of GCK-4, we revealed that it localizes to the tip of the microvilli and exerts its activity via its kinase domain. While GCK-4 does play a role in facilitating the apical recruitment of ERM-1 and NRFL-1, it sets itself apart from its orthologs by not functioning as the ERM-1 T544 kinase. In an effort to identify the kinase substrates and other interactors of GCK-4, we conducted proximity labeling and phosphoproteomics experiments. While the initial set of tested hits did not yield any significant results, the proteomics data remains a valuable resource for further exploration in search of GCK-4 interactors.

The relationship between GCK-4 and ERM-1

Morphologically, the *erm-1* and *gck-4* null phenotypes are highly similar, if not identical, as they both have a widened lumen with constrictions and result in an early larval arrest (CHAPTER 2; CHAPTER 4). Given these shared defects, to what extent do the underlying molecular mechanisms of these phenotypes align? ERM proteins are mostly known for actin regulation, by linking the cortical F-actin to the membrane and by recruiting actin regulators (McCLATCHEY, 2014; PONUWEI, 2016). This appears to hold true for ERM-1 in the *C. elegans* intestine, as depletion of ERM-1 leads to an altered apical ACT-5 network throughout development and the loss of a brush border (CHAPTER 2). LOK and SLK function as actin regulators through ERM phosphorylation of the conserved threonine residue. However, this does not apply to GCK-4, as GCK-4 knockdown did not result in loss of ERM-1 phosphorylation (CHAPTER 4; BELKINA *et al.*, 2009; VISWANATHA *et al.*, 2012). Nevertheless, GCK-4 is involved in regulation of the apical actin network in some other way, as apical ACT-5 is reduced and most of the hits found in the proximity labeling and phosphoproteomic approaches are related to the actin cytoskeleton. Collectively, ERM-1 and GCK-4 seem to act as regulators of the actin cytoskeleton in the intestine, as the loss of either of these proteins results in a disrupted apical actin network and morphological

defects that closely resemble the *act-5* knockdown phenotype (MACQUEEN *et al.*, 2005). Considering this information, along with the fact that GCK-4 is a microvillar protein and ERM-1 localization is partially dependent on GCK-4, it is likely that *gck-4* mutants also lack a brush border (CHAPTER 4). Besides the actin cytoskeleton, both ERM-1 and GCK-4 regulate the CCC, as both GCK-4 knockdown animals and *erm-1*[T544A] mutants have bright, seemingly aggregated, parts of the E-cadherin ortholog, HMR-1, in the CeAJ (CHAPTER 2; CHAPTER 4). Finally, neither ERM-1 or GCK-4 depletions have a major effect on the remaining cytoskeletal networks, remaining CeAJ complexes or epithelial cell polarity (CHAPTER 2; CHAPTER 4; GÖBEL *et al.*, 2004; VAN FÜRDEN *et al.*, 2004). To conclude, ERM-1 and GCK-4 cause a seemingly identical phenotype both morphological as well as molecularly.

If they induce the same phenotype upon depletion, how are ERM-1 and GCK-4 related? Loss of GCK-4 affects the apical recruitment of ERM-1, so GCK-4 probably acts upstream of ERM-1 (CHAPTER 4). As mentioned above, GCK-4 is not the ERM-1 kinase unlike the mammalian and *Drosophila* orthologs (CHAPTER 4; BELKINA *et al.*, 2009; HIPFNER *et al.*, 2004; VISWANATHA *et al.*, 2012). However, LOK has been shown to play a role in inducing a conformational change in Ezrin in human cell culture, transitioning it from a closed-inactive to an open-active state (PELASEYED *et al.*, 2017). This raises the possibility that GCK-4 may regulate ERM-1 directly, beyond phosphorylation. Nevertheless, we failed to detect a direct physical interaction between the two proteins. Additionally, given the that kinase domain is essential for GCK-4 activity, it appears that GCK-4 exerts its activity mainly through phosphorylation (CHAPTER 4).

Despite the established model of ERM protein recruitment via the PIP₂ binding domain, ERM proteins can also be recruited to the cortex by other proteins. In this alternative model, ERM proteins link the membrane and F-actin by binding to cortical or transmembrane proteins through the FERM domain. (MCCLATCHEY, 2014; PONUWEI, 2016). There seems to be merit for this model in the *C. elegans* intestine, as the ERM-1[4KN]::GFP is still partially recruited to the apical membrane (CHAPTER 2). Could GCK-4 potentially serve as a regulator for one of the proteins essential for ERM-1's apical recruitment? NRFL-1 was a significant hit in the GCK-4 proximity labeling suggesting they act together, and NHERF proteins are commonly involved in ERM recruitment (CHAPTER 4). Nonetheless, NRFL-1 does not influence ERM-1 localization and does not cause any overt luminal defects upon depletion, implying that GCK-4 does not control ERM-1 localization through NRFL-1 (CHAPTER 3). Besides the NHERF proteins, transmembrane proteins involved in cell-cell contacts such as CD43, CD44, ICAM1 and ICAM2 can also bind and recruit ERM proteins (BARREIRO *et al.*, 2002; CANNON *et al.*, 2011; HEISKA *et al.*, 1998; LEGG *et al.*, 2002; SERRADOR *et al.*, 1998; YONEMURA

et al., 1998). Although these proteins do not share an obvious ortholog in *C. elegans*, there might be other proteins like them in the *C. elegans* intestine that act similarly to recruit ERM-1 under control of GCK-4.

Alternatively, GCK-4 and ERM-1 may act independent of one another to control the actin cytoskeletal network. ERM-1 would in this case not be directly regulated by GCK-4, but the reduced apical ERM-1 levels would be a consequence of the loss of the apical actin network and the brush border as this is where ERM-1 resides normally. Following this logic, loss of ERM-1 also would then affect GCK-4 localization, since ERM-1 affects the microvilli in which GCK-4 resides (CHAPTER 4). How could GCK-4 affect the actin network in an ERM-independent manner? SLK has been postulated to disassemble actin stress fibers through the Rac/Rho pathways at the focal adhesions of migrating cells (AL-ZAHRANI *et al.*, 2013; SABOURIN & RUDNICKI, 1999; WAGNER & SABOURIN, 2009; WAGNER *et al.*, 2002; WAGNER *et al.*, 2008). Orthologs of the Rac/Rho pathway are predicted to be expressed in the intestine, opening the possibility that GCK-4 acts upon the apical actin network in a similar way (HASHIMSHONY *et al.*, 2015). In addition, more distant relatives of GCK-4 in the GCK protein family have been implicated in actin organization as well (POMBO *et al.*, 2007). For instance, the kinase Nak1 in fission yeast plays a crucial role in polarized actin network formation and cellular morphogenesis, mirroring the function of GCK-4 in the *C. elegans* intestine (LEONHARD & NURSE, 2005).

Dissecting the actin phenotype

The *gck-4*, *erm-1* and *act-5* phenotypes affects the morphology and physiology of the worm in four different ways: 1. Loss of the brush border in the intestine, 2. A widened and rounder intestinal lumen, 3. Constrictions in the intestinal lumen and 4. Developmental arrest as a young L1 larva. How are these four different facets of the phenotype caused and related to one another?

As the apical actin network is disrupted due to the depletion of ERM-1, GCK-4 or ACT-5, the loss of the brush border is a natural consequence. Microvilli are sustained by approximately twenty actin filaments that are regulated by actin bundlers, end capping proteins, and membrane-actin linkers. Depletion of any of these components alter the shape, length, or overall formation of microvilli in various model systems (SAUVANET *et al.*, 2015). For example, in *C. elegans* depletion of the microvillar actin plus-end capping protein EPS-8, results in a loss of brush border in the intestine (CROCE *et al.*, 2004). In addition, in mammalian cell culture Ezrin and Eps8 interact and synergistically control microvillar shape (ZWAENEPOEL *et al.*, 2012). Thus, loss of the brush border in the ERM-1, GCK-4 and ACT-5 knockdown backgrounds appears to be directly caused by a disruption of the apical actin network.

The volume and shape of a lumen is determined by a balance of two forces: the inside pressure exerting a force outwards, and the structure surrounding the lumen applying a force inwards (SCHOTTENFELD-ROAMES & GHABRIAL, 2013; SIGURBJÖRNSDÓTTIR *et al.*, 2014). Therefore, the second facet of the phenotype, the widening and loss of the oval shape of the intestinal lumen, could be explained by an imbalance of these forces. The luminal pressure is determined by the content within the lumen, originating from ingested food and influx of fluids by the intestinal cells through osmotic regulation. Food is pumped in into the *C. elegans* intestinal lumen by the pharynx, a tubular muscular motor connected to the intestine through the pharyngeal-intestinal valve (AVERY & SHTONDA, 2003). As we lack evidence of reduced pharyngeal activity in the actin mutants, it is conceivable that the lumen widens due to the accumulation of food unable to proceed due to the constrictions. In line with this is that the lumen is not widened yet during embryonic development, when the animals do not feed. However, widening of the lumen occurs in conditions without luminal constrictions, such as in the *erm-1*[T544A] mutant and animals with a disrupted IF network (CHAPTER 2; CARBERRY *et al.*, 2012; GEISLER *et al.*, 2020). In addition, in the animals with constrictions, the complete lumen is widened, and not just up to the first constriction. Thus, constipation of the intestinal content is not the main reason for a widened lumen.

Alternatively, the luminal content could be increased by osmotic pressure as altering the apical domain can affect the channels and pumps that transport water and ions across the membrane. Members of the ERM and NHERF protein families can recruit channels and pumps in various model systems, including in *C. elegans* (McCLATCHEY, 2014; PONUWEI, 2016; SHENOLIKAR & WEINMAN, 2001). For instance, in the excretory canal ERM-1 recruits AQP-8, a water channel, and together they synergistically contribute to tubulogenesis (KHAN *et al.*, 2013). In addition, NRFL-1 is important for the maintenance of AAT-6, an amino acid pump, at the apical membrane in the intestine (HAGIWARA *et al.*, 2012). Therefore, altering the localization or regulation of ERM-1 could potentially lead to the mislocalization of specific channels or pumps, subsequently causing a shift in osmotic pressure and ultimately resulting in widening of the lumen.

As mentioned above, the luminal shape is also determined by the structure surrounding the lumen applying force inwards (SIGURBJÖRNSDÓTTIR *et al.*, 2014). In the *C. elegans* intestine the terminal web, comprised of the apical actin and IF networks, is important for structural support, and therefore is essential for proper luminal morphogenesis. In support of this, both disrupting the apical actin network as well as the IF cytoskeleton causes widening of the lumen (CHAPTER 2; CHAPTER 3; CHAPTER 4; CARBERRY *et al.*, 2012; CROCE *et al.*, 2004; GEISLER *et al.*, 2020; GÖBEL *et al.*, 2004; MACQUEEN *et al.*, 2005; VAN FÜRDEN *et al.*, 2004). Therefore, it appears that the regulation of the luminal size and shape is orchestrated by

the terminal web, and that this likely accounts for the luminal widening in the various mutants explored in this thesis (CHAPTER 2; CHAPTER 3; CHAPTER 4).

In summary, the primary factor contributing to the widening of the intestinal lumen appears to be the disruption of the terminal web, although the potential influence of increased pressure within the lumen cannot be ruled out. Loss of a brush border alone does not seem to be the underlying cause of luminal expansion, as there are mutants that exhibit a widened lumen while retaining their brush border (CHAPTER 2; GEISLER *et al.*, 2020; REMMELZWAAL *et al.*, 2021). However, it is worth noting that microvillar proteins still play a role in controlling the luminal shape.

The third defect, the luminal constrictions, consistently coincide with the widened lumen and brush border defects. However, altered luminal shape and brush border issues can manifest independently from luminal constrictions (CHAPTER 2; CHAPTER 3; CHAPTER 4; CARBERRY *et al.*, 2012; CROCE *et al.*, 2004; GEISLER *et al.*, 2020; GÖBEL *et al.*, 2004; MACQUEEN *et al.*, 2005; VAN FÜRDEN *et al.*, 2004). This suggests that these defects likely share a common molecular cause, and the luminal constrictions represent an additional level of severity among these defects. This distinction becomes evident in ERM-1 phosphomutants, which predominantly exhibit luminal shape and microvillar defects, while a more severe *erm-1* null mutant leads to constrictions and the complete loss of the brush border (CHAPTER 2; GÖBEL *et al.*, 2004; VAN FÜRDEN *et al.*, 2004).

What is affected in the ERM-1, GCK-4, and ACT-5 depletion mutant backgrounds that leads to luminal constrictions, yet remains unaltered in luminal-defective mutants lacking the constrictions? In the work of van Fürden *et al.* (2004), it has been proposed that the constrictions are caused by a mislocalization of the cell-cell junctions. According to this hypothesis, ERM-1 would be involved in relocating the CeAJ components from the apical to the subapical domain. Therefore, in the absence of ERM-1 the maturing junctions would establish connections between the opposing intestinal cells causing constrictions. Since this publication, various mammalian cell culture studies showed proof of the ability of ERM proteins to influence levels and localization of the adherens junctions (CHEN *et al.*, 2012; DATTA *et al.*, 2011; JAFFE *et al.*, 2008). Furthermore, this thesis demonstrated that both the *erm-1*[T544A] mutant and GCK-4 depletion result in an altered CeAJ morphology and the aggregation of HMR-1. Additionally, for the *erm-1* phosphomutants the CeAJ coincide with the luminal constrictions (CHAPTER 2; CHAPTER 4). Thus, ERM-1 indeed seems to be involved in relocating CeAJ components from apical to subapical.

How are the apical actin regulators involved in repositioning the CeAJ? So far, ERM-1 and GCK-4, or their orthologs, have not been reported to physically interact with cell-cell junction proteins. Therefore, ERM-1 and GCK-4 do not seem to directly affect the CeAJ. In addition, the constrictions also happen in the

act-5 RNAi animals, suggesting that the CeAJ localization depends on the overall apical actin network (MACQUEEN *et al.*, 2005). In line with this, the CCC and SAX-7/MAGI-1/AFD-1 complex (SMAC) presumably directly interact with F-actin, and this interaction would be important for proper CeAJ maturation (CHAPTER 1). Furthermore, loss of other actin regulators also have been shown to influence the CeAJ (CORDOVA-BURGOS *et al.*, 2021; SASIDHARAN *et al.*, 2018). In summary, the luminal constrictions appear to arise from the mislocalization of the CeAJ, leading to the establishment of cell-cell junctions across the lumen.

The final facet of the phenotype is the L1 larval arrest, which for the apical actin proteins is exclusively observed in *erm-1*, *gck-4* and *act-5* knockdown or mutant animals (CHAPTER 4; GÖBEL *et al.*, 2004; MACQUEEN *et al.*, 2005; VAN FÜRDEN *et al.*, 2004). The depletion methods used for these animals were not specific to the intestine, so the L1 arrest phenotype could be caused independently of the intestine. Nevertheless, I hypothesize that the L1 arrest correlates with intestinal dysfunction. This conclusion is drawn from the observation that the young larval arrest only occurs in mutant backgrounds with luminal constrictions within the intestine, which impede food passage. Moreover, the striking similarity between the L1 arrest phenotype and those seen in starved animals or non-functional intestine mutants supports this assertion. For example, larvae growing up without food can alter their development, extending their life-time in the hope to reach a new food source. This can happen amongst others shortly after hatching, named the L1 diapause, in which the animal stays small and arrests development until they are fed (BAUGH, 2013; BAUGH & HU, 2020). In addition, complete loss of ELT-2, a major transcription factor for induction of the endoderm, causes a loss of the posterior part of the intestine, resulting in constipation of food and an L1 arrest (FUKUSHIGE *et al.*, 1998). While the loss of microvilli or changes in luminal shape may have an impact on intestinal physiology, we are inclined to think that these factors do not significantly contribute to the L1 arrest, as mutant backgrounds displaying only these defects do not appear to arrest as young larvae (CARBERRY *et al.*, 2012; CROCE *et al.*, 2004; GEISLER *et al.*, 2020). In addition, in *erm-1* phosphomutants we always observe at least one constriction in the intestine of arrested animals, while animals that did develop beyond L1 always have a continuous lumen

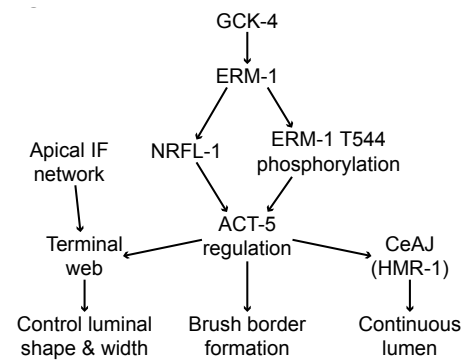


Figure 1: Schematic model on how the different actin components regulate intestinal brush border and lumen formation.

(CHAPTER 2). In summary, the L1 arrest phenotype is likely caused by the luminal constrictions that render the intestine non-functional, thereby inhibiting the animal's ability to feed and inducing the L1 diapause.

The presented data and preceding discussion collectively support a model in which ERM-1 assumes a pivotal role in orchestrating the apical actin cytoskeleton (Figure 1). ERM-1's activity in the intestine hinges on actin binding, finely tuned by the phosphocycling of the C-terminal threonine residue, and the regulation of the apical domain composition through NRFL-1. Both NRFL-1 and T544 phosphorylation redundantly govern the apical ACT-5 network. In turn, ACT-5 supports the brush border, as it is the main actin isoform for microvilli formation in the intestine (MACQUEEN *et al.*, 2005). Furthermore, ACT-5 plays a vital role in lumen morphogenesis in two key ways: Firstly, by contributing to the terminal web, thereby controlling luminal shape and size. Secondly, it ensures the accurate localization of the CeAJ, thereby maintaining a seamless lumen. Upstream of ERM-1, GCK-4 governs ERM-1 activity in a yet-to-be-determined manner. At this juncture, it remains uncertain whether GCK-4 may be reciprocally regulated by ERM-1, jointly influencing the apical actin network in a more synergistic fashion. Nevertheless, drawing from our knowledge of the GCK-4 ortholog and the data presented in this thesis, it is highly likely that GCK-4 serves as an upstream regulator of ERM-1.

Interplay between apical polarity and actin

In recent publications, the role of various intestinal apical polarity regulators were investigated using an optimized protein degradation tool allowing for intestine specific degradation (SALLEE *et al.*, 2021). It was shown that PAR-3 and HMR-1 synergistically recruit PKC-3, which ultimately results in the establishment of the apical membrane, exclusion of basolateral components and establishment of the CeAJ (NATURALE *et al.*, 2022). Interestingly, animals with intestinal knockdown of these apical polarity proteins suffer from similar defects as *erm-1*, *gck-4* and *act-5* mutant or knockdown animals, as they have a non-continuous intestinal lumen and arrest as L1 larva (PICKETT *et al.*, 2022; SALLEE *et al.*, 2021). This demonstrates a close connection between the apical polarity and actin networks in the *C. elegans* intestine. In addition, this connection does not seem unique to the intestine as depletion of apical PAR proteins or ERM-1 in the excretory canal yields strikingly similar tubulogenesis defects, causing the canal to be shortened and cystic (ABRAMS & NANCE, 2021; KHAN *et al.*, 2013). Given that both the apical polarity and actin networks result in similar morphological abnormalities when disrupted, it prompts the question of whether there is a connection between them and what the underlying relationship might be.

In order to answer this question, it is important to understand how similar the polarity and actin phenotypes actually are in the intestine. Both polarity and actin mutants have a thin intestinal lumen with gaps in the apical membrane

along the midline during embryonic development. After hatching, the arrested young larvae have a widened, round and non-continuous intestinal lumen. Although the brush border was not examined in the polarity depletion mutants, for the most part these mutants are identical to animals with an ERM-1, GCK-4 and ACT-5 depletion (CHAPTER 2; CHAPTER 4; NATURALE *et al.*, 2022; PICKETT *et al.*, 2022; SALLEE *et al.*, 2021). However, the gaps in the embryonic lumen are larger in the polarity mutants compared to the actin mutants. Furthermore, the gaps in the apical membrane remain during the larval development in the polarity mutants, while in the actin mutants the apical membrane is continuous (CHAPTER 2; CHAPTER 4; NATURALE *et al.*, 2022; PICKETT *et al.*, 2022; SALLEE *et al.*, 2021). To conclude, disruption of either apical actin or polarity networks yield nearly identical phenotypes, with the exception that gaps in the apical membrane are bigger and more persistent in the polarity knockdown animals. This suggests that the defects in establishing tissue-wide polarity is more severe in the apical polarity mutants, as there is no common apical surface throughout the tissue.

PAR-3 and HMR-1 function redundantly in recruiting PKC-3 and establishing apical polarity, albeit with distinct roles. Depletion of PAR-3 results in a loss of intercellular polarization, impeding the apical migration of the nucleus. Concurrently, the absence of HMR-1 leads to tissue polarization issues, hindering the proper fusion of apical domains among different intestinal cells. (NATURALE *et al.*, 2022). For the ERM-1 and GCK-4 depletion mutants, the intra-cellular polarity is altered as the actin cytoskeleton is not enriched properly to the apical membrane and cell-cell junctions are established at the apical membrane causing constrictions. In addition, we showed that ERM-1 is involved in the molecular specialization of the apical domain as PEPT-1 and RAB-10 were not properly enriched apically in T544 phosphomutants (CHAPTER 2). In contrast, tissue-wide polarity appears unaltered upon disruption of actin as no gaps are present in the apical membrane of larvae, demonstrating a common apical surface in the tissue. Therefore, I propose a model wherein the apical actin network appears to collaborate with PAR-3 in the induction of intra-cellular polarity, in parallel with the tissue-wide polarization induced by HMR-1 (Figure 2). As loss of ERM-1 and GCK-4 did not alter the localization of the apical PAR proteins, the actin regulators presumably act downstream of the PAR complex during polarization (CHAPTER 4; GÖBEL *et al.*, 2004; VAN FÜRDEN *et al.*, 2004). A genetic interaction between *erm-1* and *hmr-1* supports this model as animals with a combined knockdown of these genes do not form a continuous CeAJ network (VAN FÜRDEN *et al.*, 2004). The morphology of the CeAJ in these animals resembles the cell-cell junctions of animals with a knockdown of the apical PAR proteins, suggesting that the *erm-1*; *hmr-1* RNAi mimics a complete loss of apical polarity (PICKETT *et al.*, 2022).

This model also offers an explanation for the mislocalization of the CeAJ, as polarity proteins typically play a role in positioning and maturation of cell-cell junctions (FEIGIN & MUTHUSWAMY, 2009). When the intra-cellular polarity is compromised due to the disrupted apical actin organization, it may result in small localized disturbances within the polarity machinery at the apical membrane. At these sites, cell-cell junctions could mature, connecting the opposing apical surfaces and resulting in constrictions.

Evidence of these local disruptions are the small gaps in the apical membrane of embryos with a disrupted apical actin network (CHAPTER 2; CHAPTER 3; CHAPTER 4; GÖBEL *et al.*, 2004; VAN FÜRDEN *et al.*, 2004). The fact that these constrictions persist in the arrested L1 larvae, despite that the apical surface is seemingly continuous, suggests that the CeAJ can not be repositioned after maturation. Alternatively, there could be minor, yet to be identified, disruptions in the apical domain that persist post-hatching.

A close relationship between the polarity and cytoskeletal networks is not unique to the *C. elegans* intestine as they tend to be dependent on one another for their localization and regulation. For example, in the *C. elegans* one-cell embryo cortical actin flows are important for anterior localization of PAR-3, PAR-6, and PKC-3. While at the same time these anterior PAR proteins modulate and posterior PAR proteins inhibit these actin flows (MUNRO *et al.*, 2004). Thus, how could the apical polarity network regulate ERM-1 and GCK-4 in the *C. elegans* intestine?

In *Drosophila* and *Xenopus* ERM proteins can be localized apically by the polarity protein Crumbs, as Crumbs has a FERM binding domain (BURCKLÉ *et al.*, 2023; MÉDINA *et al.*, 2002; SALIS *et al.*, 2017). However, depletion of all three *C. elegans* Crumbs orthologs does not result in any major defects, so it appears unlikely that ERM-1 is dependent on the Crumbs proteins for its apical recruitment (WAAIJERS *et al.*, 2015). Mammalian PKC proteins, including the direct PKC-3 ortholog PKC ι , have been shown to phosphorylate the conserved threonine residue of ERM proteins (NG *et al.*, 2001; PIETROMONACO *et al.*, 1998; REN *et al.*, 2009). In addition, PKC proteins are able to modulate the activity and stability of EBP50/NHERF1, the closest NRFL-1 ortholog, by phosphorylating the PDZ and ERM binding domains, altering EBP50's ability to bind Ezrin and other interactors (BRYANT *et al.*, 2014; FOUASSIER *et al.*, 2005; GARBETT & BRETSCHER, 2012; GARBETT *et al.*,

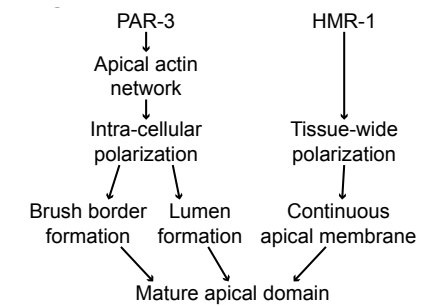


Figure 2: Schematic model on how the polarity and actin components regulate the maturation of the apical domain.

2010; Li *et al.*, 2007; RAGHURAM *et al.*, 2003). Therefore, ERM-1 activity could be regulated by PKC-3, through phosphorylation of the conserved T544 residue and regulating NRFL-1's ability to interact with its binding partners.

In contrast to the ERM proteins, orthologs of GCK-4 have not been implicated to act together with the classical polarity proteins such as the PAR and Crumbs complexes. This suggests a potential novel way on how the polarity network acts upon the actin cytoskeleton. In the GCK-4 proximity labeling data, PAR-3 came up as a strong hit, suggesting that GCK-4 and PAR-3 could interact. If indeed they interact, it is likely that PAR-3 regulates GCK-4, as we did not observe phosphorylation changes or altered localization of apical PAR proteins upon GCK-4 knockdown (CHAPTER 4).

Degradation of ERM-1

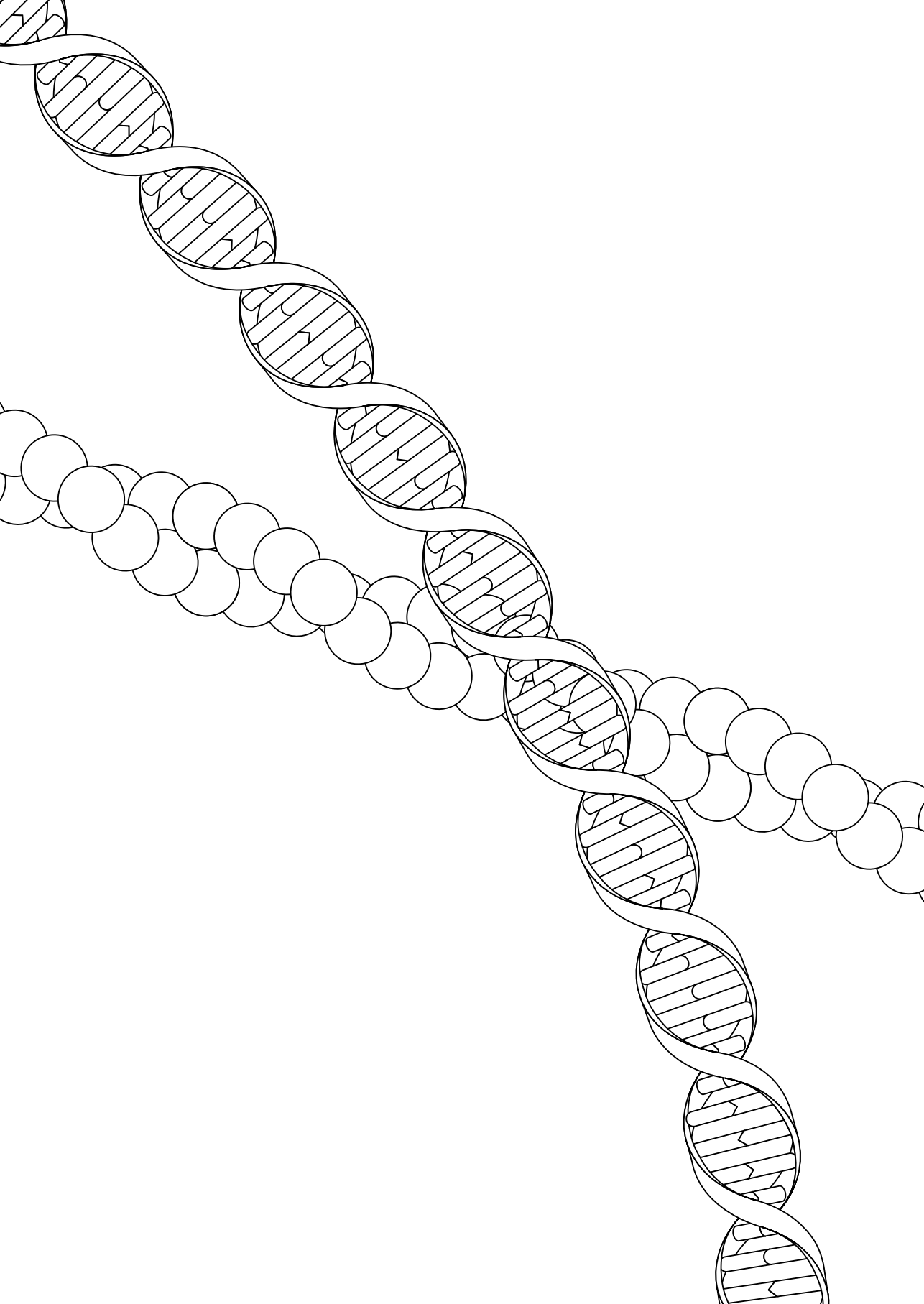
In Chapter 5, we set out to improve the auxin-inducible degradation (AID) system, by increasing the degradation dynamics of the technology. For this, we made use of a novel mIAA7 degron and adapted it for *C. elegans*. We showed that this degron can improve degradation compared to the conventional AID* degron for multiple proteins in various tissues, and that it is compatible with the novel AID2 system. In addition, we aimed to improve degradation even further, by analyzing the effects of the position of the degron in respect to the tagged protein, and by increasing the number of degrons attached to the target protein. Although degron position did not matter, attaching more than one degron improves degradation significantly. Collectively, we managed to improve the degradation efficiency of the AID system and provided a toolkit for others to include the new degron in their AID-based experiments.

Our improvements to the AID system did not yield strong enough degradation to fully degrade ERM-1 (CHAPTER 5). What optimizations could be implemented to improve ERM-1 degradation, so that it could be used for studying the *erm-1* phenotype? As mentioned in the discussion of Chapter 5, the rate limiting factor of ERM-1 degradation seem to be related to the stability and abundance of the protein, as adding more than two mIAA7 degrons did not further improve the degradation efficiency. Using the Fluorescence Recovery After Photobleaching (FRAP) technique, ERM-1 recovery is minimal after 45 minutes during larval development, while during the initial phases of embryonic lumen formation ERM-1 recovers within minutes (CHAPTER 2; BIDAUD-MEYNARD *et al.*, 2021). Therefore, ERM-1 degradation could be improved by applying it during embryonic development, as ERM-1 is more dynamic and complete degradation should be more efficient. Embryonic degradation also makes more sense as the apical polarity and actin defects are initiated early on during intestinal development (CHAPTER 4; SALLEE *et al.*, 2021). Embryonic degradation using AID does require a specific auxin derivative, IAA-AM, as the conventional auxin does not pass the eggshell efficiently (NEGISHI *et al.*, 2019). Alternatively, the tissue-specific ZIF-1

degradation system could be employed, as it has been demonstrated to be effective in studying apical polarity proteins during intestinal polarization (NATURALE *et al.*, 2022; PICKETT *et al.*, 2022; SALLEE *et al.*, 2021). However, the AID system could be desired for certain biological questions as the degradation is reversible. For the *act-5* RNAi animals, some arrested L1 larvae could be rescued by removing the RNAi, showing that the defects are reversible (MACQUEEN *et al.*, 2005). In the *erm-1* phosphomutant animals, we observe something similar. Embryos, on average, have more intestinal constrictions than larvae, suggesting that these constrictions can be resolved over time (CHAPTER 2). In order to investigate this aspect of the actin phenotype, the AID system would be more suitable as knockdowns can be stopped upon removal of auxin (ZHANG *et al.*, 2015).

Conclusion

The work in this thesis demonstrates how the *C. elegans* intestine provides an excellent model to study tubulogenesis. Our research has elucidated how the interplay among the cell polarity network, cytoskeleton, and cell-cell junctions collectively provide the necessary cues and structure to form a fully functional intestine. Moreover, we have introduced a comprehensive model detailing how these distinct cellular networks synergistically collaborate to achieve a functional apical membrane and lumen. To facilitate further exploration of tubulogenesis in *C. elegans*, we have also introduced and improved upon a range of molecular tools in this thesis. Future research should prioritize the validation of this model, with a specific focus on understanding how the polarity network exerts regulatory control over the actin cytoskeleton. Furthermore, it is imperative to investigate the role of the actin cytoskeleton in microvilli formation, terminal web development, and CeAJ localization to gain deeper insights into the underlying mechanisms contributing to the various facets of the actin-defective phenotype. Ideally, addressing these questions will yield a more comprehensive understanding of the precise involvement of ERM-1, NRFL-1 and GCK-4 in the regulation of the apical actin network.



Appendix

References

English summary

Dutch summary (Nederlandse samenvatting)

Curriculum vitae

List of publications

Acknowledgments (Dankwoord)

References

- Abbattiscianni, A. C., Favia, M., Mancini, M. T., Cardone, R. A., Guerra, L., Monterisi, S., Castellani, S., Laselva, O., Di Sole, F., Conese, M., Zaccolo, M. and Casavola, V., 2016 Correctors of mutant CFTR enhance subcortical cAMP-PKA signaling through modulating ezrin phosphorylation and cytoskeleton organization. *Journal of Cell Science* 129:1128–1140 <https://doi.org/10.1242/jcs.177907>.
- Abrams, J. and Nance, J., 2021 A polarity pathway for exocyst-dependent intracellular tube extension. *eLife* 10:e65169 <https://doi.org/10.7554/eLife.65169>.
- Achilleos, A., Wehman, A. M. and Nance, J., 2010 PAR-3 mediates the initial clustering and apical localization of junction and polarity proteins during *C. elegans* intestinal epithelial cell polarization. *Development* 137:1833–1842 <https://doi.org/10.1242/dev.047647>.
- Aher, A. and Akhmanova, A., 2018 Tipping microtubule dynamics, one protofilament at a time. *Current Opinion in Cell Biology* 50:86–93 <https://doi.org/10.1016/j.ceb.2018.02.015>.
- Akhmanova, A. and Steinmetz, M. O., 2015 Control of microtubule organization and dynamics: two ends in the limelight. *Nat Rev Mol Cell Biol* 16:711–726 <https://doi.org/10.1038/nrm4084>.
- Al-Zahrani, K. N., Baron, K. D. and Sabourin, L. A., 2013 Ste20-like kinase SLK, at the crossroads. *Cell Adhesion & Migration* 7:1–10 <https://doi.org/10.4161/cam.22495>.
- Angeles-Albores, D., Lee, R. Y. N., Chan, J. and Sternberg, P. W., 2018 Two new functions in the WormBase Enrichment Suite. *microPublication Biology* <https://doi.org/10.17912/W25Q2N>.
- Armenti, S. T., Lohmer, L. L., Sherwood, D. R. and Nance, J., 2014 Repurposing an endogenous degradation system for rapid and targeted depletion of *C. elegans* proteins. *Development* 141:4640–4647 <https://doi.org/10.1242/dev.115048>.
- Arribere, J. A., Bell, R. T., Fu, B. X. H., Artiles, K. L., Hartman, P. S. and Fire, A. Z., 2014 Efficient Marker-Free Recovery of Custom Genetic Modifications with CRISPR/Cas9 in *Caenorhabditis elegans*. *Genetics* 198:837–846 <https://doi.org/10.1534/genetics.114.169730>.
- Artan, M., Barratt, S., Flynn, S. M., Begum, F., Skehel, M., Nicolas, A. and Bono, M. de, 2021 Interactome analysis of *Caenorhabditis elegans* synapses by TurboID-based proximity labeling. *Journal of Biological Chemistry* 297 <https://doi.org/10.1016/j.jbc.2021.101094>.
- Asan, A., Raiders, S. A. and Priess, J. R., 2016 Morphogenesis of the *C. elegans* Intestine Involves Axon Guidance Genes. *PLoS Genetics* 12:e1005950 <https://doi.org/10.1371/journal.pgen.1005950>.
- Ashley, G. E., Duong, T., Levenson, M. T., Martinez, M. A. Q., Johnson, L. C., Hibshman, J. D., Saeger, H. N., Palmisano, N. J., Doonan, R., Martinez-Mendez, R., Davidson, B. R., Zhang, W., Ragle, J. M., Medwig-Kinney, T. N., Sirota, S. S., Goldstein, B., Matus, D. Q., Dickinson, D. J., Reiner, D. J. and Ward, J. D., 2021 An expanded auxin-inducible degron toolkit for *Caenorhabditis elegans*. *Genetics* 217:iyab006 <https://doi.org/10.1093/genetics/iyab006>.
- Avery, L. and Shtonda, B. B., 2003 Food transport in the *C. elegans* pharynx. *Journal of Experimental Biology* 206:2441–2457 <https://doi.org/10.1242/jeb.00433>.

Babich, V. and Sole, F. D., 2015 The Na⁺/H⁺ Exchanger-3 (NHE3) Activity Requires Ezrin Binding to Phosphoinositide and Its Phosphorylation. *PLoS ONE* 10:e0129306 <https://doi.org/10.1371/journal.pone.0129306>.

Bagci, H., Sriskandarajah, N., Robert, A., Boulais, J., Elkholi, I. E., Tran, V., Lin, Z.-Y., Thibault, M.-P., Dubé, N., Faubert, D., Hipfner, D. R., Gingras, A.-C. and Côté, J.-F., 2020 Mapping the proximity interaction network of the Rho-family GTPases reveals signalling pathways and regulatory mechanisms. *Nat Cell Biol* 22:120–134 <https://doi.org/10.1038/s41556-019-0438-7>.

Baker, J. P. and Titus, M. A., 1997 A family of unconventional myosins from the nematode *Caenorhabditis elegans*. *Journal of Molecular Biology* 272:523–535 <https://doi.org/10.1006/jmbi.1997.1232>.

Barreiro, O., Yáñez-Mó, M., Serrador, J. M., Montoya, M. C., Vicente-Manzanares, M., Tejedor, R., Furthmayr, H. and Sánchez-Madrid, F., 2002 Dynamic interaction of VCAM-1 and ICAM-1 with moesin and ezrin in a novel endothelial docking structure for adherent leukocytes. *Journal of Cell Biology* 157:1233–1245 <https://doi.org/10.1083/jcb.200112126>.

Barret, C., Roy, C., Montcourrier, P., Mangeat, P. and Niggli, V., 2000 Mutagenesis of the Phosphatidylinositol 4,5-Bisphosphate (Pip2) Binding Site in the Nh2-Terminal Domain of Ezrin Correlates with Its Altered Cellular Distribution. *Journal of Cell Biology* 151:1067–1080 <https://doi.org/10.1083/jcb.151.5.1067>.

Baugh, L. R., 2013 To Grow or Not to Grow: Nutritional Control of Development During *Caenorhabditis elegans* L1 Arrest. *Genetics* 194:539–555 <https://doi.org/10.1534/genetics.113.150847>.

Baugh, L. R. and Hu, P. J., 2020 Starvation Responses Throughout the *Caenorhabditis elegans* Life Cycle. *Genetics* 216:837–878 <https://doi.org/10.1534/genetics.120.303565>.

Bei, Y., Hogan, J., Berkowitz, L. A., Soto, M., Rocheleau, C. E., Pang, K. M., Collins, J. and Mello, C. C., 2002 SRC-1 and Wnt Signaling Act Together to Specify Endoderm and to Control Cleavage Orientation in Early *C. elegans* Embryos. *Developmental Cell* 3:113–125 [https://doi.org/10.1016/S1534-5807\(02\)00185-5](https://doi.org/10.1016/S1534-5807(02)00185-5).

Belkina, N. V., Liu, Y., Hao, J.-J., Karasuyama, H. and Shaw, S., 2009 LOK is a major ERM kinase in resting lymphocytes and regulates cytoskeletal rearrangement through ERM phosphorylation. *Proceedings of the National Academy of Sciences* 106:4707–4712 <https://doi.org/10.1073/pnas.0805963106>.

Ben-Aissa, K., Patino-Lopez, G., Belkina, N. V., Maniti, O., Rosales, T., Hao, J.-J., Kruhlak, M. J., Knutson, J. R., Picart, C. and Shaw, S., 2012 Activation of Moesin, a Protein That Links Actin Cytoskeleton to the Plasma Membrane, Occurs by Phosphatidylinositol 4,5-bisphosphate (PIP2) Binding Sequentially to Two Sites and Releasing an Autoinhibitory Linker *. *Journal of Biological Chemistry* 287:16311–16323 <https://doi.org/10.1074/jbc.M111.304881>.

Berg, M., Zhou, X. Y. and Shapira, M., 2016a Host-Specific Functional Significance of *Caenorhabditis* Gut Commensals. *Frontiers in Microbiology* 7 <https://doi.org/10.3389/fmicb.2016.01622>.

- Berg, M., Stenuit, B., Ho, J., Wang, A., Parke, C., Knight, M., Alvarez-Cohen, L. and Shapira, M., 2016b Assembly of the *Caenorhabditis elegans* gut microbiota from diverse soil microbial environments. *ISME J* 10:1998–2009 <https://doi.org/10.1038/ismej.2015.253>.
- Bernadskaya, Y. Y., Patel, F. B., Hsu, H.-T. and Soto, M. C., 2011 Arp2/3 promotes junction formation and maintenance in the *Caenorhabditis elegans* intestine by regulating membrane association of apical proteins. *MBoC* 22:2886–2899 <https://doi.org/10.1091/mbc.e10-10-0862>.
- Berryman, M., Gary, R. and Bretscher, A., 1995 Ezrin oligomers are major cytoskeletal components of placental microvilli: a proposal for their involvement in cortical morphogenesis. *Journal of Cell Biology* 131:1231–1242 <https://doi.org/10.1083/jcb.131.5.1231>.
- Bhoi, A., Palladino, F. and Fabrizio, P., 2021 Auxin confers protection against ER stress in *Caenorhabditis elegans*. *Biology Open* 10:bio057992 <https://doi.org/10.1242/bio.057992>.
- Bidaud-Meynard, A., Demouchy, F., Nicolle, O., Pacquelet, A., Suman, S. K., Plancke, C. N., Robin, F. B. and Michaux, G., 2021 High-resolution dynamic mapping of the *C. elegans* intestinal brush border. *Development* 148:dev200029 <https://doi.org/10.1242/dev.200029>.
- Bonilha, V. L., Finnemann, S. C. and Rodriguez-Boulan, E., 1999 Ezrin Promotes Morphogenesis of Apical Microvilli and Basal Infoldings in Retinal Pigment Epithelium. *Journal of Cell Biology* 147:1533–1548 <https://doi.org/10.1083/jcb.147.7.1533>.
- Bonilha, V. L., Rayborn, M. E., Saotome, I., McClatchey, A. I. and Hollyfield, J. G., 2006 Microvilli defects in retinas of ezrin knockout mice. *Experimental Eye Research* 82:720–729 <https://doi.org/10.1016/j.exer.2005.09.013>.
- Boratkó, A. and Csontos, C., 2013 NHERF2 is crucial in ERM phosphorylation in pulmonary endothelial cells. *Cell Communication and Signaling* 11:99 <https://doi.org/10.1186/1478-811X-11-99>.
- Bosk, S., Braunger, J. A., Gerke, V. and Steinem, C., 2011 Activation of F-Actin Binding Capacity of Ezrin: Synergism of PIP2 Interaction and Phosphorylation. *Biophysical Journal* 100:1708–1717 <https://doi.org/10.1016/j.bpj.2011.02.039>.
- Bossinger, O., Klebes, A., Segbert, C., Theres, C. and Knust, E., 2001 Zonula Adherens Formation in *Caenorhabditis elegans* Requires *dlg-1*, the Homologue of the *Drosophila* Gene discs large. *Developmental Biology* 230:29–42 <https://doi.org/10.1006/dbio.2000.0113>.
- Bossinger, O., Fukushige, T., Claeys, M., Borgonie, G. and McGhee, J. D., 2004 The apical disposition of the *Caenorhabditis elegans* intestinal terminal web is maintained by LET-413. *Developmental Biology* 268:448–456 <https://doi.org/10.1016/j.ydbio.2004.01.003>.
- Bowerman, B., Eaton, B. A. and Priess, J. R., 1992 *skn-1*, a maternally expressed gene required to specify the fate of ventral blastomeres in the early *C. elegans* embryo. *Cell* 68:1061–1075 [https://doi.org/10.1016/0092-8674\(92\)90078-Q](https://doi.org/10.1016/0092-8674(92)90078-Q).
- Bowerman, B., Draper, B. W., Mello, C. C. and Priess, J. R., 1993 The maternal gene *skn-1* encodes a protein that is distributed unequally in early *C. elegans* embryos. *Cell* 74:443–452 [https://doi.org/10.1016/0092-8674\(93\)80046-H](https://doi.org/10.1016/0092-8674(93)80046-H).

- Branon, T. C., Bosch, J. A., Sanchez, A. D., Udeshi, N. D., Svinkina, T., Carr, S. A., Feldman, J. L., Perrimon, N. and Ting, A. Y., 2018 Efficient proximity labeling in living cells and organisms with TurboID. *Nat Biotechnol* 36:880–887 <https://doi.org/10.1038/nbt.4201>.
- Braunger, J. A., Brückner, B. R., Nehls, S., Pietuch, A., Gerke, V., Mey, I., Janshoff, A. and Steinem, C., 2014 Phosphatidylinositol 4,5-Bisphosphate Alters the Number of Attachment Sites between Ezrin and Actin Filaments. *Journal of Biological Chemistry* 289:9833–9843 <https://doi.org/10.1074/jbc.M113.530659>.
- Brenner, S., 1974 The genetics of *Caenorhabditis elegans*. *Genetics* 77:71–94 <https://doi.org/10.1093/genetics/77.1.71>.
- Broere, N., Chen, M., Cinar, A., Singh, A. K., Hillesheim, J., Riederer, B., Lünemann, M., Rottinghaus, I., Krabbenhöft, A., Engelhardt, R., Rausch, B., Weinman, E. J., Donowitz, M., Hubbard, A., Kocher, O., de Jonge, H. R., Hogema, B. M. and Seidler, U., 2009 Defective jejunal and colonic salt absorption and altered Na⁺/H⁺ exchanger 3 (NHE3) activity in NHE regulatory factor 1 (NHERF1) adaptor protein-deficient mice. *Pflugers Arch - Eur J Physiol* 457:1079–1091 <https://doi.org/10.1007/s00424-008-0579-1>.
- Broitman-Maduro, G., Maduro, M. F. and Rothman, J. H., 2005 The Noncanonical Binding Site of the MED-1 GATA Factor Defines Differentially Regulated Target Genes in the *C. elegans* Mesendoderm. *Developmental Cell* 8:427–433 <https://doi.org/10.1016/j.devcel.2005.01.014>.
- Broitman-Maduro, G., Lin, K. T.-H., Hung, W. W. K. and Maduro, M. F., 2006 Specification of the *C. elegans* MS blastomere by the T-box factor TBX-35. *Development* 133:3097–3106 <https://doi.org/10.1242/dev.02475>.
- Broitman-Maduro, G., Owrighi, M., Hung, W. W. K., Kuntz, S., Sternberg, P. W. and Maduro, M. F., 2009 The NK-2 class homeodomain factor CEH-51 and the T-box factor TBX-35 have overlapping function in *C. elegans* mesoderm development. *Development* 136:2735–2746 <https://doi.org/10.1242/dev.038307>.
- Bryant, D. M., Datta, A., Rodríguez-Fraticelli, A. E., Peränen, J., Martín-Belmonte, F. and Mostov, K. E., 2010 A molecular network for *de novo* generation of the apical surface and lumen. *Nat Cell Biol* 12:1035–1045 <https://doi.org/10.1038/ncb2106>.
- Bryant, D. M., Roinot, J., Datta, A., Overeem, A. W., Kim, M., Yu, W., Peng, X., Eastburn, D. J., Ewald, A. J., Werb, Z. and Mostov, K. E., 2014 A Molecular Switch for the Orientation of Epithelial Cell Polarization. *Developmental Cell* 31:171–187 <https://doi.org/10.1016/j.devcel.2014.08.027>.
- Bulgakova, N. A. and Knust, E., 2009 The Crumbs complex: from epithelial-cell polarity to retinal degeneration. *Journal of Cell Science* 122:2587–2596 <https://doi.org/10.1242/jcs.023648>.
- Burcklé, C., Raitière, J., Kodjabachian, L. and Bivic, A. L., 2023 Crb3 stabilizes activated Ezrin-Radixin-Moesin to organize the apical domain of multiciliated cells. *bioRxiv* :2023.01.24.525309 <https://doi.org/10.1101/2023.01.24.525309>.
- Cadigan, K. M. and Waterman, M. L., 2012 TCF/LEFs and Wnt Signaling in the Nucleus. *Cold Spring Harbor Perspectives in Biology* 4:a007906–a007906 <https://doi.org/10.1101/cshperspect.a007906>.

- Calderón Villalobos, L. I. A., Lee, S., De Oliveira, C., Ivetac, A., Brandt, W., Armitage, L., Sheard, L. B., Tan, X., Parry, G., Mao, H., Zheng, N., Napier, R., Kepinski, S. and Estelle, M., 2012 A combinatorial TIR1/AFB-Aux/IAA co-receptor system for differential sensing of auxin. *Nat Chem Biol* 8:477–485 <https://doi.org/10.1038/nchembio.926>.
- Calvo, D., Victor, M., Gay, F., Sui, G., Po-Shan Luke, M., Dufourcq, P., Wen, G., Maduro, M., Rothman, J. and Shi, Y., 2001 A POP-1 repressor complex restricts inappropriate cell type-specific gene transcription during *Caenorhabditis elegans* embryogenesis. *The EMBO Journal* 20:7197–7208 <https://doi.org/10.1093/emboj/20.24.7197>.
- Cani, P. D., 2018 Human gut microbiome: hopes, threats and promises. *Gut* 67:1716–1725 <https://doi.org/10.1136/gutjnl-2018-316723>.
- Cannon, J. L., Mody, P. D., Blaine, K. M., Chen, E. J., Nelson, A. D., Sayles, L. J., Moore, T. V., Clay, B. S., Dulin, N. O., Shilling, R. A., Burkhardt, J. K. and Sperling, A. I., 2011 CD43 interaction with ezrin-radixin-moesin (ERM) proteins regulates T-cell trafficking and CD43 phosphorylation. *MBoC* 22:954–963 <https://doi.org/10.1091/mbc.e10-07-0586>.
- Cao, X., Ding, X., Guo, Z., Zhou, R., Wang, F., Long, F., Wu, F., Bi, F., Wang, Q., Fan, D., Forte, J. G., Teng, M. and Yao, X., 2005 PALS1 Specifies the Localization of Ezrin to the Apical Membrane of Gastric Parietal Cells*. *Journal of Biological Chemistry* 280:13584–13592 <https://doi.org/10.1074/jbc.M411941200>.
- Captan, V. V., Goszczynski, B. and McGhee, J. D., 2007 Neither Maternal nor Zygotic *med-1/med-2* Genes Play a Major Role in Specifying the *Caenorhabditis elegans* Endoderm. *Genetics* 175:969–974 <https://doi.org/10.1534/genetics.106.066662>.
- Carberry, K., Wiesenfahrt, T., Windoffer, R., Bossinger, O. and Leube, R. E., 2009 Intermediate filaments in *Caenorhabditis elegans*. *Cell Motility* 66:852–864 <https://doi.org/10.1002/cm.20372>.
- Carberry, K., Wiesenfahrt, T., Geisler, F., Stöcker, S., Gerhardus, H., Überbach, D., Davis, W., Jorgensen, E., Leube, R. E. and Bossinger, O., 2012 The novel intestinal filament organizer IFO-1 contributes to epithelial integrity in concert with ERM-1 and DLG-1. *Development* 139:1851–1862 <https://doi.org/10.1242/dev.075788>.
- Carmeliet, P. and Jain, R. K., 2000 Angiogenesis in cancer and other diseases. *Nature* 407:249–257 <https://doi.org/10.1038/35025220>.
- Carreno, S., Kouranti, I., Glusman, E. S., Fuller, M. T., Echard, A. and Payre, F., 2008 Moesin and its activating kinase Slik are required for cortical stability and microtubule organization in mitotic cells. *Journal of Cell Biology* 180:739–746 <https://doi.org/10.1083/jcb.200709161>.
- Casaleto, J. B., Saotome, I., Curto, M. and McClatchey, A. I., 2011 Ezrin-mediated apical integrity is required for intestinal homeostasis. *Proceedings of the National Academy of Sciences* 108:11924–11929 <https://doi.org/10.1073/pnas.1103418108>.
- Castiglioni, V. G., Pires, H. R., Rosas Bertolini, R., Riga, A., Kerver, J. and Boxem, M., 2020 Epidermal PAR-6 and PKC-3 are essential for larval development of *C. elegans* and organize non-centrosomal microtubules. *eLife* 9:e62067 <https://doi.org/10.7554/eLife.62067>.

- Castiglioni, V. G., Ramalho, J. J., Kroll, J. R., Stucchi, R., Beuzekom, H. van, Schmidt, R., Altelaar, M. and Boxem, M., 2022 Identification and characterization of Crumbs polarity complex proteins in *Caenorhabditis elegans*. *Journal of Biological Chemistry* 298 <https://doi.org/10.1016/j.jbc.2022.101786>.
- Chambers, D. N. and Bretscher, A., 2005 Ezrin Mutants Affecting Dimerization and Activation. *Biochemistry* 44:3926–3932 <https://doi.org/10.1021/bi0480382>.
- Charras, G. T., Hu, C.-K., Coughlin, M. and Mitchison, T. J., 2006 Reassembly of contractile actin cortex in cell blebs. *Journal of Cell Biology* 175:477–490 <https://doi.org/10.1083/jcb.200602085>.
- Chen, J., Cohn, J. A. and Mandel, L. J., 1995 Dephosphorylation of ezrin as an early event in renal microvillar breakdown and anoxic injury. *Proceedings of the National Academy of Sciences* 92:7495–7499 <https://doi.org/10.1073/pnas.92.16.7495>.
- Chen, L., Ong, B. and Bennett, V., 2001 LAD-1, the *Caenorhabditis elegans* L1CAM homologue, participates in embryonic and gonadal morphogenesis and is a substrate for fibroblast growth factor receptor pathway-dependent phosphotyrosine-based signaling. *Journal of Cell Biology* 154:841–856 <https://doi.org/10.1083/jcb.200009004>.
- Chen, S.-D., Song, M.-M., Zhong, Z.-Q., Li, N., Wang, P.-L., Cheng, S., Bai, R.-X. and Yuan, H.-S., 2012 Knockdown of Radixin by RNA interference Suppresses the Growth of Human Pancreatic Cancer Cells *in vitro* and *in vivo*. *Asian Pacific Journal of Cancer Prevention* 13:753–759 <https://doi.org/10.7314/APJCP.2012.13.3.753>.
- Chen, S. G., Stribinskis, V., Rane, M. J., Demuth, D. R., Gozal, E., Roberts, A. M., Jagadapillai, R., Liu, R., Choe, K., Shivakumar, B., Son, F., Jin, S., Kerber, R., Adame, A., Masliah, E. and Friedland, R. P., 2016 Exposure to the Functional Bacterial Amyloid Protein Curli Enhances Alpha-Synuclein Aggregation in Aged Fischer 344 Rats and *Caenorhabditis elegans*. *Sci Rep* 6:34477 <https://doi.org/10.1038/srep34477>.
- Chen, K., Franz, C. J., Jiang, H., Jiang, Y. and Wang, D., 2017 An evolutionarily conserved transcriptional response to viral infection in *Caenorhabditis* nematodes. *BMC Genomics* 18:303 <https://doi.org/10.1186/s12864-017-3689-3>.
- Cheng, Z., Yi, P., Wang, X., Chai, Y., Feng, G., Yang, Y., Liang, X., Zhu, Z., Li, W. and Ou, G., 2013 Conditional targeted genome editing using somatically expressed TALENs in *C. elegans*. *Nat Biotechnol* 31:934–937 <https://doi.org/10.1038/nbt.2674>.
- Chihara, D. and Nance, J., 2012 An E-cadherin-mediated hitchhiking mechanism for *C. elegans* germ cell internalization during gastrulation. *Development* 139:2547–2556 <https://doi.org/10.1242/dev.079863>.
- Chirivino, D., Del Maestro, L., Formstecher, E., Hupé, P., Raposo, G., Louvard, D. and Arpin, M., 2011 The ERM proteins interact with the HOPS complex to regulate the maturation of endosomes. *MBoC* 22:375–385 <https://doi.org/10.1091/mbc.e10-09-0796>.
- Cho, U., Zimmerman, S. M., Chen, L., Owen, E., Kim, J. V., Kim, S. K. and Wandless, T. J., 2013 Rapid and Tunable Control of Protein Stability in *Caenorhabditis elegans* Using a Small Molecule. *PLOS ONE* 8:e72393 <https://doi.org/10.1371/journal.pone.0072393>.

Conway, J., Al-Zahrani, K. N., Pryce, B. R., Abou-Hamad, J. and Sabourin, L. A., 2017 Transforming growth factor β -induced epithelial to mesenchymal transition requires the Ste20-like kinase SLK independently of its catalytic activity. *Oncotarget* 8:98745–98756 <https://doi.org/10.18632/oncotarget.21928>.

Cordova-Burgos, L., Patel, F. B. and Soto, M. C., 2021 E-Cadherin/HMR-1 Membrane Enrichment Is Polarized by WAVE-Dependent Branched Actin. *Journal of Developmental Biology* 9:19 <https://doi.org/10.3390/jdb9020019>.

Coscoy, S., Waharte, F., Gautreau, A., Martin, M., Louvard, D., Mangeat, P., Arpin, M. and Amblard, F., 2002 Molecular analysis of microscopic ezrin dynamics by two-photon FRAP. *Proceedings of the National Academy of Sciences* 99:12813–12818 <https://doi.org/10.1073/pnas.192084599>.

Costa, M., Raich, W., Agbunag, C., Leung, B., Hardin, J. and Priess, J. R., 1998 A Putative Catenin-Cadherin System Mediates Morphogenesis of the *Caenorhabditis elegans* Embryo. *Journal of Cell Biology* 141:297–308 <https://doi.org/10.1083/jcb.141.1.297>.

Croce, A., Cassata, G., Disanza, A., Gagliani, M. C., Tacchetti, C., Malabarba, M. G., Carlier, M.-F., Scita, G., Baumeister, R. and Fiore, P. P. D., 2004 A novel actin barbed-end-capping activity in EPS-8 regulates apical morphogenesis in intestinal cells of *Caenorhabditis elegans*. *Nat Cell Biol* 6:1173–1179 <https://doi.org/10.1038/ncb1198>.

Datta, A., Bryant, D. M. and Mostov, K. E., 2011 Molecular Regulation of Lumen Morphogenesis. *Current Biology* 21:R126–R136 <https://doi.org/10.1016/j.cub.2010.12.003>.

Davis, M. W., Morton, J. J., Carroll, D. and Jorgensen, E. M., 2008 Gene Activation Using FLP Recombinase in *C. elegans*. *PLoS Genetics* 4:e1000028 <https://doi.org/10.1371/journal.pgen.1000028>.

Dejima, K., Hori, S., Iwata, S., Suehiro, Y., Yoshina, S., Motohashi, T. and Mitani, S., 2018 An Aneuploidy-Free and Structurally Defined Balancer Chromosome Toolkit for *Caenorhabditis elegans*. *Cell Rep* 22:232–241 <https://doi.org/10.1016/j.celrep.2017.12.024>.

DeMasco, C. R., Kovacevic, I., Uzun, A. and Cram, E. J., 2011 Structural and Functional Evaluation of *C. elegans* Filamins FLN-1 and FLN-2. *PLoS ONE* 6:e22428 <https://doi.org/10.1371/journal.pone.0022428>.

Deppe, U., Schierenberg, E., Cole, T., Krieg, C., Schmitt, D., Yoder, B. and von Ehrenstein, G., 1978 Cell lineages of the embryo of the nematode *Caenorhabditis elegans*. *Proceedings of the National Academy of Sciences* 75:376–380 <https://doi.org/10.1073/pnas.75.1.376>.

Deretic, D., Traverso, V., Parkins, N., Jackson, F., de Turco, E. B. R. and Ransom, N., 2004 Phosphoinositides, Ezrin/Moesin, and rac1 Regulate Fusion of Rhodopsin Transport Carriers in Retinal Photoreceptors. *MBoC* 15:359–370 <https://doi.org/10.1091/mbc.e03-04-0203>.

Dickinson, D. J., Pani, A. M., Heppert, J. K., Higgins, C. D. and Goldstein, B., 2015 Streamlined Genome Engineering with a Self-Excising Drug Selection Cassette. *Genetics* 200:1035–1049 <https://doi.org/10.1534/genetics.115.178335>.

Dirksen, P., Marsh, S. A., Braker, I., Heitland, N., Wagner, S., Nakad, R., Mader, S., Petersen, C., Kowallik, V., Rosenstiel, P., Félix, M.-A. and Schulenburg, H., 2016 The native microbiome of the nematode *Caenorhabditis elegans*: gateway to a new host-microbiome model. *BMC Biology* 14:38 <https://doi.org/10.1186/s12915-016-0258-1>.

Dokshin, G. A., Ghanta, K. S., Piscopo, K. M. and Mello, C. C., 2018 Robust Genome Editing with Short Single-Stranded and Long, Partially Single-Stranded DNA Donors in *Caenorhabditis elegans*. *Genetics* 210:781–787 <https://doi.org/10.1534/genetics.118.301532>.

Dominguez, R. and Holmes, K. C., 2011 Actin Structure and Function. *Annu. Rev. Biophys.* 40:169–186 <https://doi.org/10.1146/annurev-biophys-042910-155359>.

Dreher, K. A., Brown, J., Saw, R. E. and Callis, J., 2006 The Arabidopsis Aux/IAA Protein Family Has Diversified in Degradation and Auxin Responsiveness. *The Plant Cell* 18:699–714 <https://doi.org/10.1105/tpc.105.039172>.

Duong, T., Rasmussen, N. R., Ballato, E., Mote, F. S. and Reiner, D. J., 2020 The Rheb-TORC1 signaling axis functions as a developmental checkpoint. *Development* 147:dev181727 <https://doi.org/10.1242/dev.181727>.

Edgar, B. A., Zielke, N. and Gutierrez, C., 2014 Endocycles: a recurrent evolutionary innovation for post-mitotic cell growth. *Nat Rev Mol Cell Biol* 15:197–210 <https://doi.org/10.1038/nrm3756>.

El Mouridi, S., Peng, Y. and Frøkjær-Jensen, C., 2020 Characterizing a strong pan-muscular promoter (*Pmlc-1*) as a fluorescent co-injection marker to select for single-copy insertions. *microPublication Biology* <https://doi.org/10.17912/micropub.biology.000302>.

Eldirany, S. A., Lomakin, I. B., Ho, M. and Bunick, C. G., 2021 Recent insight into intermediate filament structure. *Current Opinion in Cell Biology* 68:132–143 <https://doi.org/10.1016/j.ccb.2020.10.001>.

Ellis, H. M. and Horvitz, H. R., 1986 Genetic control of programmed cell death in the nematode *C. elegans*. *Cell* 44:817–829 [https://doi.org/10.1016/0092-8674\(86\)90004-8](https://doi.org/10.1016/0092-8674(86)90004-8).

Endo, J., Toyama-Sorimachi, N., Taya, C., Kuramochi-Miyagawa, S., Nagata, K., Kuida, K., Takashi, T., Yonekawa, H., Yoshizawa, Y., Miyasaka, N. and Karasuyama, H., 2000 Deficiency of a STE20/PAK family kinase LOK leads to the acceleration of LFA-1 clustering and cell adhesion of activated lymphocytes. *FEBS Letters* 468:234–238 [https://doi.org/10.1016/S0014-5793\(00\)01219-9](https://doi.org/10.1016/S0014-5793(00)01219-9).

Ewe, C. K., Sommermann, E. M., Kenchel, J., Flowers, S. E., Maduro, M. F., Joshi, P. M. and Rothman, J. H., 2022 Feedforward regulatory logic controls the specification-to-differentiation transition and terminal cell fate during *Caenorhabditis elegans* endoderm development. *Development* 149:dev200337 <https://doi.org/10.1242/dev.200337>.

Farley, B. M., Pagano, J. M. and Ryder, S. P., 2008 RNA target specificity of the embryonic cell fate determinant POS-1. *RNA* 14:2685–2697 <https://doi.org/10.1261/rna.1256708>.

Fehon, R. G., McClatchey, A. I. and Bretscher, A., 2010 Organizing the cell cortex: the role of ERM proteins. *Nat Rev Mol Cell Biol* 11:276–287 <https://doi.org/10.1038/nrm2866>.



- Feigin, M. E. and Muthuswamy, S. K., 2009 Polarity proteins regulate mammalian cell-cell junctions and cancer pathogenesis. *Current Opinion in Cell Biology* 21:694–700 <https://doi.org/10.1016/j.ceb.2009.07.003>.
- Feldman, J. L. and Priess, J. R., 2012 A Role for the Centrosome and PAR-3 in the Hand-Off of MTOC Function during Epithelial Polarization. *Current Biology* 22:575–582 <https://doi.org/10.1016/j.cub.2012.02.044>.
- Félix, M.-A., Ashe, A., Piffaretti, J., Wu, G., Nuez, I., Béliard, T., Jiang, Y., Zhao, G., Franz, C. J., Goldstein, L. D., Sanroman, M., Miska, E. A. and Wang, D., 2011 Natural and Experimental Infection of *Caenorhabditis* Nematodes by Novel Viruses Related to Nodaviruses. *PLoS Biology* 9:e1000586 <https://doi.org/10.1371/journal.pbio.1000586>.
- Feng, W., Long, J. and Zhang, M., 2005 A unified assembly mode revealed by the structures of tetrameric L27 domain complexes formed by mLin-2/mLin-7 and Patj/Pals1 scaffold proteins. *Proceedings of the National Academy of Sciences* 102:6861–6866 <https://doi.org/10.1073/pnas.0409346102>.
- Fievet, B. T., Gautreau, A., Roy, C., Del Maestro, L., Mangeat, P., Louvard, D. and Arpin, M., 2004 Phosphoinositide binding and phosphorylation act sequentially in the activation mechanism of ezrin. *Journal of Cell Biology* 164:653–659 <https://doi.org/10.1083/jcb.200307032>.
- Finnerty, C. M., Chambers, D., Ingraffea, J., Faber, H. R., Karplus, P. A. and Bretscher, A., 2004 The EBP50-moesin interaction involves a binding site regulated by direct masking on the FERM domain. *Journal of Cell Science* 117:1547–1552 <https://doi.org/10.1242/jcs.01038>.
- Fire, A., Xu, S., Montgomery, M. K., Kostas, S. A., Driver, S. E. and Mello, C. C., 1998 Potent and specific genetic interference by double-stranded RNA in *Caenorhabditis elegans*. *Nature* 391:806–811 <https://doi.org/10.1038/35888>.
- Firestein, B. L. and Rongo, C., 2001 DLG-1 Is a MAGUK Similar to SAP97 and Is Required for Adherens Junction Formation. *MBoC* 12:3465–3475 <https://doi.org/10.1091/mbc.12.11.3465>.
- Fouassier, L., Nichols, M. T., Gidey, E., McWilliams, R. R., Robin, H., Finnigan, C., Howell, K. E., Housset, C. and Doctor, R. B., 2005 Protein kinase C regulates the phosphorylation and oligomerization of ERM binding phosphoprotein 50. *Experimental Cell Research* 306:264–273 <https://doi.org/10.1016/j.yexcr.2005.02.011>.
- Fritzsche, M., Thorogate, R. and Charras, G., 2014 Quantitative Analysis of Ezrin Turnover Dynamics in the Actin Cortex. *Biophysical Journal* 106:343–353 <https://doi.org/10.1016/j.bpj.2013.11.4499>.
- Fukushige, T., Hawkins, M. G. and McGhee, J. D., 1998 The GATA-factor *elt-2* is essential for formation of the *Caenorhabditis elegans* intestine. *Developmental Biology* 198:286–302 [https://doi.org/10.1016/S0012-1606\(98\)80006-7](https://doi.org/10.1016/S0012-1606(98)80006-7).
- Fukushige, T., Hendzel, M. J., Bazett-Jones, D. P. and McGhee, J. D., 1999 Direct visualization of the *elt-2* gut-specific GATA factor binding to a target promoter inside the living *Caenorhabditis elegans* embryo. *Proceedings of the National Academy of Sciences* 96:11883–11888 <https://doi.org/10.1073/pnas.96.21.11883>.

- Fukushige, T., Goszczynski, B., Tian, H. and McGhee, J. D., 2003 The Evolutionary Duplication and Probable Demise of an Endodermal GATA Factor in *Caenorhabditis elegans*. *Genetics* 165:575–588 <https://doi.org/10.1093/genetics/165.2.575>.
- Garbett, D. and Bretscher, A., 2012 PDZ interactions regulate rapid turnover of the scaffolding protein EBP50 in microvilli. *Journal of Cell Biology* 198:195–203 <https://doi.org/10.1083/jcb.201204008>.
- Garbett, D., LaLonde, D. P. and Bretscher, A., 2010 The scaffolding protein EBP50 regulates microvillar assembly in a phosphorylation-dependent manner. *Journal of Cell Biology* 191:397–413 <https://doi.org/10.1083/jcb.201004115>.
- Garland, B., Delisle, S., Al-Zahrani, K. N., Pryce, B. R. and Sabourin, L. A., 2021 The Ste20-like kinase – a Jack of all trades? *Journal of Cell Science* 134:jcs258269 <https://doi.org/10.1242/jcs.258269>.
- Gary, R. and Bretscher, A., 1995 Ezrin self-association involves binding of an N-terminal domain to a normally masked C-terminal domain that includes the F-actin binding site. *MBoC* 6:1061–1075 <https://doi.org/10.1091/mbc.6.8.1061>.
- Gautreau, A., Louvard, D. and Arpin, M., 2000 Morphogenic Effects of Ezrin Require a Phosphorylation-Induced Transition from Oligomers to Monomers at the Plasma Membrane. *Journal of Cell Biology* 150:193–204 <https://doi.org/10.1083/jcb.150.1.193>.
- Geisler, F., Gerhardus, H., Carberry, K., Davis, W., Jorgensen, E., Richardson, C., Bossinger, O. and Leube, R. E., 2016 A novel function for the MAP kinase SMA-5 in intestinal tube stability. *Mol Biol Cell* 27:3855–3868 <https://doi.org/10.1091/mbc.E16-02-0099>.
- Geisler, F., Coch, R. A., Richardson, C., Goldberg, M., Bevilacqua, C., Prevedel, R. and Leube, R. E., 2020 Intestinal intermediate filament polypeptides in *C. elegans*: Common and isotype-specific contributions to intestinal ultrastructure and function. *Sci Rep* 10:3142 <https://doi.org/10.1038/s41598-020-59791-w>.
- Georgescu, M.-M., Cote, G., Agarwal, N. K. and White, C. L., 2014 NHERF1/EBP50 Controls Morphogenesis of 3D Colonic Glands by Stabilizing PTEN and Ezrin-Radixin-Moesin Proteins at the Apical Membrane. *Neoplasia* 16:365–374.e2 <https://doi.org/10.1016/j.neo.2014.04.004>.
- Ghanta, K. S., Ishidate, T. and Mello, C. C., 2021 Microinjection for precision genome editing in *Caenorhabditis elegans*. *STAR Protoc* 2:100748 <https://doi.org/10.1016/j.xpro.2021.100748>.
- Gibson, D. G., Young, L., Chuang, R.-Y., Venter, J. C., Hutchison, C. A. and Smith, H. O., 2009 Enzymatic assembly of DNA molecules up to several hundred kilobases. *Nat Methods* 6:343–345 <https://doi.org/10.1038/nmeth.1318>.
- Gilkerson, J., Kelley, D. R., Tam, R., Estelle, M. and Callis, J., 2015 Lysine Residues Are Not Required for Proteasome-Mediated Proteolysis of the Auxin/Indole Acidic Acid Protein IAA1. *Plant Physiology* 168:708–720 <https://doi.org/10.1104/pp.15.00402>.
- Göbel, V., Barrett, P. L., Hall, D. H. and Fleming, J. T., 2004 Lumen morphogenesis in *C. elegans* requires the membrane-cytoskeleton linker erm-1. *Dev Cell* 6:865–873 <https://doi.org/10.1016/j.devcel.2004.05.018>.

- Goldstein, B., 1993 Establishment of gut fate in the E lineage of *C. elegans*: the roles of lineage-dependent mechanisms and cell interactions. *Development* 118:1267–1277 <https://doi.org/10.1242/dev.118.4.1267>.
- Goldstein, B. and Macara, I. G., 2007 The PAR Proteins: Fundamental Players in Animal Cell Polarization. *Developmental Cell* 13:609–622 <https://doi.org/10.1016/j.devcel.2007.10.007>.
- Goodson, H. V. and Jonasson, E. M., 2018 Microtubules and Microtubule-Associated Proteins. *Cold Spring Harb Perspect Biol* 10:a022608 <https://doi.org/10.1101/cshperspect.a022608>.
- Grana, T. M., Cox, E. A., Lynch, A. M. and Hardin, J., 2010 SAX-7/L1CAM and HMR-1/cadherin function redundantly in blastomere compaction and non-muscle myosin accumulation during *Caenorhabditis elegans* gastrulation. *Developmental Biology* 344:731–744 <https://doi.org/10.1016/j.ydbio.2010.05.507>.
- Gray, W. M., Kepinski, S., Rouse, D., Leyser, O. and Estelle, M., 2001 Auxin regulates SCFTIR1-dependent degradation of AUX/IAA proteins. *Nature* 414:271–276 <https://doi.org/10.1038/35104500>.
- Guilluy, C., Rolli-Derkinderen, M., Loufrani, L., Bourgé, A., Henrion, D., Sabourin, L., Loirand, G. and Pacaud, P., 2008 Ste20-Related Kinase SLK Phosphorylates Ser188 of RhoA to Induce Vasodilation in Response to Angiotensin II Type 2 Receptor Activation. *Circulation Research* 102:1265–1274 <https://doi.org/10.1161/CIRCRESAHA.107.164764>.
- Hagiwara, K., Nagamori, S., Umemura, Y. M., Ohgaki, R., Tanaka, H., Murata, D., Nakagomi, S., Nomura, K. H., Kage-Nakadai, E., Mitani, S., Nomura, K. and Kanai, Y., 2012 NRFL-1, the *C. elegans* NHERF Orthologue, Interacts with Amino Acid Transporter 6 (AAT-6) for Age-Dependent Maintenance of AAT-6 on the Membrane. *PLOS ONE* 7:e43050 <https://doi.org/10.1371/journal.pone.0043050>.
- Han, H.-F. and Beckerle, M. C., 2009 The ALP-Enigma Protein ALP-1 Functions in Actin Filament Organization to Promote Muscle Structural Integrity in *Caenorhabditis elegans*. *MBoC* 20:2361–2370 <https://doi.org/10.1091/mbc.e08-06-0584>.
- Han, B., Sivaramakrishnan, P., Lin, C.-C. J., Neve, I. A. A., He, J., Tay, L. W. R., Sowa, J. N., Sizovs, A., Du, G., Wang, J., Herman, C. and Wang, M. C., 2017 Microbial Genetic Composition Tunes Host Longevity. *Cell* 169:1249–1262.e13 <https://doi.org/10.1016/j.cell.2017.05.036>.
- Hao, J.-J., Liu, Y., Kruhlak, M., Debell, K. E., Rellahan, B. L. and Shaw, S., 2009 Phospholipase C-mediated hydrolysis of PIP2 releases ERM proteins from lymphocyte membrane. *Journal of Cell Biology* 184:451–462 <https://doi.org/10.1083/jcb.200807047>.
- Harris, T. W., Arnaboldi, V., Cain, S., Chan, J., Chen, W. J., Cho, J., Davis, P., Gao, S., Grove, C. A., Kishore, R., Lee, R. Y. N., Muller, H.-M., Nakamura, C., Nuin, P., Paulini, M., Raciti, D., Rodgers, F. H., Russell, M., Schindelman, G., Auken, K. V., Wang, Q., Williams, G., Wright, A. J., Yook, K., Howe, K. L., Schedl, T., Stein, L. and Sternberg, P. W., 2020 WormBase: a modern Model Organism Information Resource. *Nucleic Acids Res* 48:D762–D767 <https://doi.org/10.1093/nar/gkz920>.
- Hashimshony, T., Feder, M., Levin, M., Hall, B. K. and Yanai, I., 2015 Spatiotemporal transcriptomics reveals the evolutionary history of the endoderm germ layer. *Nature* 519:219–222 <https://doi.org/10.1038/nature13996>.

- Heiska, L., Alfthan, K., Grönholm, M., Vilja, P., Vaheri, A. and Carpén, O., 1998 Association of Ezrin with Intercellular Adhesion Molecule-1 and -2 (ICAM-1 and ICAM-2): Regulation by Phosphatidylinositol 4,5-Bisphosphate*. *Journal of Biological Chemistry* 273:21893–21900 <https://doi.org/10.1074/jbc.273.34.21893>.
- Herrmann, H. and Aebi, U., 2016 Intermediate Filaments: Structure and Assembly. *Cold Spring Harb Perspect Biol* 8:a018242 <https://doi.org/10.1101/cshperspect.a018242>.
- Herwig, L., Blum, Y., Krudewig, A., Ellertsdottir, E., Lenard, A., Belting, H.-G. and Affolter, M., 2011 Distinct Cellular Mechanisms of Blood Vessel Fusion in the Zebrafish Embryo. *Current Biology* 21:1942–1948 <https://doi.org/10.1016/j.cub.2011.10.016>.
- Hetherington, S., Gally, C., Fritz, J.-A., Polanowska, J., Reboul, J., Schwab, Y., Zahreddine, H., Behm, C. and Labouesse, M., 2011 PAT-12, a potential anti-nematode target, is a new spectraplakins partner essential for *Caenorhabditis elegans* hemidesmosome integrity and embryonic morphogenesis. *Developmental Biology* 350:267–278 <https://doi.org/10.1016/j.ydbio.2010.11.025>.
- Hills-Muckey, K., Martinez, M. A. Q., Stec, N., Hebbar, S., Saldanha, J., Medwig-Kinney, T. N., Moore, F. E. Q., Ivanova, M., Morao, A., Ward, J. D., Moss, E. G., Ercan, S., Zinovyeva, A. Y., Matus, D. Q. and Hammell, C. M., 2022 An engineered, orthogonal auxin analog/AtTIR1(F79G) pairing improves both specificity and efficacy of the auxin degradation system in *Caenorhabditis elegans*. *Genetics* 220:iyab174 <https://doi.org/10.1093/genetics/iwab174>.
- Hipfner, D. R., Keller, N. and Cohen, S. M., 2004 Slik Sterile-20 kinase regulates Moesin activity to promote epithelial integrity during tissue growth. *Genes Dev.* 18:2243–2248 <https://doi.org/10.1101/gad.303304>.
- Hoier, E. F., Mohler, W. A., Kim, S. K. and Hajnal, A., 2000 The *Caenorhabditis elegans* APC-related gene *apr-1* is required for epithelial cell migration and Hox gene expression. *Genes Dev.* 14:874–886 <https://doi.org/10.1101/gad.14.7.874>.
- Housden, B. E., Muhar, M., Gemberling, M., Gersbach, C. A., Stainier, D. Y. R., Seydoux, G., Mohr, S. E., Zuber, J. and Perrimon, N., 2017 Loss-of-function genetic tools for animal models: cross-species and cross-platform differences. *Nat Rev Genet* 18:24–40 <https://doi.org/10.1038/nrg.2016.118>.
- Huang, L., Wong, T. Y. W., Lin, R. C. C. and Furthmayr, H., 1999 Replacement of Threonine 558, a Critical Site of Phosphorylation of Moesin *in vivo*, with Aspartate Activates F-actin Binding of Moesin: Regulation by Conformational Change*. *Journal of Biological Chemistry* 274:12803–12810 <https://doi.org/10.1074/jbc.274.18.12803>.
- Huang, S., Shetty, P., Robertson, S. M. and Lin, R., 2007 Binary cell fate specification during *C. elegans* embryogenesis driven by reiterated reciprocal asymmetry of TCF POP-1 and its coactivator β -catenin SYS-1. *Development* 134:2685–2695 <https://doi.org/10.1242/dev.008268>.
- Hughes, S. C., Formstecher, E. and Fehon, R. G., 2010 Sip1, the *Drosophila* orthologue of EBP50/NHERF1, functions with the sterile 20 family kinase Slik to regulate Moesin activity. *Journal of Cell Science* 123:1099–1107 <https://doi.org/10.1242/jcs.059469>.
- Hüsken, K., Wiesenfahrt, T., Abraham, C., Windoffer, R., Bossinger, O. and Leube, R. E., 2008 Maintenance of the intestinal tube in *Caenorhabditis elegans*: the role of the intermediate filament protein IFC-2. *Differentiation* 76:881–896 <https://doi.org/10.1111/j.1432-0436.2008.00264.x>.

- Ikenouchi, J., Hirata, M., Yonemura, S. and Umeda, M., 2013 Sphingomyelin clustering is essential for the formation of microvilli. *Journal of Cell Science* 126:3585–3592 <https://doi.org/10.1242/jcs.122325>.
- Ingraffea, J., Reczek, D. and Bretscher, A., 2002 Distinct cell type-specific expression of scaffolding proteins EBP50 and E3KARP: EBP50 is generally expressed with ezrin in specific epithelia, whereas E3KARP is not. *European Journal of Cell Biology* 81:61–68 <https://doi.org/10.1078/0171-9335-00218>.
- Jaffe, A. B., Kaji, N., Durgan, J. and Hall, A., 2008 Cdc42 controls spindle orientation to position the apical surface during epithelial morphogenesis. *Journal of Cell Biology* 183:625–633 <https://doi.org/10.1083/jcb.200807121>.
- Janski, N., Masoud, K., Batzenschlager, M., Herzog, E., Evrard, J.-L., Houlné, G., Bourge, M., Chabouté, M.-E. and Schmit, A.-C., 2012 The GCP3-Interacting Proteins GIP1 and GIP2 Are Required for γ -Tubulin Complex Protein Localization, Spindle Integrity, and Chromosomal Stability. *The Plant Cell* 24:1171–1187 <https://doi.org/10.1105/tpc.111.094904>.
- Jiang, H. and Wang, D., 2018 The Microbial Zoo in the *C. elegans* Intestine: Bacteria, Fungi and Viruses. *Viruses* 10:85 <https://doi.org/10.3390/v10020085>.
- Jiang, H., Chen, K., Sandoval, L. E., Leung, C. and Wang, D., 2017 An Evolutionarily Conserved Pathway Essential for Orsay Virus Infection of *Caenorhabditis elegans*. *mBio* 8:10.1128/mbio.00940-17 <https://doi.org/10.1128/mbio.00940-17>.
- Johnson, C. A., Behbehani, R. and Buss, F., 2022 Unconventional Myosins from *Caenorhabditis elegans* as a Probe to Study Human Orthologues. *Biomolecules* 12:1889 <https://doi.org/10.3390/biom12121889>.
- Johnson, L. C., Vo, A. A., Clancy, J. C., Myles, K. M., Pooranachithra, M., Aguilera, J., Levenson, M. T., Wohlenberg, C., Rechtsteiner, A., Ragle, J. M., Chisholm, A. D. and Ward, J. D., 2023 NHR-23 activity is necessary for *C. elegans* developmental progression and apical extracellular matrix structure and function. *Development* 150:dev201085 <https://doi.org/10.1101/2021.10.27.465992>.
- Kagawa, H., Gengyo, K., Mclachlan, A. D., Brenner, S. and Karn, J., 1989 Paramyosin gene (unc-15) of *Caenorhabditis elegans*: Molecular cloning, nucleotide sequence and models for thick filament structure. *Journal of Molecular Biology* 207:311–333 [https://doi.org/10.1016/0022-2836\(89\)90257-X](https://doi.org/10.1016/0022-2836(89)90257-X).
- Karagiosis, S. A. and Ready, D. F., 2004 Moesin contributes an essential structural role in *Drosophila* photoreceptor morphogenesis. *Development* 131:725–732 <https://doi.org/10.1242/dev.00976>.
- Katzemich, A., Long, J. Y., Panneton, V., Fisher, L. A. B., Hipfner, D. and Schöck, F., 2019 Slik phosphorylation of Talin T152 is crucial for proper Talin recruitment and maintenance of muscle attachment in *Drosophila*. *Development* 146:dev176339 <https://doi.org/10.1242/dev.176339>.
- Khan, L. A., Zhang, H., Abraham, N., Sun, L., Fleming, J. T., Buechner, M., Hall, D. H. and Gobel, V., 2013 Intracellular lumen extension requires ERM-1-dependent apical membrane expansion and AQP-8-mediated flux. *Nat Cell Biol* 15:143–156 <https://doi.org/10.1038/ncb2656>.

- Klompstra, D., Anderson, D. C., Yeh, J. Y., Zilberman, Y. and Nance, J., 2015 An instructive role for *C. elegans* E-cadherin in translating cell contact cues into cortical polarity. *Nat Cell Biol* 17:726–735 <https://doi.org/10.1038/ncb3168>.
- Kodama, Y. and Hu, C.-D., 2010 An improved bimolecular fluorescence complementation assay with a high signal-to-noise ratio. *BioTechniques* 49:793–805 <https://doi.org/10.2144/000113519>.
- Kolotuev, I., Hyenne, V., Schwab, Y., Rodriguez, D. and Labouesse, M., 2013 A pathway for unicellular tube extension depending on the lymphatic vessel determinant Prox1 and on osmoregulation. *Nat Cell Biol* 15:157–168 <https://doi.org/10.1038/ncb2662>.
- Kondo, T., Takeuchi, K., Doi, Y., Yonemura, S., Nagata, S., Tsukita, S. and Tsukita, S., 1997 ERM (Ezrin/Radixin/Moesin)-based Molecular Mechanism of Microvillar Breakdown at an Early Stage of Apoptosis. *Journal of Cell Biology* 139:749–758 <https://doi.org/10.1083/jcb.139.3.749>.
- Koorman, T., Klompstra, D., van der Voet, M., Lemmens, I., Ramalho, J. J., Nieuwenhuize, S., van den Heuvel, S., Tavernier, J., Nance, J. and Boxem, M., 2016 A combined binary interaction and phenotypic map of *C. elegans* cell polarity proteins. *Nat Cell Biol* 18:337–346 <https://doi.org/10.1038/ncb3300>.
- Köppen, M., Simske, J. S., Sims, P. A., Firestein, B. L., Hall, D. H., Radice, A. D., Rongo, C. and Hardin, J. D., 2001 Cooperative regulation of AJM-1 controls junctional integrity in *Caenorhabditis elegans* epithelia. *Nat Cell Biol* 3:983–991 <https://doi.org/10.1038/ncb1101-983>.
- Kreimann, E. L., Morales, F. C., de Orbeta-Cruz, J., Takahashi, Y., Adams, H., Liu, T.-J., McCrea, P. D. and Georgescu, M.-M., 2007 Cortical stabilization of β -catenin contributes to NHERF1/EBP50 tumor suppressor function. *Oncogene* 26:5290–5299 <https://doi.org/10.1038/sj.onc.1210336>.
- Kroll, J. R., Rimmelzwaal, S. and Boxem, M., 2021 CeLINC, a fluorescence-based protein–protein interaction assay in *Caenorhabditis elegans*. *Genetics* 219:iyab163 <https://doi.org/10.1093/genetics/iwab163>.
- Kubota, T., Nishimura, K., Kanemaki, M. T. and Donaldson, A. D., 2013 The Elg1 Replication Factor C-like Complex Functions in PCNA Unloading during DNA Replication. *Molecular Cell* 50:273–280 <https://doi.org/10.1016/j.molcel.2013.02.012>.
- Kumar, A., Baruah, A., Tomioka, M., Iino, Y., Kalita, M. C. and Khan, M., 2020 *Caenorhabditis elegans*: a model to understand host–microbe interactions. *Cell. Mol. Life Sci.* 77:1229–1249 <https://doi.org/10.1007/s00018-019-03319-7>.
- Kunda, P., Pelling, A. E., Liu, T. and Baum, B., 2008 Moesin Controls Cortical Rigidity, Cell Rounding, and Spindle Morphogenesis during Mitosis. *Current Biology* 18:91–101 <https://doi.org/10.1016/j.cub.2007.12.051>.
- Kurz, C. L., Chauvet, S., Andrès, E., Aurouze, M., Vallet, I., Michel, G. P. F., Uh, M., Celli, J., Filloux, A., de Bentzmann, S., Steinmetz, I., Hoffmann, J. A., Finlay, B. B., Gorvel, J.-P., Ferrandon, D. and Ewbank, J. J., 2003 Virulence factors of the human opportunistic pathogen *Serratia marcescens* identified by *in vivo* screening. *The EMBO Journal* 22:1451–1460 <https://doi.org/10.1093/emboj/cdg159>.

Kvalvaag, A. S., Pust, S., Sundet, K. I., Engedal, N., Simm, R. and Sandvig, K., 2013 The ERM Proteins Ezrin and Moesin Regulate Retrograde Shiga Toxin Transport. *Traffic* 14:839–852 <https://doi.org/10.1111/tra.12077>.

Labouesse, M., 2006 Epithelial junctions and attachments. *WormBook* <https://doi.org/10.1895/wormbook.1.56.1>.

LaLonde, D. P. and Bretscher, A., 2009 The Scaffold Protein PDZK1 Undergoes a Head-to-Tail Intramolecular Association That Negatively Regulates Its Interaction with EBP50. *Biochemistry* 48:2261–2271 <https://doi.org/10.1021/bi802089k>.

LaLonde, D. P., Garbett, D. and Bretscher, A., 2010 A Regulated Complex of the Scaffolding Proteins PDZK1 and EBP50 with Ezrin Contribute to Microvillar Organization. *MBoC* 21:1519–1529 <https://doi.org/10.1091/mbc.e10-01-0008>.

Lamprecht, G., Weinman, E. J. and Yun, C.-H. C., 1998 The Role of NHERF and E3KARP in the cAMP-mediated Inhibition of NHE3*. *Journal of Biological Chemistry* 273:29972–29978 <https://doi.org/10.1074/jbc.273.45.29972>.

Lazar, C. S., Cresson, C. M., Lauffenburger, D. A. and Gill, G. N., 2004 The Na⁺/H⁺ Exchanger Regulatory Factor Stabilizes Epidermal Growth Factor Receptors at the Cell Surface. *MBoC* 15:5470–5480 <https://doi.org/10.1091/mbc.e04-03-0239>.

Legg, J. W., Lewis, C. A., Parsons, M., Ng, T. and Isacke, C. M., 2002 A novel PKC-regulated mechanism controls CD44–ezrin association and directional cell motility. *Nat Cell Biol* 4:399–407 <https://doi.org/10.1038/ncb797>.

Leonhard, K. and Nurse, P., 2005 Ste20/GCK kinase Nak1/Orb3 polarizes the actin cytoskeleton in fission yeast during the cell cycle. *Journal of Cell Science* 118:1033–1044 <https://doi.org/10.1242/jcs.01690>.

Leung, B., Hermann, G. J. and Priess, J. R., 1999 Organogenesis of the *Caenorhabditis elegans* Intestine. *Developmental Biology* 216:114–134 <https://doi.org/10.1006/dbio.1999.9471>.

Li, J., Poulikakos, P. I., Dai, Z., Testa, J. R., Callaway, D. J. E. and Bu, Z., 2007 Protein Kinase C Phosphorylation Disrupts Na⁺/H⁺ Exchanger Regulatory Factor 1 Autoinhibition and Promotes Cystic Fibrosis Transmembrane Conductance Regulator Macromolecular Assembly *. *Journal of Biological Chemistry* 282:27086–27099 <https://doi.org/10.1074/jbc.M702019200>.

Li, S., Prasanna, X., Salo, V. T., Vattulainen, I. and Ikonen, E., 2019 An efficient auxin-inducible degron system with low basal degradation in human cells. *Nat Methods* 16:866–869 <https://doi.org/10.1038/s41592-019-0512-x>.

Liégeois, S., Benedetto, A., Garnier, J.-M., Schwab, Y. and Labouesse, M., 2006 The V0-ATPase mediates apical secretion of exosomes containing Hedgehog-related proteins in *Caenorhabditis elegans*. *Journal of Cell Biology* 173:949–961 <https://doi.org/10.1083/jcb.200511072>.

Liégeois, S., Benedetto, A., Michaux, G., Belliard, G. and Labouesse, M., 2007 Genes Required for Osmoregulation and Apical Secretion in *Caenorhabditis elegans*. *Genetics* 175:709–724 <https://doi.org/10.1534/genetics.106.066035>.

Lin, R., Thompson, S. and Priess, J. R., 1995 *pop-1* Encodes an HMG box protein required for the specification of a mesoderm precursor in Early *C. elegans* embryos. *Cell* 83:599–609 [https://doi.org/10.1016/0092-8674\(95\)90100-0](https://doi.org/10.1016/0092-8674(95)90100-0).

Lin, R., Hill, R. J. and Priess, J. R., 1998 POP-1 and Anterior–Posterior Fate Decisions in *C. elegans* Embryos. *Cell* 92:229–239 [https://doi.org/10.1016/S0092-8674\(00\)80917-4](https://doi.org/10.1016/S0092-8674(00)80917-4).

Liscum, E. and Reed, J. W., 2002 Genetics of Aux/IAA and ARF action in plant growth and development. *Plant Mol Biol* 49:387–400 <https://doi.org/10.1023/A:1015255030047>.

Little, M., Georgas, K., Pennisi, D. and Wilkinson, L., 2010 Chapter Five - Kidney Development: Two Tales of Tubulogenesis. *Current Topics in Developmental Biology* 90:193–229 [https://doi.org/10.1016/S0070-2153\(10\)90005-7](https://doi.org/10.1016/S0070-2153(10)90005-7).

Liu, H., Wang, S., Hang, W., Gao, J., Zhang, W., Cheng, Z., Yang, C., He, J., Zhou, J., Chen, J. and Shi, A., 2018 LET-413/Erbin acts as a RAB-5 effector to promote RAB-10 activation during endocytic recycling. *J Cell Biol* 217:299–314 <https://doi.org/10.1083/jcb.201705136>.

Lo, M.-C., Gay, F., Odom, R., Shi, Y. and Lin, R., 2004 Phosphorylation by the β -Catenin/MAPK Complex Promotes 14-3-3-Mediated Nuclear Export of TCF/POP-1 in Signal-Responsive Cells in *C. elegans*. *Cell* 117:95–106 [https://doi.org/10.1016/S0092-8674\(04\)00203-X](https://doi.org/10.1016/S0092-8674(04)00203-X).

Loose, J. A. and Ghazi, A., 2021 Auxin treatment increases lifespan in *Caenorhabditis elegans*. *Biology Open* 10:bio058703 <https://doi.org/10.1242/bio.058703>.

Lozano, E., Sáez, A. G., Flemming, A. J., Cunha, A. and Leroi, A. M., 2006 Regulation of Growth by Ploidy in *Caenorhabditis elegans*. *Current Biology* 16:493–498 <https://doi.org/10.1016/j.cub.2006.01.048>.

Luo, J., Zhou, J.-J. and Zhang, J.-Z., 2018 Aux/IAA Gene Family in Plants: Molecular Structure, Regulation, and Function. *International Journal of Molecular Sciences* 19:259 <https://doi.org/10.3390/ijms19010259>.

Lynch, A. M. and Hardin, J., 2009 The assembly and maintenance of epithelial junctions in *C. elegans*. *Front Biosci* 14:1414–1432 <https://doi.org/10.2741/3316>.

Lynch, A. M., Grana, T., Cox-Paulson, E., Couthier, A., Cameron, M., Chin-Sang, I., Pettitt, J. and Hardin, J., 2012 A Genome-wide Functional Screen Shows MAGI-1 Is an L1CAM-Dependent Stabilizer of Apical Junctions in *C. elegans*. *Current Biology* 22:1891–1899 <https://doi.org/10.1016/j.cub.2012.08.024>.

MacQueen, A. J., Baggett, J. J., Perumov, N., Bauer, R. A., Januszewski, T., Schriefer, L. and Waddle, J. A., 2005 ACT-5 Is an Essential *Caenorhabditis elegans* Actin Required for Intestinal Microvilli Formation. *MBoC* 16:3247–3259 <https://doi.org/10.1091/mbc.e04-12-1061>.

Maduro, M. F., 2017 Gut development in *C. elegans*. *Seminars in Cell & Developmental Biology* 66:3–11 <https://doi.org/10.1016/j.semcdb.2017.01.001>.



- Maduro, M. F., Meneghini, M. D., Bowerman, B., Broitman-Maduro, G. and Rothman, J. H., 2001 Restriction of Mesendoderm to a Single Blastomere by the Combined Action of SKN-1 and a GSK-3 β Homolog Is Mediated by MED-1 and -2 in *C. elegans*. *Molecular Cell* 7:475–485 [https://doi.org/10.1016/S1097-2765\(01\)00195-2](https://doi.org/10.1016/S1097-2765(01)00195-2).
- Maduro, M. F., Lin, R. and Rothman, J. H., 2002 Dynamics of a Developmental Switch: Recursive Intracellular and Intranuclear Redistribution of *Caenorhabditis elegans* POP-1 Parallels Wnt-Inhibited Transcriptional Repression. *Developmental Biology* 248:128–142 <https://doi.org/10.1006/dbio.2002.0721>.
- Maduro, M. F., Hill, R. J., Heid, P. J., Newman-Smith, E. D., Zhu, J., Priess, J. R. and Rothman, J. H., 2005a Genetic redundancy in endoderm specification within the genus *Caenorhabditis*. *Developmental Biology* 284:509–522 <https://doi.org/10.1016/j.ydbio.2005.05.016>.
- Maduro, M. F., Kasmir, J. J., Zhu, J. and Rothman, J. H., 2005b The Wnt effector POP-1 and the PAL-1/Caudal homeoprotein collaborate with SKN-1 to activate *C. elegans* endoderm development. *Developmental Biology* 285:510–523 <https://doi.org/10.1016/j.ydbio.2005.06.022>.
- Maduro, M. F., Broitman-Maduro, G., Mengarelli, I. and Rothman, J. H., 2007 Maternal deployment of the embryonic SKN-1–MED-1,2 cell specification pathway in *C. elegans*. *Developmental Biology* 301:590–601 <https://doi.org/10.1016/j.ydbio.2006.08.029>.
- Maduro, M. F., Broitman-Maduro, G., Choi, H., Carranza, F., Wu, A. C.-Y. and Rifkin, S. A., 2015 MED GATA factors promote robust development of the *C. elegans* endoderm. *Developmental Biology* 404:66–79 <https://doi.org/10.1016/j.ydbio.2015.04.025>.
- Magendantz, M., Henry, M. D., Lander, A. and Solomon, F., 1995 Interdomain Interactions of Radixin *in vitro*(*). *Journal of Biological Chemistry* 270:25324–25327 <https://doi.org/10.1074/jbc.270.43.25324>.
- Martinez, M. A. Q., Kinney, B. A., Medwig-Kinney, T. N., Ashley, G., Ragle, J. M., Johnson, L., Aguilera, J., Hammell, C. M., Ward, J. D. and Matus, D. Q., 2020 Rapid Degradation of *Caenorhabditis elegans* Proteins at Single-Cell Resolution with a Synthetic Auxin. *G3 Genes/Genomes/Genetics* 10:267–280 <https://doi.org/10.1534/g3.119.400781>.
- Matsui, T., Maeda, M., Doi, Y., Yonemura, S., Amano, M., Kaibuchi, K., Tsukita, S. and Tsukita, S., 1998 Rho-Kinase Phosphorylates COOH-terminal Threonines of Ezrin/Radixin/Moesin (ERM) Proteins and Regulates Their Head-to-Tail Association. *Journal of Cell Biology* 140:647–657 <https://doi.org/10.1083/jcb.140.3.647>.
- Maudsley, S., Zamah, A. M., Rahman, N., Blitzer, J. T., Luttrell, L. M., Lefkowitz, R. J. and Hall, R. A., 2000 Platelet-Derived Growth Factor Receptor Association with Na⁺/H⁺ Exchanger Regulatory Factor Potentiates Receptor Activity. *Molecular and Cellular Biology* 20:8352–8363 <https://doi.org/10.1128/MCB.20.22.8352-8363.2000>.
- McClatchey, A. I., 2014 ERM proteins at a glance. *Journal of Cell Science* 127:3199–3204 <https://doi.org/10.1242/jcs.098343>.
- McGhee, J., 2007 The *C. elegans* intestine. *WormBook* <https://doi.org/10.1895/wormbook.1.133.1>.

- McGhee, J. D., 2013 The *Caenorhabditis elegans* intestine. *Wiley Interdiscip Rev Dev Biol* 2:347–367 <https://doi.org/10.1002/wdev.93>.
- McKeown, C. R., Han, H.-F. and Beckerle, M. C., 2006 Molecular characterization of the *Caenorhabditis elegans* ALP/Enigma gene *alp-1*. *Developmental Dynamics* 235:530–538 <https://doi.org/10.1002/dvdy.20633>.
- McMahon, L., Legouis, R., Vonesch, J.-L. and Labouesse, M., 2001 Assembly of *C. elegans* apical junctions involves positioning and compaction by LET-413 and protein aggregation by the MAGUK protein DLG-1. *Journal of Cell Science* 114:2265–2277 <https://doi.org/10.1242/jcs.114.12.2265>.
- Médina, E., Williams, J., Klipfell, E., Zarnescu, D., Thomas, C. M. and Le Bivic, A., 2002 Crumbs interacts with moesin and β Heavy-spectrin in the apical membrane skeleton of *Drosophila*. *Journal of Cell Biology* 158:941–951 <https://doi.org/10.1083/jcb.200203080>.
- Mello, C. C., Kramer, J. M., Stinchcomb, D. and Ambros, V., 1991 Efficient gene transfer in *C. elegans*: extrachromosomal maintenance and integration of transforming sequences. *EMBO J* 10:3959–3970 <https://doi.org/10.1002/j.1460-2075.1991.tb04966.x>.
- Mello, C. C., Draper, B. W., Krause, M., Weintraub, H. and Priess, J. R., 1992 The *pie-1* and *mex-1* genes and maternal control of blastomere identity in early *C. elegans* embryos. *Cell* 70:163–176 [https://doi.org/10.1016/0092-8674\(92\)90542-K](https://doi.org/10.1016/0092-8674(92)90542-K).
- Mendoza-Ochoa, G. I., Barrass, J. D., Terlouw, B. R., Maudlin, I. E., de Lucas, S., Sani, E., Aslanzadeh, V., Reid, J. A. E. and Beggs, J. D., 2019 A fast and tuneable auxin-inducible degron for depletion of target proteins in budding yeast. *Yeast* 36:75–81 <https://doi.org/10.1002/yea.3362>.
- Meneghini, M. D., Ishitani, T., Carter, J. C., Hisamoto, N., Ninomiya-Tsuji, J., Thorpe, C. J., Hamill, D. R., Matsumoto, K. and Bowerman, B., 1999 MAP kinase and Wnt pathways converge to downregulate an HMG-domain repressor in *Caenorhabditis elegans*. *Nature* 399:793–797 <https://doi.org/10.1038/21666>.
- Minna Roh-Johnson, Gidi Shemer, Christopher D. Higgins, Joseph H. McClellan, Adam D. Werts, U. Serdar Tulu, Liang Gao, Eric Betzig, Daniel P. Kiehart, and Bob Goldstein, 2012 Triggering a Cell Shape Change by Exploiting Preexisting Actomyosin Contractions. *Science* 335:1232–1235 <https://doi.org/10.1126/science.1217869>.
- Montalvo-Katz, S., Huang, H., Appel, M. D., Berg, M. and Shapira, M., 2013 Association with Soil Bacteria Enhances p38-Dependent Infection Resistance in *Caenorhabditis elegans*. *Infect Immun* 81:514–520 <https://doi.org/10.1128/IAI.00653-12>.
- Morales, F. C., Takahashi, Y., Kreimann, E. L. and Georgescu, M.-M., 2004 Ezrin–radixin–moesin (ERM)-binding phosphoprotein 50 organizes ERM proteins at the apical membrane of polarized epithelia. *Proceedings of the National Academy of Sciences* 101:17705–17710 <https://doi.org/10.1073/pnas.0407974101>.
- Morawska, M. and Ulrich, H. D., 2013 An expanded tool kit for the auxin-inducible degron system in budding yeast. *Yeast* 30:341–351 <https://doi.org/10.1002/yea.2967>.

- Morffy, N. and Strader, L. C., 2022 Structural Aspects of Auxin Signaling. *Cold Spring Harb Perspect Biol* 14:a039883 <https://doi.org/10.1101/cshperspect.a039883>.
- Morita, K., Flemming, A. J., Sugihara, Y., Mochii, M., Suzuki, Y., Yoshida, S., Wood, W. B., Kohara, Y., Leroi, A. M. and Ueno, N., 2002 A *Caenorhabditis elegans* TGF- β , DBL-1, controls the expression of LON-1, a PR-related protein, that regulates polyploidization and body length. *The EMBO Journal* 21:1063–1073 <https://doi.org/10.1093/emboj/21.5.1063>.
- Moss, B. L., Mao, H., Guseman, J. M., Hinds, T. R., Hellmuth, A., Kovenock, M., Noorassa, A., Lanctot, A., Villalobos, L. I. A. C., Zheng, N. and Nemhauser, J. L., 2015 Rate Motifs Tune Auxin/Indole-3-Acetic Acid Degradation Dynamics. *Plant Physiology* 169:803–813 <https://doi.org/10.1104/pp.15.00587>.
- Muñoz-Jiménez, C., Ayuso, C., Dobrzynska, A., Torres-Mendéz, A., Ruiz, P. de la C. and Askjaer, P., 2017 An Efficient FLP-Based Toolkit for Spatiotemporal Control of Gene Expression in *Caenorhabditis elegans*. *Genetics* 206:1763–1778 <https://doi.org/10.1534/genetics.117.201012>.
- Munro, E., Nance, J. and Priess, J. R., 2004 Cortical Flows Powered by Asymmetrical Contraction Transport PAR Proteins to Establish and Maintain Anterior-Posterior Polarity in the Early *C. elegans* Embryo. *Developmental Cell* 7:413–424 <https://doi.org/10.1016/j.devcel.2004.08.001>.
- Na, K., Shin, H., Cho, J.-Y., Jung, S. H., Lim, J., Lim, J.-S., Kim, E. A., Kim, H. S., Kang, A. R., Kim, J. H., Shin, J. M., Jeong, S.-K., Kim, C.-Y., Park, J. Y., Chung, H.-M., Omenn, G. S., Hancock, W. S. and Paik, Y.-K., 2017 Systematic Proteogenomic Approach To Exploring a Novel Function for NHERF1 in Human Reproductive Disorder: Lessons for Exploring Missing Proteins. *J. Proteome Res.* 16:4455–4467 <https://doi.org/10.1021/acs.jproteome.7b00146>.
- Nagle, R. B. and Cress, A. E., 2011 Metastasis Update: Human Prostate Carcinoma Invasion via Tubulogenesis. *Prostate Cancer* 2011:e249290 <https://doi.org/10.1155/2011/249290>.
- Nakamura, F., Amieva, M. R. and Furthmayr, H., 1995 Phosphorylation of Threonine 558 in the Carboxyl-terminal Actin-binding Domain of Moesin by Thrombin Activation of Human Platelets (*). *Journal of Biological Chemistry* 270:31377–31385 <https://doi.org/10.1074/jbc.270.52.31377>.
- Nakamura, F., Huang, L., Pestonjamas, K., Luna, E. J. and Furthmayr, H., 1999 Regulation of F-Actin Binding to Platelet Moesin *In vitro* by Both Phosphorylation of Threonine 558 and Polyphosphatidylinositides. *MBoC* 10:2669–2685 <https://doi.org/10.1091/mbc.10.8.2669>.
- Nakamura, F., Osborn, T. M., Hartemink, C. A., Hartwig, J. H. and Stossel, T. P., 2007 Structural basis of filamin A functions. *Journal of Cell Biology* 179:1011–1025 <https://doi.org/10.1083/jcb.200707073>.
- Nance, J., 2005 Gastrulation in *C. elegans*. *WormBook* <https://doi.org/10.1895/wormbook.1.23.1>.
- Nance, J. and Frøkjær-Jensen, C., 2019 The *Caenorhabditis elegans* Transgenic Toolbox. *Genetics* 212:959–990 <https://doi.org/10.1534/genetics.119.301506>.
- Natsume, T., Kiyomitsu, T., Saga, Y. and Kanemaki, M. T., 2016 Rapid Protein Depletion in Human Cells by Auxin-Inducible Degron Tagging with Short Homology Donors. *Cell Reports* 15:210–218 <https://doi.org/10.1016/j.celrep.2016.03.001>.

- Naturale, V., Pickett, M. and Feldman, J., 2022 E-Cadherin/HMR-1 and PAR-3 Break Symmetry at Stable Cell Contacts in a Developing Epithelium. *bioRxiv* <https://doi.org/10.2139/ssrn.4227255>.
- Negishi, T., Asakawa, M., Kanemaki, M. T. and Sawa, H., 2019 Modified auxin improves the auxin-inducible degradation (AID) system for laid *C. elegans* embryos. *microPublication Biology* <https://doi.org/10.17912/micropub.biology.000190>.
- Neisch, A. L. and Fehon, R. G., 2011 Ezrin, Radixin and Moesin: key regulators of membrane-cortex interactions and signaling. *Current Opinion in Cell Biology* 23:377–382 <https://doi.org/10.1016/j.celb.2011.04.011>.
- Ng, T., Parsons, M., Hughes, W. E., Monypenny, J., Zicha, D., Gautreau, A., Arpin, M., Gschmeissner, S., Vermeer, P. J., Bastiaens, P. I. H. and Parker, P. J., 2001 Ezrin is a downstream effector of trafficking PKC-integrin complexes involved in the control of cell motility. *The EMBO Journal* 20:2723–2741 <https://doi.org/10.1093/emboj/20.11.2723>.
- Niemeyer, M., Moreno Castillo, E., Ihling, C. H., Iacobucci, C., Wilde, V., Hellmuth, A., Hoehenwarter, W., Samodelov, S. L., Zurbriggen, M. D., Kastritis, P. L., Sinz, A. and Calderón Villalobos, L. I. A., 2020 Flexibility of intrinsically disordered degrons in AUX/IAA proteins reinforces auxin co-receptor assemblies. *Nat Commun* 11:2277 <https://doi.org/10.1038/s41467-020-16147-2>.
- Nishimura, K., Fukagawa, T., Takisawa, H., Kakimoto, T. and Kanemaki, M., 2009 An auxin-based degron system for the rapid depletion of proteins in nonplant cells. *Nat Methods* 6:917–922 <https://doi.org/10.1038/nmeth.1401>.
- Nono, M., Kishimoto, S., Sato-Carlton, A., Carlton, P. M., Nishida, E. and Uno, M., 2020 Intestine-to-Germline Transmission of Epigenetic Information Intergenerationally Ensures Systemic Stress Resistance in *C. elegans*. *Cell Reports* 30:3207–3217.e4 <https://doi.org/10.1016/j.celrep.2020.02.050>.
- O'Brien, L. E., Jou, T.-S., Pollack, A. L., Zhang, Q., Hansen, S. H., Yurchenco, P. and Mostov, K. E., 2001 Rac1 orientates epithelial apical polarity through effects on basolateral laminin assembly. *Nat Cell Biol* 3:831–838 <https://doi.org/10.1038/ncb0901-831>.
- Oh, Y.-S., Heo, K., Kim, E.-K., Jang, J.-H., Bae, S. S., Park, J. B., Kim, Y. H., Song, M., Kim, S. R., Ryu, S. H., Kim, I.-H. and Suh, P.-G., 2017 Dynamic relocalization of NHERF1 mediates chemotactic migration of ovarian cancer cells toward lysophosphatidic acid stimulation. *Exp Mol Med* 49:e351–e351 <https://doi.org/10.1038/emm.2017.88>.
- Ono, K., Yu, R., Mohri, K. and Ono, S., 2006 *Caenorhabditis elegans* Kettin, a Large Immunoglobulin-like Repeat Protein, Binds to Filamentous Actin and Provides Mechanical Stability to the Contractile Apparatuses in Body Wall Muscle. *Mol Biol Cell* 17:2722–2734 <https://doi.org/10.1091/mbc.E06-02-0114>.
- Oshiro, N., Fukata, Y. and Kaibuchi, K., 1998 Phosphorylation of Moesin by Rho-associated Kinase (Rho-kinase) Plays a Crucial Role in the Formation of Microvilli-like Structures *. *Journal of Biological Chemistry* 273:34663–34666 <https://doi.org/10.1074/jbc.273.52.34663>.
- Owraghi, M., Broitman-Maduro, G., Luu, T., Roberson, H. and Maduro, M. F., 2010 Roles of the Wnt effector POP-1/TCF in the *C. elegans* endomesoderm specification gene network. *Developmental Biology* 340:209–221 <https://doi.org/10.1016/j.ydbio.2009.09.042>.

Page, B. D., Diede, S. J., Tenlen, J. R. and Ferguson, E. L., 2007 EEL-1, a Hect E3 ubiquitin ligase, controls asymmetry and persistence of the SKN-1 transcription factor in the early *C. elegans* embryo. *Development* 134:2303–2314 <https://doi.org/10.1242/dev.02855>.

Paix, A., Folkmann, A., Rasoloson, D. and Seydoux, G., 2015 High Efficiency, Homology-Directed Genome Editing in *Caenorhabditis elegans* Using CRISPR-Cas9 Ribonucleoprotein Complexes. *Genetics* 201:47–54 <https://doi.org/10.1534/genetics.115.179382>.

Pal, S., Lant, B., Yu, B., Tian, R., Tong, J., Krieger, J. R., Moran, M. F., Gingras, A.-C. and Derry, W. B., 2017 CCM-3 Promotes *C. elegans* Germline Development by Regulating Vesicle Trafficking Cytokinesis and Polarity. *Current Biology* 27:868–876 <https://doi.org/10.1016/j.cub.2017.02.028>.

Panneton, V., Nath, A., Sader, F., Delaunay, N., Pelletier, A., Maier, D., Oh, K. and Hipfner, D. R., 2015 Regulation of Catalytic and Non-catalytic Functions of the *Drosophila* Ste20 Kinase Slik by Activation Segment Phosphorylation. *J Biol Chem* 290:20960–20971 <https://doi.org/10.1074/jbc.M115.645952>.

Parameswaran, N. and Gupta, N., 2013 Re-defining ERM function in lymphocyte activation and migration. *Immunological Reviews* 256:63–79 <https://doi.org/10.1111/imr.12104>.

Parameswaran, N., Matsui, K. and Gupta, N., 2011 Conformational Switching in Ezrin Regulates Morphological and Cytoskeletal Changes Required for B Cell Chemotaxis. *The Journal of Immunology* 186:4088–4097 <https://doi.org/10.4049/jimmunol.1001139>.

Parry, G., Calderon-Villalobos, L. I., Prigge, M., Peret, B., Dharmasiri, S., Itoh, H., Lechner, E., Gray, W. M., Bennett, M. and Estelle, M., 2009 Complex regulation of the TIR1/AFB family of auxin receptors. *Proceedings of the National Academy of Sciences* 106:22540–22545 <https://doi.org/10.1073/pnas.0911967106>.

Pásti, G. and Labouesse, M., 2018 Epithelial junctions, cytoskeleton, and polarity. *WormBook: The Online Review of C. elegans Biology* <https://doi.org/10.1895/wormbook.1.56.2>.

Patel, T. and Hobert, O., 2017 Coordinated control of terminal differentiation and restriction of cellular plasticity. *eLife* <https://doi.org/10.7554/eLife.24100>.

Paul, S. M., Ternet, M., Salvaterra, P. M. and Beitel, G. J., 2003 The Na⁺/K⁺ ATPase is required for septate junction function and epithelial tube-size control in the *Drosophila* tracheal system. *Development* 130:4963–4974 <https://doi.org/10.1242/dev.00691>.

Pearson, M. A., Reczek, D., Bretscher, A. and Karplus, P. A., 2000 Structure of the ERM Protein Moesin Reveals the FERM Domain Fold Masked by an Extended Actin Binding Tail Domain. *Cell* 101:259–270 [https://doi.org/10.1016/S0092-8674\(00\)80836-3](https://doi.org/10.1016/S0092-8674(00)80836-3).

Pelaseyed, T. and Bretscher, A., 2018 Regulation of actin-based apical structures on epithelial cells. *Journal of Cell Science* 131:jcs221853 <https://doi.org/10.1242/jcs.221853>.

Pelaseyed, T., Viswanatha, R., Sauvanet, C., Filter, J. J., Goldberg, M. L. and Bretscher, A., 2017 Ezrin activation by LOK phosphorylation involves a PIP2-dependent wedge mechanism. *eLife* 6:e22759 <https://doi.org/10.7554/eLife.22759>.

Pettitt, J., Cox, E. A., Broadbent, I. D., Flett, A. and Hardin, J., 2003 The *Caenorhabditis elegans* p120 catenin homologue, JAC-1, modulates cadherin-catenin function during epidermal morphogenesis. *Journal of Cell Biology* 162:15–22 <https://doi.org/10.1083/jcb.200212136>.

Phillips, B. T., Kidd, A. R., King, R., Hardin, J. and Kimble, J., 2007 Reciprocal asymmetry of SYS-1/ β -catenin and POP-1/TCF controls asymmetric divisions in *Caenorhabditis elegans*. *Proceedings of the National Academy of Sciences* 104:3231–3236 <https://doi.org/10.1073/pnas.0611507104>.

Pickett, M. A., Sallee, M. D., Cote, L., Naturale, V. F., Akpınaroglu, D., Lee, J., Shen, K. and Feldman, J. L., 2022 Separable mechanisms drive local and global polarity establishment in the *Caenorhabditis elegans* intestinal epithelium. *Development* 149:dev200325 <https://doi.org/10.1242/dev.200325>.

Pietromonaco, S. F., Simons, P. C., Altman, A. and Elias, L., 1998 Protein Kinase C- θ Phosphorylation of Moesin in the Actin-binding Sequence *. *Journal of Biological Chemistry* 273:7594–7603 <https://doi.org/10.1074/jbc.273.13.7594>.

Pilot, F., Philippe, J.-M., Lemmers, C. and Lecuit, T., 2006 Spatial control of actin organization at adherens junctions by a synaptotagmin-like protein. *Nature* 442:580–584 <https://doi.org/10.1038/nature04935>.

Polesello, C., Delon, I., Valenti, P., Ferrer, P. and Payre, F., 2002 Dmoesin controls actin-based cell shape and polarity during *Drosophila melanogaster* oogenesis. *Nat Cell Biol* 4:782–789 <https://doi.org/10.1038/ncb856>.

Pollard, T. D., 2016 Actin and Actin-Binding Proteins. *Cold Spring Harb Perspect Biol* 8:a018226 <https://doi.org/10.1101/cshperspect.a018226>.

Pombo, C. M., Force, T., Kyriakis, J., Nogueira, E., Fidalgo, M. and Zalvide, J., 2007 The GCK II and III subfamilies of the STE20 group kinases. *Front Biosci* 12:850–859 <https://doi.org/10.2741/2107>.

Ponuwei, G. A., 2016 A glimpse of the ERM proteins. *J Biomed Sci* 23:35 <https://doi.org/10.1186/s12929-016-0246-3>.

Pradel, E., Zhang, Y., Pujol, N., Matsuyama, T., Bargmann, C. I. and Ewbank, J. J., 2007 Detection and avoidance of a natural product from the pathogenic bacterium *Serratia marcescens* by *Caenorhabditis elegans*. *Proceedings of the National Academy of Sciences* 104:2295–2300 <https://doi.org/10.1073/pnas.0610281104>.

Qadota, H., Inoue, M., Hikita, T., Köppen, M., Hardin, J. D., Amano, M., Moerman, D. G. and Kaibuchi, K., 2007 Establishment of a tissue-specific RNAi system in *C. elegans*. *Gene* 400:166–173 <https://doi.org/10.1016/j.gene.2007.06.020>.

Quintin, S., Gally, C. and Labouesse, M., 2016 Noncentrosomal microtubules in *C. elegans* epithelia. *genesis* 54:229–242 <https://doi.org/10.1002/dvg.22921>.

Quizi, J. L., Baron, K., Al-Zahrani, K. N., O'Reilly, P., Sriram, R. K., Conway, J., Laurin, A.-A. and Sabourin, L. A., 2013 SLK-mediated phosphorylation of paxillin is required for focal adhesion turnover and cell migration. *Oncogene* 32:4656–4663 <https://doi.org/10.1038/onc.2012.488>.



- Raghuram, V., Hormuth, H. and Foskett, J. K., 2003 A kinase-regulated mechanism controls CFTR channel gating by disrupting bivalent PDZ domain interactions. *Proceedings of the National Academy of Sciences* 100:9620–9625 <https://doi.org/10.1073/pnas.1633250100>.
- Raj, A., Rifkin, S. A., Andersen, E. and van Oudenaarden, A., 2010 Variability in gene expression underlies incomplete penetrance. *Nature* 463:913–918 <https://doi.org/10.1038/nature08781>.
- Ramalho, J. J., Sepers, J. J., Nicolle, O., Schmidt, R., Cravo, J., Michaux, G. and Boxem, M., 2020 C-terminal phosphorylation modulates ERM-1 localization and dynamics to control cortical actin organization and support lumen formation during *Caenorhabditis elegans* development. *Development* 147:dev188011 <https://doi.org/10.1242/dev.188011>.
- Ramos, J. A., Zenser, N., Leyser, O. and Callis, J., 2001 Rapid Degradation of Auxin/Indoleacetic Acid Proteins Requires Conserved Amino Acids of Domain II and Is Proteasome Dependent. *Plant Cell* 13:2349–2360 <https://doi.org/10.1105/tpc.010244>.
- Rasmussen, J. P., Feldman, J. L., Reddy, S. S. and Priess, J. R., 2013 Cell Interactions and Patterned Intercalations Shape and Link Epithelial Tubes in *C. elegans*. *PLoS Genetics* 9:e1003772 <https://doi.org/10.1371/journal.pgen.1003772>.
- Rechavi, O. and Lev, I., 2017 Principles of Transgenerational Small RNA Inheritance in *Caenorhabditis elegans*. *Current Biology* 27:R720–R730 <https://doi.org/10.1016/j.cub.2017.05.043>.
- Rechavi, O., Hourri-Ze'evi, L., Anava, S., Goh, W. S. S., Kerk, S. Y., Hannon, G. J. and Hobert, O., 2014 Starvation-Induced Transgenerational Inheritance of Small RNAs in *C. elegans*. *Cell* 158:277–287 <https://doi.org/10.1016/j.cell.2014.06.020>.
- Reczek, D. and Bretscher, A., 1998 The Carboxyl-terminal Region of EBP50 Binds to a Site in the Amino-terminal Domain of Ezrin That Is Masked in the Dormant Molecule *. *Journal of Biological Chemistry* 273:18452–18458 <https://doi.org/10.1074/jbc.273.29.18452>.
- Reczek, D., Berryman, M. and Bretscher, A., 1997 Identification of EBP50: A PDZ-containing Phosphoprotein that Associates with Members of the Ezrin-Radixin-Moesin Family. *Journal of Cell Biology* 139:169–179 <https://doi.org/10.1083/jcb.139.1.169>.
- Remmelzwaal, S., Geisler, F., Stucchi, R., van der Horst, S., Pasolli, M., Kroll, J. R., Jarosinska, O. D., Akhmanova, A., Richardson, C. A., Altelaar, M., Leube, R. E., Ramalho, J. J. and Boxem, M., 2021 BBLN-1 is essential for intermediate filament organization and apical membrane morphology. *Current Biology* 31:2334–2346.e9 <https://doi.org/10.1016/j.cub.2021.03.069>.
- Ren, L., Hong, S. H., Cassavaugh, J., Osborne, T., Chou, A. J., Kim, S. Y., Gorlick, R., Hewitt, S. M. and Khanna, C., 2009 The actin-cytoskeleton linker protein ezrin is regulated during osteosarcoma metastasis by PKC. *Oncogene* 28:792–802 <https://doi.org/10.1038/onc.2008.437>.
- Riddle, M. R., Weintraub, A., Nguyen, K. C. Q., Hall, D. H. and Rothman, J. H., 2013 Transdifferentiation and remodeling of post-embryonic *C. elegans* cells by a single transcription factor. *Development* 140:4844–4849 <https://doi.org/10.1242/dev.103010>.

- Riddle, M. R., Spickard, E. A., Jevince, A., Nguyen, K. C. Q., Hall, D. H., Joshi, P. M. and Rothman, J. H., 2016 Transorganogenesis and transdifferentiation in *C. elegans* are dependent on differentiated cell identity. *Dev Biol* 420:136–147 <https://doi.org/10.1016/j.ydbio.2016.09.020>.
- Riga, A., Castiglioni, V. G. and Boxem, M., 2020 New insights into apical-basal polarization in epithelia. *Current Opinion in Cell Biology* 62:1–8 <https://doi.org/10.1016/j.ceb.2019.07.017>.
- Riga, A., Cravo, J., Schmidt, R., Pires, H. R., Castiglioni, V. G., van den Heuvel, S. and Boxem, M., 2021 *Caenorhabditis elegans* LET-413 Scribble is essential in the epidermis for growth, viability, and directional outgrowth of epithelial seam cells. *PLoS Genet* 17:e1009856 <https://doi.org/10.1371/journal.pgen.1009856>.
- Rijnberk, L. M. van, Barrull-Mascaró, R., Palen, R. L. van der, Schild, E. S., Korswagen, H. C. and Galli, M., 2022 Endomitosis controls tissue-specific gene expression during development. *PLoS Biology* 20:e3001597 <https://doi.org/10.1371/journal.pbio.3001597>.
- Roch, F., Polesello, C., Roubinet, C., Martin, M., Roy, C., Valenti, P., Carreno, S., Mangeat, P. and Payre, F., 2010 Differential roles of PtdIns(4,5)P₂ and phosphorylation in moesin activation during *Drosophila* development. *Journal of Cell Science* 123:2058–2067 <https://doi.org/10.1242/jcs.064550>.
- Rocheleau, C. E., Yasuda, J., Shin, T. H., Lin, R., Sawa, H., Okano, H., Priess, J. R., Davis, R. J. and Mello, C. C., 1999 WRM-1 Activates the LIT-1 Protein Kinase to Transduce Anterior/Posterior Polarity Signals in *C. elegans*. *Cell* 97:717–726 [https://doi.org/10.1016/S0092-8674\(00\)80784-9](https://doi.org/10.1016/S0092-8674(00)80784-9).
- Rodriguez-Boulan, E. and Macara, I. G., 2014 Organization and execution of the epithelial polarity programme. *Nat Rev Mol Cell Biol* 15:225–242 <https://doi.org/10.1038/nrm3775>.
- Roosjen, M., Kuhn, A., Mutte, S., Boeren, S., Krupar, P., Koehorst, J., Fendrych, M., Friml, J. and Weijers, D., 2022 An ultra-fast, proteome-wide response to the plant hormone auxin. *bioRxiv* <https://doi.org/10.1101/2022.11.25.517949>.
- Rose, A. M. and Baillie, D. L., 1980 Genetic organization of the region around UNC-15 (I), a gene affecting paramyosin in *Caenorhabditis elegans*. *Genetics* 96:639–648 <https://doi.org/10.1093/genetics/96.3.639>.
- Rual, J.-F., Ceron, J., Koreth, J., Hao, T., Nicot, A.-S., Hirozane-Kishikawa, T., Vandenhaute, J., Orkin, S. H., Hill, D. E., van den Heuvel, S. and Vidal, M., 2004 Toward Improving *Caenorhabditis elegans* Phenome Mapping With an ORFeome-Based RNAi Library. *Genome Res* 14:2162–2168 <https://doi.org/10.1101/gr.2505604>.
- Rueden, C. T., Schindelin, J., Hiner, M. C., DeZonia, B. E., Walter, A. E., Arena, E. T. and Eliceiri, K. W., 2017 ImageJ2: ImageJ for the next generation of scientific image data. *BMC Bioinformatics* 18:529 <https://doi.org/10.1186/s12859-017-1934-z>.
- Ruijtenberg, S. and Heuvel, S. van den, 2015 G1/S Inhibitors and the SWI/SNF Complex Control Cell-Cycle Exit during Muscle Differentiation. *Cell* 162:300–313 <https://doi.org/10.1016/j.cell.2015.06.013>.
- Sabourin, L. A. and Rudnicki, M. A., 1999 Induction of apoptosis by SLK, a Ste20-related kinase. *Oncogene* 18:7566–7575 <https://doi.org/10.1038/sj.onc.1203119>.

Salis, P., Payre, F., Valenti, P., Bazellieres, E., Bivic, A. L. and Mottola, G., 2017 Crumbs, Moesin and Yurt regulate junctional stability and dynamics for a proper morphogenesis of the *Drosophila* pupal wing epithelium. *Sci Rep* 7:1–14 <https://doi.org/10.1038/s41598-017-15272-1>.

Sallee, M. D., Zonka, J. C., Skokan, T. D., Raftrey, B. C. and Feldman, J. L., 2018 Tissue-specific degradation of essential centrosome components reveals distinct microtubule populations at microtubule organizing centers. *PLoS Biology* 16:e2005189 <https://doi.org/10.1371/journal.pbio.2005189>.

Sallee, M. D., Pickett, M. A. and Feldman, J. L., 2021 Apical PAR complex proteins protect against programmed epithelial assaults to create a continuous and functional intestinal lumen. *eLife* 10 <https://doi.org/10.7554/elife.64437>.

Samuel, B. S., Rowedder, H., Braendle, C., Félix, M.-A. and Ruvkun, G., 2016 *Caenorhabditis elegans* responses to bacteria from its natural habitats. *Proceedings of the National Academy of Sciences* 113:E3941–E3949 <https://doi.org/10.1073/pnas.1607183113>.

Sanchez, A. D. and Feldman, J. L., 2017 Microtubule-organizing centers: from the centrosome to non-centrosomal sites. *Current Opinion in Cell Biology* 44:93–101 <https://doi.org/10.1016/j.ceb.2016.09.003>.

Saotome, I., Curto, M. and McClatchey, A. I., 2004 Ezrin Is Essential for Epithelial Organization and Villus Morphogenesis in the Developing Intestine. *Developmental Cell* 6:855–864 <https://doi.org/10.1016/j.devcel.2004.05.007>.

Sasidharan, S., Borinskaya, S., Patel, F., Bernadskaya, Y., Mandalapu, S., Agapito, M. and Soto, M. C., 2018 WAVE regulates Cadherin junction assembly and turnover during epithelial polarization. *Developmental Biology* 434:133–148 <https://doi.org/10.1016/j.ydbio.2017.12.002>.

Sathyan, K. M., McKenna, B. D., Anderson, W. D., Duarte, F. M., Core, L. and Guertin, M. J., 2019 An improved auxin-inducible degron system preserves native protein levels and enables rapid and specific protein depletion. *Genes Dev.* 33:1441–1455 <https://doi.org/10.1101/gad.328237.119>.

Sauvanet, C., Wayt, J., Pelaseyed, T. and Bretscher, A., 2015 Structure, regulation, and functional diversity of microvilli on the apical domain of epithelial cells. *Annu Rev Cell Dev Biol* 31:593–621 <https://doi.org/10.1146/annurev-cellbio-100814-125234>.

Sawyer, J. M., Harrell, J. R., Shemer, G., Sullivan-Brown, J., Roh-Johnson, M. and Goldstein, B., 2010 Apical constriction: A cell shape change that can drive morphogenesis. *Developmental Biology* 341:5–19 <https://doi.org/10.1016/j.ydbio.2009.09.009>.

Schierenberg, E., 1987 Reversal of cellular polarity and early cell-cell interaction in the embryo of *Caenorhabditis elegans*. *Developmental Biology* 122:452–463 [https://doi.org/10.1016/0012-1606\(87\)90309-5](https://doi.org/10.1016/0012-1606(87)90309-5).

Schiksnis, E. C., Nicholson, A. L., Modena, M. S., Pule, M. N., Arribere, J. A. and Pasquinelli, A. E., 2020 Auxin-independent depletion of degron-tagged proteins by TIR1. *microPublication Biology* <https://doi.org/10.17912/micropub.biology.000213>.

Schindelin, J., Arganda-Carreras, I., Frise, E., Kaynig, V., Longair, M., Pietzsch, T., Preibisch, S., Rueden, C., Saalfeld, S., Schmid, B., Tinevez, J.-Y., White, D. J., Hartenstein, V., Eliceiri, K., Tomancak, P. and Cardona, A., 2012 Fiji: an open-source platform for biological-image analysis. *Nat Methods* 9:676–682 <https://doi.org/10.1038/nmeth.2019>.

Schottenfeld-Roames, J. and Ghabrial, A. S., 2013 Osmotic regulation of seamless tube growth. *Nat Cell Biol* 15:137–139 <https://doi.org/10.1038/ncb2683>.

Schwartz, M. L. and Jorgensen, E. M., 2016 SapTrap, a Toolkit for High-Throughput CRISPR/Cas9 Gene Modification in *Caenorhabditis elegans*. *Genetics* 202:1277–1288 <https://doi.org/10.1534/genetics.115.184275>.

Segbert, C., Johnson, K., Theres, C., van Fürden, D. and Bossinger, O., 2004 Molecular and functional analysis of apical junction formation in the gut epithelium of *Caenorhabditis elegans*. *Developmental Biology* 266:17–26 <https://doi.org/10.1016/j.ydbio.2003.10.019>.

Seidler, U., Singh, A. K., Cinar, A., Chen, M., Hillesheim, J., Hogema, B. and Riederer, B., 2009 The Role of the NHERF Family of PDZ Scaffolding Proteins in the Regulation of Salt and Water Transport. *Annals of the New York Academy of Sciences* 1165:249–260 <https://doi.org/10.1111/j.1749-6632.2009.04046.x>.

Senju, Y., Kalimeri, M., Koskela, E. V., Somerharju, P., Zhao, H., Vattulainen, I. and Lappalainen, P., 2017 Mechanistic principles underlying regulation of the actin cytoskeleton by phosphoinositides. *Proceedings of the National Academy of Sciences* 114:E8977–E8986 <https://doi.org/10.1073/pnas.1705032114>.

Sepers, J. J., Ramalho, J. J., Kroll, J. R., Schmidt, R. and Boxem, M., 2022a ERM-1 Phosphorylation and NRFL-1 Redundantly Control Lumen Formation in the *C. elegans* Intestine. *Frontiers in Cell and Developmental Biology* 10:769862 <https://doi.org/10.3389/fcell.2022.769862>.

Sepers, J. J., Verstappen, N. H. M., Vo, A. A., Ragle, J. M., Ruijtenberg, S., Ward, J. D. and Boxem, M., 2022b The mIAA7 degron improves auxin-mediated degradation in *Caenorhabditis elegans*. *G3 Genes/Genomes/Genetics* 12:jkac222 <https://doi.org/10.1093/g3journal/jkac222>.

Serrador, J. M., Nieto, M., Alonso-Lebrero, J. L., del Pozo, M. A., Calvo, J., Furthmayr, H., Schwartz-Albiez, R., Lozano, F., González-Amaro, R., Sánchez-Mateos, P. and Sánchez-Madrid, F., 1998 CD43 Interacts With Moesin and Ezrin and Regulates Its Redistribution to the Uropods of T Lymphocytes at the Cell-Cell Contacts. *Blood* 91:4632–4644 <https://doi.org/10.1182/blood.V91.12.4632>.

Serrano-Saiz, E., Leyva-Díaz, E., Cruz, E. D. L. and Hobert, O., 2018 BRN3-type POU Homeobox Genes Maintain the Identity of Mature Postmitotic Neurons in Nematodes and Mice. *Current Biology* 28:2813–2823.e2 <https://doi.org/10.1016/j.cub.2018.06.045>.

Shen, Z., Zhang, X., Chai, Y., Zhu, Z., Yi, P., Feng, G., Li, W. and Ou, G., 2014 Conditional Knockouts Generated by Engineered CRISPR-Cas9 Endonuclease Reveal the Roles of Coronin in *C. elegans* Neural Development. *Developmental Cell* 30:625–636 <https://doi.org/10.1016/j.devcel.2014.07.017>.

- Shenolikar, S. and Weinman, Edward. J., 2001 NHERF: targeting and trafficking membrane proteins. *American Journal of Physiology-Renal Physiology* 280:F389–F395 <https://doi.org/10.1152/ajprenal.2001.280.3.F389>.
- Shetty, P., Lo, M.-C., Robertson, S. M. and Lin, R., 2005 *C. elegans* TCF protein, POP-1, converts from repressor to activator as a result of Wnt-induced lowering of nuclear levels. *Developmental Biology* 285:584–592 <https://doi.org/10.1016/j.ydbio.2005.07.008>.
- Shin, T. H., Yasuda, J., Rocheleau, C. E., Lin, R., Soto, M., Bei, Y., Davis, R. J. and Mello, C. C., 1999 MOM-4, a MAP Kinase Kinase Kinase-Related Protein, Activates WRM-1/LIT-1 Kinase to Transduce Anterior/Posterior Polarity Signals in *C. elegans*. *Molecular Cell* 4:275–280 [https://doi.org/10.1016/S1097-2765\(00\)80375-5](https://doi.org/10.1016/S1097-2765(00)80375-5).
- Shreiner, A. B., Kao, J. Y. and Young, V. B., 2015 The gut microbiome in health and in disease. *Curr Opin Gastroenterol* 31:69–75 <https://doi.org/10.1097/MOG.000000000000139>.
- Sigurbjörnsdóttir, S., Mathew, R. and Leptin, M., 2014 Molecular mechanisms of de novo lumen formation. *Nat Rev Mol Cell Biol* 15:665–676 <https://doi.org/10.1038/nrm3871>.
- Simons, P. C., Pietromonaco, S. F., Reczek, D., Bretscher, A. and Elias, L., 1998 C-Terminal Threonine Phosphorylation Activates ERM Proteins to Link the Cell's Cortical Lipid Bilayer to the Cytoskeleton. *Biochemical and Biophysical Research Communications* 253:561–565 <https://doi.org/10.1006/bbrc.1998.9823>.
- Sommermann, E. M., Strohmaier, K. R., Maduro, M. F. and Rothman, J. H., 2010 Endoderm development in *Caenorhabditis elegans*: The synergistic action of ELT-2 and -7 mediates the specification–differentiation transition. *Developmental Biology* 347:154–166 <https://doi.org/10.1016/j.ydbio.2010.08.020>.
- Song, X., Wang, W., Wang, H., Yuan, X., Yang, F., Zhao, L., Mullen, M., Du, S., Zohbi, N., Muthusamy, S., Cao, Y., Jiang, J., Xia, P., He, P., Ding, M., Emmett, N., Ma, M., Wu, Q., Green, H.-N., Ding, X., Wang, D., Wang, F. and Liu, X., 2020 Acetylation of ezrin regulates membrane–cytoskeleton interaction underlying CCL18-elicited cell migration. *Journal of Molecular Cell Biology* 12:424–437 <https://doi.org/10.1093/jmcb/mjz099>.
- Spanier, B., 2014 Transcriptional and functional regulation of the intestinal peptide transporter PEPT1. *The Journal of Physiology* 592:871–879 <https://doi.org/10.1113/jphysiol.2013.258889>.
- Speck, O., Hughes, S. C., Noren, N. K., Kulikauskas, R. M. and Fehon, R. G., 2003 Moesin functions antagonistically to the Rho pathway to maintain epithelial integrity. *Nature* 421:83–87 <https://doi.org/10.1038/nature01295>.
- Stephens, R., Lim, K., Portela, M., Kvensakul, M., Humbert, P. O. and Richardson, H. E., 2018 The Scribble Cell Polarity Module in the Regulation of Cell Signaling in Tissue Development and Tumorigenesis. *Journal of Molecular Biology* 430:3585–3612 <https://doi.org/10.1016/j.jmb.2018.01.011>.
- Stetak, A. and Hajnal, A., 2011 The *C. elegans* MAGI-1 protein is a novel component of cell junctions that is required for junctional compartmentalization. *Developmental Biology* 350:24–31 <https://doi.org/10.1016/j.ydbio.2010.10.026>.

- Sulston, J. E., Schierenberg, E., White, J. G. and Thomson, J. N., 1983 The embryonic cell lineage of the nematode *Caenorhabditis elegans*. *Dev Biol* 100:64–119 [https://doi.org/10.1016/0012-1606\(83\)90201-4](https://doi.org/10.1016/0012-1606(83)90201-4).
- Tanguy, M., Véron, L., Stempor, P., Ahringer, J., Sarkies, P. and Miska, E. A., 2017 An Alternative STAT Signaling Pathway Acts in Viral Immunity in *Caenorhabditis elegans*. *mBio* 8:e00924-17 <https://doi.org/10.1128/mBio.00924-17>.
- Tauffenberger, A. and Parker, J. A., 2014 Heritable Transmission of Stress Resistance by High Dietary Glucose in *Caenorhabditis elegans*. *PLoS Genetics* 10:e1004346 <https://doi.org/10.1371/journal.pgen.1004346>.
- Tenenhaus, C., Subramaniam, K., Dunn, M. A. and Seydoux, G., 2001 PIE-1 is a bifunctional protein that regulates maternal and zygotic gene expression in the embryonic germ line of *Caenorhabditis elegans*. *Genes Dev* 15:1031–1040 <https://doi.org/10.1101/gad.876201>.
- Thorpe, C. J., Schlesinger, A., Carter, J. C. and Bowerman, B., 1997 Wnt Signaling Polarizes an Early *C. elegans* Blastomere to Distinguish Endoderm from Mesoderm. *Cell* 90:695–705 [https://doi.org/10.1016/S0092-8674\(00\)80530-9](https://doi.org/10.1016/S0092-8674(00)80530-9).
- Timmons, L. and Fire, A., 1998 Specific interference by ingested dsRNA. *Nature* 395:854–854 <https://doi.org/10.1038/27579>.
- Totong, R., Achilleos, A. and Nance, J., 2007 PAR-6 is required for junction formation but not apicobasal polarization in *C. elegans* embryonic epithelial cells. *Development* 134:1259–1268 <https://doi.org/10.1242/dev.02833>.
- Troemel, E. R., Félix, M.-A., Whiteman, N. K., Barrière, A. and Ausubel, F. M., 2008 Microsporidia Are Natural Intracellular Parasites of the Nematode *Caenorhabditis elegans*. *PLoS Biology* 6:e309 <https://doi.org/10.1371/journal.pbio.0060309>.
- Tsarouhas, V., Senti, K.-A., Jayaram, S. A., Tiklová, K., Hemphälä, J., Adler, J. and Samakovlis, C., 2007 Sequential Pulses of Apical Epithelial Secretion and Endocytosis Drive Airway Maturation in *Drosophila*. *Developmental Cell* 13:214–225 <https://doi.org/10.1016/j.devcel.2007.06.008>.
- Ukken, F. P., Aprill, I., JayaNandanan, N. and Leptin, M., 2014 Slik and the Receptor Tyrosine Kinase Breathless Mediate Localized Activation of Moesin in Terminal Tracheal Cells. *PLoS ONE* 9:e103323 <https://doi.org/10.1371/journal.pone.0103323>.
- van Fürden, D., Johnson, K., Segbert, C. and Bossinger, O., 2004 The *C. elegans* ezrin-radixin-moesin protein ERM-1 is necessary for apical junction remodelling and tubulogenesis in the intestine. *Dev Biol* 272:262–276 <https://doi.org/10.1016/j.ydbio.2004.05.012>.
- Venz, R., Pekec, T., Katic, I., Ciosk, R. and Ewald, C. Y., 2021 End-of-life targeted degradation of DAF-2 insulin/IGF-1 receptor promotes longevity free from growth-related pathologies. *eLife* 10:e71335 <https://doi.org/10.7554/eLife.71335>.

- Virtanen, P., Gommers, R., Oliphant, T. E., Haberland, M., Reddy, T., Cournapeau, D., Burovski, E., Peterson, P., Weckesser, W., Bright, J., van der Walt, S. J., Brett, M., Wilson, J., Millman, K. J., Mayorov, N., Nelson, A. R. J., Jones, E., Kern, R., Larson, E., Carey, C. J., Polat, İ., Feng, Y., Moore, E. W., VanderPlas, J., Laxalde, D., Perktold, J., Cimrman, R., Henriksen, I., Quintero, E. A., Harris, C. R., Archibald, A. M., Ribeiro, A. H., Pedregosa, F. and van Mulbregt, P., 2020 SciPy 1.0: fundamental algorithms for scientific computing in Python. *Nat Methods* 17:261–272 <https://doi.org/10.1038/s41592-019-0686-2>.
- Viswanatha, R., Ohouo, P. Y., Smolka, M. B. and Bretscher, A., 2012 Local phosphocycling mediated by LOK/SLK restricts ezrin function to the apical aspect of epithelial cells. *Journal of Cell Biology* 199:969–984 <https://doi.org/10.1083/jcb.201207047>.
- Viswanatha, R., Wayt, J., Ohouo, P. Y., Smolka, M. B. and Bretscher, A., 2013 Interactome Analysis Reveals Ezrin Can Adopt Multiple Conformational States *. *Journal of Biological Chemistry* 288:35437–35451 <https://doi.org/10.1074/jbc.M113.505669>.
- Vo, A. A., Levenson, M. T., Ragle, J. M. and Ward, J. D., 2021 Efficient generation of a single-copy eft-3p::TIR1::F2A::BFP::AID*::NLS allele in the *C. elegans* ttTi5605 insertion site through recombination-mediated cassette exchange. *microPublication Biology* <https://doi.org/10.17912/micropub.biology.000425>.
- Waaijers, S., Portegijs, V., Kerver, J., Lemmens, B. B. L. G., Tijsterman, M., van den Heuvel, S. and Boxem, M., 2013 CRISPR/Cas9-Targeted Mutagenesis in *Caenorhabditis elegans*. *Genetics* 195:1187–1191 <https://doi.org/10.1534/genetics.113.156299>.
- Waaijers, S., Ramalho, J. J., Koorman, T., Kruse, E. and Boxem, M., 2015 The *C. elegans* Crumbs family contains a CRB3 homolog and is not essential for viability. *Biology Open* 4:276–284 <https://doi.org/10.1242/bio.201410744>.
- Waaijers, S., Muñoz, J., Berends, C., Ramalho, J. J., Goerdayal, S. S., Low, T. Y., Zoumaro-Djayoon, A. D., Hoffmann, M., Koorman, T., Tas, R. P., Harterink, M., Seelk, S., Kerver, J., Hoogenraad, C. C., Bossinger, O., Tursun, B., van den Heuvel, S., Heck, A. J. R. and Boxem, M., 2016 A tissue-specific protein purification approach in *Caenorhabditis elegans* identifies novel interaction partners of DLG-1/Discs large. *BMC Biology* 14:66 <https://doi.org/10.1186/s12915-016-0286-x>.
- Wagner, S. M. and Sabourin, L. A., 2009 A novel role for the Ste20 kinase SLK in adhesion signaling and cell migration. *Cell Adhesion & Migration* 3:182–184 <https://doi.org/10.4161/cam.3.2.7229>.
- Wagner, S., Flood, T. A., O'Reilly, P., Hume, K. and Sabourin, L. A., 2002 Association of the Ste20-like Kinase (SLK) with the Microtubule: Role in Rac1-Mediated Regulation of Actin Dynamics during Cell Adhesion and Spreading *. *Journal of Biological Chemistry* 277:37685–37692 <https://doi.org/10.1074/jbc.M205899200>.
- Wagner, S., Storbeck, C. J., Roovers, K., Chaar, Z. Y., Kolodziej, P., McKay, M. and Sabourin, L. A., 2008 FAK/src-Family Dependent Activation of the Ste20-Like Kinase SLK Is Required for Microtubule-Dependent Focal Adhesion Turnover and Cell Migration. *PLOS ONE* 3:e1868 <https://doi.org/10.1371/journal.pone.0001868>.
- Wang, S., Tang, N. H., Lara-Gonzalez, P., Zhao, Z., Cheerambathur, D. K., Prevo, B., Chisholm, A. D., Desai, A. and Oegema, K., 2017 A toolkit for GFP-mediated tissue-specific protein degradation in *C. elegans*. *Development* 144:2694–2701 <https://doi.org/10.1242/dev.150094>.

- Wang, X., Yan, R., Chen, Y.-Z. and Wang, Y., 2021 Computational identification of ubiquitination sites in *Arabidopsis thaliana* using convolutional neural networks. *Plant Mol Biol* 105:601–610 <https://doi.org/10.1007/s11103-020-01112-w>.
- Ward, J. D., 2015 Rapid and Precise Engineering of the *Caenorhabditis elegans* Genome with Lethal Mutation Co-Conversion and Inactivation of NHEJ Repair. *Genetics* 199:363–377 <https://doi.org/10.1534/genetics.114.172361>.
- Weinman, E. J., Steplock, D. and Shenolikar, S., 1993 CAMP-mediated inhibition of the renal brush border membrane Na⁺-H⁺ exchanger requires a dissociable phosphoprotein cofactor. *J Clin Invest* 92:1781–1786 <https://doi.org/10.1172/JCI116767>.
- Welz, T., Wellbourne-Wood, J. and Kerkhoff, E., 2014 Orchestration of cell surface proteins by Rab11. *Trends in Cell Biology* 24:407–415 <https://doi.org/10.1016/j.tcb.2014.02.004>.
- Wickham, H., 2016 *ggplot2*. Cham: Springer International Publishing <https://doi.org/10.1007/978-3-319-24277-4>.
- Winter, J. F., Höpfner, S., Korn, K., Farnung, B. O., Bradshaw, C. R., Marsico, G., Volkmer, M., Habermann, B. and Zerial, M., 2012 *Caenorhabditis elegans* screen reveals role of PAR-5 in RAB-11-recycling endosome positioning and apicobasal cell polarity. *Nat Cell Biol* 14:666–676 <https://doi.org/10.1038/ncb2508>.
- Wu, Y. and Griffin, E. E., 2017 Chapter Eleven - Regulation of Cell Polarity by PAR-1/MARK Kinase. In *Current Topics in Developmental Biology* (ed. Jenny, A.), pp. 365–397. Academic Press <https://doi.org/10.1016/bs.ctdb.2016.11.001>.
- Yang, X.-D., Huang, S., Lo, M.-C., Mizumoto, K., Sawa, H., Xu, W., Robertson, S. and Lin, R., 2011 Distinct and mutually inhibitory binding by two divergent β -catenins coordinates TCF levels and activity in *C. elegans*. *Development* 138:4255–4265 <https://doi.org/10.1242/dev.069054>.
- Yao, Z., Aboualizadeh, F., Kroll, J., Akula, I., Snider, J., Lyakisheva, A., Tang, P., Kotlyar, M., Jurisica, I., Boxem, M. and Stagljar, I., 2020 Split Intein-Mediated Protein Ligation for detecting protein-protein interactions and their inhibition. *Nat Commun* 11:2440 <https://doi.org/10.1038/s41467-020-16299-1>.
- Yesbolatova, A., Natsume, T., Hayashi, K.-I. and Kanemaki, M. T., 2019 Generation of conditional auxin-inducible degron (AID) cells and tight control of degron-fused proteins using the degradation inhibitor auxinole. *Methods* 164–165:73–80 <https://doi.org/10.1016/j.ymeth.2019.04.010>.
- Yesbolatova, A., Saito, Y., Kitamoto, N., Makino-Itou, H., Ajima, R., Nakano, R., Nakaoka, H., Fukui, K., Gamo, K., Tominari, Y., Takeuchi, H., Saga, Y., Hayashi, K.-I. and Kanemaki, M. T., 2020 The auxin-inducible degron 2 technology provides sharp degradation control in yeast, mammalian cells, and mice. *Nat Commun* 11:5701 <https://doi.org/10.1038/s41467-020-19532-z>.
- Yonemura, S., Hirao, M., Doi, Y., Takahashi, N., Kondo, T., Tsukita, S. and Tsukita, S., 1998 Ezrin/Radixin/Moesin (ERM) Proteins Bind to a Positively Charged Amino Acid Cluster in the Juxta-Membrane Cytoplasmic Domain of CD44, CD43, and ICAM-2. *Journal of Cell Biology* 140:885–895 <https://doi.org/10.1083/jcb.140.4.885>.

Yonemura, S., Matsui, T., Tsukita, S. and Tsukita, S., 2002 Rho-dependent and -independent activation mechanisms of ezrin/radixin/moesin proteins: an essential role for polyphosphoinositides *in vivo*. *Journal of Cell Science* 115:2569–2580 <https://doi.org/10.1242/jcs.115.12.2569>.

Yu, W., Shewan, A. M., Brakeman, P., Eastburn, D. J., Datta, A., Bryant, D. M., Fan, Q.-W., Weiss, W. A., Zegers, M. M. P. and Mostov, K. E., 2008 Involvement of RhoA, ROCK I and myosin II in inverted orientation of epithelial polarity. *EMBO reports* 9:923–929 <https://doi.org/10.1038/embor.2008.135>.

Yu, C.-W., Luk, T. C. and Liao, V. H.-C., 2021 Long-term nanoplastics exposure results in multi and trans-generational reproduction decline associated with germline toxicity and epigenetic regulation in *Caenorhabditis elegans*. *Journal of Hazardous Materials* 412:125173 <https://doi.org/10.1016/j.jhazmat.2021.125173>.

Yun, C. H. C., Oh, S., Zizak, M., Steplock, D., Tsao, S., Tse, C.-M., Weinman, E. J. and Donowitz, M., 1997 cAMP-mediated inhibition of the epithelial brush border Na⁺/H⁺ exchanger, NHE3, requires an associated regulatory protein. *Proceedings of the National Academy of Sciences* 94:3010–3015 <https://doi.org/10.1073/pnas.94.7.3010>.

Zacharias, A. L., Walton, T., Preston, E. and Murray, J. I., 2015 Quantitative Differences in Nuclear β -catenin and TCF Pattern Embryonic Cells in *C. elegans*. *PLOS Genetics* 11:e1005585 <https://doi.org/10.1371/journal.pgen.1005585>.

Zhang, H., Abraham, N., Khan, L. A., Hall, D. H., Fleming, J. T. and Göbel, V., 2011 Apicobasal domain identities of expanding tubular membranes depend on glycosphingolipid biosynthesis. *Nat Cell Biol* 13:1189–1201 <https://doi.org/10.1038/ncb2328>.

Zhang, H., Kim, A., Abraham, N., Khan, L. A., Hall, D. H., Fleming, J. T. and Gobel, V., 2012 Clathrin and AP-1 regulate apical polarity and lumen formation during *C. elegans* tubulogenesis. *Development* 139:2071–2083 <https://doi.org/10.1242/dev.077347>.

Zhang, H., Kim, A., Abraham, N., Khan, L. A. and Göbel, V., 2013 Vesicular sorting controls the polarity of expanding membranes in the *C. elegans* intestine. *Worm* 2:e23702 <https://doi.org/10.4161/worm.23702>.

Zhang, L., Ward, J. D., Cheng, Z. and Dernburg, A. F., 2015 The auxin-inducible degradation (AID) system enables versatile conditional protein depletion in *C. elegans*. *Development* 142:4374–4384 <https://doi.org/10.1242/dev.129635>.

Zhang, X.-R., Zhao, L., Suo, F., Gao, Y., Wu, Q., Qi, X. and Du, L.-L., 2022 An improved auxin-inducible degron system for fission yeast. *G3 Genes/Genomes/Genetics* 12:jkab393 <https://doi.org/10.1093/g3journal/jkab393>.

Zhapparova, O. N., Fokin, A. I., Vorobyeva, N. E., Bryantseva, S. A. and Nadezhdina, E. S., 2013 Ste20-like protein kinase SLK (LOSK) regulates microtubule organization by targeting dynactin to the centrosome. *Mol Biol Cell* 24:3205–3214 <https://doi.org/10.1091/mbc.E13-03-0137>.

Zhou, X., Massol, R. H., Nakamura, F., Chen, X., Gewurz, B. E., Davis, B. M., Lencer, W. I. and Waldor, M. K., 2014 Remodeling of the Intestinal Brush Border Underlies Adhesion and Virulence of an Enteric Pathogen. *mBio* 5:e01639-14 <https://doi.org/10.1128/mBio.01639-14>.

Zhu, J., Hill, R. J., Heid, P. J., Fukuyama, M., Sugimoto, A., Priess, J. R. and Rothman, J. H., 1997 *end-1* encodes an apparent GATA factor that specifies the endoderm precursor in *Caenorhabditis elegans* embryos. *Genes Dev.* 11:2883–2896 <https://doi.org/10.1101/gad.11.21.2883>.

Zhu, J., Fukushige, T., McGhee, J. D. and Rothman, J. H., 1998 Reprogramming of early embryonic blastomeres into endodermal progenitors by a *Caenorhabditis elegans* GATA factor. *Genes Dev.* 12:3809–3814 <https://doi.org/10.1101/gad.12.24.3809>.

Zhu, L., Zhou, R., Mettler, S., Wu, T., Abbas, A., Delaney, J. and Forte, J. G., 2007 High turnover of ezrin T567 phosphorylation: conformation, activity, and cellular function. *American Journal of Physiology-Cell Physiology* 293:C874–C884 <https://doi.org/10.1152/ajpcell.00111.2007>.

Zwaenepoel, I., Naba, A., Menezes Lyra Da Cunha, M., Del Maestro, L., Formstecher, E., Louvard, D. and Arpin, M., 2012 Ezrin regulates microvillus morphogenesis by promoting distinct activities of Eps8 proteins. *Mol Biol Cell* 23:1080–1095 <https://doi.org/10.1091/mbc.E11-07-0588>.

English summary

Most organs in the body consist of tubular structures responsible for the transport of nutrients and waste products. Examples include blood vessels through which our blood flows, the intestines where we digest food, and airways through which air reaches our lungs. An important aspect of forming these biological tubes is creating a lumen, which is the hole in the tube. This can happen in various ways, such as eliminating cells in a tissue to create an open space, or by neighboring cells breaking their connections, allowing the space between them to be filled with fluid. Complications in the formation of biological tubes can lead to various diseases, such as kidney abnormalities and cardiovascular diseases. Additionally, certain forms of cancer utilize the mechanisms involved in tube formation to become more aggressive or even spread to other organs.

The formation of these biological tubes is coordinated by a close collaboration of various structures and networks within the cells that compose the tube. An example of this is cell polarity, where cells divide into two domains, or sides: the apical domain facing the lumen, and the basolateral domain that is in contact with neighboring cells. Cell polarization is essential during tube development, as cells need to know where the lumen should be formed. Cell polarization is also important for tissue function. For example, in our intestines each individual intestinal cell knows on which side to digest and absorb food while simultaneously keeping pathogens out. In addition to cell polarization, the connections between neighboring cells, the cell junctions, are important for formation of biological tubes. These connect the neighboring cells so that the tissue as a whole is stronger and the tubes do not leak. The cells can also communicate with each other through these cell junctions. For example, this ensures that all cells polarize in the same way, so they all face the same direction. In this way, all individual cells collectively work together to form a barrier between the internal and external environment.

In this thesis, the focus is primarily on the role of the cytoskeleton in lumen formation. The cytoskeleton provides structural support and shapes the cells, similar to the skeleton in our body. The cytoskeleton is made up of different types of proteins that come together to form rods. These rods support the cell, much like how individual bones support our body. The different components of the cytoskeleton have different functions; some rods are long and shape the cell, while others are shorter and hold various components within the cell in place. My research focuses mainly on one specific component of the cytoskeleton called actin. The actin cytoskeleton is made up of relatively small rods that are mainly located just beneath the cell membrane. The cell membrane is the structure that separates the inside of a cell from the outside, similar to the skin of our body. Here, actin locally shapes and supports the cell membrane, for example in the small intestine actin forms microvilli: small finger-like

structures on the apical cell membrane to increase the surface area for better nutrient exchange. In the cells of the biological tubes, you mainly find actin at the apical membrane to shape the lumen. We have a fairly good understanding of how the actin cytoskeleton contributes to the formation of biological tubes, but the exact mechanism of how the apical actin network is regulated and which molecular players are involved remains unclear.

To gain a better understanding of how actin is regulated during the formation of tubular structures, we use the *C. elegans* model organism. *C. elegans* are one-millimeter-long roundworms that live in damp soil and feed on bacteria. These animals have several advantages for genetic studies. To start, they are hermaphrodites, meaning they are both male and female and can self-fertilize. This eliminates the need to mate worms of different sexes, allowing us to obtain genetic copies of a single parent worm. Additionally, this single parent can produce nearly three hundred offspring within a week, and these offspring grow to maturity within a few days. This allows us to easily analyze and study a large number of offspring in a short amount of time. Moreover, these animals have been used for research in the lab for about fifty years, and as a result, we have extensive knowledge on how to maintain, study, and genetically manipulate them.

Although the worm may not seem similar to us at first glance, it serves as an excellent model organism. At a genetic and molecular level, they exhibit similarities with us, therefore the cells and fundamental processes occurring within these cells resemble those of humans. Studying *C. elegans* helps scientists to better understand the human body. A good example of this is the organ primarily discussed in this thesis, namely the worm's intestine. Although on a smaller scale, this is a tube consisting of so-called epithelial cells, just like in humans. Moreover, the worm's intestine exhibits similar properties, such as digesting and absorbing food, and it has microvilli and a microbiota. Additionally, the intestine affects other organs in the worm, such as the nervous system and the immune system, similar to humans. In **Chapter 1**, I delve deeper into the development and functions of the *C. elegans* intestine. I also discuss various types of research conducted using this model organ.

For my research, I focus on proteins that play a role in regulating the actin cytoskeleton and the formation of the lumen in the intestine of *C. elegans*. Proteins are biological molecules that form the basis of all cellular processes. These proteins are genetically encoded in an organism's genome in the form of genes. In my research, I use a technique called CRISPR/Cas9, which allows us to modify these genes. This enables us to remove or partially inactivate proteins, allowing us to determine their role. The underlying idea is that by observing which process is disrupted after manipulating the gene, we can infer what the gene does. Additionally, the CRISPR/Cas9 technique allows us to introduce new genetic material. This allows us, for example, to attach something to a protein

or introduce new proteins into the worm. An example of this is attaching a fluorescent protein to a protein we are investigating, causing the protein to light up under a microscope. This allows us to see where the protein is located in the cell and to track it during intestine development. These techniques, combined with a few others, help us study how specific proteins regulate actin and their role during intestine development in *C. elegans*.

In **Chapter 2**, we worked on ERM-1, a protein that is part of the ERM family, the members of which are known as linkers between the cell membrane and the underlying actin. Previous studies have shown that ERM-1 is located in the microvilli in the *C. elegans* intestine and that the protein is important for actin regulation and lumen formation. Inactivating ERM-1 results in the loss of microvilli, along with the widening of the lumen and the presence of obstructions that hinder the passage of food. In this chapter, we investigated how ERM-1 is regulated. To start, we looked at the role of ERM-1's ability to bind to the cell membrane and found that this is essential for ERM-1 activity. Additionally, we examined the role of ERM-1's ability to bind actin by investigating the phosphorylation of the portion of ERM-1 responsible for actin binding. Phosphorylation is a modification of a protein generally associated with its activation. To our surprise, this phosphorylation is not essential for ERM-1 activity, and it seems to have a more subtle role in the regulation and localization of ERM-1 in the intestinal cells.

In **Chapter 3**, we looked at NRFL-1, a protein that is part of the NHERF family and binds to proteins of the ERM family. ERM proteins not only act as linkers between the cell membrane and actin but can also together with NHERF proteins recruit other regulators of actin or the apical domain to the cell membrane. We demonstrated that NRFL-1 is recruited to the microvilli by ERM-1 and that this is essential for the function of NRFL-1. Depletion of NRFL-1 does not result in obvious defects. However, the simultaneous loss of ERM-1 phosphorylation and NRFL-1 results in defects that are nearly identical to the loss of ERM-1, with widened intestinal lumen accompanied by constrictions. We assume that ERM-1 has two functions in the intestine: actin binding regulated by phosphorylation, and organizing the apical domain via NRFL-1.

In **Chapter 4**, we conducted a genetic screen to find new regulators of lumen formation in the *C. elegans* intestine. In a genetic screen, genes are systematically inactivated to see if defects occur, which are then linked to a biological process. Using this screen, we identified a protein called GCK-4 located in the microvilli. Loss of GCK-4 results in widening of the lumen with multiple constrictions in the intestine, as well as a disrupted actin network. The protein family to which GCK-4 belongs is primarily known for phosphorylating ERM proteins. Since similar defects arise when ERM-1 is inactivated, this suggests that GCK-4 phosphorylates ERM-1. Surprisingly, this turned out not to be the case in the *C. elegans* intestine, so it seems that ERM-1 and GCK-4 independently contribute

to the formation of the intestinal lumen. Finally, we used two different techniques to identify interactors of GCK-4, of which the resulting data will be a valuable resource in the search for GCK-4 interactors.

In **Chapter 5**, we did not focus on lumen formation in the *C. elegans* intestine, but on improving a technique we often use in the lab, called auxin-inducible degradation (AID). This is a protein depletion system originally from plants, which we integrated into the worm. The great advantage of this technique is that it allows us to degrade proteins in one specific tissue. Most proteins have a function in various tissues, which means that genetic inactivation of a protein can lead to defects in multiple organs simultaneously. Since the AID technology only removes a protein in one tissue, we can specifically study the role of that protein in that tissue without influencing other tissues. However, sometimes this technology is not sufficient to completely degrade proteins and thus not inducing defects. Therefore, our goal was to improve the degradation of the AID technology. To degrade a protein, it must be genetically labeled with a degron, a piece that we attach to the protein that the degradation system recognizes. To improve degradation, we found a new degron called mIAA7, and implemented it in *C. elegans*. Additionally, we discovered that labeling a protein with more than one degron can further improve degradation. Finally, we made DNA constructs with the mIAA7-degron available to others in the *C. elegans* research field to help them integrate this degron into their experiments.

In **Chapter 6**, I discuss my results and the drawn conclusions. I compare the defects of the ERM-1, NRFL-1, and GCK-4 mutants with each other and with actin mutants found in other studies. I try to determine if my data align with the current theories and perspectives we have about the role of actin in lumen formation, and I debate outstanding questions in this field. Ultimately, I discuss my ideas, based on my research, about the collaboration between the actin cytoskeleton, the cell polarity network, and the cell junctions during the formation of the lumen in the *C. elegans* intestine. Finally, I briefly address how the AID system could potentially be further improved to investigate lumen formation in the *C. elegans* intestine.

Dutch summary (Nederlandse samenvatting)

De meeste organen in het lichaam bestaan uit buisvormige structuren die verantwoordelijk zijn voor het transport van voedings- en afvalstoffen. Voorbeelden hiervan zijn de bloedvaten waar ons bloed doorheen stroomt, de darmen waarin we voedsel verteren, en de luchtwegen waarmee lucht onze longen bereikt. Een belangrijk aspect van het vormen van deze biologische buizen is het creëren van een lumen, oftewel het gat in de buis. Dit kan op verschillende manieren gebeuren, zoals door het elimineren van cellen in een weefsel, waardoor een open ruimte ontstaat, of doordat aangrenzende cellen hun verbindingen verbreken, waardoor de ruimte ertussen gevuld wordt met vloeistof. Complicaties in het vormen van biologische buizen kunnen leiden tot verschillende ziektes, zoals nierafwijkingen en hart- en vaatziekten. Bovendien worden bepaalde vormen van kanker agressiever of zaaien uit door gebruik te maken van de mechanismen die betrokken zijn bij het vormen van biologische buizen.

De formatie van deze biologische buizen wordt gecoördineerd door een nauwe samenwerking van verschillende structuren en netwerken in de cellen waaruit de buis bestaat. Een voorbeeld hiervan is celpolariteit waarbij cellen zich opdelen in twee domeinen, oftewel kanten: het apicale domein gericht naar het lumen, en het basolaterale domein dat in contact staat met de buurcellen. Celpolarisatie is essentieel tijdens de ontwikkeling van de buis, aangezien de cellen moeten weten waar het lumen gevormd moet worden. Ook is celpolarisatie belangrijk voor het functioneren van het weefsel. Denk hierbij bijvoorbeeld aan onze darmen, waarin elke individuele darmcel weet aan welke zijde voedsel verteerd en opgenomen moet worden en tegelijkertijd ziekteverwekkers buiten moet houden. Naast celpolarisatie zijn de connecties tussen de buurcellen, de celverbindingen, belangrijk voor het vormen van biologische buizen. Deze verbinden de buurcellen zodat het weefsel als geheel sterker is en de buizen niet lekken. Ook kunnen de cellen met elkaar communiceren via de celverbindingen. Hierdoor zorgen ze bijvoorbeeld dat alle cellen op dezelfde manier polariseren, zodat ze allemaal dezelfde kant opstaan. Op deze manier werken alle individuele cellen collectief samen om een barrière te vormen tussen het interne en externe milieu.

In dit proefschrift ligt de focus voornamelijk op de rol van het cytoskelet tijdens de vorming van een lumen. Het cytoskelet zorgt voor structurele ondersteuning en geeft vorm aan de cellen, vergelijkbaar met het skelet in ons lichaam. Het cytoskelet bestaat uit verschillende soorten eiwitten die samenkomen om staven te vormen. Deze staven ondersteunen de cel, net zoals individuele botten ons lichaam ondersteunen. De verschillende onderdelen van het cytoskelet hebben verschillende functies; sommige staven zijn lang en geven vorm aan de cel, terwijl andere korter zijn en de verschillende onderdelen in de cel op hun plek houden. In mijn onderzoek richt ik mij voornamelijk op één specifiek

onderdeel van het cytoskelet genaamd actine. Het actine cytoskelet is gemaakt van relatief kleine staven die zich voornamelijk vlak onder het celmembraan bevinden. Het celmembraan is de structuur die de binnenkant van een cel scheidt van de buitenkant, vergelijkbaar met de huid van ons lichaam. Hier geeft actine lokaal vorm en ondersteuning aan het celmembraan. In bijvoorbeeld de dunne darm zorgt actine voor microvilli: kleine vingerachtige structuren op het apicale celmembraan om het oppervlak te vergroten voor een betere uitwisseling van voedingsstoffen. In de cellen van de biologische buizen vind je actine voornamelijk aan het apicale membraan waar het vorm geeft aan het lumen. We hebben een redelijk goed begrip van hoe het actine cytoskelet bijdraagt aan het vormen van biologische buizen, echter blijft het exacte mechanisme van hoe het apicale actine netwerk gereguleerd wordt en welke moleculaire spelers hierbij betrokken zijn nog onduidelijk.

Om een beter begrip te krijgen van hoe actine gereguleerd wordt tijdens het vormen van buisvormige structuren, maken we gebruik van het *C. elegans* modelorganisme. *C. elegans* zijn één millimeter lange rondwormen die in vochtige aarde leven en zich voeden met bacteriën. Deze dieren hebben een aantal grote voordelen voor genetische studies. Om te beginnen zijn ze hermafrodit, wat betekent dat ze zowel mannelijk als vrouwelijk zijn en zichzelf kunnen bevruchten. Dit houdt in dat het niet nodig is om wormen van verschillende geslachten te laten paren, en zo kunnen we genetische kopieën krijgen van een enkele ouderworm. Daarnaast kan deze ene ouder bijna driehonderd nakomelingen produceren binnen een week en groeien deze nakomelingen binnen enkele dagen op. Hierdoor kunnen we gemakkelijk een grote hoeveelheid nageslacht analyseren en bestuderen in korte tijd. Ook worden deze dieren al ongeveer vijftig jaar gebruikt voor onderzoek in het lab, waardoor we over uitgebreide kennis beschikken om ze te onderhouden, bestuderen en genetisch manipuleren.

Hoewel de worm op het eerste gezicht totaal niet op ons lijkt, dient hij toch als een uitstekend modeldier. Op genetisch en moleculair niveau vertonen ze namelijk gelijkenissen met ons, waardoor de cellen en basale processen die in deze cellen plaatsvinden overeenkomsten hebben met die van de mens. Het bestuderen van *C. elegans* helpt wetenschappers dus om het menselijk lichaam beter te begrijpen. Een goed voorbeeld hiervan is het orgaan waar voornamelijk in dit proefschrift over gesproken wordt, namelijk de darm van de worm. Hoewel op een kleinere schaal, is dit een buis die bestaat uit zogenaamde epitheelcellen, net zoals in de mens. Bovendien vertoont de darm van de worm vergelijkbare eigenschappen, zoals het verteren en opnemen van voedsel, en heeft microvilli en een microbiota. Ook beïnvloedt de darm andere organen in de worm, zoals het zenuwstelsel en het immuunsysteem, net zoals bij de mens. In **Hoofdstuk 1** ga ik dieper in op de ontwikkeling en functies van



de *C. elegans* darm. Ook bespreek ik diverse soorten onderzoek die met behulp van dit modelorgaan worden uitgevoerd.

Voor mijn onderzoek richt ik me op eiwitten die een rol spelen in de regulatie van het actine cytoskelet en de vorming van het lumen in de darm van *C. elegans*. Eiwitten zijn biologische moleculen die aan de basis liggen van alle cellulaire processen. Deze eiwitten zijn genetisch geschreven in het genoom van een organisme in de vorm van genen. In mijn onderzoek maak ik gebruik van een techniek genaamd CRISPR/Cas9, waarmee deze genen aangepast kunnen worden. Hiermee kunnen we eiwitten verwijderen of gedeeltelijk inactiveren, waardoor we kunnen achterhalen wat de rol van het eiwit is. Het idee hierachter is dat door te observeren welk proces verstoord raakt na manipulatie van het gen, we kunnen afleiden wat het gen doet. Daarnaast stelt de CRISPR/Cas9 techniek ons in staat om nieuw genetisch materiaal in te brengen. Hierdoor kunnen we bijvoorbeeld iets aan een eiwit plakken of nieuwe eiwitten introduceren in de worm. Een voorbeeld hiervan is het plakken van een fluorescerend eiwit aan een eiwit waarnaar we onderzoek doen, waardoor het eiwit onder een microscoop oplicht. Hierdoor kunnen we zien waar het eiwit zich in de cel bevindt en kunnen we het volgen tijdens de ontwikkeling van de darm. Deze technieken, in combinatie met een aantal andere, helpen ons bij het bestuderen van hoe specifieke eiwitten actine reguleren en hun rol tijdens de ontwikkeling van de darm in *C. elegans*.

In **Hoofdstuk 2** hebben we gewerkt aan ERM-1, een eiwit dat deel uitmaakt van de ERM-familie waarvan de leden bekend staan als koppelaars tussen het celmembraan en de onderliggende actine. Voorgaande studies hebben laten zien dat ERM-1 zich in de microvilli van de *C. elegans* darm bevindt en dat het eiwit belangrijk is voor actineregulatie en lumenformatie. De inactivatie van ERM-1 leidt tot het verlies van microvilli en verwijding van het lumen, evenals obstructies die de doorgang van voedsel belemmeren. In dit hoofdstuk hebben we onderzocht hoe ERM-1 wordt gereguleerd. Om te beginnen hebben we gekeken naar het effect van ERM-1's vermogen om aan het celmembraan te binden en zagen dat dit essentieel is voor ERM-1 activiteit. Daarnaast onderzochten we de rol van het vermogen van ERM-1 om aan actine te binden door de fosforylering van het deel van ERM-1 dat verantwoordelijk is voor de actinebinding te onderzoeken. Fosforylatie is een modificatie van een eiwit die over het algemeen geassocieerd wordt met de activatie van het eiwit. Tot onze verrassing is deze fosforylatie niet essentieel voor ERM-1 activiteit en lijkt het een meer subtiele rol te hebben in de regulatie en lokalisatie van ERM-1 in de darmcellen.

In **Hoofdstuk 3** keken we naar NRFL-1, een eiwit dat onderdeel is van de NHERF-familie en dat bindt aan eiwitten van de ERM-familie. ERM-eiwitten fungeren niet alleen als koppelaars tussen het celmembraan en actine, maar kunnen ook samen met NHERF-eiwitten andere regulatoren van actine of het

apicale domein naar het celmembraan rekruteren. We lieten zien dat NRFL-1 naar de microvilli wordt gerekruteerd door ERM-1 en dat dit essentieel is voor de functie van NRFL-1. De depletie van NRFL-1 resulteert niet in overduidelijke defecten. Echter, gelijktijdig verlies van ERM-1 fosforylatie en NRFL-1 zorgt voor defecten die nagenoeg identiek zijn aan het verlies van ERM-1, met een verdikking van en obstructies in het darmlumen tot gevolg. We veronderstellen dat ERM-1 twee functies heeft in de darm: actinebinding die wordt gereguleerd door fosforylatie en het organiseren van het apicale domein via NRFL-1.

In **Hoofdstuk 4** hebben we een genetische screen uitgevoerd om nieuwe lumenregulators te vinden in de *C. elegans* darm. In een genetische screen worden genen systematisch geïnactiveerd om te kijken welke defecten ontstaan, en deze worden vervolgens gekoppeld aan een biologisch proces. Met behulp van deze screen hebben we een eiwit genaamd GCK-4 geïdentificeerd dat zich bevindt in de microvilli. Verlies van GCK-4 resulteert in een verwijding van het lumen met meerdere vernauwingen in de darm, evenals een verstoord actine-netwerk. De eiwitfamilie waartoe GCK-4 behoort staat vooral bekend om fosforylatie van ERM-eiwitten. Aangezien vergelijkbare defecten ontstaan bij het inactiveren van ERM-1, suggereert dit dat GCK-4 ERM-1 fosforyleert. Dit bleek echter niet waar te zijn in de *C. elegans* darm en dus lijkt het erop dat ERM-1 en GCK-4 onafhankelijk van elkaar bijdragen aan de vorming van het darmlumen. Ten slotte hebben we gebruikgemaakt van twee verschillende technieken om interactoren voor GCK-4 te identificeren, waarvan de resulterende data een waardevolle bron zal zijn in de zoektocht naar GCK-4 interactoren.

In **Hoofdstuk 5** hebben we ons niet gericht op de lumenformatie in de *C. elegans* darm, maar op het verbeteren van een techniek die we vaak gebruiken in het lab, genaamd auxin-inducible degradation (AID). Dit is een eiwitdegradatiesysteem dat oorspronkelijk uit planten komt, en dat we hebben geïntegreerd in de worm. Het grote voordeel van deze techniek is dat we hiermee eiwitten kunnen degraderen in één specifiek weefsel. De meeste eiwitten hebben namelijk een functie in verschillende soorten weefsels, waardoor een genetische inactivatie van een eiwit ervoor kan zorgen dat defecten ontstaan in meerdere organen tegelijkertijd. Omdat de AID-technologie een eiwit in één weefsel verwijdert, kunnen we de specifieke rol van dat eiwit in dat weefsel bestuderen, zonder beïnvloeding van andere weefsels. Echter, soms is deze technologie niet voldoende om eiwitten volledig te degraderen en daarmee defecten te veroorzaken. Daarom was ons doel om de degradatie van de AID-technologie te verbeteren. Om een eiwit te degraderen moet het genetisch gelabeld worden met een degron, een stuk dat we aan het eiwit plakken dat het degradatiesysteem herkent. Om de degradatie te verbeteren hebben we een nieuwe degron, genaamd mIAA7, gevonden en geïmplementeerd in *C. elegans*. Daarnaast hebben we ontdekt dat het labelen van een eiwit met meer



dan één degron de degradatie nog verder kan verbeteren. Tot slot hebben we DNA-constructen met de mIAA7-degron beschikbaar gemaakt om anderen binnen het *C. elegans*-onderzoeksveld te helpen deze degron te integreren in hun experimenten.

In **Hoofdstuk 6** bespreek ik mijn resultaten en de getrokken conclusies. Hierbij vergelijk ik de defecten van de ERM-1, NRFL-1 en GCK-4 mutanten onderling en met actinemutanten die gevonden zijn in andere studies. Ik probeer hierbij te achterhalen of mijn data in lijn zijn met de theorieën en denkwijzen die we momenteel hebben over de rol van actine in lumenformatie en ik behandel openstaande vragen binnen dit vakgebied. Uiteindelijk bespreek ik mijn ideeën, gebaseerd op mijn onderzoek, over de samenwerking tussen het actine cytoskelet, het celpolariteitsnetwerk en de celverbindingen tijdens de vorming van het lumen in de *C. elegans* darm. Als laatste behandel ik kort hoe het AID-systeem eventueel nog verbeterd kan worden om lumenformatie in de *C. elegans* darm verder te onderzoeken.

Curriculum vitae

Johannes Jan “Jorian” Sepers was born on June 22, 1994 in Gorinchem, the Netherlands. He completed his pre-university education with a focus on science, health, and engineering at CS De Hoven locatie Lyceum Oudehoven in Gorinchem. He then pursued a bachelor’s degree in Biology followed by a master’s degree in Molecular and Cellular Life Sciences at Utrecht University, The Netherlands, in 2013 and 2016, respectively. Throughout his bachelor’s and master’s programs, he demonstrated a keen interest and specialization in cell biology, developmental biology, and genetics. He completed his bachelor’s degree with a literature research thesis entitled “The Role of the Epithelial-Mesenchymal Transition in Cancer” and a brief practical research internship under the guidance of Prof. Dr. Mike Boxem. For his first master’s internship, he continued his work at the Boxem lab, utilizing CRISPR/Cas9 technology and live imaging to investigate the interdependency between the isoforms of PAR-3 and PAR-6 in *Caenorhabditis elegans* epithelial tissues. Before starting his second internship, Jorian wrote his master’s literature research thesis entitled “Organization of the Microtubule Cytoskeleton in Neurons” under the supervision of Prof. Dr. Lukas C. Kapitein. For Jorian’s second internship, he relocated to California, USA. At the University of California Berkeley, in the group of Prof. Dr. David Bilder, he investigated the systemic effects of polarity-deficient ovarian tumors in *Drosophila melanogaster* flies. Jorian contributed to this research by conducting immunohistochemistry on ovarian tumors and preparing RNA samples from these tumors for transcriptomic analysis, ultimately resulting in a scientific publication. Upon completing his master’s degree in 2018, he returned to the lab of Prof. Dr. Mike Boxem at Utrecht University as a PhD student. In this role, he focused on studying the morphogenesis, tubulogenesis, and cell polarity of the *C. elegans* intestine. Additionally, he worked on improving the Auxin-Inducible Degradation technology commonly used within the *C. elegans* research community. The results of this research are outlined in this thesis, of which three chapters have been published in scientific journals. During his PhD, he was part of the Cancer, Stem Cells & Developmental Biology PhD program for which he served as a member of the PhD students committee for a year. Jorian will further his academic career as a postdoctoral researcher in the lab of Dr. Baoxu Pang at the LUMC in Leiden, The Netherlands, where he will investigate the role of the non-coding regulatory genome through comprehensive genome-wide approaches.

List of publications

Hsi, T. C., Ong, K. L., **Sepers, J. J.**, Kim, J., & Bilder, D., 2023. Systemic coagulopathy promotes host lethality in a new *Drosophila* tumor model. *Current Biology*, 33(14), 3002-3010.e6

Sepers, J.J., Verstappen, N.H., Vo, A.A., Ragle, J.M., Ruijtenberg, S., Ward, J.D. and Boxem, M., 2022. The mIAA7 degron improves auxin-mediated degradation in *Caenorhabditis elegans*. *G3 Genes|Genomes|Genetics*, 12(10), jkac22.

Sepers, J.J., Ramalho, J.J., Kroll, J.R., Schmidt, R. and Boxem, M., 2022. ERM-1 phosphorylation and NRFL-1 redundantly control lumen formation in the *C. elegans* intestine. *Frontiers in Cell and Developmental Biology*, 10, 769862.

Ramalho, J.J., **Sepers, J.J.**, Nicolle, O., Schmidt, R., Cravo, J., Michaux, G. and Boxem, M., 2020. C-terminal phosphorylation modulates ERM-1 localization and dynamics to control cortical actin organization and support lumen formation during *Caenorhabditis elegans* development. *Development*, 147(14), dev188011.

Acknowledgments (Dankwoord)

Mike, we already got to know each other in my first year of my bachelor (2013) as you were my mentor, although both of us recall little from that time. A few years later, I started working in your lab for my bachelor's and master's internships. Finally, two years later, I returned as a PhD student. The fact that I came back so many times stems from the fact that I have always enjoyed working with you, both as a student and employee, and I think we are alike in many ways regarding science as well as outside the lab life. As a supervisor, you are an enthusiastic and approachable person, who encourages his students to be critical, creative and independent. All of this contributed to making my PhD trajectory feel relatively smooth and enjoyable. Additionally, I believe that you, together with **Sander**, have formed a great department, where everybody is very sociable and open. Obviously, there were ups and downs, but I have always enjoyed going to the Kruyt building and working with the people within the department. You are both social and fun people who always encourage social interaction within and outside the department. I have deeply appreciated this aspect and will seek out similar environments in future jobs. **Suzan & Saskia**, first, I want to apologize for not always speaking highly of organoid research or fully appreciating the value of ribosomal proteins. Of course, all of this was in good fun. I genuinely think you are both great scientists, and I truly admire the research that you are doing. Secondly, you two joined the department halfway through my PhD, and I can already see the great influence you have had on the department. In my future endeavors, I aspire to work with progressive leadership like yours. **Vincent & Ruben**, here I will start (again) with an apology: sorry for the number of times you had to remind me to put on a lab coat. I do appreciate the work that you are doing for the lab. You are both very knowledgeable on how to run the lab, and it always felt like you were able to provide a solution to every problem. This way, you two make everybody's lab lives a lot easier and smoother. Vincent, I also enjoyed sharing the office with you. You always seem open to conversations and providing support, whether it is about serious PhD matters or just catching up on the latest football events.

Victoria, after I asked you to be my paranymph, both Jack and Eva separately came to me to tell me that you had excitedly informed them that you would be my paranymph. This confirmed to me that I made the right choice. I want to thank you for being my paranymph and for undertaking all the responsibilities that come with it for me. Even though, at the moment of writing this, I do not know exactly all the things you did, I am sure it will be great. During your time in the lab, I considered you an inspiring person. I witnessed a significant change from when I left after my master's internship until I started my PhD. You became very engaged in science and the discussions around it, becoming a very knowledgeable member of the lab. Even now, hearing about your current scientific research, it is very impressive, and I am sure you will succeed in

your future goals. In the acknowledgments of your thesis, you mentioned that I am welcome to visit you in Valencia. This, of course, happened during your wedding, which I am grateful to have attended. However, I would still love to visit it properly with you, including a climbing session in the nearby area. Besides that, I also hope to still run into you during conferences, as I have enjoyed the EWM in Vienna a lot with you. Unfortunately, our fields are a bit separated now, so we will have to see what is possible. **Ana**, I also have to thank you for being my paranymph and for undertaking all the responsibilities that come with it for me. I hope I will be able to do at least the same for you as your paranymph. You joined the lab later during my PhD at a time when many southern Europeans had just left. However, you were a great replacement for them, not just because you talk as much as all of them combined, but mostly because of your significant influence on the lab. We organized borrels and other out-of-the-lab activities together, and you are always open for a conversation. One influence, however, that I do not agree with is that since you introduced your intestinal and pancreatic organoids, I have noticed that many people in the department are shifting away from *C. elegans*. Besides the department, for me personally, you have also been an amazing influence. With the many beers, parties, and re-dinners we have shared, you have been a great support during the last two years of my PhD. In addition, working together from home was always fun, and way better than writing the thesis alone. Finalmente, muchas gracias por las clases de español! Ahora tengo que visitarte en Valladolid, porque necesito practicar el idioma. También extraño mucho nuestras noches en 'Beer & Barrels' y 'Back & Fourth', así que quiero vivir la versión española!

Helena, I always thought of you as the mother-figure in the lab, looking after people to help them both in the lab and with personal matters. Many others and I often came to you for advice when needed, as you always provided a safe space to talk. Additionally, you were my supervisor during my internships, showing me all the fundamentals in the lab and thinking along about future steps to take in my career. One piece of advice ultimately led to this book as one morning, you told me to go talk to Mike because he had discussed with you that I could be a suitable candidate for a PhD. Thank you for all your help and guidance, my career would not have been where it is now without you. **João**, I also have to thank you for a similar reason, as you were an important exemplary figure during my internships and at the start of my PhD. In addition, a lot of my research stems from projects that you started, as you probably recognize many chapters in this book. I will always appreciate that you showed me all the ins-and-outs of the projects in the first months of my PhD. Even though these were not your happiest times in the lab, you still took me along with a positive and accepting attitude. I'm excited to hear that you are back at Dev Bio now, although it saddens me that it is after I left, as I would have liked to spend more time in the lab together.



Janine, we met each other during our first experiences in the Kruyt building, me as a bachelor student and you as a PhD student. But we really got to know each other a couple of months later when we were working back-to-back in the so-called Gossip lab, where I got to hear all the gossip of the department. By the way, you still owe me over a 1000 NGM plates from this time... You are an optimistic and happy person, and even though there have been obstacles or setbacks, you remained an enjoyable lab member, always happily singing along with the radio in the lab. **Amalia**, we also got to know each other during my master in the Gossip lab, which reminds me that you also owe me many plates! You are a very chatty and 'gezellig' person, often sparking conversations and drawing the attention of the room. You are also very expressive, always telling people what is on your mind. This may have led to some awkward situations, as not all Dutch people are prepared for that, but I think you should never change this. Overall, I always enjoyed having you around, both in the lab as well as in the office decorated with Corfu postcards. **Sanne**, you are the last person who still owes me many plates, especially considering you took many in your last months in the lab. I think I have never met anybody with such a wide variety of musical interests, and I have enjoyed a great mix of styles over the years when you played them loudly in the lab. In addition, I always appreciated our long chats in the lab, regardless of whether they were about our political differences or the latest gossip. I am excited to hear that you moved to Leiden recently, as I just started at the LUMC. I look forward to having a drink once in a while there! **Jason**, we bonded in the beginning mostly by complaining about how intense and argumentative the lab meetings were. We would occasionally make eye contact during those meetings, looking at each other like 'pfff.. not one of those discussions again', and afterwards we would complain in the lab about how long it took. I have always liked working with you in the same lab space, as you gave off a relaxed vibe and provided pleasant conversations while picking worms. Also, your previous experiences made you an insightful person. **Olga**, I will never forgive you for spending the whole student market talking with me, only to ultimately pick Sanne as your supervisor even though she did not even attend the market! But regardless, I do appreciate that you joined the lab both as a master and later as a PhD student. You are very social and fit well within the Boxem group. This was already evident when you were a master student, as you joined me and the other PhDs more often than your fellow master students. I hope you are adjusting well to being the most senior member of the Boxem group now. I am sure you will make the last part of the PhD a success. **Merel**, you are a very energetic and enthusiastic person who shares her opinions whether people are ready for them or not. I see you as a compassionate individual, always looking out for those around you, although do not forget to take care of yourself as well from time-to-time. You were a great addition to the lab, and I enjoyed your company from as close as the lab to as far as Spain, where we went together with Olga and Ana.

Ben, you are such a happy person, and I always enjoyed chatting with you. You are also very insightful and have your own unique opinions, which suits you well in your educational position. **Tessa**, I admire your passion about science. It may not have always gone your way in the lab, but I'm glad to see that you stayed for the education. You always talked excitingly about science, so I believe you will be a very inspiring teacher! **Elise**, when I see bubble wrap, I think of you. You would be popping the bubbles one-by-one in the office, not hearing the sound with your headphones on, while others looked around trying to figure out where the noise came from. Goodluck with the final stretch of your PhD. From now on, when you get ERM-1 related questions during meetings, you really have to answer them yourself. **Alex**, thanks to you I will never forget what a UMI is. After one of your presentations, I asked about it, and what could have been a brief explanation turned into a 30-minute lecture on the reasons why there are biases in sequencing libraries and the history on how scientists used to deal with them. It really showed your interest in the smallest details of science and your willingness to share it with others. **Kaila**, it was very nice to share the office with you. You are a calm and organized person who does not bother anybody, while at the same time offering a listening ear or a nice gesture for those who need it. **Loes**, the sound of a phone connecting to a Bluetooth speaker reminds me of you, as the speaker in our lab space would always make a sound when you entered. You were the DJ of our lab, always ensuring there was music playing. **Mario**, to be honest, we hardly know each other as colleagues since we rarely find ourselves in the same country. And when we do meet, it is usually over drinks at a bar or a party rather than in the Kruyt building. Nevertheless, I thoroughly enjoyed those nights, whether in Utrecht or Madrid. **Joren, Mohamed & Stefanos**, our overlap in the lab was relatively short, but I can already tell that you are very fun and smart people. I believe the future of Dev Bio is in good hands. Goodluck!

Sander, Noud & Savvas, thank you for your contributions to my PhD as my master students. All three of you were insightful and great people to work with, and the supervision was an enrichment to my PhD journey. Sander, you were my first master student, and it was not only a learning experience for you, but I also learned a lot from it. You were a very nice and calm person, and despite realizing early on during your internship that lab work was not your passion, you persevered to produce results and to finish the internship. It is great to see you still working in the Kruyt building, now in an educational role. Noud, I mostly remember you as an enthusiastic student. You often came up with your own ideas or experiments beyond the projects you were assigned, such as improving the gel electrophoresis buffers. I also appreciated your directness, you tend to speak your mind regardless of the audience. This is definitely a strong point, especially for a master student, who tends to be more timid. Savvas, you were my last master student, whom I shared with Jason. You really

integrated with the other PhDs in the group, as if you were already a part of it. You even joined parties and a festival with us! Additionally, you were very insightful and independent in the lab, and showed genuine excitement about the topic we worked on. I am excited to hear that you are back in Mike's group, although it is a pity that it is after I left. However, if you ever need me, feel free to give me a call, especially if you need help discriminating between the intestine and the excretory canal.

Boris, Jey, Josiah, Milena, Kyle & Ilya, what started as invitation to a bouldering WhatsApp group from Boris, turned into weekly climbing sessions, secret borrels, and many other activities, even after some of us left the Kruyt building already. I feel like this group brought me, along with some other members from Dev Bio, closer to and getting to know better the Cell Bio department. Thank you for hosting me, a Dev Bio person, in your Cell Bio dominated group.

Mama & Papa, dank jullie wel voor alle onvoorwaardelijke steun, niet alleen voor afgelopen jaren, maar natuurlijk in heel mijn leven. Jullie hebben ons de ruimte en de vrijheid gegeven om te maken van ons leven wat we wilden. Van jongs af aan, werden we altijd gestimuleerd en geholpen dingen te leren en te doen, of het nou een moestuin was die het gezicht van de tuin verpestte waar jullie hard aan hadden gewerkt, of het houden van cavia's waar papa allergisch voor is. Ook nu we ouder zijn is niets te gek, met buitenlandse stages, drie verhuizingen per jaar of de wekelijkse oppas. Met alles zijn we altijd gesteund, zowel praktisch, financieel als emotioneel. Mama, jij biedt altijd een luisterend oor, en ik voel me daardoor veilig om mijn problemen te delen. Hierdoor lijken ze direct minder zwaar, en kom je vaak met oplossingen om het in de toekomst beter te doen. Ook ben je altijd de regelaar binnen het gezin, die ervoor zorgde dat alles op zijn plek zit en iedereen tevreden is. Jij had altijd al heel de reis uitgestippeld voordat we op vakantie gingen en zorgt ervoor dat iedereen aanwezig is op de volgende familiegelegenheid. Af en toe gaat het regelen zover dat we je ervan moeten weerhouden onze huizen op te ruimen en te reorganiseren. Echter maakt dit alles ons leven een stuk beter, en zorg je ervoor dat iedereen zijn ding kan blijven doen. Papa, zolang als ik me kan herinneren, probeer jij ons al uit te leggen hoe de wereld in elkaar steekt, zoals waarom de vogels nesten bouwen in de tuin of de politieke zaken die zich afspeelden op tv. Toepasselijk voor dit boekje, ik kan me zelfs herinneren dat ik mijn eerste genetecales van jou kreeg, waarin je tijdens het avondeten uitlegde hoe genen worden doorgegeven en dat dit opgeschreven wordt in een kruistabel met een 'kleine b' en een 'grote B'. Niet dat ik er destijds iets van begreep, aangezien ik nog veel te jong was. Deze leergierigheid en je bereidheid om deze kennis te delen met je omgeving, heeft enorm bijgedragen aan de nieuwsgierige en kritische persoon die ik nu ben. Ik vind het bijzonder om te zien dat je deze nieuwsgierigheid ook weer weet over te brengen naar de volgende generatie. Want wanneer ik in het voorjaar de tuin inloop, kan Julian mij in detail vertellen

waarom de bijtjes naar de bloemen vliegen en wat ze daar doen. Of Merijn, die zodra het regent vraagt of we naar buiten kunnen gaan, want nu komen de slakken tevoorschijn en kunnen we ze makkelijk vinden. Voor dit alles wil ik jullie beiden bedanken, omdat dit enorm heeft bijgedragen aan de persoon die ik nu ben en het pad dat ik bewandel. **Eline & Bernice**, ook jullie bieden veel steun. Als oudere zussen lopen jullie altijd een stapje voor op mij, en daarom staan jullie altijd klaar met adviezen en ideeën. Daarnaast dienen jullie ook als voorbeeld voor mij. Eline, door te laten zien dat met de juiste motivatie en doorzettingsvermogen heel veel mogelijk is, ongeacht of het meezit of niet. En Bernice is meer een voorbeeld in letterlijke zin, gezien wij een vergelijkbaar opleidings- en carrièrepad bewandelen. Dank jullie wel voor al jullie adviezen en inzichten! **Julian, Merijn & Olivier**, bedankt voor alle dagen LEGO'en, voetballen, stoeien, en nog veel meer. Jullie zijn een van de dingen in mijn leven die mij onvoorwaardelijk plezier brengen!

Kira, er zijn maar weinig mensen in de wereld die mij zo goed kennen als jij. Zolang als ik me kan herinneren, zijn wij al vrienden en hebben we enorm veel samen meegemaakt. Elke beslissing en elk probleem delen we eigenlijk wel met elkaar. Jij bent een persoon op wie ik altijd heb kunnen bouwen en vertrouwen, en daar ben ik je enorm dankbaar voor! **Jeroen, Jeffrey, Joost, Richard, Robin, Romy, Iris & Kyara**, jullie zouden eens moeten weten hoe vaak ik de vraag heb gekregen waarom ik nog steeds in Gorinchem woon terwijl ik zoveel tijd in Utrecht doorbreng. Als ik deze mensen vervolgens uitleg hoe vaak ik jullie zie in een week en wat dit voor mij betekent, begrijpen de meesten waarom. Jullie zijn heel belangrijk voor mij en bieden mij enorm veel steun, in goede en slechte tijden. We zijn al heel lang vrienden, sommigen al meer dan 20 jaar, en we hebben veel samen meegemaakt. Ik hoop dat dit nog lang zo zal blijven. **Alex, Myrddin & Wouter**, inmiddels kennen we elkaar ook al een tijdje, sinds de bachelor Biologie. Jullie zijn altijd een gezellige afleiding van het lableven en het leven in Gorinchem. Ondanks dat dit vaak betekent dat we levensbedreigende sporten beoefenen in de Zwitserse bergen, een film kijken waar Alex van tevoren al grotendeels de verhaallijn heeft verklapt, of jullie weer eens iets uit mijn persoonlijke leven proberen te ontfutselen. Ik hoop dat we nog vele weekjes naar Zwitserland gaan, weekendjes Zeeland beleven en nog veel meer avonturen meemaken! **Raimon**, I truly value our friendship, and now that my PhD is finished, I hope we can climb together frequently, go on more trips, and of course, I will have additional time to respond more quickly to your messages.

